Nuclear Science
NEA/NSC/DOC(2003)5

ISBN 92-64-02160-4

Benchmark on the Three-dimensional VENUS-2 MOX Core Measurements

Final Report

January 2004

NEA No. 4438

NUCLEAR ENERGY AGENCY
ORGANISATION FOR ECONOMIC CO-OPERATION AND DEVELOPMENT

ORGANISATION FOR ECONOMIC CO-OPERATION AND DEVELOPMENT

Pursuant to Article 1 of the Convention signed in Paris on 14th December 1960, and which came into force on 30th September 1961, the Organisation for Economic Co-operation and Development (OECD) shall promote policies designed:

- to achieve the highest sustainable economic growth and employment and a rising standard of living in member countries, while maintaining financial stability, and thus to contribute to the development of the world economy;
- to contribute to sound economic expansion in member as well as non-member countries in the process of economic development; and
- to contribute to the expansion of world trade on a multilateral, non-discriminatory basis in accordance with international obligations.

The original member countries of the OECD are Austria, Belgium, Canada, Denmark, France, Germany, Greece, Iceland, Ireland, Italy, Luxembourg, the Netherlands, Norway, Portugal, Spain, Sweden, Switzerland, Turkey, the United Kingdom and the United States. The following countries became members subsequently through accession at the dates indicated hereafter: Japan (28th April 1964), Finland (28th January 1969), Australia (7th June 1971), New Zealand (29th May 1973), Mexico (18th May 1994), the Czech Republic (21st December 1995), Hungary (7th May 1996), Poland (22nd November 1996), Korea (12th December 1996) and the Slovak Republic (14 December 2000). The Commission of the European Communities takes part in the work of the OECD (Article 13 of the OECD Convention).

NUCLEAR ENERGY AGENCY

The OECD Nuclear Energy Agency (NEA) was established on 1st February 1958 under the name of the OEEC European Nuclear Energy Agency. It received its present designation on 20th April 1972, when Japan became its first non-European full member. NEA membership today consists of 28 OECD member countries: Australia, Austria, Belgium, Canada, Czech Republic, Denmark, Finland, France, Germany, Greece, Hungary, Iceland, Ireland, Italy, Japan, Luxembourg, Mexico, the Netherlands, Norway, Portugal, Republic of Korea, Slovak Republic, Spain, Sweden, Switzerland, Turkey, the United Kingdom and the United States. The Commission of the European Communities also takes part in the work of the Agency.

The mission of the NEA is:

- to assist its member countries in maintaining and further developing, through international co-operation, the scientific, technological and legal bases required for a safe, environmentally friendly and economical use of nuclear energy for peaceful purposes, as well as
- to provide authoritative assessments and to forge common understandings on key issues, as input to government decisions on nuclear energy policy and to broader OECD policy analyses in areas such as energy and sustainable development.

Specific areas of competence of the NEA include safety and regulation of nuclear activities, radioactive waste management, radiological protection, nuclear science, economic and technical analyses of the nuclear fuel cycle, nuclear law and liability, and public information. The NEA Data Bank provides nuclear data and computer program services for participating countries.

In these and related tasks, the NEA works in close collaboration with the International Atomic Energy Agency in Vienna, with which it has a Co-operation Agreement, as well as with other international organisations in the nuclear field.

FOREWORD

In the framework of the joint activities of the OECD/NEA Working Party on the Physics of Plutonium Fuels and Innovative Fuel Cycles (WPPR) and the Task Force on Reactor-based Plutonium Disposition (TFRPD), the two-dimensional VENUS-2 MOX core benchmark was launched in 1999 and completed in 2000. Overall, the results were very encouraging and confirmed that present methods using the latest nuclear data sets can adequately calculate MOX-fuelled systems. However, the calculation overestimated fission rates of MOX pins and slightly underestimated those of UO_2 pins.

A three-dimensional VENUS-2 MOX core benchmark was therefore launched in 2001 to lead a more thorough investigation of the calculation methods used for MOX-fuelled systems. Twelve participants contributed to the 3-D benchmark, providing more than 20 solutions. The calculated axial pin power distributions were compared with the experimental results. This report provides details of the comparative analysis of calculated results against experimental data.

Acknowledgements

The Secretariat expresses its sincere gratitude to the participants who willingly devoted their time and effort to this benchmark exercise and to SCK•CEN (Mol, Belgium) for the release of the valuable experimental data. Special thanks go to Dr. Y. Nagaya of JAERI for his valuable comments on the report.

TABLE OF CONTENTS

List of tables

List of figures

EXECUTIVE SUMMARY

The management of excess plutonium produced during the operation of commercial power plants has become an important issue facing the nuclear community. More recently, the USA and the Russian Federation have declared some of their weapons-grade plutonium stockpiles surplus to their national defence needs. Many possible approaches to this matter have been envisaged, and two options are currently practised:

- vitrification and geological disposal with other nuclear waste without prior reprocessing;
- utilisation of plutonium as mixed-oxide (MOX) uranium and plutonium fuel in existing or advanced nuclear power plants.

The preferred option depends upon whether plutonium is perceived as waste or as a high-quality nuclear fuel.

Several countries use plutonium recovered from nuclear waste in the form of MOX fuel in existing power plants. Although the actual practice for MOX fuel use is well developed with many years of experience, the quantity utilised is still limited from the practical point of view (degradation of plutonium quality and decrease of safety margins). This practice alone is therefore not sufficient to stabilise the stockpile of plutonium extracted from spent fuel. If the extension of current constraints is envisaged (i.e. a larger quantity, multiple recycle and high burn-up of plutonium in PWRs), it is still necessary to validate both the basic nuclear data and calculational methods to better understand the behaviour of MOX fuel in challenging situations and to identify possible improvements in nuclear data and physics modelling methods.

Within the framework of the Nuclear Science Committee of the OECD/NEA, theoretical physics benchmarks and multiple recycling issues of various MOX-fuelled systems have been addressed. From the results of theoretical benchmarks performed, many improvements and clarifications in nuclear data libraries and calculation methods have been achieved. However, it was also felt that there was a need to link these findings to data from experiments. Hence, a blind international benchmark exercise based on the two-dimensional VENUS-2 MOX core measurement data was launched in 1999 and was completed in 2000. Overall, the results were very encouraging and confirmed that present methods using the latest nuclear data sets can adequately calculate MOX-fuelled systems. However, the calculation overestimated fission rates of MOX pins and slightly underestimated those of UO_2 pins.

A three-dimensional VENUS-2 MOX core benchmark was therefore launched in 2001 for a more thorough investigation into the calculation methods used for MOX-fuelled systems. Twelve participants contributed to the 3-D benchmark, providing more than 20 solutions. The calculated axial pin power distributions were compared with the experimental results.

Various nuclear data sets such as ENDF/B-IV, ENDF/B-VI, JEF-2.2, JENDL-3.2 and JENDL-3.3 were investigated. For axial power distribution calculations, four participants used deterministic codes such as TORT, DANTSYS and PARCS; eight participants applied continuous-energy Monte Carlo codes such as MCNP-4B, MCNP-4C, MVP and MCU-REA and a multi-group Monte Carlo code MOCA.

With regard to cell calculations, although the maximum spreads in k_∞ from the average values are 1.1% for 3/0 UO_2, 1.5% for 4/0 UO_2 and 1.4% for MOX cells, most of the results report a deviation of less than 0.5%. In particular most of the Monte Carlo calculations give results with a deviation of less than 0.2%.

The reaction rate results are in general consistent. However, differences in basic data among the libraries used are observed for some isotopes and it seems that the reaction rate results are sensitive to basic data processing procedures, especially for the preparation of cross-section data for deterministic cell calculations.

All reported k_{eff} show, in general, very good agreement with the experimental value ($k_{eff} = 1$). The average k_{eff} from all calculations is 1.00122±0.00394. The deterministic calculations give an average of 0.99828±0.00402 and the Monte Carlo calculations lead to an average of 1.00232±0.00341. Various nuclear data sets were examined. However, the calculated k_{eff} results show that there is no clear dependency on basic nuclear libraries. Differences observed among them could be due to different nuclear data processing procedures and calculation models used. A further investigation into nuclear data processing procedures and calculation models used by the participants might better clarify the origin of the discrepancies observed in k_{eff} results.

For the MOX pins, averaged pin powers from both deterministic and Monte Carlo calculations give a scatter band less than ±2% for most of the axial positions. For a few axial positions, both calculations report more than ±3% of scatter band. For 4/0 UO_2 pins, both deterministic and Monte Carlo calculations give an excellent agreement (within ±1%) of discrepancy for almost all positions. A slight increase of discrepancies up to 3% is observed at both extremities of the fuel pins. As for 3/0 UO_2 pins, an agreement within ±1% is observed for almost all positions in both deterministic and Monte Carlo calculation results. A slight overestimation up to 2.5% is observed in the pin (-11,+2) at positions near the axial reflectors. For the pin (-6,-6), a slight overestimation of less than 2% is observed near the upper reflector, as is an underestimation of pin powers of about 2% emerging from both calculation methods.

With regard to somewhat larger discrepancies observed in UO_2 pins at axial positions near the upper and lower reflector regions, this could result from the fact that most of the calculation models ignored the detailed structures above and below the active fuel pins, i.e. top and bottom stops of the active fuel pins and top and bottom blankets in the axial reflector regions.

This will be further studied by performing supplementary calculations to quantify the influence of detailed axial structures on calculated pin powers near the axial reflectors.

A comparison calculation undertaken by SCK•CEN found that ignoring the thermal scattering by Plexiglas, which is the main component of the axial reflectors, does not have an important influence on larger discrepancies observed at positions near the axial reflectors.

In conclusion, the results confirm that all combinations of the present methods using the latest nuclear data sets can adequately calculate MOX-fuelled systems in 3-D geometry, producing reasonably accurate axial pin power distributions.

The 3-D VENUS-2 MOX core experimental data provided by SCK•CEN were very useful for comparison of the calculated results to investigate current methods and nuclear data. The reported uncertainties of the measured data (1σ) for the six fuel pins are ±2.2% in UO_2 and ±3.4% in MOX pins. Further studies using experimental data with smaller uncertainties would contribute to additional refinements of calculation methods used for MOX-fuelled systems.

Chapter 1

INTRODUCTION

The management of excess plutonium produced during the operation of commercial power plants has become an important issue facing the nuclear community. Many possible approaches to this problem have been envisaged, with options including vitrification of the spent fuel and geological disposal with other nuclear waste without prior reprocessing, and burning of the plutonium fuels in nuclear power plants for the production of electricity. The preferred option depends on whether plutonium is perceived as a waste or a high-quality nuclear fuel.

Several countries use plutonium recovered from nuclear waste in the form of mixed-oxide (MOX) uranium and plutonium fuel in existing power plants, a well-established technology with which the nuclear industry has many years of experience. From the practical viewpoint, re-use of plutonium in PWRs is limited in quantity as well as in quality. Loading of plutonium assembly in a PWR core is recommended only up to 30% of the total loading to avoid any problems which might be caused by power peaking or degradation of safety parameters. The quality of plutonium decreases after a few recycles [1-4].

Even though the actual practice for MOX fuel use is well developed, this process alone is not sufficient to stabilise the stockpile of plutonium extracted from spent fuel. For a larger quantity, multiple recycle and high burn-up of plutonium in PWRs, it is still necessary to validate both the basic nuclear data and calculational methods to better understand the behaviour of MOX fuel in challenging situations and to identify possible improvements in nuclear data and physics modelling methods.

Therefore, in the framework of joint activities carried out by the OECD/NEA Working Party on the Physics of Plutonium Fuels and Innovative Fuel Cycles (WPPR) and the Task Force on Reactor-based Plutonium Disposition (TFRPD), a blind international benchmark exercise for the prediction of power distribution in the two-dimensional VENUS-2 MOX core experiments was launched in 1999. This was the first experiment-based benchmark; it was completed in 2000 [5-7]. Analysis of the two-dimensional benchmark results showed that present methods using the latest nuclear data sets could adequately calculate MOX-fuelled systems. However, the calculation overestimated fission rates of MOX pins and slightly underestimated those of UO_2 pins. This was reflected in all combinations of codes and data. Therefore, a three-dimensional VENUS-2 MOX core benchmark was launched in 2001 for a more thorough investigation of the calculation methods used for MOX-fuelled systems [8,9].

In the 3-D VENUS-2 measurements, the axial fission rate distributions of six fuel pins in the core were measured by γ-scanning at 21 different axial levels. The main objective of the benchmark is to calculate the axial fission rates of the six fuel pins and to compare them with the measured values. Additionally, fission chamber measurements (^{235}U and ^{237}Np) and activation foil measurements were performed at different axial levels at positions outside the core. These additional results could be used for a 3-D dosimetry benchmark.

As in the previous two-dimensional benchmark, the three-dimensional benchmark exercise discussed here was a blind test; hence the axially measured pin power values of the six fuel pins at specified VENUS locations were not revealed to the participants. Twelve participants contributed to the benchmark, providing more than 20 solutions. The calculated pin power distributions were compared with the experimental results. Various nuclear data sets such as ENDF/B-IV, ENDF/B-VI, JEF-2.2, JENDL-3.2 and JENDL-3.3 were investigated. For the axial power distribution calculations, four participants used deterministic codes such as TORT, DANTSYS and PARCS; eight participants applied continuous-energy Monte Carlo codes such as MCNP-4B, MCNP-4C, MVP and MCU-REA and a multi-group Monte Carlo code MOCA. This report provides details of the comparison analysis of calculated results against experimental data.

Chapter 2

BENCHMARK MODEL

The objective of the benchmark was to validate and compare the nuclear data sets and production codes used for MOX-fuelled system calculations in NEA member countries. The comparison with experimental data would allow to identify the origins of discrepancies between calculations and measurements and to quantify the relative merits of the different calculational methods.

A complete description of the benchmark specification, including details of the VENUS-2 core, is given in Appendix A. Included in this specification are all geometry and material data required to develop the detailed three-dimensional computational model of the 1/4 fraction of the VENUS-2 reactor core. Apart from the geometry and material data, the isotopic concentrations of each medium were also provided to minimise the discrepancies from the atomic density calculations as in the 2-D case.

The VENUS facility is a zero power critical reactor located at SCK•CEN in Belgium. As shown in Figure 2.1, the core is comprised of 12 "15×15" subassemblies, instead of those of "17×17" (the pin-to-pin pitch remains typical of the "17×17" subassembly). The central part of the core (four 15×15 assemblies) consists of fuel pins 3.3 wt.% enriched in ^{235}U (called 3/0 UO_2 pins). There are five Pyrex pins in 1/8 of the core. Of the eight assemblies on the periphery of the core, all of which contain fuel pins 4.0 wt.% enriched in ^{235}U (called 4/0 UO_2 pins), eight rows of the most external fuel pins have been replaced by mixed-oxide fuel pins (UO_2-PuO_2) enriched 2.0 wt.% in ^{235}U and 2.7 wt.% in high-grade plutonium (called 2/2.7 MOX pins).

The average fission rate in the core which corresponds to the absolute reference irradiation is 1.87E+08 fissions/cm/sec at the mid-plane. This average fission rate corresponds to a power of 595 Watts. In the two-dimensional pin power measurements (i.e. at the mid-plane of the core), the fission rate distributions of 128 fuel rods in the whole core were measured after an irradiation of 13.5 h at 90% of the VENUS maximum power. The 1/8 of the core comprises 325 fuel rods in which the pin powers of 121 fuel rods (41 3/0 UO_2, 35 4/0 UO_2 and 45 MOX pins) were directly measured and the pin powers of 204 fuel rods were interpolated from the measured values to have a complete pin-to-pin fission rate distribution of the 1/4 core. The additional seven fuel pins measured were located in symmetric positions out of 1/8 of the core.

In the three-dimensional pin power measurements, the fission rate distributions of six fuel pins (two 3/0 UO_2, two 4/0 UO_2 and two 2/2.7 MOX pins) were measured axially by γ-scanning after an irradiation of 8 h at 90% of the VENUS maximum power. The axial measurements were carried out at 21 different vertical planes along 50 cm of the fuel pin length (from 105 cm to 155 cm): starting from 110 cm, and at every 2 cm upwards to 150 cm. Originally, this method was employed in order to obtain vertical buckling representative of the core. The experimental data were taken from the gamma activity of the ^{140}La (fission yields ~6.3% for ^{235}U and ~5.5% for ^{239}Pu, energy ~1.6 MeV, effective half-life ~12.8 d).

The measured fuel pin positions in VENUS-2 are shown in Figure 2.2. Among the measured pins, fuel pin numbers 30, 74, 115, 131, 240 and 325 are axially measured pins. Figure 2.3 shows a vertical cross-section of the VENUS-2 core with corresponding axial co-ordinates for 3-D modelling of the core.

Results requested are as follows:

Cell calculations

For each fuel cell (3/0 UO_2, 4/0 UO_2, 2/2.7 MOX), the participants should provide the following results:

- k_∞;
- reaction rates (absorption and fission) per isotope (one group and three groups involving the 5 keV and 4 eV boundaries).

Core calculations

- k_{eff};
- normalised radial fission rate distribution at 325 fuel pin positions (315 pins on 1/8 of the core, plus 10 diagonal pins);
- normalised axial fission rate distribution of six fuel pins.

Chapter 3

PARTICIPANTS, CODES AND DATA

Twelve participants contributed to the benchmark, providing more than 20 solutions. The complete list of participants, basic libraries and codes used are presented below and summarised in Table 3.1. Calculation details provided by the participants can be found in Appendix B.

1. ***FRAMATOME ANP GmbH, Germany***
   Participants: W. Hofmann, J. Koban and W. Timm
   Basic library: ENDF/B-IV
   Cell code: CASMO-4 (70 groups)
   Core calculation: TORT 2.7.3 (5 groups)
   Remarks: S_8P_0 approximation, 55×55 meshes in (x,y) directions and 25 equidistant regions for the active fuel length, used the cross-section data generated for MOCA calculations

2. ***KAERI, Korea***
   Participants: Do-Heon Kim, Jung-Do Kim, Choong-Sub Gil and Jonghwa Chang
   Basic library: ENDF/B-VI Release 7 (natural S_n from ENDL-84)
   Cell code: TRANSX 2.15 (190 groups)
   Core calculation: DANTSYS 3.0 (35 groups)
   Remarks: S_8P_3 approximation, mesh sizes are less than 0.03 cm for the fuel regions

3. ***NEA+KAERI, Korea***
   Participants: Byung-Chan Na (NEA) and Gyu-Hong Roh (KAERI)
   Basic library: ENDF/B-VI Release 5 and JENDL-3.2
   Cell code: TRANSX 2.15 (190 groups)
   Core calculation: TORT 3.2 (35 groups)
   Remarks: S_8P_3 approximation, $100 \times 102 \times 72$ meshes in x,y,z directions

4. ***Purdue University, USA***
   Participants: Tomasz Kozlowski, Chang-Ho Lee and Thomas Downar
   Basic library: ENDF/B-VI Release 3
   Cell code: HELIOS 1.7 (190 groups)
   Core calculation: PARCS 2.1 (8 groups)
   Remarks: Used SP3 kernel with one mesh per pin cell and SPH factors

5. ***FRAMATOME ANP GmbH, Germany***
   Participants: W. Timm, S. Misu and D. Porsch
   Basic library: ENDF/B-IV
   Cell code: CASMO-4 (70 groups)
   Core calculation: MOCA (5 groups)
   Remarks: Multi-group Monte Carlo calculations

6. ***JAERI, Japan***
   Participants: Yasunobu Nagaya, Keisuke Okumura and Takamasa Mori
   Basic library: JENDL-3.2 and JENDL-3.3
   Cell code: MVP
   Core calculation: MVP
   Remarks: Number of histories used – 49 million (cell) and 199 million (core)

7. ***SCK•CEN, Belgium***
   Participants: Nadia Messaoudi and Hamid Ait Abderrahim
   Basic library: ENDF/B-VI Release 5 and JEF-2.2
   Cell code: MCNP-4C
   Core calculation: MCNP-4C
   Remarks: Number of histories used – 1 million (cell) and 350 million (core)

8. ***KAERI+NEA, Korea***
   Participants: Gyu-Hong Roh (KAERI) and Byung-Chan Na (NEA)
   Basic library: ENDF60 (MCNP package library), ENDF/B-VI Release 5, JENDL-3.2, JEF-2.2
   Cell code: MCNP-4B
   Core calculation: MCNP-4B
   Remarks: Number of histories used – 1 million (cell) and 50/200/300 million (core)

9. ***KFKI, Hungary***
   Participants: Gábor Hordósy
   Basic library: ENDF/B-VI Release 2 (structural material data from ENDF/B-V)
   Cell code: MCNP-4C
   Core calculation: MCNP-4C
   Remarks: Number of histories used – 12.5 million (cell) and 37 million (core)

10. ***KI, Russian Federation***
    Participants: E. Gomin and M. Kalugin
    Basic library: MCU data library based on ENDF/B-VI, JENDL-3.2 and BROND
    Cell code: MCU-REA
    Core calculation: MCU-REA
    Remarks: Number of histories used – 1 million (cell) and 40 million (core)

11. ***GRS+IKE, Germany***
    Participants: Winfried Zwermann (GRS) and Margarete Mattes (IKE)
    Basic library: JEF-2.2, ENDF/B-VI Release 5 and JENDL-3.2
    Cell code: MCNP-4C
    Core calculation: MCNP-4C
    Remarks: Number of histories used – 4 million (cell) and 40 million (core)

12. ***SEA, Spain***
    Participants: David Lopez Maganto
    Basic library: ENDF/B-VI for fuel, water, some elements of steel structures (for the rest from ENDF/B-V)
    Cell code: MCNP-4C
    Core calculation: MCNP-4C
    Remarks: Number of histories used – 40 million (cell) and 40-60 million (core)

Chapter 4

RESULTS OF THE BENCHMARK

4.1 Calculational methods

Cell calculation methods

FRAMATOME-ANP GmbH applied CASMO-4, a multi-group two-dimensional transport theory code for burn-up calculations on BWR and PWR assemblies. The standard Studvik "L-library" in 70 energy groups was used. In this library, most of the data are based on ENDF/B-IV. The shielded resonance data for Pu were taken from JEF libraries. The default number of energy groups for MOX fuel in CASMO-4 were used. The calculation started with a simplified geometry and 70 neutron energy groups: 14 fast groups, 13 resonance groups and 43 thermal (below 4 eV). Energy groups were then collapsed as spatial detail was increased. For the present benchmark, a five-group condensation scheme was chosen with the upper boundaries 10 MeV, 821 keV, 5.53 keV, 4 eV and 0.625 eV. The flux distributions and the eigenvalue were calculated based upon methods of characteristics.

The fission spectrum assumed for the benchmark is somewhat harder than the CASMO fission spectrum, but gives an overall better adaptation to the CASMO k_∞ and the CASMO group fluxes. There are some more approximations:

- only isotropic scattering was assumed (P_0);
- (n,2n) reactions were ignored in the five-group scheme;
- the transport cross-section was assumed to be the inverse diffusion constant divided by three (3), the in-group scattering cross-section then being the difference between this transport cross-section and the total removal cross-section;
- upscattering was only taken into account approximately via a correction term in the downscattering cross-section to the last group (similar to the standard CASMO procedure for the two-group condensation); upscattering above 0.625 eV is generally small anyway.

In general, cross-sections for infinite pin lattice (homogeneous calculations) have been used. For specific materials heterogeneous cell calculations have been performed:

- For the Pyrex pin cell, a (infinite lattice) 3×3 cell was assumed with one Pyrex pin in the centre being surrounded by eight 3/0 fuel pins. The cross-sections are then condensed only for the central Pyrex pin.
- For the fuel rods adjacent to the baffle reflector it was investigated whether this environment has an effect on the condensed cross-sections of the fuel row directly adjacent to the baffle and on the cross-sections of the baffle steel. To this end an 8×8 cell was calculated with two "rows" of water, three "rows" of baffle steel and three "rows" of each fuel type, all rows

having a thickness of 1.26 cm and the 8×8 cell having reflective boundary conditions. It was found that only for the UO_2 fuel was there a noticeable effect (the thermal fission and absorption cross-sections are smaller by a few per cent near the baffle), whereas the baffle had only a negligible influence on the MOX cross-sections. It was found that the five-group cross-section data of the baffle steel were almost independent of the adjacent fuel type and were taken as identical for the inner and outer baffle.

- A similar CASMO cell calculation was performed for the interface between the 3/0 and the 4/0 UO_2 fuel. Here the interface had the strongest effect on the thermal cross-sections of the 4/0 UO_2 fuel, where an increase of around 2% was seen due to increased moderation. The influence on the 3/0 UO_2 cross-sections at this interface is smaller (around 1% decrease) and can be ignored.

In accordance with these CASMO results, the thermal cross-sections of the UO_2 fuel (both 3/0 and 4/0) adjacent to the baffle steel and those of the 4/0 UO_2 fuel at the interface to the 3/0 fuel have been slightly modified in the thermal range below 0.625 eV. It should be kept in mind that the effect of these modifications of the cross-sections in a limited number of pins is negligible with regard to the core k_{eff}. Regarding pin powers the impact is of the order of a few per cent only.

Both KAERI and NEA+KAERI followed the same procedure for cross-section generations by using the code TRANSX. MATXS-format master libraries in 190 energy groups (i.e. HELIOS neutron energy group structure) based on ENDF/B-VI (releases 5 and 7) and JENDL-3.2 were generated by using the MATSXR module of NJOY except for the natural S_n, which was obtained from ENDL84. Using these 190-group neutron libraries, ONEDANT calculations for three fuel pin cell types and for a Pyrex super-cell were undertaken to obtain weight flux for generating the region-wise homogenised cross-sections collapsed to 35 groups. For the resonance shielding treatment, the Bondarenko method or background cross-section method in TRANSX was used. Neither overlapping of resonances nor (n,2n) reactions were taken into account. Flux-, mixture-, and region-dependent fission spectra were used. Since the energy group structure used was based on that of HELIOS, the energy cut-offs for reaction rate calculations are different from those given in the benchmark specification. The adopted energy group boundaries were 4.881 keV and 3.9279 eV instead of 5 keV and 4 eV.

Purdue University used the current coupling and collision probability code HELIOS 1.7 for pin cell calculations and few group cross-section generation. For resonance treatment, the subgroup method was used. Sets of weights and cross-sections are stored in the nuclear data library for each resonance isotope. To describe the interaction of resonance isotopes, they are grouped in categories inside which the resonances are assumed to overlap, while there is no overlap between the different categories. A weighted mix of fissionable isotopes was used for fission spectrum calculations. In the transport calculations, (n,2n) and (n,3n) reactions were included by adjusting absorption cross-sections and scattering matrices. As in KAERI and NEA+KAERI calculations, the energy cut-offs for cell calculation reaction rates were 4.881 keV and 3.9279 eV.

For the continuous-energy Monte Carlo methods, MVP was used by JAERI (JENDL-3.2 and JENDL-3.3), MCNP-4C was widely used by SCK•CEN (ENDF/B-VI.5 and JEF-2.2), KFKI (ENDF/B-VI.2), GRS (ENDF/B-VI.5, JENDL-3.2 and JEF-2.2), SEA (ENDF/B-VI). KAERI+NEA used MCNP-4B (MCNP package library ENDF60, ENDF/B-VI.5, JENDL-3.2 and JEF-2.2), and the Kurchatov Institute used their own Monte Carlo code MCU-REA (MCUDAT based on ENDF/B-VI, JENDL-3.2 and BROND).

In MVP calculations, resonance shielding, mutual shielding, and (n,2n) reactions were explicitly taken into account. Unresolved resonances were treated by probability tables. Nuclide-wise fission spectrum was used. The number of histories used for cell calculations was 49 million.

In SCK•CEN MCNP-4C calculations, self-shielding effects in the unresolved resonance range was taken into account using a probability table treatment for some isotopes, and (n,2n) reactions were also treated explicitly. Watt fission spectrum was used. The number of histories used for cell calculations was one million: 1 000 neutrons per cycle with 1 100 cycles (100 were inactive).

In KAERI+NEA MCNP-4B calculations, the mutual shielding effect was not taken into account. (n,2n) reactions were treated explicitly and Watt fission spectrum was used. The number of histories used for cell calculations was one million: 1 000 neutrons per cycle with 1 000 cycles.

In KFKI MCNP-4C calculations, the probability table treatment was used for the unresolved resonances. The number of histories used for cell calculations was 12.5 million: 25 000 particles per cycle, 50 passive and 500 active cycles.

KI simulated one million histories for MCU-REA cell calculations. Four million (8 000 neutrons per cycle and 500 cycles) histories were used by GRS MCNP-4C cell calculations. In SEA MCNP-4C calculations, no special treatment of unresolved resonances was given. However, (n,2n) reactions were treated explicitly, Watt fission spectrum was used and 2.5 million histories for k_∞ calculations and 40 million for reaction rate calculations were used.

Core calculation methods

FRAMATOME-ANP GmbH used both the deterministic S_N code TORT and the multi-group Monte Carlo code MOCA. In both TORT and MOCA core calculations, the uniform grid with a pitch of 1.26 cm in x-y direction has been preserved in all regions outside the fissile zones, i.e. baffle, water, barrel. Therefore, baffle, barrel and neutron pad have been modelled only approximately in this uniform grid, i.e. in such a way that the masses (areas) of these materials are approximately preserved. In the geometrical model a size of 55×55 “meshes” has been assumed in the x-y direction. The geometrical model was limited to a core quadrant. Axially, only two additional materials have been introduced:

- rods with Plexiglas (surrounded by water) above and below the 3/0 UO_2 zone;
- rods with Plexiglas (surrounded by water) above and below the 4/0 UO_2 zone and the 2/2.7 MOX zone.

In TORT calculations for the upper axial reflector a thickness of 13 cm has been assumed and for the lower a thickness of 21.5 cm. For these regions a combination of Plexiglas and water zones has been used. The 3-D TORT calculations were performed in x-y-z geometry with S_8P_0 approximation. For comparison with the S_8 calculation an extra S_2 calculation was performed. In order to obtain an accurate axial power profile in the specified fuel rods, the rods were split axially into 25 equidistant regions (2 cm per region). All results have been obtained by assuming quarter core symmetry.

In MOCA calculations, all grid plate materials have been neglected. For the upper axial reflector a thickness of 13 cm has been assumed and for the lower a thickness of 30 cm. In order to obtain a sufficiently accurate axial power profile in the specified fuel rods, these were split axially into seven almost equidistant regions (around 7 cm per region) and the axial fission rate distribution was then calculated by a simple spline interpolation preserving the rates of these seven axial zones. Since no statistically significant axial asymmetry was detected, axial profiles were symmetrised. All results have

been obtained by assuming quarter core symmetry. Comparisons with full core calculations (taking into account the barrel and neutron pad only in one quarter of the core) gave a k_{eff} which seemed to be around 20 to 30 pcm lower than the symmetrical core (high statistical uncertainty here), so the presence of the barrel seems to slightly increase the k_{eff}. However the pin power distribution was not affected with full core geometry (no statistically significant effects were detected).

KAERI used the 3-D S_N code THREEDANT in the DANTSYS 3.0 system and NEA+KAERI applied the 3-D S_N code TORT in the DOORS 3.2 system. Both calculations applied S_8P_3 approximation for angular descretisation. In KAERI calculations, the mesh sizes were less than ~0.03 cm for three fuel cells. The VENUS-2 core was modelled explicitly from bottom to top with the proper use of homogenisation for the grid regions and the core was modelled up to the barrel in the x- and y-direction. The regions beyond the barrel were filled with water and the neutron pad was not taken into account. In NEA+KAERI calculations, the geometrical model for TORT inputs was prepared by using the pre- and post-processing code BOT3P [10]. One quarter of the full 3-D VENUS-2 core was modelled with $100 \times 102 \times 72$ spatial meshes in the (x,y,z) geometry. Fully symmetrical quadrature sets were introduced. The point-wise flux convergence criterion used was 1.0E-4 and the eigenvalue convergence criterion applied was 1.0E-5.

In Purdue University core calculations, the PARCS core simulator was applied using fine mesh finite difference SP_3 kernel with one mesh per pin cell and SPH factors. Fuel and radial reflector cross-sections and corresponding SPH factors were generated from a VENUS-2 2-D HELIOS solution. Axial reflector cross-sections and SPH factors were generated from a 1-D homogeneous fuel-heterogeneous reflector HELIOS solution.

For JAERI MVP calculations, a quarter-symmetric core model was developed. This model included lower filling, reactor support, bottom, intermediate and upper grids, top and bottom reflectors, top and bottom stops and upper filling axially. It also included reactor vessel, jacket, neutron pad, barrel, outer and inner baffles radially. The neutron pad was assumed to be a part of a cylindrical tube, though the real pad does not have uniform thickness. A full-core calculation was performed to investigate the asymmetric effect of the barrel and neutron pad on the pin power distribution but no difference was seen between the full-core and quarter-symmetric models. Thus the quarter-symmetric model was employed to reduce statistical errors. No data were available for the top and bottom reflectors and tops for MOX pins. Thus the same data were assumed as for 4/0 UO_2 pins The scattering law $S(\alpha,\beta)$ of polyethylene was used for Plexiglas as no scattering law was available for this material. Tally regions for pin power distribution include not only the single unit cells of interest but also symmetric cells, though the geometry is not symmetric with regard to the diagonal due to the neutron pad. Histories for 3-D core calculation were 199 million: 9 950 cycles and 20 000 neutrons per cycle (not including 50 cycles for initial guess).

In SCK•CEN MCNP-4C core calculations, one quarter of the full 3-D core was explicitly modelled in three-dimensional geometry. All fuel rods and Pyrex rods were fully modelled including the fuel pellet, fuel gap in UO_2 pin cells, clad and coolant. The radial core components such as the reactor vessel, jacket, neutron pad, barrel, reflector, outer baffle, inner baffle and inner hole, etc., were also fully modelled. The core was modelled vertically from bottom to top, i.e. lower filling, reactor support, bottom grid, lower reflector, upper grid, upper filling, etc. In order to obtain the axial fission rate distributions in the core, the core was divided into 25 axial layers. Since no thermal scattering data for Plexiglas (upper and lower reflectors) are available, one set of calculations was performed using the scattering data of polyethylene in place of Plexiglas and another set of calculations was undertaken which ignored the thermal scattering of axial reflectors. It was shown that the thermal scattering of the axial reflectors did not play an important role in calculated axial pin power results. Therefore, they were not taken into account in the final calculations. Three hundred fifty (350) million histories (500 000 neutrons per cycle with 700 cycles) were used.

In KAERI+NEA MCNP-4B calculations, one quarter of the full 3-D core was explicitly modelled. The number of histories originally used was 50×10^6 (100 000 neutrons/cycle and 500 cycles after 100 inactive cycles) as a reference calculation. To investigate the influence of the number of histories on calculated results, they were increased to 200×10^6 and then to 300×10^6 (100 000 neutrons/cycle and 3 000 cycles after 100 inactive cycles). The thermal scattering of Plexiglas was not taken into account.

GRS also developed one quarter of the 3-D core model. Forty (40) million histories were used (4 000 neutrons per cycle and 10 000 cycles). Since no $S(\alpha,\beta)$ data are available for Plexiglas, polyethylene data were used to describe the thermal scattering of the axial reflectors. Due to the neutron pad, the arrangement is not totally symmetric with regard to the diagonal; each pin fission rate value was therefore calculated by taking the average of pins (i,j) and (j,i).

KFKI, KI and SEA provided no details on calculation models and assumptions. However, it is believed that they developed 1/4 of the full 3-D core model. In KFKI MCNP-4C calculations, for the axial power distribution calculations, the pins were divided into 2-cm high cells, and the volume averaged fission rate of these segments was used. Thirty-seven (37) million histories were used. In KI MCU-REA calculations, 40 million histories were used. No specific assumptions for the calculation model were made, but the neutron pad outer radius used was 65.073 cm instead of the value given in the specification. In SEA MCNP-4C calculations, 40 million neutron histories were used for all calculations, but for the axial fission rates in the MOX zone, 60 million neutron histories were used.

4.2 Cell calculations

Three types of pin cells have been studied: two cells fuelled with UO_2 3.3 wt.% and 4.0 wt.% enriched in ^{235}U and one cell fuelled with MOX 2.0 wt.% enriched in ^{235}U and 2.7 wt.% enriched in high-quality plutonium. In cell calculations, two main parameters, e.g. k_∞ and reaction rates (fission and absorption) in one group and in three groups were investigated. However, all the deterministic cell calculations reported three-group reaction rates with different three-energy group boundaries from those given in the benchmark specification. Therefore, a direct comparison of these three-group reaction rate results is not so meaningful, and the analysis is mainly focused on the energy group integrated (i.e. total) reaction rates. All the Monte Carlo calculations reported three-group reaction rates with energy group boundaries of 5 keV and 4 eV as given in the specification.

Infinite multiplication factor

The calculated k_∞ results are summarised in Table 4.1. For a relative comparison of calculated results, they are plotted together with the average values in Figures 4.1, 4.2 and 4.3. The average k_∞ values are 1.40656±0.00491 for 3/0 UO_2, 1.33769±0.00556 for 4/0 UO_2 and 1.25737±0.00561 for MOX cells. The maximum differences between the highest and the lowest values are 1 632 pcm, 1 956 pcm, and 1 934 pcm for 3/0 UO_2, 4/0 UO_2 and MOX cells, respectively. These values represent deviations of 1.1% for 3/0 UO_2, 1.5% for 4/0 UO_2 and 1.4% for MOX pins from the average k_∞ values. Although these rather high maximum spreads in k_∞ differ from the average values, most of the results report a deviation of less than 0.5%. In particular the Monte Carlo calculations give results with a deviation of less than 0.2% which is the claimed uncertainty on reactivity in current nuclear design methods.

For all three pin types, the results obtained by deterministic codes give smaller values than the average values, except for the values from Purdue University. Most of the Monte Carlo results show larger values than the average values. This could be partially explained by the fact that the deterministic

calculations use in general a cylindrical cell geometry whereas the Monte Carlo calculations and Purdue University's HELIOS calculations describe the "true" square cell geometry for cell calculations. As has been well demonstrated in previous studies [11,12], the cylindrical model provides equivalent moderator volumes in a cell, however the effective moderation is higher in the square cell than in the cylindrical cell, resulting in more thermal flux in the square cell than in the cylindrical cell. Uranium is not as sensitive to this small spectral change; therefore the effect of the cylindrical cell is rather small. However, for MOX cells, the largest effect observed in previous studies by going from the cylindrical cell to the square cell is a decrease of resonance absorption (mainly by ^{238}U). This leads to an increase in the thermal flux promoting fissions primarily by ^{239}Pu at that energy region. Therefore the square cell provides a larger increase in the multiplication factor, as is indeed observed.

Anther observation is that, in general, deviations in deterministic code results are slightly higher than those in Monte Carlo calculation results.

KAERI and NEA+KAERI results, in which the same cross-section generation methods were used, indicate no differences in k_∞ values calculated with the two different versions of ENDF/B-VI.

In NEA+KAERI deterministic calculations, JENDL-3.2 gives slightly larger k_∞ values than ENDF/B-VI for all three types of fuel pins: +595 pcm for 3/0 UO_2, +414 pcm for 4/0 UO_2, +311 pcm for MOX pins. The same trend is observed in KAERI+NEA and GRS Monte Carlo calculations, which show larger k_∞ values with JENDL-3.2 than with ENDF/B-VI.

SCK•CEN Monte Carlo calculations examined differences between ENDF/B-VI and JEF-2.2. These calculations show that JEF-2.2 produces larger k_∞ values than ENDF/B-VI for all three types of fuel pins: +862 pcm for 3/0 UO_2, +727 pcm for 4/0 UO_2, +284 pcm for MOX pins. KAERI+NEA and GRS Monte Carlo calculations confirm this observation, giving larger k_∞ values with JEF-2.2 than with ENDF/B-VI: from KAERI+NEA, +403 pcm (3/0 UO_2), +614 pcm (4/0 UO_2), +83 pcm (MOX) and from GRS, +480 pcm (3/0 UO_2), +593 pcm (4/0 UO_2), +258 pcm (MOX).

KAERI+NEA and GRS examined the differences between JENDL-3.2 and JEF-2.2; in their calculations, JENDL-3.2 gives larger k_∞ values for 3/0 UO_2 and MOX pins (+110 pcm and +150 pcm, respectively), but smaller value for 4/0 UO_2 pins (-138 pcm) than JEF-2.2. However, in GRS calculations, JENDL-3.2 produces slightly smaller k_∞ values for 3/0 UO_2 and 4/0 UO_2 pins (-42 pcm and -124 pcm, respectively), and a larger value for MOX pin (+29 pcm) than JEF-2.2. In all cases, the differences between JENDL-3.2 and JEF-2.2 are small and less than 150 pcm.

JAERI examined differences between the two versions of the JENDL libraries (3.2 and 3.3). The differences between them are very small. However JENDL-3.2 gives larger k_∞ values for all three types of fuel pin than JENDL-3.3: +473 pcm for 3/0 UO_2, +684 pcm for 4/0 UO_2, and +174 pcm for MOX pins. It is interesting to note that JENDL-3.3-based values are close to the average values.

Even though the maximum spread in k_∞ values is larger in MOX pin cell calculations than in UO_2 pins, the differences in k_∞ values among different libraries are smaller in MOX than in UO_2 pins.

A comparison of calculated k_∞ values among libraries used is summarised in Table 4.2. Different Monte Carlo calculations with the same library provide consistent results. JEF-based results always produce higher values than those based on other libraries.

Absorption and fission reaction rates

For simplicity of comparison, the reported reaction rates were normalised to the total fission equal to 1.0, although the usual method is to normalise the total absorption equal to 1.0. Only for a relative comparison of provided results, the GRS ENDF/B-VI reaction rates were arbitrarily taken as the references and deviations from the references were compared. The relative comparison results are shown in Tables 4.3 to 4.15.

As mentioned in the section concerning calculation methods, KAERI, NEA+KAERI, and Purdue University adopted different three-energy group boundaries (4.881 keV and 3.9279 eV instead of 5 keV and 4 eV). FRAMATOME-ANP calculations also applied different energy group boundaries such as 5.53 keV and 4 eV. Therefore, a direct and rigorous comparison of reaction rates in three-energy groups is not possible, and the analysis below mainly focuses on the total reaction rates, i.e. energy group integrated reaction rates. Total absorption and fission rates per isotope relative to GRS ENDF/B-VI based results are plotted in Figures 4.4 to 4.16.

MOX fuel pin

For ^{234}U, ENDF-based absorption rates show a good agreement among them except results from FRAMATOME-ANP (ENDF/B-IV) and SEA. Both results give absorption reaction rates about 8% and 7% less than the other ENDF-based results. KAERI and NEA+KAERI TRANSX results produce about 2% smaller absorption rates than other ENDF-based results. JEF-based results give slightly smaller (about 0.5%) absorption rates than those based on ENDF. The discrepancies between ENDF- and JENDL-based results become larger, up to 6%. Moreover, for each energy group, JENDL gives about 5% less absorption rates than ENDF.

The agreement among ENDF-based results is excellent for total fission reaction rates. However, the FRAMATOME-ANP result again shows a difference of about 8% compared to other ENDF-based results. The discrepancies between ENDF- and JEF-based results become larger than in absorption rates, which are about 2%. The KAERI+NEA JEF result gives about 3% smaller fission rates and it is so in the energy group (g=1). About 5% smaller fission rates are reported from JEDL-based results when compared to ENDF-based results. The discrepancies are very pronounced in the energy groups (g=2 and g=3). Compared to ENDF, JENDL produces about 50% more fissions in g=2, about 100% less fissions with JENDL-3.2 and about 35% less with JENDL-3.3 in g=3.

Large discrepancies observed in FRAMATOME-ANP results may be due to the basic library ENDF/B-IV. However, the absolute contributions of ^{234}U to the total neutronic balance are very small compared with other isotopes, hence the large deviations observed for ^{234}U would not play an important role.

For ^{235}U, all results except SEA values are consistent for both absorption and fission reaction rates. For most of the calculations, the discrepancies among them are less than 0.5% for both absorption and fission rates. All libraries used give consistent reaction rate values and no library-dependent trend is observed. For absorption rates, discrepancies are slightly higher in g=2 than in other energy groups.

For ^{236}U, ENDF-based absorption rates show a good agreement. The discrepancies are less than 0.5% among most of the ENDF-based results. The KAERI+NEA ENDF60 result provides slightly higher absorption rate values (1.6%) than the others. JEF-based results report about 4-5% larger absorption rates than those based on ENDF. Especially, JEF-based results produce about 17% more absorption rates in g=1 than ENDF. All JENDL-based results give slightly larger absorption rates (2%) than those based on ENDF.

ENDF-based fission rates are consistent. The differences between ENDF- and JEF-based fission rates are negligible. JENDL-based results show slightly smaller fission rates (about 1%) than those based on ENDF. However, the discrepancies between the two libraries in g=3 are about 20%.

For ^{238}U, ENDF-based absorption rates are slightly discrepant: in average about 1.5%. KAERI and NEA+KAERI TRANSX results give higher values (about 3%) and Purdue University HELIOS produces a smaller value (about 3%) than other ENDF results. The differences between ENDF- and JEF-based absorption rates are negligible. JENDL-based results also give absorption rates similar to those based on ENDF and JEF. However, the JENDL-3.2-based NEA+KAERI TRANSX result gives 3% larger absorption rates than other JENDL-based results.

Regarding fission reaction rates, the results from ENDF are very consistent. However, HELIOS and CASMO calculations give about 2% less fissions and about 9% more fissions, respectively, compared to the other ENDF-based results. JEF-based results show very similar values to those of ENDF, but the KAERI+NEA result gives a larger value by 2% than the other JEF-based results. JENDL-based results produce about 1% less fission rates compared to those based on ENDF. For g=2, JENDL gives up to 5% more fission rates than ENDF.

For ^{239}Pu, an excellent agreement among the results provided is observed for both total absorption and total fission rates. The deviations are less than 0.2% among most of the results provided.

For ^{240}Pu, KAERI and NEA+KAERI TRANSX results show about 3% larger absorption rates and FRAMATOME-ANP CASMO calculations give about a 2% larger value than the other ENDF-based results. Although JEF- and JENDL-based results are similar to those from ENDF, JEF and JENDL produce about 4% and 6% more absorption rates, respectively, in the energy group g=2. A 3% larger absorption rate is provided by the JENDL-3.2-based NEA+KAERI result as compared with other JENDL-based results. The JENDL-3.3 absorption rate result is closer to the ENDF results than that of JENDL-3.2.

For fission reaction rates, the results can be grouped depending on the libraries used. Except HELIOS and CASMO results, ENDF-based results show a good agreement. Compared to ENDF-based results, JEF produces about 4% more fission rates and JENDL gives about 3% less fission rates. It is interesting to note that in the energy group g=3, JENDL-3.2 gives about 6% less fissions, but JENDL-3.3 gives 30% more fissions than ENDF.

For ^{241}Pu, ENDF- and JENDL-based calculations produce similar results for both absorption and fission reaction rates. However, JEF-based results are about 1.5% of more absorption and about 2% more fission rates than ENDF and JENDL. The KI MCU-REA calculation reported slightly larger value of absorption (3%) and fission rates (1%) than the others.

For ^{242}Pu, discrepancies in absorption and fission reaction rates become large. The discrepancies in absorption reaction rates among ENDF-based results are about 1-3%, except the CASMO result (-10%). JEF and JENDL give about 10-12% less absorption rates compared to ENDF. This is mainly due to 10-12% less absorption reactions estimated in the energy group g=3 with JEF and JENDL. As in the absorption rates, the CASMO result shows a larger discrepancy (about 7%) for fission rates compared with the other ENDF-based results. JEF-based results give slightly larger fission rates (about 3%) whereas JENDL produces slightly smaller values of fission rates (about -3%) compared to ENDF. Considerable differences in fission rates between ENDF and JEF/JENDL are observed in the energy group g=3. However, this may not play a role due to its small contribution to the total neutronic balance.

For ^{241}Am, the agreement among results provided is rather good. The discrepancies in absorption rates among ENDF-based results are about 1%. JEF produces about 4-5% more absorption rates than ENDF, showing large discrepancies in the energy group g=1. All JENDL-3.2-based results show about 3% less absorption rates than those based on ENDF, whereas JENDL-3.3 gives a value about 5% higher than ENDF.

For fission rates, an excellent agreement is shown among most of the ENDF-based results. The discrepancies among them are about 0.5%. As with absorption rates, JEF produces about 5% more fission rates than ENDF, but the most pronounced differences are shown in the energy group g=3 (more than +20% compared to ENDF). All JENDL-3.2 based results show about 4% less fission rates than those based on ENDF whereas JENDL-3.3 gives a slightly higher value fission rate (0.6%) than ENDF.

It is interesting to note that there are large differences between JENDL-3.2 and JENDL-3.3 results for both reactions. For absorption reaction rates, the JENDL-3.3 result is similar to JEF-based results, and for fission reaction rates it is similar to the ENDF-based result.

3/0 and 4/0 UO_2 fuel pins

For ^{235}U, the agreement among results provided is excellent for both reaction rates. For most of the results, the discrepancies among them are less than 0.2%.

For ^{238}U, discrepancies in absorption rates among ENDF-based results become larger. JEF and JENDL produce close results. For fission reaction rates, ENDF and JEF give similar results whereas JENDL-based results provide smaller fission rate values (about 3-5%) than the two other libraries.

The reaction rate results are in general consistent. However, differences in basic data among the libraries used are observed for some isotopes and it seems that the reaction rate results are sensitive to basic data processing procedures, especially for the preparation of cross-section data for deterministic cell calculations.

4.3 Core calculations

For the core calculations, k_{eff}, normalised radial fission rate distribution at 325 fuel pin positions at the code mid-plane, and normalised axial fission rate distribution of six fuel pins were requested.

However, in this report, the analysis is focused on k_{eff} and axial fission rate distributions of six fuel pins, since the radial fission rate distribution of 325 fuel pins at the core mid-plane was analysed in detail in the previous two-dimensional benchmark [6,7].

The six axially measured fuel pins consists of two 3/0 UO_2, two 4/0 UO_2 and two MOX pins. Their positions are shown in Figure 2.2 and their pin position numbers are 30, 74, 115, 131, 240 and 325. The axial measurements were carried out at 21 different vertical planes along 50 cm of the fuel pin length (from 105 cm to 155 cm) starting from 110 cm, and at every 2 cm upwards to 150 cm.

The measured k_{eff} value is 1 with an uncertainty of ±32 pcm, and the reported uncertainties of the measured data (1σ) of pin power distributions of the six fuel pins are ±2.2% in UO_2 and ±3.4% in MOX pins.

Effective multiplication factor

The calculated k_{eff} values are presented in Table 4.16. All reported k_{eff} show in general a very good agreement with the experimental value (k_{eff} = 1). The average k_{eff} from all calculations is 1.00122±0.00394. The deterministic calculations produce an average of 0.99828±0.00402 and the Monte Carlo calculations lead to an average of 1.00232±0.00341. The maximum discrepancy reported is about 1% by the KAERI+NEA calculation with JENDL-3.2. This represents about 1 000 pcm of differences. The origin of this large discrepancy is not clearly understood, since no abnormal behaviour was observed in reaction rate results obtained by KAERI+NEA cell calculations with the JENDL-3.2 library. The other JENDL-3.2 based calculations report less than 0.5% of discrepancies. Except for the NEA+KAERI TORT calculation with JENDL-3.2, all four deterministic calculation results show a slight underestimation of k_{eff} (but less than 0.5%). Most of the Monte Carlo calculations reported k_{eff} values with a discrepancy of less than 0.1%. Two JEF-based results reported by SCK•CEN and KAERI+NEA show discrepancies of about 0.7% whereas the GRS JEF-based result gives a discrepancy of less than 0.3%.

Between two versions of the JENDL library, JENDL-3.3 gives a better result than JENDL-3.2. However, no clear advantage of one library over the others was observed and no systematic dependency on basic libraries in k_{eff} calculations was seen. Again, differences in reported k_{eff} values would be due to different nuclear data processing procedures and the calculation models used. A further investigation into nuclear data processing procedures and calculation models used by the participants could better clarify the origin of the discrepancies observed in k_{eff} results.

Axial pin power distribution

The axially measured fission rate values of the six fuel pins are normalised to one (1) and presented in Table 4.17. The measured fission rate value at 132 cm of the MOX pin (-27,-12) and those at 114 and 148 cm of the MOX pin (-22,-2) were not available, and the values given in the table for these three positions are interpolated values. The calculated axial pin power distribution results provided by each participant and their comparison with the measured values are presented in Tables 4.18 to 4.37.

General comparison

For a relative comparison of the calculated results against measured power distributions, (C/E)-1 values in % are plotted in Figures 4.17 to 4.22 for deterministic calculations and in Figures 4.23 to 4.28 for Monte Carlo calculations.

For the MOX pin (-27,-12), deterministic calculations show about ±2% of scatter band for most of the axial positions. However, the scatter band becomes larger near the axial lower and upper reflectors. Monte Carlo calculations show a statistical perturbation giving a larger scatter band than deterministic calculations. For most of the axial positions, the scatter band is about ±3% and it becomes larger near the axial reflectors as in deterministic calculations. The large statistical perturbation in Monte Carlo calculations and a larger scatter band near the axial reflectors in both deterministic and Monte Carlo calculations might be partially due to the extreme position of the pin (-27,12), which is located next to the outer baffle. The Monte Carlo calculations that used a smaller number of particle histories show a more pronounced statistical perturbation.

For the MOX pin (-22,-2), deterministic calculation results give about ±2% of scatter band for most of the axial positions. Larger discrepancies near the axial reflectors are still observed in the pin (-22,-2), however these are less pronounced in the pin (-22,-2) than in the pin (-27,-12). All five

calculation results reported more than 4% of discrepancy for the axial position at 116 cm. Monte Carlo calculations give better results for this pin than for the pin (-27,-12) and show less statistical perturbation. The scatter band is about ±2% for most of the axial positions. As in deterministic calculations, most of the Monte Carlo calculations reported more than 4% of discrepancy for the axial position at 116 cm. The accuracy of the measurement for this position may be doubtful.

For the 4/0 UO_2 pin (-15,+2), an excellent agreement is observed in the results obtained by deterministic calculations. For most of the axial positions, the scatter band is less than ±1%. Near the upper axial reflector, the scatter band becomes a bit larger (about 3%). The same trend is observed in Monte Carlo calculation results. A slightly larger scatter band is seen in some Monte Carlo calculation results, probably due to their statistical perturbation. Again, as in deterministic calculations, near the upper axial reflector, the scatter band becomes larger, up to 2-4%. Most of the Monte Carlo results show a very similar profile of pin powers, however some results seem to suffer from a more pronounced statistical perturbation. This might be simply the question of the total number of particle histories used, and could be corrected by increasing the number of histories.

For the 4/0 UO_2 pin (-13,-12), deterministic calculation results show an excellent agreement with experimental results. For most of the axial positions, the scatter band is between almost 0 and 1%. However, a trend of slight overestimation of pin powers is observed near the lower and upper axial reflectors. Monte Carlo calculations also report a good agreement giving a scatter band of less than ±2% for most of the axial positions. A trend of slightly overestimating of the pin powers near the axial reflectors is observed. FRAMATOME-ANP MOCA results give highly overestimated pin powers for the positions at 110 cm and 150 cm. This problem could be the result of a rough extrapolation of pin powers at the boundaries in MOCA calculations (the axial meshes used in MOCA fission rate calculations were larger than 2 cm) and this could be remedied by a better extrapolation.

The 3/0 UO_2 pin (-11,+2) is located next to a Pyrex pin which contains the absorbing material. Both deterministic and Monte Carlo calculation results show almost the same profile of pin powers. For the axial positions in the middle, the scatter band is less than or about ±1% from deterministic calculations and about ±1% from Monte Carlo calculations. A trend of slight overestimation of pin powers is observed at positions near the lower and upper axial reflectors. No noticeable influence of the Pyrex pin on calculated pin powers is observed.

For the 3/0 UO_2 pin (-6,-6), deterministic calculations report less than ±1% of scatter band and Monte Carlo results about ±1% for most of the axial positions in the central part of the pin, as in the pin (-11,+2). However, a slight overestimation at positions near the upper reflector and a slight underestimation of pin powers at positions near the lower reflector region in both deterministic and Monte Carlo calculation results are observed.

Comparison of deterministic and Monte Carlo calculations

To summarise the analysis undertaken above and to compare the general trend of results, average values of axial pin powers obtained by deterministic and Monte Carlo methods were calculated and compared as (C/E)-1 values in Figures 4.29 to 4.31.

For the MOX pin (-27,-12), averaged pin powers from both deterministic and Monte Carlo calculations give a scatter band less than ±2% for most of the axial positions. For the position at 112 cm, the discrepancies are about 3% from Monte Carlo calculations and about 3.5% from deterministic calculations. For the MOX pin (-22,-2), both calculations show a scatter band of ±2% for most of

the positions, however for the positions at 116, 136 and 150 cm, the discrepancies reported by both Monte Carlo calculations and deterministic calculations are more than 3%. Hence, the accuracy of measurement for these positions might be questionable.

For 4/0 UO_2 pins (-15,+2) and (-13,-12), both deterministic and Monte Carlo calculations provide an excellent agreement within ±1% of discrepancy for almost all positions. A slight increase of discrepancies up to 3% is observed at both extremities of the fuel pins.

For 3/0 UO_2 pins (-11,+2) and (-6,-6), again both deterministic and Monte Carlo calculations give an excellent agreement within ±1% of discrepancy for almost all positions. A slight overestimation up to 2.5% is observed in the pin (-11,+2) at positions near the axial reflectors. For the pin (-6,-6), a slight overestimation of less than 2% near the upper reflector and an underestimation of pin powers about 2% from both calculation methods are observed.

To summarise, the two different methods produce very similar results within the measurement uncertainties for most of the axial positions, as expected.

In general, for power distribution calculations of the six fuel pins, most of the calculation results show a good agreement with experimental data within the reported measurement uncertainties (1σ) which are ±2.2% in UO_2 and ±3.4% in MOX pins. Due to the statistical perturbation, Monte Carlo calculations give slightly larger scatter band than deterministic calculations.

Comparison of libraries

JAERI applied two versions of the JENDL library (3.2 and 3.3). SCK•CEN used two libraries based on ENDF/B-VI.5 and JEF-2.2. Both KAERI+NEA and GRS examined three libraries based on ENDF/B-VI.5, JENDL-3.2 and JEF-2.2. In addition, KAERI+NEA also applied the MCNP-4B package library ENDF60. These results are presented in Figures 4.32 to 4.37.

Due to the fact that all Monte Carlo results show the statistical perturbation and that for some positions one library gives a better result, but worse results for other positions with other libraries, an absolute comparison of results with different libraries is not possible. The accuracy of pin power results seem to be more dependent on how the core is modelled and how the cross-sections are prepared.

Comparison of number of particle histories

KAERI+NEA performed a series of supplementary calculations to investigate the influence of the number of particle histories on the accuracy of pin power results. For this, all the calculations were carried out with the MCNP package library ENDF60, increasing the number of histories for each step. The reference case was undertaken with 50×10^6 of histories (100 000 neutrons/cycle and 500 cycles after 100 inactive cycles). However, the calculation model does not take into account the top and bottom stops of the active fuel pins and top and bottom blankets in the axial reflector regions, which might cause larger discrepancies of pin powers near the axial reflectors. The comparative results of this study are presented in Figures 4.38 and 4.43.

When the number of histories is increased to 200×10^6 (100 000 neutrons/cycle and 2 000 cycles after 100 inactive cycles), the relative errors (1σ) are about 1.8% for the MOX pin (-27,-12) and about 1.0% for the MOX pin (-22,-2), while they are about 0.7% for the four UO_2 pins. In consequence, the scatter bands become much smaller for both MOX and UO_2 pins than in the reference calculation with 50×10^6 histories. However, larger discrepancies near the axial reflectors are still observed, especially

for the UO_2 pins. For the MOX (-27,-12) pin, all 21 axial positions give a discrepancy of less than 3.4%, which is the reported uncertainty of the measurement. In the MOX (-22,-2) pin, 18 positions out of 21 show about or less than 2%. In the UO_2 pins, for most of the axial positions (18 positions for the 4/0 UO_2 and 19-20 for UO_2 3/0 pins), the agreements between calculated and measured pin power values are very good (less than ±2%). The slightly worse results for the UO_2 pins are due to the pronounced reflector effect near the axial upper and lower reflectors.

The standard deviations of differences between calculated and measured values are 1.7% for the MOX pin (-27,-12) and 2.0% for the MOX pin (-22,-2). For the two 4/0 UO_2 pins, the standard deviations of differences between calculated and measured values are 1.8%. For the 3/0 UO_2 pins, the standard deviations of differences between calculated and measured values are 1.4% for the UO_2 pin (-11,+2) and 1.0% for the UO_2 pin (-6,-6).

To examine more thoroughly the influence of the number of histories on results, the histories were again increased up to 300×10^6 (100 000 neutrons/cycle and 3 000 cycles after 100 inactive cycles). From the latter calculation, the reported relative errors (1σ) are about 1.5% for the MOX pin (-27,-12) and about 0.8% for the MOX pin (-22,-2), and they are about 0.6% for the four UO_2 pins. However, the pin power results obtained show almost the same trend as those from the calculations with 200×10^6 histories. The standard deviations of differences between calculated and measured values are 1.6% for the MOX pin (-27,-12) and 1.9% for the MOX pin (-22,-2). The standard deviations of differences between calculated and measured values are 1.6% for the UO_2 pin (-15,+2) and 1.9% for the UO_2 pin (-13,-12). For the 3/0 UO_2 pins, the standard deviations of differences between calculated and measured values are 1.4% for the pin (-11,+2) and 1.0% for the pin (-6,-6). Therefore, compared to the calculated results with 200×10^6 histories, no real advantage is obtained when the number of histories is increased to 300×10^6.

To summarise, some Monte Carlo calculation results that showed a statistical perturbation with the limited number of histories used might be improved to some extent if a sufficient number of histories were to be applied.

Comments on pin power discrepancies near the axial reflectors

With regard to somewhat larger discrepancies observed in UO_2 pins at axial positions near the upper and lower reflector regions, even though discrepancies are often within the reported measurement uncertainties in many calculation results, this could originate from the fact that most of the calculation models ignored the detailed structures above and below the active fuel pins, i.e. top and bottom stops of the active fuel pins and top and bottom blankets in the axial reflector regions.

According to the calculation details provided by JAERI and Ref. [13], JAERI took into account the detailed structures above and below the active fuel pins in its calculation model and JAERI results do not show pronounced discrepancies of pin powers observed in UO_2 pins at positions near the axial reflectors.

It is therefore believed that ignoring detailed structures above and below the active fuel pins in the calculation model may cause about 1 or 2% of pin power discrepancy at axial positions near the axial reflectors.

Moreover, according to the benchmark specification and the original document on the experiments provided by SCK•CEN, the reflector composition changes a little from one fuel region to another, depending on the structure of the corresponding fuel pins. However, the detailed information on these

composition changes was not available and could not be given to the participants. Therefore, some approximations made by each participant to describe the lower and upper reflectors as a mixture of water, grid and Plexiglas would affect pin power results near the axial reflectors.

This will be further studied by performing supplementary calculations to quantify the influence of detailed axial structures on calculated pin powers near the axial reflectors.

Through a comparison calculation undertaken by SCK•CEN, it was found that ignoring the thermal scattering by Plexiglas, which is the main component of the axial reflectors, does not have an important influence on larger discrepancies observed at positions near the axial reflectors.

Chapter 5

CONCLUSIONS

Following the two-dimensional VENUS-2 MOX core benchmark, an international benchmark exercise based on the three-dimensional VENUS-2 MOX core experiment results was organised by the OECD/NEA. The benchmark aimed at validating three-dimensional calculation methods together with the latest nuclear data used for MOX-fuelled systems. Therefore, the measured axial pin power distributions of the six fuel pins at 21 axial positions were main investigative purpose of the benchmark. Twelve participants contributed to the benchmark, providing more than 20 solutions. Various nuclear data sets such as ENDF/B-IV, several versions of ENDF/B-VI, JEF-2.2 and two versions of JENDL (3.2 and 3.3) were used. For core calculations predicting axial power distributions, four participants applied deterministic codes such as TORT, DANTSYS and PARCS, and eight participants used continuous-energy Monte Carlo codes such as MCNP-4B, MCNP-4C, MVP and MCU-REA, and the multi-group Monte Carlo code MOCA.

From the cell calculations, k_∞ and reaction rates were investigated. The average k_∞ values are 1.40656±0.00491 for 3/0 UO_2, 1.33769±0.00556 for 4/0 UO_2 and 1.25737±0.00561 for MOX cells. Although the maximum spreads in k_∞ from the average values are 1.1% for 3/0 UO_2, 1.5% for 4/0 UO_2 and 1.4% for MOX cells, most of the results report a deviation of less than 0.5%. In particular, most of the Monte Carlo calculations give results with a deviation of less than 0.2%, which is the claimed uncertainty on reactivity in current nuclear design methods. For all three types of fuel pins, the results obtained by deterministic codes give smaller values than the average values (except for the values from Purdue University) and most of the Monte Carlo results show larger values than the average values. This could partially be explained by the fact that the deterministic calculations generally use a cylindrical cell geometry whereas the Monte Carlo calculations and Purdue University's HELIOS calculations describe the "true" square cell geometry for cell calculations.

The reaction rate results are in general consistent. However, differences in basic data among libraries used are observed for some isotopes and it seems that the reaction rate results are sensitive to basic data processing procedures, especially for the preparation of cross-section data for deterministic cell calculations.

Concerning core calculations, k_{eff}, normalised radial fission rate distribution at 325 fuel pin positions at the core mid-plane, and normalised axial fission rate distribution of six fuel pins were reported. In this study, the calculated k_{eff} values and axial fission rate distribution of six fuel pins were analysed and compared with the experimental values. The measured k_{eff} value is one (1) with an uncertainty of ±32 pcm, and the reported uncertainties of the measured data (1σ) of pin power distributions of the six fuel pins are ±2.2% in UO_2 and ±3.4% in MOX pins.

All reported k_{eff} show in general a very good agreement with the experimental value (k_{eff} = 1). The average k_{eff} from all calculations is 1.00122±0.00394. The deterministic calculations give an average of 0.99828±0.00402 and the Monte Carlo calculations lead to an average of 1.00232±0.00341. Various nuclear data sets were examined. However, the calculated k_{eff} results show that there is no

clear dependency on basic nuclear libraries. Differences observed among them would rather be due to different nuclear data processing procedures and calculation models used. A further investigation into nuclear data processing procedures and calculation models used by the participants could better clarify the origin of the discrepancies observed in k_{eff} results.

For the MOX pins, averaged pin powers from both deterministic and Monte Carlo calculations give a scatter band less than ±2% for most of the axial positions. For a few axial positions, both calculations report more than ±3% of scatter band. For 4/0 UO_2 pins, both deterministic and Monte Carlo calculations give an excellent agreement within ±1% of discrepancy for almost all positions. A slight increase of discrepancies up to 3% is observed at both extremities of the fuel pins. As for 3/0 UO_2 pins, agreement within ±1% is observed for almost all positions in both deterministic and Monte Carlo calculation results. A slight overestimation up to 2.5% is observed in the pin (-11,+2) at positions near the axial reflectors. For the pin (-6,-6), a slight overestimation of less than 2% is observed near the upper reflector, as is an underestimation of pin powers of about 2% from both calculation methods.

As expected, the two methods produce very similar results within the reported measurement uncertainties for most of the axial positions. However, some Monte Carlo calculations seem to suffer from statistical perturbation and the results might be improved by increasing the total number of particle histories used.

From an intercomparison of results when different libraries are used, a general observation is that there are no great differences and that, for most of the axial positions, the calculated pin power results show a scatter band of less than ±2% when compared with experimental values. Therefore, the “best” library cannot be determined.

The results of a separate study show that the statistical perturbation observed in Monte Carlo calculations can be decreased by increasing the total number of particle histories. However, after a certain threshold, there is no real gain.

With regard to somewhat larger discrepancies observed in UO_2 pins at axial positions near the upper and lower reflector regions, this could originate from the fact that most of the calculation models ignored the detailed structures above and below the active fuel pins, i.e. top and bottom stops of the active fuel pins and top and bottom blankets in the axial reflector regions.

This will be further studied by performing supplementary calculations to quantify the influence of detailed axial structures on calculated pin powers near the axial reflectors.

Through a comparison calculation undertaken by SCK•CEN, it was found that ignoring the thermal scattering by Plexiglas, which is the main component of the axial reflectors, does not have an important influence on larger discrepancies observed at positions near the axial reflectors.

In conclusion, the results confirm that all combinations of the present methods using the latest nuclear data sets can adequately calculate MOX-fuelled systems in 3-D geometry, producing reasonably accurate axial pin power distributions.

The 3-D VENUS-2 MOX core experimental data provided by SCK•CEN were very useful for comparison of calculated results against them to investigate current methods and nuclear data. The reported uncertainties of the measured data (1σ) for the six fuel pins are ±2.2% in UO_2 and ±3.4% in MOX pins. Further studies using experimental data with smaller uncertainties would contribute to additional refinements of calculation methods used for MOX-fuelled systems.

REFERENCES

[1] *Physics of Plutonium Recycling: Issues and Perspectives*, Volume I, OECD/NEA report, ISBN 92-64-14538-9 (1995).

[2] *Physics of Plutonium Recycling: Plutonium Recycling in Pressurised Water Reactors*, Volume II, OECD/NEA report, ISBN 92-64-14590-7 (1995).

[3] *Physics of Plutonium Recycling: Void Reactivity Effect in Pressurised Water Reactors*, Volume III, OECD/NEA report, ISBN 92-64-14591-5 (1995).

[4] *Physics of Plutonium Recycling: Multiple Plutonium Recycling in Advanced PWRs*, Volume VI, OECD/NEA report, ISBN 92-64-19957-8 (2002).

[5] Na, Byung-Chan and Enrico Sartori, *Blind Benchmark on the VENUS-2 MOX Core Measurements*, OECD/NEA document, NEA/SEN/NSC/WPPR(99)2, May 1999.

[6] Na, Byung-Chan, *Benchmark on the VENUS-2 MOX Core Measurements*, OECD/NEA report, NEA/NSC/DOC(2000)7, ISBN 92-64-18276-4 (2000).

[7] Na, Byung-Chan and Enrico Sartori, "OECD/NEA International Benchmark on the VENUS-2 MOX Core Measurements," *Nuclear Science and Engineering*, 142, 37-47 (2002).

[8] van der Meer, Klaas, *et al*., *Additional Data for the 3-D VENUS-2 Benchmark*, SCK•CEN report, TN-0008, September 2000.

[9] Na, Byung-Chan and Nadia Messaoudi, *Blind Benchmark on the 3-D VENUS-2 MOX Core Measurements: Final Specification*, OECD/NEA document, NEA/SEN/NSC/WPPR(2001)1, May 2001.

[10] Orsi, R., *The ENEA-Bologna Pre-post Processor Package BOT3P for the DORT and TORT Transport Codes (Version 1.0)*, December 1999.

[11] *Light Water Reactor (LWR) Pin Cell Benchmark Intercomparisons*, JEFF report 15, OECD/NEA report, September 1999.

[12] DeHart, M.D., "A Deterministic Study of the Deficiency of the Wigner-Seitz Approximation for Pu/MOX Fuel Pins", *Proc. Int. Conf. on Mathematics and Computation, Reactor Physics and Environmental Analysis in Nuclear Applications*, Madrid, Spain, 27-30 September 1999, p. 689.

[13] Nagaya, Y., K. Okumura and T. Mori, "Analysis of VENUS-2 MOX Core Measurements with a Monte Carlo Code MVP", *Proc. Int. Conf. on the New Frontiers of Nuclear Technology: Reactor Physics, Safety and High Performance Computing (PHYSOR 2002)*, Seoul, Korea, 7-10 October 2002, 4A-04.

TABLES

Table 3.1. Participants, basic library and computer codes used

Institution (Country)	Participants	Codes used	Data used	Energy group
FRAMATOME-ANP (Germany)	W. Hofmann J. Koban W. Timm	CASMO-4 TORT-2.7.3	ENDF/B-IV (Er and Tm data from JEF-1 and JEF-2.1)	5 groups
KAERI (Korea)	D.H. Kim J.D. Kim C.S. Gil J.H. Chang	TRANSX-2.15 DANTSYS-3.0	ENDF/B-VI.7 (Sn from ENDL84)	35 groups
NEA+ KAERI (Korea)	B-C. Na (NEA) G.H. Roh (KAERI)	TRANSX-2.15 TORT-3.2	ENDF/B-VI.5 JENDL-3.2	35 groups
Purdue Univ. (USA)	T. Kozlowski C.H. Lee T.J. Downar	HELIOS-1.7 PARCS-2.1	ENDF/B-VI.3	8 groups
FRAMATOME-ANP (Germany)	W. Timm S. Misu D. Porsch	CASMO-4 MOCA	ENDF/B-IV (Er and Tm data from JEF-1 and JEF-2.1)	Multi-group Monte Carlo: 5 groups
JAERI (Japan)	Y. Nagaya K. Okumura T. Mori	MVP	JENDL-3.2 (Sn from CENDL-2) JENDL-3.3 (S, Si, Mo from JENDL-3.2 and Sn from CENDL-2)	Continuous
SCK•CEN (Belgium)	N. Messaoudi H.A. Abderrahim	MCNP-4C	ENDF/B-VI.5 JEF-2.2	Continuous
KAERI (Korea) + NEA	G.H. Roh (KAERI) B-C. Na (NEA)	MCNP-4B	ENDF/B-VI.5 JENDL-3.2 JEF-2.2	Continuous
KFKI (Hungary)	G. Hordósy	MCNP-4C	ENDF/B-VI.2 (structural material data from ENDF/B-V)	Continuous
KI (Russia)	E. Gomin M. Kalugin	MCU-REA	MCU data library (based on ENDF/B-VI, JENDL-3.2 and BROND)	Continuous
GRS+IKE (Germany)	W. Zwermann (GRS) M. Mattes (IKE)	MCNP-4C	ENDF/B-VI.5 JENDL-3.2 JEF-2.2	Continuous
SEA (Spain)	D.L. Maganto	MCNP-4C	ENDF/B-VI for fuel, water, some elements of steel structures (for the rest from ENDF/B-V)	Continuous

Table 4.1. k_∞ values of cell calculations

Institution	Code	Basic library	3/0 UO_2	Deviation (%)	4/0 UO_2	Deviation (%)	MOX	Deviation (%)
FRAMATOME-ANP	CASMO-4	ENDF/B-IV	1.40394	-0.19	1.33469	-0.22	1.25550	-0.15
KAERI	TRANSX-2.15	ENDF/B-VI.7	1.39612^{L}	-0.74	1.32679^{L}	-0.82	1.24636^{L}	-0.88
NEA+KAERI	TRANSX-2.15	ENDF/B-VI.5	1.39612^{L}	-0.74	1.32679^{L}	-0.82	1.24636^{L}	-0.88
		JENDL-3.2	1.40207	-0.32	1.33093	-0.51	1.24947	-0.63
Purdue Univ.	HELIOS-1.7	ENDF/B-VI.3	1.40850	0.14	1.34331	0.42	1.26339	0.48
JAERI	MVP	JENDL-3.2	1.41183	0.37	1.34635^{H}	0.65	1.26383	0.51
		JENDL-3.3	1.40710	0.04	1.33951	0.14	1.26209	0.38
SCK•CEN	MCNP-4C	ENDF/B-VI.5	1.40382	-0.19	1.33572	-0.15	1.25555	-0.14
		JEF-2.2	1.41244^{H}	0.42	1.34299	0.40	1.25839	0.08
KAERI+NEA	MCNP-4B	ENDF60	1.40479	-0.13	1.33635	-0.10	1.25447	-0.23
		ENDF/B-VI.5	1.40726	0.05	1.33677	-0.07	1.25876	0.11
		JENDL-3.2	1.41239	0.41	1.34153	0.29	1.26109	0.30
		JEF-2.2	1.41129	0.34	1.34291	0.39	1.25959	0.18
KFKI	MCNP-4C	ENDF/B-VI.2	1.40430	-0.16	1.33519	-0.19	1.25339	-0.32
KI	MCU-REA	MCUDAT	1.40710	0.04	1.33650	-0.09	1.25490	-0.20
GRS	MCNP-4C	ENDF/B-VI.5	1.40690	0.02	1.33798	0.02	1.25859	0.10
		JENDL-3.2	1.41128	0.34	1.34267	0.37	1.26146	0.33
		JEF-2.2	1.41170	0.37	1.34391	0.46	1.26117	0.30
SEA	MCNP-4C	ENDF/B-VI	1.40570	-0.06	1.33530	-0.18	1.26570^{H}	0.66
Average			1.40656		1.33769		1.25737	
Standard deviation			0.00491		0.00556		0.00561	

Table 4.2. Comparison of calculated k_∞ values with different nuclear data libraries

ENDF/B								
Institution	**Method**	**Library**	**3/0 UO_2**	**Deviation (%)**	**4/0 UO_2**	**Deviation (%)**	**MOX**	**Deviation (%)**
FRAMATOME	CASMO-4	ENDF/B-IV	1.40394	-0.19	1.33469	-0.22	1.25550	-0.15
SEA	MCNP-4C	ENDF/B-VI	1.4057	-0.06	1.3353	-0.18	1.2657	0.66
KFKI	MCNP-4C	ENDF/B-VI.2	1.40430	-0.16	1.33519	-0.19	1.25339	-0.32
Purdue Univ.	HELIOS-1.7	ENDF/B-VI.3	1.40850	0.14	1.34331	0.42	1.26339	0.48
NEA+KAERI	TRANSX	ENDF/B-VI.5	1.39612	-0.74	1.32679	-0.82	1.24636	-0.88
SCK•CEN	MCNP-4C	ENDF/B-VI.5	1.40382	-0.19	1.33572	-0.15	1.25555	-0.14
KAERI+NEA	MCNP-4B	ENDF/B-VI.5	1.40726	0.05	1.33677	-0.07	1.25876	0.11
GRS	MCNP-4C	ENDF/B-VI.5	1.4069	0.02	1.33798	0.02	1.25859	0.10
KAERI	TRANSX	ENDF/B-VI.7	1.39612	-0.74	1.32679	-0.82	1.24636	-0.88
KAERI+NEA	MCNP-4B	ENDF60	1.40479	-0.13	1.33635	-0.10	1.25447	-0.23
Average			1.40375		1.33489		1.25581	
Standard deviation			0.00430		0.00493		0.00631	

JEF-2.2								
Institution	**Method**	**Library**	**3/0 UO_2**	**Deviation (%)**	**4/0 UO_2**	**Deviation (%)**	**MOX**	**Deviation (%)**
SCK•CEN	MCNP-4C	JEF-2.2	1.41244	0.42	1.34299	0.40	1.25839	0.08
KAERI+NEA	MCNP-4B	JEF-2.2	1.41129	0.34	1.34291	0.39	1.25959	0.18
GRS	MCNP-4C	JEF-2.2	1.4117	0.37	1.34391	0.46	1.26117	0.30
Average			1.41181		1.34327		1.25972	
Standard deviation			0.00058		0.00056		0.00139	

JENDL								
Institution	**Method**	**Library**	**3/0 UO_2**	**Deviation (%)**	**4/0 UO_2**	**Deviation (%)**	**MOX**	**Deviation (%)**
NEA+KAERI	TRANSX	JENDL-3.2	1.40207	-0.32	1.33093	-0.51	1.24947	-0.63
JAERI	MVP	JENDL-3.2	1.41183	0.37	1.34635	0.65	1.26383	0.51
KAERI+NEA	MCNP-4B	JENDL-3.2	1.41239	0.41	1.34153	0.29	1.26109	0.30
GRS	MCNP-4C	JENDL-3.2	1.41128	0.34	1.34267	0.37	1.26146	0.33
JAERI	MVP	JENDL-3.3	1.40710	0.04	1.33951	0.14	1.26209	0.38
Average			1.40893		1.34020		1.25959	
Standard deviation			0.00437		0.00575		0.00575	

Table 4.3. ^{234}U reaction rates in MOX fuel pin (relative to the arbitrary reference GRS ENDF-VI.5 values)

Institution (code, library)	g=1	Dev. (%)	g=2	Dev. (%)	g=3	Dev. (%)	Total	Dev. (%)
Absorption rates								
KFKI (MCNP-4C, ENDF/B-VI.2)	7.250E-05	0.50	1.541E-03	-0.34	3.443E-04	-0.79	1.958E-03	-0.39
Purdue Univ. (HELIOS, ENDF/B-VI.3)	7.088E-05	-1.74	1.536E-03	-0.66	3.451E-04	-0.56	1.952E-03	-0.68
KAERI+NEA (MCNP-4B, ENDF/B-VI.5)	7.208E-05	-0.07	1.545E-03	-0.10	3.470E-04	-0.02	1.964E-03	-0.09
SCK•CEN (MCNP-4C, ENDF/B-VI.5)	7.218E-05	0.07	1.523E-03	-1.52	3.446E-04	-0.69	1.940E-03	-1.31
KAERI (TRANSX, ENDF/B-VI.7)	7.246E-05	0.45	1.505E-03	-2.67	3.421E-04	-1.42	1.920E-03	-2.33
KAERI+NEA (MCNP-4B, ENDF60)	7.238E-05	0.33	1.540E-03	-0.41	3.449E-04	-0.62	1.957E-03	-0.42
FRAMATOME-ANP (CASMO, ENDF/B-IV)	–	–	–	–	–	–	1.801E-03	-8.34
SEA (MCNP-4C, ENDF/B-VI)	7.038E-05	-2.43	1.387E-03	-10.31	3.696E-04	6.50	1.827E-03	-7.04
GRS (MCNP-4C, ENDF/B-VI.5)	7.214E-05	0.00	1.546E-03	0.00	3.470E-04	0.00	1.965E-03	0.00
NEA+KAERI (TRANSX, ENDF/B-VI.5)	–	–	–	–	–	–	1.920E-03	-2.33
KAERI+NEA (MCNP-4B, JEF-2.2)	7.026E-05	-2.60	1.534E-03	-0.79	3.477E-04	0.19	1.952E-03	-0.68
GRS (MCNP-4C, JEF-2.2)	7.101E-05	-1.56	1.544E-03	-0.13	3.472E-04	0.04	1.962E-03	-0.15
SCK•CEN (MCNP-4C, JEF-2.2)	7.101E-05	-1.57	1.537E-03	-0.59	3.462E-04	-0.22	1.954E-03	-0.56
KAERI+NEA (MCNP-4B, JENDL-3.2)	6.904E-05	-4.28	1.504E-03	-2.75	3.276E-04	-5.60	1.900E-03	-3.31
GRS (MCNP-4C, JENDL-3.2)	7.059E-05	-2.14	1.551E-03	0.30	3.467E-04	-0.09	1.968E-03	0.14
JAERI (MVP, JENDL-3.2)	6.881E-05	-4.60	1.469E-03	-4.99	3.273E-04	-5.68	1.865E-03	-5.09
NEA+KAERI (TRANSX, JENDL-3.2)	–	–	–	–	–	–	1.837E-03	-6.52
JAERI (MVP, JENDL-3.3)	6.880E-05	-4.63	1.472E-03	-4.78	3.286E-04	-5.31	1.870E-03	-4.87
KI (MCU-REA, MCUDAT)	7.066E-05	-2.05	1.468E-03	-5.06	3.335E-04	-3.91	1.872E-03	-4.74
Fission rates								
KFKI (MCNP-4C, ENDF/B-VI.2)	5.137E-05	0.46	1.424E-06	0.11	1.464E-06	-0.90	5.426E-05	0.42
Purdue Univ. (HELIOS, ENDF/B-VI.3)	4.996E-05	-2.31	1.419E-06	-0.27	1.472E-06	-0.41	5.285E-05	-2.20
KAERI+NEA (MCNP-4B, ENDF/B-VI.5)	5.108E-05	-0.10	1.420E-06	-0.22	1.477E-06	-0.04	5.398E-05	-0.10
SCK•CEN (MCNP-4C, ENDF/B-VI.5)	5.116E-05	0.05	1.409E-06	-0.98	1.466E-06	-0.78	5.404E-05	0.00
KAERI (TRANSX, ENDF/B-VI.7)	5.114E-05	0.00	1.413E-06	-0.70	1.458E-06	-1.35	5.401E-05	-0.05
KAERI+NEA (MCNP-4B, ENDF60)	5.128E-05	0.28	1.421E-06	-0.12	1.467E-06	-0.72	5.417E-05	0.25
FRAMATOME-ANP (CASMO, ENDF/B-IV)	–	–	–	–	–	–	4.990E-05	-7.65
SEA (MCNP-4C, ENDF/B-VI)	5.026E-05	-1.72	1.293E-06	-9.10	1.589E-06	7.56	5.314E-05	-1.65
GRS (MCNP-4C, ENDF/B-VI.5)	5.114E-05	0.00	1.423E-06	0.00	1.478E-06	0.00	5.403E-05	0.00
NEA+KAERI (TRANSX, ENDF/B-VI.5)	–	–	–	–	–	–	5.401E-05	-0.05
KAERI+NEA (MCNP-4B, JEF-2.2)	4.950E-05	-3.20	1.416E-06	-0.44	1.480E-06	0.14	5.239E-05	-3.04
GRS (MCNP-4C, JEF-2.2)	5.021E-05	-1.82	1.425E-06	0.15	1.478E-06	0.03	5.311E-05	-1.71
SCK•CEN (MCNP-4C, JEF-2.2)	5.020E-05	-1.84	1.415E-06	-0.52	1.473E-06	-0.33	5.308E-05	-1.76
KAERI+NEA (MCNP-4B, JENDL-3.2)	4.928E-05	-3.62	2.127E-06	49.49	2.943E-08	-98.01	5.144E-05	-4.80
GRS (MCNP-4C, JENDL-3.2)	4.977E-05	-2.67	1.424E-06	0.05	1.476E-06	-0.10	5.267E-05	-2.53
JAERI (MVP, JENDL-3.2)	4.909E-05	-4.00	2.100E-06	47.60	2.931E-08	-98.02	5.122E-05	-5.21
NEA+KAERI (TRANSX, JENDL-3.2)	–	–	–	–	–	–	5.135E-05	-4.97
JAERI (MVP, JENDL-3.3)	4.908E-05	-4.02	2.060E-06	44.78	9.543E-07	-35.42	5.209E-05	-3.59
KI (MCU-REA, MCUDAT)	4.964E-05	-2.93	1.394E-06	-2.03	2.048E-06	38.60	5.308E-05	-1.77

Table 4.4. ^{235}U reaction rates in MOX fuel pin (relative to the arbitrary reference GRS ENDF-VI.5 values)

Institution (code, library)	g=1	Dev. (%)	g=2	Dev. (%)	g=3	Dev. (%)	Total	Dev. (%)
Absorption rates								
KFKI (MCNP-4C, ENDF/B-VI.2)	1.371E-02	0.53	9.383E-02	-1.22	2.690E-01	-0.62	3.765E-01	-0.73
Purdue Univ. (HELIOS, ENDF/B-VI.3)	1.350E-02	-1.03	9.699E-02	2.11	2.715E-01	0.30	3.820E-01	0.70
KAERI+NEA (MCNP-4B, ENDF/B-VI.5)	1.364E-02	-0.01	9.516E-02	0.17	2.706E-01	-0.03	3.794E-01	0.02
SCK•CEN (MCNP-4C, ENDF/B-VI.5)	1.365E-02	0.05	8.735E-02	-8.04	2.693E-01	-0.50	3.767E-01	-0.67
KAERI (TRANSX, ENDF/B-VI.7)	1.378E-02	1.03	9.693E-02	2.05	2.673E-01	-1.25	3.780E-01	-0.34
KAERI+NEA (MCNP-4B, ENDF60)	1.369E-02	0.36	9.361E-02	-1.46	2.695E-01	-0.43	3.768E-01	-0.66
FRAMATOME-ANP (CASMO, ENDF/B-IV)	–	–	–	–	–	–	3.755E-01	-1.00
SEA (MCNP-4C, ENDF/B-VI)	1.316E-02	-3.54	8.556E-02	-9.93	2.919E-01	7.83	3.906E-01	2.98
GRS (MCNP-4C, ENDF/B-VI.5)	1.364E-02	0.00	9.499E-02	0.00	2.707E-01	0.00	3.793E-01	0.00
NEA+KAERI (TRANSX, ENDF/B-VI.5)	–	–	–	–	–	–	3.780E-01	-0.34
KAERI+NEA (MCNP-4B, JEF-2.2)	1.347E-02	-1.28	9.319E-02	-1.89	2.711E-01	0.18	3.778E-01	-0.39
GRS (MCNP-4C, JEF-2.2)	1.353E-02	-0.84	9.299E-02	-2.11	2.709E-01	0.08	3.774E-01	-0.50
SCK•CEN (MCNP-4C, JEF-2.2)	1.353E-02	-0.79	9.321E-02	-1.88	2.699E-01	-0.27	3.767E-01	-0.69
KAERI+NEA (MCNP-4B, JENDL-3.2)	1.354E-02	-0.73	9.262E-02	-2.50	2.704E-01	-0.10	3.766E-01	-0.72
GRS (MCNP-4C, JENDL-3.2)	1.352E-02	-0.91	9.254E-02	-2.58	2.710E-01	0.14	3.771E-01	-0.58
JAERI (MVP, JENDL-3.2)	1.351E-02	-0.96	9.266E-02	-2.46	2.703E-01	-0.15	3.764E-01	-0.76
NEA+KAERI (TRANSX, JENDL-3.2)	–	–	–	–	–	–	3.758E-01	-0.92
JAERI (MVP, JENDL-3.3)	1.364E-02	-0.03	9.491E-02	-0.08	2.700E-01	-0.26	3.785E-01	-0.20
KI (MCU-REA, MCUDAT)	1.370E-02	0.46	9.396E-02	-1.08	2.716E-01	0.35	3.794E-01	0.03
Fission rates								
KFKI (MCNP-4C, ENDF/B-VI.2)	1.161E-02	0.52	6.037E-02	1.94	2.284E-01	-0.44	3.004E-01	0.07
Purdue Univ. (HELIOS, ENDF/B-VI.3)	1.146E-02	-0.80	6.001E-02	1.33	2.304E-01	0.43	3.019E-01	0.56
KAERI+NEA (MCNP-4B, ENDF/B-VI.5)	1.155E-02	-0.02	5.933E-02	0.19	2.293E-01	-0.05	3.002E-01	0.00
SCK•CEN (MCNP-4C, ENDF/B-VI.5)	1.156E-02	0.05	6.029E-02	1.80	2.287E-01	-0.31	3.005E-01	0.12
KAERI (TRANSX, ENDF/B-VI.7)	1.166E-02	0.92	6.008E-02	1.45	2.264E-01	-1.29	2.982E-01	-0.66
KAERI+NEA (MCNP-4B, ENDF60)	1.159E-02	0.35	6.024E-02	1.72	2.288E-01	-0.25	3.006E-01	0.16
FRAMATOME-ANP (CASMO, ENDF/B-IV)	–	–	–	–	–	–	2.973E-01	-0.95
SEA (MCNP-4C, ENDF/B-VI)	1.117E-02	-3.33	5.504E-02	-7.05	2.481E-01	8.15	3.143E-01	4.71
GRS (MCNP-4C, ENDF/B-VI.5)	1.155E-02	0.00	5.922E-02	0.00	2.294E-01	0.00	3.002E-01	0.00
NEA+KAERI (TRANSX, ENDF/B-VI.5)	–	–	–	–	–	–	2.982E-01	-0.66
KAERI+NEA (MCNP-4B, JEF-2.2)	1.138E-02	-1.43	6.014E-02	1.55	2.299E-01	0.24	3.015E-01	0.44
GRS (MCNP-4C, JEF-2.2)	1.144E-02	-0.91	6.003E-02	1.36	2.297E-01	0.14	3.012E-01	0.35
SCK•CEN (MCNP-4C, JEF-2.2)	1.145E-02	-0.88	6.021E-02	1.68	2.289E-01	-0.22	3.005E-01	0.13
KAERI+NEA (MCNP-4B, JENDL-3.2)	1.143E-02	-1.03	5.971E-02	0.83	2.296E-01	0.11	3.008E-01	0.21
GRS (MCNP-4C, JENDL-3.2)	1.141E-02	-1.19	5.959E-02	0.63	2.302E-01	0.35	3.012E-01	0.35
JAERI (MVP, JENDL-3.2)	1.140E-02	-1.27	5.960E-02	0.64	2.296E-01	0.07	3.006E-01	0.13
NEA+KAERI (TRANSX, JENDL-3.2)	–	–	–	–	–	–	2.993E-01	-0.27
JAERI (MVP, JENDL-3.3)	1.145E-02	-0.83	5.918E-02	-0.06	2.288E-01	-0.27	2.994E-01	-0.25
KI (MCU-REA, MCUDAT)	1.158E-02	0.26	5.987E-02	1.11	2.304E-01	0.46	3.019E-01	0.57

Table 4.5. ^{236}U reaction rates in MOX fuel pin (relative to the arbitrary reference GRS ENDF-VI.5 values)

Institution (code, library)	g=1	Dev. (%)	g=2	Dev. (%)	g=3	Dev. (%)	Total	Dev. (%)
Absorption rates								
KFKI (MCNP-4C, ENDF/B-VI.2)	2.919E-05	0.50	6.594E-04	0.55	1.799E-05	-0.25	7.066E-04	0.53
Purdue Univ. (HELIOS, ENDF/B-VI.3)	2.846E-05	-2.01	6.488E-04	-1.06	1.787E-05	-0.93	6.952E-04	-1.09
KAERI+NEA (MCNP-4B, ENDF/B-VI.5)	2.903E-05	-0.05	6.563E-04	0.08	1.805E-05	0.05	7.034E-04	0.08
SCK•CEN (MCNP-4C, ENDF/B-VI.5)	2.907E-05	0.07	6.571E-04	0.21	1.800E-05	-0.23	7.042E-04	0.19
KAERI (TRANSX, ENDF/B-VI.7)	2.919E-05	0.49	6.558E-04	0.01	1.778E-05	-1.45	7.028E-04	-0.01
KAERI+NEA (MCNP-4B, ENDF60)	2.913E-05	0.29	6.672E-04	1.74	1.801E-05	-0.14	7.143E-04	1.63
FRAMATOME-ANP (CASMO, ENDF/B-IV)	–	–	–	–	–	–	7.096E-04	0.96
SEA (MCNP-4C, ENDF/B-VI)	2.813E-05	-3.17	6.003E-04	-8.46	1.846E-05	2.35	6.469E-04	-7.96
GRS (MCNP-4C, ENDF/B-VI.5)	2.905E-05	0.00	6.558E-04	0.00	1.804E-05	0.00	7.029E-04	0.00
NEA+KAERI (TRANSX, ENDF/B-VI.5)	–	–	–	–	–	–	7.028E-04	-0.01
KAERI+NEA (MCNP-4B, JEF-2.2)	3.367E-05	15.93	6.785E-04	3.47	1.812E-05	0.46	7.303E-04	3.91
GRS (MCNP-4C, JEF-2.2)	3.397E-05	16.94	6.778E-04	3.36	1.807E-05	0.20	7.298E-04	3.84
SCK•CEN (MCNP-4C, JEF-2.2)	3.398E-05	16.99	6.860E-04	4.61	1.810E-05	0.33	7.381E-04	5.01
KAERI+NEA (MCNP-4B, JENDL-3.2)	2.909E-05	0.16	6.689E-04	2.00	1.836E-05	1.76	7.163E-04	1.92
GRS (MCNP-4C, JENDL-3.2)	2.850E-05	-1.88	6.616E-04	0.89	1.803E-05	-0.04	7.081E-04	0.75
JAERI (MVP, JENDL-3.2)	2.902E-05	-0.09	6.704E-04	2.23	1.831E-05	1.50	7.177E-04	2.11
NEA+KAERI (TRANSX, JENDL-3.2)	–	–	–	–	–	–	7.193E-04	2.35
JAERI (MVP, JENDL-3.3)	2.910E-05	0.20	6.690E-04	2.02	1.833E-05	1.62	7.165E-04	1.94
KI (MCU-REA, MCUDAT)	2.860E-05	-1.55	6.630E-04	1.10	1.773E-05	-1.69	7.094E-04	0.93
Fission rates								
KFKI (MCNP-4C, ENDF/B-VI.2)	1.749E-05	0.45	8.742E-06	0.62	1.727E-07	-0.15	2.640E-05	0.51
Purdue Univ. (HELIOS, ENDF/B-VI.3)	1.704E-05	-2.09	8.607E-06	-0.94	1.711E-07	-1.05	2.582E-05	-1.70
KAERI+NEA (MCNP-4B, ENDF/B-VI.5)	1.739E-05	-0.09	8.696E-06	0.08	1.731E-07	0.07	2.626E-05	-0.03
SCK•CEN (MCNP-4C, ENDF/B-VI.5)	1.742E-05	0.07	8.735E-06	0.53	1.727E-07	-0.15	2.633E-05	0.22
KAERI (TRANSX, ENDF/B-VI.7)	1.735E-05	-0.32	8.701E-06	0.14	1.703E-07	-1.52	2.622E-05	-0.17
KAERI+NEA (MCNP-4B, ENDF60)	1.744E-05	0.21	8.845E-06	1.80	1.729E-07	-0.05	2.646E-05	0.74
FRAMATOME-ANP (CASMO, ENDF/B-IV)	–	–	–	–	–	–	2.700E-05	2.79
SEA (MCNP-4C, ENDF/B-VI)	1.699E-05	-2.36	7.947E-06	-8.54	1.753E-07	1.34	2.512E-05	-4.38
GRS (MCNP-4C, ENDF/B-VI.5)	1.741E-05	0.00	8.689E-06	0.00	1.730E-07	0.00	2.627E-05	0.00
NEA+KAERI (TRANSX, ENDF/B-VI.5)	–	–	–	–	–	–	2.622E-05	-0.17
KAERI+NEA (MCNP-4B, JEF-2.2)	1.718E-05	-1.29	8.644E-06	-0.51	1.722E-07	-0.41	2.600E-05	-1.03
GRS (MCNP-4C, JEF-2.2)	1.744E-05	0.21	8.630E-06	-0.68	1.717E-07	-0.71	2.624E-05	-0.09
SCK•CEN (MCNP-4C, JEF-2.2)	1.745E-05	0.23	8.746E-06	0.66	1.721E-07	-0.49	2.636E-05	0.37
KAERI+NEA (MCNP-4B, JENDL-3.2)	1.724E-05	-0.98	8.530E-06	-1.83	2.113E-07	22.15	2.598E-05	-1.11
GRS (MCNP-4C, JENDL-3.2)	1.692E-05	-2.76	8.753E-06	0.74	1.729E-07	-0.03	2.585E-05	-1.59
JAERI (MVP, JENDL-3.2)	1.718E-05	-1.28	8.550E-06	-1.60	2.107E-07	21.83	2.594E-05	-1.23
NEA+KAERI (TRANSX, JENDL-3.2)	–	–	–	–	–	–	2.594E-05	-1.23
JAERI (MVP, JENDL-3.3)	1.726E-05	-0.84	8.531E-06	-1.81	2.110E-07	21.98	2.600E-05	-1.01
KI (MCU-REA, MCUDAT)	1.700E-05	-2.35	8.039E-06	-7.48	2.265E-07	30.97	2.527E-05	-3.81

Table 4.6. ^{238}U reaction rates in MOX fuel pin (relative to the arbitrary reference GRS ENDF-VI.5 values)

Institution (code, library)	g=1	Dev. (%)	g=2	Dev. (%)	g=3	Dev. (%)	Total	Dev. (%)
Absorption rates								
KFKI (MCNP-4C, ENDF/B-VI.2)	1.285E-01	0.55	3.356E-01	2.68	6.574E-02	-0.41	5.299E-01	1.77
Purdue Univ. (HELIOS, ENDF/B-VI.3)	1.224E-01	-4.24	3.185E-01	-2.57	6.506E-02	-1.45	5.059E-01	-2.84
KAERI+NEA (MCNP-4B, ENDF/B-VI.5)	1.278E-01	-0.02	3.271E-01	0.05	6.601E-02	0.00	5.209E-01	0.03
SCK•CEN (MCNP-4C, ENDF/B-VI.5)	1.280E-01	0.15	3.343E-01	2.25	6.577E-02	-0.37	5.280E-01	1.41
KAERI (TRANSX, ENDF/B-VI.7)	1.277E-01	-0.13	3.448E-01	5.47	6.527E-02	-1.13	5.377E-01	3.26
KAERI+NEA (MCNP-4B, ENDF60)	1.282E-01	0.31	3.350E-01	2.47	6.582E-02	-0.29	5.290E-01	1.59
FRAMATOME-ANP (CASMO, ENDF/B-IV)	–	–	–	–	–	–	5.278E-01	1.37
SEA (MCNP-4C, ENDF/B-VI)	1.235E-01	-3.38	3.085E-01	-5.64	6.816E-02	3.25	5.001E-01	-3.96
GRS (MCNP-4C, ENDF/B-VI.5)	1.278E-01	0.00	3.269E-01	0.00	6.601E-02	0.00	5.207E-01	0.00
NEA+KAERI (TRANSX, ENDF/B-VI.5)	–	–	–	–	–	–	5.377E-01	3.26
KAERI+NEA (MCNP-4B, JEF-2.2)	1.259E-01	-1.52	3.282E-01	0.41	6.619E-02	0.26	5.203E-01	-0.08
GRS (MCNP-4C, JEF-2.2)	1.268E-01	-0.78	3.272E-01	0.10	6.612E-02	0.16	5.202E-01	-0.11
SCK•CEN (MCNP-4C, JEF-2.2)	1.261E-01	-1.32	3.276E-01	0.21	6.606E-02	0.07	5.198E-01	-0.18
KAERI+NEA (MCNP-4B, JENDL-3.2)	1.258E-01	-1.60	3.273E-01	0.14	6.591E-02	-0.16	5.190E-01	-0.32
GRS (MCNP-4C, JENDL-3.2)	1.256E-01	-1.73	3.266E-01	-0.09	6.598E-02	-0.05	5.182E-01	-0.49
JAERI (MVP, JENDL-3.2)	1.247E-01	-2.45	3.263E-01	-0.19	6.583E-02	-0.28	5.168E-01	-0.76
NEA+KAERI (TRANSX, JENDL-3.2)	–	–	–	–	–	–	5.357E-01	2.87
JAERI (MVP, JENDL-3.3)	1.260E-01	-1.43	3.265E-01	-0.13	6.590E-02	-0.17	5.184E-01	-0.45
KI (MCU-REA, MCUDAT)	1.285E-01	0.52	3.295E-01	0.81	6.541E-02	-0.92	5.236E-01	0.56
Fission rates								
KFKI (MCNP-4C, ENDF/B-VI.2)	6.554E-02	0.46	2.365E-05	3.22	2.725E-07	-0.50	6.556E-02	0.46
Purdue Univ. (HELIOS, ENDF/B-VI.3)	6.371E-02	-2.34	0.000E+00	-100.00	2.541E-07	-7.25	6.371E-02	-2.38
KAERI+NEA (MCNP-4B, ENDF/B-VI.5)	6.519E-02	-0.08	2.356E-05	2.81	2.739E-07	-0.03	6.522E-02	-0.08
SCK•CEN (MCNP-4C, ENDF/B-VI.5)	6.530E-02	0.09	2.390E-05	4.31	2.727E-07	-0.45	6.533E-02	0.09
KAERI (TRANSX, ENDF/B-VI.7)	6.516E-02	-0.13	2.359E-05	2.95	2.710E-07	-1.08	6.518E-02	-0.13
KAERI+NEA (MCNP-4B, ENDF60)	6.534E-02	0.16	2.449E-05	6.88	2.729E-07	-0.37	6.537E-02	0.16
FRAMATOME-ANP (CASMO, ENDF/B-IV)	–	–	–	–	–	–	7.114E-02	9.00
SEA (MCNP-4C, ENDF/B-VI)	6.353E-02	-2.63	2.196E-05	-4.18	2.848E-07	3.96	6.355E-02	-2.63
GRS (MCNP-4C, ENDF/B-VI.5)	6.524E-02	0.00	2.291E-05	0.00	2.739E-07	0.00	6.527E-02	0.00
NEA+KAERI (TRANSX, ENDF/B-VI.5)	–	–	–	–	–	–	6.518E-02	-0.13
KAERI+NEA (MCNP-4B, JEF-2.2)	6.390E-02	-2.06	2.275E-05	-0.72	2.745E-07	0.22	6.392E-02	-2.06
GRS (MCNP-4C, JEF-2.2)	6.484E-02	-0.62	2.322E-05	1.32	2.743E-07	0.15	6.486E-02	-0.62
SCK•CEN (MCNP-4C, JEF-2.2)	6.489E-02	-0.55	2.391E-05	4.36	2.739E-07	-0.02	6.491E-02	-0.54
KAERI+NEA (MCNP-4B, JENDL-3.2)	6.446E-02	-1.20	2.406E-05	5.01	2.734E-07	-0.21	6.449E-02	-1.20
GRS (MCNP-4C, JENDL-3.2)	6.442E-02	-1.26	2.376E-05	3.69	2.738E-07	-0.06	6.444E-02	-1.26
JAERI (MVP, JENDL-3.2)	6.429E-02	-1.46	2.373E-05	3.56	2.732E-07	-0.27	6.431E-02	-1.46
NEA+KAERI (TRANSX, JENDL-3.2)	–	–	–	–	–	–	6.434E-02	-1.43
JAERI (MVP, JENDL-3.3)	6.475E-02	-0.76	2.380E-05	3.86	2.735E-07	-0.16	6.477E-02	-0.76
KI (MCU-REA, MCUDAT)	6.493E-02	-0.48	–	–	–	–	6.493E-02	-0.52

Table 4.7. ^{239}Pu reaction rates in MOX fuel pin (relative to the arbitrary reference GRS ENDF-VI.5 values)

Institution (code, library)	g=1	Dev. (%)	g=2	Dev. (%)	g=3	Dev. (%)	Total	Dev. (%)
Absorption rates								
KFKI (MCNP-4C, ENDF/B-VI.2)	1.665E-02	0.51	1.175E-01	0.50	7.866E-01	-0.15	9.208E-01	-0.05
Purdue Univ. (HELIOS, ENDF/B-VI.3)	1.636E-02	-1.23	1.165E-01	-0.38	7.872E-01	-0.07	9.201E-01	-0.13
KAERI+NEA (MCNP-4B, ENDF/B-VI.5)	1.656E-02	-0.04	1.170E-01	0.03	7.878E-01	0.01	9.214E-01	0.01
SCK•CEN (MCNP-4C, ENDF/B-VI.5)	1.657E-02	0.05	1.170E-01	0.02	7.872E-01	-0.07	9.207E-01	-0.06
KAERI (TRANSX, ENDF/B-VI.7)	1.669E-02	0.76	1.173E-01	0.33	7.918E-01	0.51	9.258E-01	0.50
KAERI+NEA (MCNP-4B, ENDF60)	1.662E-02	0.34	1.174E-01	0.41	7.861E-01	-0.20	9.202E-01	-0.11
FRAMATOME-ANP (CASMO, ENDF/B-IV)	–	–	–	–	–	–	9.165E-01	-0.51
SEA (MCNP-4C, ENDF/B-VI)	1.607E-02	-2.99	1.075E-01	-8.10	7.668E-01	-2.66	8.906E-01	-3.33
GRS (MCNP-4C, ENDF/B-VI.5)	1.656E-02	0.00	1.170E-01	0.00	7.878E-01	0.00	9.213E-01	0.00
NEA+KAERI (TRANSX, ENDF/B-VI.5)	–	–	–	–	–	–	9.258E-01	0.50
KAERI+NEA (MCNP-4B, JEF-2.2)	1.672E-02	0.93	1.167E-01	-0.24	7.891E-01	0.17	9.225E-01	0.13
GRS (MCNP-4C, JEF-2.2)	1.683E-02	1.63	1.164E-01	-0.46	7.882E-01	0.06	9.215E-01	0.02
SCK•CEN (MCNP-4C, JEF-2.2)	1.667E-02	0.62	1.167E-01	-0.24	7.897E-01	0.24	9.230E-01	0.19
KAERI+NEA (MCNP-4B, JENDL-3.2)	1.658E-02	0.09	1.168E-01	-0.11	7.889E-01	0.15	9.224E-01	0.12
GRS (MCNP-4C, JENDL-3.2)	1.655E-02	-0.06	1.171E-01	0.15	7.877E-01	-0.01	9.214E-01	0.01
JAERI (MVP, JENDL-3.2)	1.653E-02	-0.21	1.168E-01	-0.13	7.898E-01	0.26	9.231E-01	0.20
NEA+KAERI (TRANSX, JENDL-3.2)	–	–	–	–	–	–	9.258E-01	0.49
JAERI (MVP, JENDL-3.3)	1.655E-02	-0.06	1.170E-01	-0.01	7.906E-01	0.36	9.241E-01	0.31
KI (MCU-REA, MCUDAT)	1.679E-02	1.34	1.206E-01	3.09	7.858E-01	-0.24	9.233E-01	0.22
Fission rates								
KFKI (MCNP-4C, ENDF/B-VI.2)	1.490E-02	0.50	6.820E-02	0.44	5.214E-01	-0.24	6.045E-01	-0.15
Purdue Univ. (HELIOS, ENDF/B-VI.3)	1.463E-02	-1.33	6.772E-02	-0.26	5.224E-01	-0.04	6.048E-01	-0.10
KAERI+NEA (MCNP-4B, ENDF/B-VI.5)	1.482E-02	-0.05	6.796E-02	0.09	5.226E-01	-0.01	6.054E-01	0.00
SCK•CEN (MCNP-4C, ENDF/B-VI.5)	1.483E-02	0.05	6.794E-02	0.06	5.218E-01	-0.16	6.046E-01	-0.13
KAERI (TRANSX, ENDF/B-VI.7)	1.491E-02	0.54	6.833E-02	0.63	5.241E-01	0.28	6.074E-01	0.32
KAERI+NEA (MCNP-4B, ENDF60)	1.488E-02	0.33	6.825E-02	0.52	5.213E-01	-0.27	6.044E-01	-0.17
FRAMATOME-ANP (CASMO, ENDF/B-IV)	–	–	–	–	–	–	6.017E-01	-0.60
SEA (MCNP-4C, ENDF/B-VI)	1.443E-02	-2.70	6.238E-02	-8.12	5.156E-01	-1.35	5.924E-01	-2.15
GRS (MCNP-4C, ENDF/B-VI.5)	1.483E-02	0.00	6.790E-02	0.00	5.227E-01	0.00	6.054E-01	0.00
NEA+KAERI (TRANSX, ENDF/B-VI.5)	–	–	–	–	–	–	6.074E-01	0.32
KAERI+NEA (MCNP-4B, JEF-2.2)	1.478E-02	-0.34	6.655E-02	-1.99	5.235E-01	0.15	6.048E-01	-0.10
GRS (MCNP-4C, JEF-2.2)	1.490E-02	0.46	6.636E-02	-2.27	5.229E-01	0.05	6.042E-01	-0.20
SCK•CEN (MCNP-4C, JEF-2.2)	1.474E-02	-0.59	6.650E-02	-2.05	5.235E-01	0.16	6.048E-01	-0.10
KAERI+NEA (MCNP-4B, JENDL-3.2)	1.472E-02	-0.70	6.773E-02	-0.24	5.231E-01	0.09	6.056E-01	0.03
GRS (MCNP-4C, JENDL-3.2)	1.470E-02	-0.84	6.795E-02	0.07	5.226E-01	-0.02	6.052E-01	-0.03
JAERI (MVP, JENDL-3.2)	1.468E-02	-1.02	6.777E-02	-0.19	5.236E-01	0.18	6.061E-01	0.11
NEA+KAERI (TRANSX, JENDL-3.2)	–	–	–	–	–	–	6.071E-01	0.28
JAERI (MVP, JENDL-3.3)	1.470E-02	-0.88	6.783E-02	-0.10	5.242E-01	0.29	6.067E-01	0.21
KI (MCU-REA, MCUDAT)	1.489E-02	0.41	6.931E-02	2.07	5.197E-01	-0.57	6.038E-01	-0.27

Table 4.8. ^{240}Pu reaction rates in MOX fuel pin (relative to the arbitrary reference GRS ENDF-VI.5 values)

Institution (code, library)	g=1	Dev. (%)	g=2	Dev. (%)	g=3	Dev. (%)	Total	Dev. (%)
Absorption rates								
KFKI (MCNP-4C, ENDF/B-VI.2)	2.113E-03	0.50	9.648E-03	0.33	1.755E-01	0.82	1.873E-01	0.79
Purdue Univ. (HELIOS, ENDF/B-VI.3)	2.068E-03	-1.64	9.876E-03	2.70	1.742E-01	0.08	1.862E-01	0.19
KAERI+NEA (MCNP-4B, ENDF/B-VI.5)	2.101E-03	-0.07	9.637E-03	0.22	1.748E-01	0.39	1.865E-01	0.38
SCK•CEN (MCNP-4C, ENDF/B-VI.5)	2.104E-03	0.06	9.687E-03	0.73	1.756E-01	0.88	1.874E-01	0.87
KAERI (TRANSX, ENDF/B-VI.7)	2.110E-03	0.37	1.022E-02	6.25	1.786E-01	2.58	1.909E-01	2.75
KAERI+NEA (MCNP-4B, ENDF60)	2.109E-03	0.31	9.669E-03	0.55	1.767E-01	1.49	1.885E-01	1.43
FRAMATOME-ANP (CASMO, ENDF/B-IV)	–	–	–	–	–	–	1.896E-01	2.06
SEA (MCNP-4C, ENDF/B-VI)	2.053E-03	-2.36	8.856E-03	-7.91	1.552E-01	-10.85	1.661E-01	-10.59
GRS (MCNP-4C, ENDF/B-VI.5)	2.103E-03	0.00	9.617E-03	0.00	1.741E-01	0.00	1.858E-01	0.00
NEA+KAERI (TRANSX, ENDF/B-VI.5)	–	–	–	–	–	–	1.909E-01	2.75
KAERI+NEA (MCNP-4B, JEF-2.2)	2.083E-03	-0.94	1.003E-02	4.34	1.728E-01	-0.75	1.849E-01	-0.49
GRS (MCNP-4C, JEF-2.2)	2.106E-03	0.18	1.004E-02	4.43	1.717E-01	-1.38	1.838E-01	-1.06
SCK•CEN (MCNP-4C, JEF-2.2)	2.107E-03	0.19	1.001E-02	4.07	1.737E-01	-0.23	1.858E-01	0.00
KAERI+NEA (MCNP-4B, JENDL-3.2)	2.102E-03	-0.02	1.016E-02	5.64	1.735E-01	-0.35	1.857E-01	-0.04
GRS (MCNP-4C, JENDL-3.2)	2.100E-03	-0.11	1.009E-02	4.91	1.739E-01	-0.09	1.861E-01	0.17
JAERI (MVP, JENDL-3.2)	2.096E-03	-0.32	1.014E-02	5.39	1.754E-01	0.78	1.877E-01	1.00
NEA+KAERI (TRANSX, JENDL-3.2)	–	–	–	–	–	–	1.913E-01	2.94
JAERI (MVP, JENDL-3.3)	2.070E-03	-1.56	9.684E-03	0.70	1.747E-01	0.39	1.865E-01	0.38
KI (MCU-REA, MCUDAT)	2.070E-03	-1.54	9.581E-03	-0.37	1.702E-01	-2.24	1.818E-01	-2.14
Fission rates								
KFKI (MCNP-4C, ENDF/B-VI.2)	1.642E-03	0.47	6.740E-05	-0.01	3.523E-05	0.79	1.744E-03	0.46
Purdue Univ. (HELIOS, ENDF/B-VI.3)	1.600E-03	-2.08	6.549E-05	-2.84	3.498E-05	0.07	1.700E-03	-2.06
KAERI+NEA (MCNP-4B, ENDF/B-VI.5)	1.632E-03	-0.09	6.602E-05	-2.05	3.509E-05	0.39	1.733E-03	-0.16
SCK•CEN (MCNP-4C, ENDF/B-VI.5)	1.635E-03	0.06	6.692E-05	-0.72	3.525E-05	0.85	1.737E-03	0.04
KAERI (TRANSX, ENDF/B-VI.7)	1.633E-03	-0.03	6.808E-05	1.00	3.583E-05	2.50	1.737E-03	0.06
KAERI+NEA (MCNP-4B, ENDF60)	1.638E-03	0.28	6.744E-05	0.06	3.546E-05	1.45	1.741E-03	0.30
FRAMATOME-ANP (CASMO, ENDF/B-IV)	–	–	–	–	–	–	1.902E-03	9.55
SEA (MCNP-4C, ENDF/B-VI)	1.607E-03	-1.65	6.197E-05	-8.07	3.130E-05	-10.47	1.700E-03	-2.07
GRS (MCNP-4C, ENDF/B-VI.5)	1.634E-03	0.00	6.740E-05	0.00	3.496E-05	0.00	1.736E-03	0.00
NEA+KAERI (TRANSX, ENDF/B-VI.5)	–	–	–	–	–	–	1.737E-03	0.06
KAERI+NEA (MCNP-4B, JEF-2.2)	1.586E-03	-2.95	1.567E-04	132.47	3.456E-05	-1.14	1.777E-03	2.35
GRS (MCNP-4C, JEF-2.2)	1.609E-03	-1.50	1.570E-04	132.89	3.435E-05	-1.74	1.801E-03	3.71
SCK•CEN (MCNP-4C, JEF-2.2)	1.609E-03	-1.52	1.571E-04	133.07	3.473E-05	-0.64	1.801E-03	3.72
KAERI+NEA (MCNP-4B, JENDL-3.2)	1.585E-03	-2.98	6.750E-05	0.15	3.268E-05	-6.50	1.685E-03	-2.93
GRS (MCNP-4C, JENDL-3.2)	1.584E-03	-3.04	6.717E-05	-0.34	3.277E-05	-6.26	1.684E-03	-3.00
JAERI (MVP, JENDL-3.2)	1.579E-03	-3.33	6.714E-05	-0.38	3.305E-05	-5.45	1.680E-03	-3.26
NEA+KAERI (TRANSX, JENDL-3.2)	–	–	–	–	–	–	1.685E-03	-2.97
JAERI (MVP, JENDL-3.3)	1.579E-03	-3.36	7.308E-05	8.43	4.543E-05	29.97	1.698E-03	-2.23
KI (MCU-REA, MCUDAT)	1.594E-03	-2.46	6.663E-05	-1.15	3.433E-05	-1.80	1.695E-03	-2.39

Table 4.9. ^{241}Pu reaction rates in MOX fuel pin (relative to the arbitrary reference GRS ENDF-VI.5 values)

Institution (code, library)	g=1	Dev. (%)	g=2	Dev. (%)	g=3	Dev. (%)	Total	Dev. (%)
Absorption rates								
KFKI (MCNP-4C, ENDF/B-VI.2)	6.979E-04	-0.49	8.050E-03	0.00	2.807E-02	0.87	3.681E-02	0.65
Purdue Univ. (HELIOS, ENDF/B-VI.3)	6.858E-04	-2.22	8.164E-03	1.42	2.814E-02	1.11	3.699E-02	1.12
KAERI+NEA (MCNP-4B, ENDF/B-VI.5)	7.013E-04	-0.02	8.066E-03	0.19	2.789E-02	0.23	3.666E-02	0.21
SCK•CEN (MCNP-4C, ENDF/B-VI.5)	6.946E-04	-0.96	8.000E-03	-0.63	2.809E-02	0.95	3.679E-02	0.57
KAERI (TRANSX, ENDF/B-VI.7)	7.084E-04	1.01	8.272E-03	2.75	2.772E-02	-0.37	3.670E-02	0.34
KAERI+NEA (MCNP-4B, ENDF60)	6.968E-04	-0.66	8.066E-03	0.19	2.809E-02	0.95	3.685E-02	0.75
FRAMATOME-ANP (CASMO, ENDF/B-IV)	–	–	–	–	–	–	3.703E-02	1.24
SEA (MCNP-4C, ENDF/B-VI)	6.708E-04	-4.36	7.307E-03	-9.23	2.922E-02	5.01	3.719E-02	1.68
GRS (MCNP-4C, ENDF/B-VI.5)	7.014E-04	0.00	8.050E-03	0.00	2.783E-02	0.00	3.658E-02	0.00
NEA+KAERI (TRANSX, ENDF/B-VI.5)	–	–	–	–	–	–	3.670E-02	0.34
KAERI+NEA (MCNP-4B, JEF-2.2)	7.377E-04	5.18	8.081E-03	0.38	2.835E-02	1.87	3.716E-02	1.60
GRS (MCNP-4C, JEF-2.2)	7.416E-04	5.74	8.040E-03	-0.13	2.827E-02	1.59	3.705E-02	1.28
SCK•CEN (MCNP-4C, JEF-2.2)	7.418E-04	5.77	8.052E-03	0.03	2.825E-02	1.52	3.704E-02	1.27
KAERI+NEA (MCNP-4B, JENDL-3.2)	7.173E-04	2.28	8.093E-03	0.53	2.783E-02	0.02	3.664E-02	0.17
GRS (MCNP-4C, JENDL-3.2)	7.161E-04	2.10	8.067E-03	0.21	2.781E-02	-0.06	3.659E-02	0.05
JAERI (MVP, JENDL-3.2)	7.156E-04	2.03	8.056E-03	0.07	2.780E-02	-0.11	3.657E-02	-0.03
NEA+KAERI (TRANSX, JENDL-3.2)	–	–	–	–	–	–	3.672E-02	0.39
JAERI (MVP, JENDL-3.3)	7.142E-04	1.83	8.063E-03	0.16	2.782E-02	-0.01	3.660E-02	0.06
KI (MCU-REA, MCUDAT)	7.007E-04	-0.10	8.399E-03	4.33	2.860E-02	2.77	3.770E-02	3.07
Fission rates								
KFKI (MCNP-4C, ENDF/B-VI.2)	6.309E-04	0.51	6.082E-03	1.76	2.098E-02	1.31	2.769E-02	1.39
Purdue Univ. (HELIOS, ENDF/B-VI.3)	6.228E-04	-0.78	6.188E-03	3.52	2.101E-02	1.44	2.782E-02	1.84
KAERI+NEA (MCNP-4B, ENDF/B-VI.5)	6.276E-04	-0.02	5.987E-03	0.17	2.075E-02	0.23	2.737E-02	0.21
SCK•CEN (MCNP-4C, ENDF/B-VI.5)	6.280E-04	0.04	6.048E-03	1.19	2.100E-02	1.39	2.767E-02	1.32
KAERI (TRANSX, ENDF/B-VI.7)	6.335E-04	0.92	6.155E-03	2.99	2.062E-02	-0.41	2.741E-02	0.36
KAERI+NEA (MCNP-4B, ENDF60)	6.298E-04	0.34	6.091E-03	1.92	2.100E-02	1.39	2.772E-02	1.48
FRAMATOME-ANP (CASMO, ENDF/B-IV)	–	–	–	–	–	–	2.778E-02	1.73
SEA (MCNP-4C, ENDF/B-VI)	6.071E-04	-3.29	5.526E-03	-7.54	2.181E-02	5.35	2.794E-02	2.31
GRS (MCNP-4C, ENDF/B-VI.5)	6.277E-04	0.00	5.977E-03	0.00	2.071E-02	0.00	2.731E-02	0.00
NEA+KAERI (TRANSX, ENDF/B-VI.5)	–	–	–	–	–	–	2.741E-02	0.36
KAERI+NEA (MCNP-4B, JEF-2.2)	6.244E-04	-0.52	6.104E-03	2.13	2.120E-02	2.37	2.793E-02	2.25
GRS (MCNP-4C, JEF-2.2)	6.279E-04	0.03	6.079E-03	1.70	2.114E-02	2.07	2.784E-02	1.94
SCK•CEN (MCNP-4C, JEF-2.2)	6.281E-04	0.06	6.092E-03	1.92	2.112E-02	2.01	2.784E-02	1.94
KAERI+NEA (MCNP-4B, JENDL-3.2)	6.332E-04	0.87	5.994E-03	0.28	2.071E-02	0.01	2.733E-02	0.08
GRS (MCNP-4C, JENDL-3.2)	6.321E-04	0.70	5.984E-03	0.12	2.069E-02	-0.06	2.731E-02	-0.01
JAERI (MVP, JENDL-3.2)	6.316E-04	0.62	5.972E-03	-0.08	2.068E-02	-0.15	2.728E-02	-0.12
NEA+KAERI (TRANSX, JENDL-3.2)	–	–	–	–	–	–	2.741E-02	0.35
JAERI (MVP, JENDL-3.3)	6.308E-04	0.50	5.978E-03	0.01	2.070E-02	-0.05	2.731E-02	-0.02
KI (MCU-REA, MCUDAT)	6.336E-04	0.94	6.140E-03	2.73	2.085E-02	0.68	2.762E-02	1.12

Table 4.10. ^{242}Pu reaction rates in MOX fuel pin (relative to the arbitrary reference GRS ENDF-VI.5 values)

Institution (code, library)	g=1	Dev. (%)	g=2	Dev. (%)	g=3	Dev. (%)	Total	Dev. (%)
Absorption rates								
KFKI (MCNP-4C, ENDF/B-VI.2)	4.400E-05	0.50	1.116E-04	0.90	2.336E-03	2.04	2.491E-03	1.97
Purdue Univ. (HELIOS, ENDF/B-VI.3)	4.297E-05	-1.83	1.084E-04	-2.02	2.292E-03	0.15	2.444E-03	0.02
KAERI+NEA (MCNP-4B, ENDF/B-VI.5)	4.375E-05	-0.07	1.119E-04	1.15	2.316E-03	1.17	2.471E-03	1.15
SCK•CEN (MCNP-4C, ENDF/B-VI.5)	4.380E-05	0.07	1.103E-04	-0.32	2.319E-03	1.31	2.473E-03	1.22
KAERI (TRANSX, ENDF/B-VI.7)	4.393E-05	0.36	1.099E-04	-0.63	2.283E-03	-0.25	2.437E-03	-0.25
KAERI+NEA (MCNP-4B, ENDF60)	4.391E-05	0.32	1.111E-04	0.39	2.368E-03	3.44	2.523E-03	3.25
FRAMATOME-ANP (CASMO, ENDF/B-IV)	–	–	–	–	–	–	2.200E-03	-9.94
SEA (MCNP-4C, ENDF/B-VI)	4.278E-05	-2.28	1.016E-04	-8.20	2.014E-03	-12.02	2.158E-03	-11.67
GRS (MCNP-4C, ENDF/B-VI.5)	4.378E-05	0.00	1.106E-04	0.00	2.289E-03	0.00	2.443E-03	0.00
NEA+KAERI (TRANSX, ENDF/B-VI.5)	–	–	–	–	–	–	2.437E-03	-0.25
KAERI+NEA (MCNP-4B, JEF-2.2)	4.372E-05	-0.12	1.170E-04	5.78	2.052E-03	-10.35	2.213E-03	-9.43
GRS (MCNP-4C, JEF-2.2)	4.422E-05	1.02	1.172E-04	5.94	2.014E-03	-12.03	2.175E-03	-10.98
SCK•CEN (MCNP-4C, JEF-2.2)	4.423E-05	1.03	1.172E-04	5.90	2.069E-03	-9.60	2.231E-03	-8.71
KAERI+NEA (MCNP-4B, JENDL-3.2)	4.391E-05	0.30	1.183E-04	6.92	2.077E-03	-9.24	2.240E-03	-8.34
GRS (MCNP-4C, JENDL-3.2)	4.386E-05	0.19	1.167E-04	5.47	2.031E-03	-11.26	2.192E-03	-10.29
JAERI (MVP, JENDL-3.2)	4.379E-05	0.02	1.166E-04	5.41	1.982E-03	-13.40	2.143E-03	-12.30
NEA+KAERI (TRANSX, JENDL-3.2)	–	–	–	–	–	–	2.195E-03	-10.16
JAERI (MVP, JENDL-3.3)	4.383E-05	0.13	1.095E-04	-1.02	1.985E-03	-13.28	2.138E-03	-12.48
KI (MCU-REA, MCUDAT)	4.256E-05	-2.78	1.145E-04	3.51	1.935E-03	-15.46	2.092E-03	-14.38
Fission rates								
KFKI (MCNP-4C, ENDF/B-VI.2)	3.342E-05	0.47	4.527E-07	0.78	2.864E-09	-0.58	3.388E-05	0.47
Purdue Univ. (HELIOS, ENDF/B-VI.3)	3.258E-05	-2.07	4.318E-07	-3.87	2.868E-09	-0.45	3.301E-05	-2.09
KAERI+NEA (MCNP-4B, ENDF/B-VI.5)	3.323E-05	-0.10	4.476E-07	-0.34	2.880E-09	-0.04	3.368E-05	-0.10
SCK•CEN (MCNP-4C, ENDF/B-VI.5)	3.328E-05	0.05	4.537E-07	1.00	2.866E-09	-0.52	3.374E-05	0.06
KAERI (TRANSX, ENDF/B-VI.7)	3.322E-05	-0.14	4.372E-07	-2.68	2.850E-09	-1.06	3.366E-05	-0.17
KAERI+NEA (MCNP-4B, ENDF60)	3.336E-05	0.27	4.498E-07	0.14	2.868E-09	-0.44	3.381E-05	0.27
FRAMATOME-ANP (CASMO, ENDF/B-IV)	–	–	–	–	–	–	3.620E-05	7.36
SEA (MCNP-4C, ENDF/B-VI)	3.276E-05	-1.51	4.122E-07	-8.24	3.010E-09	4.49	3.318E-05	-1.59
GRS (MCNP-4C, ENDF/B-VI.5)	3.327E-05	0.00	4.492E-07	0.00	2.881E-09	0.00	3.372E-05	0.00
NEA+KAERI (TRANSX, ENDF/B-VI.5)	–	–	–	–	–	–	3.366E-05	-0.17
KAERI+NEA (MCNP-4B, JEF-2.2)	3.241E-05	-2.58	4.647E-07	3.46	1.378E-06	X	3.425E-05	1.57
GRS (MCNP-4C, JEF-2.2)	3.290E-05	-1.09	4.650E-07	3.51	1.352E-06	X	3.472E-05	2.97
SCK•CEN (MCNP-4C, JEF-2.2)	3.289E-05	-1.12	4.676E-07	4.09	1.390E-06	X	3.475E-05	3.06
KAERI+NEA (MCNP-4B, JENDL-3.2)	3.230E-05	-2.90	3.359E-07	-25.22	1.690E-07	X	3.281E-05	-2.70
GRS (MCNP-4C, JENDL-3.2)	3.227E-05	-2.99	3.330E-07	-25.86	1.654E-07	X	3.277E-05	-2.81
JAERI (MVP, JENDL-3.2)	3.219E-05	-3.23	3.317E-07	-26.17	1.614E-07	X	3.269E-05	-3.06
NEA+KAERI (TRANSX, JENDL-3.2)	–	–	–	–	–	–	3.273E-05	-2.93
JAERI (MVP, JENDL-3.3)	3.224E-05	-3.08	2.843E-07	-36.70	1.815E-07	X	3.270E-05	-3.00
KI (MCU-REA, MCUDAT)	3.182E-05	-4.34	3.973E-07	-11.56	1.568E-07	X	3.239E-05	-3.95

Table 4.11. ^{241}Am reaction rates in MOX fuel pin (relative to the arbitrary reference GRS ENDF-VI.5 values)

Institution (code, library)	g=1	Dev. (%)	g=2	Dev. (%)	g=3	Dev. (%)	Total	Dev. (%)
Absorption rates								
KFKI (MCNP-4C, ENDF/B-VI.2)	1.291E-05	0.53	9.982E-05	0.50	6.797E-04	0.55	7.924E-04	0.54
Purdue Univ. (HELIOS, ENDF/B-VI.3)	1.436E-05	11.83	1.065E-04	7.19	6.766E-04	0.09	7.974E-04	1.18
KAERI+NEA (MCNP-4B, ENDF/B-VI.5)	1.284E-05	-0.02	9.940E-05	0.08	6.764E-04	0.06	7.886E-04	0.06
SCK•CEN (MCNP-4C, ENDF/B-VI.5)	1.285E-05	0.08	9.948E-05	0.16	6.795E-04	0.52	7.918E-04	0.46
KAERI (TRANSX, ENDF/B-VI.7)	1.295E-05	0.81	1.075E-04	8.23	6.767E-04	0.10	7.971E-04	1.14
KAERI+NEA (MCNP-4B, ENDF60)	1.289E-05	0.35	1.001E-04	0.80	6.786E-04	0.39	7.916E-04	0.44
FRAMATOME-ANP (CASMO, ENDF/B-IV)	–	–	–	–	–	–	8.104E-04	2.83
SEA (MCNP-4C, ENDF/B-VI)	1.242E-05	-3.32	9.098E-05	-8.40	6.220E-04	-7.98	7.254E-04	-7.96
GRS (MCNP-4C, ENDF/B-VI.5)	1.284E-05	0.00	9.932E-05	0.00	6.760E-04	0.00	7.881E-04	0.00
NEA+KAERI (TRANSX, ENDF/B-VI.5)	–	–	–	–	–	–	7.971E-04	1.14
KAERI+NEA (MCNP-4B, JEF-2.2)	1.411E-05	9.85	1.016E-04	2.35	7.026E-04	3.93	8.183E-04	3.83
GRS (MCNP-4C, JEF-2.2)	1.421E-05	10.61	1.013E-04	2.02	7.030E-04	4.00	8.186E-04	3.86
SCK•CEN (MCNP-4C, JEF-2.2)	1.421E-05	10.67	1.017E-04	2.41	7.081E-04	4.75	8.240E-04	4.55
KAERI+NEA (MCNP-4B, JENDL-3.2)	1.305E-05	1.62	1.031E-04	3.76	6.478E-04	-4.17	7.639E-04	-3.07
GRS (MCNP-4C, JENDL-3.2)	1.303E-05	1.46	1.031E-04	3.85	6.455E-04	-4.51	7.616E-04	-3.36
JAERI (MVP, JENDL-3.2)	1.302E-05	1.41	1.028E-04	3.51	6.493E-04	-3.95	7.651E-04	-2.92
NEA+KAERI (TRANSX, JENDL-3.2)	–	–	–	–	–	–	7.714E-04	-2.12
JAERI (MVP, JENDL-3.3)	1.363E-05	6.12	1.001E-04	0.81	7.193E-04	6.41	8.331E-04	5.70
KI (MCU-REA, MCUDAT)	1.389E-05	8.18	1.068E-04	7.57	7.371E-04	9.04	8.579E-04	8.86
Fission rates								
KFKI (MCNP-4C, ENDF/B-VI.2)	6.675E-06	0.47	7.920E-07	0.55	3.705E-06	0.59	1.117E-05	0.52
Purdue Univ. (HELIOS, ENDF/B-VI.3)	6.651E-06	0.10	8.331E-07	5.77	3.691E-06	0.21	1.118E-05	0.54
KAERI+NEA (MCNP-4B, ENDF/B-VI.5)	6.638E-06	-0.09	7.885E-07	0.10	3.687E-06	0.09	1.111E-05	-0.02
SCK•CEN (MCNP-4C, ENDF/B-VI.5)	6.648E-06	0.06	7.880E-07	0.03	3.705E-06	0.58	1.114E-05	0.23
KAERI (TRANSX, ENDF/B-VI.7)	6.626E-06	-0.28	8.409E-07	6.76	3.704E-06	0.56	1.117E-05	0.50
KAERI+NEA (MCNP-4B, ENDF60)	6.661E-06	0.25	7.956E-07	1.01	3.701E-06	0.48	1.116E-05	0.38
FRAMATOME-ANP (CASMO, ENDF/B-IV)	–	–	–	–	–	–	1.190E-05	7.06
SEA (MCNP-4C, ENDF/B-VI)	6.532E-06	-1.69	7.216E-07	-8.38	3.378E-06	-8.29	1.063E-05	-4.34
GRS (MCNP-4C, ENDF/B-VI.5)	6.644E-06	0.00	7.877E-07	0.00	3.683E-06	0.00	1.111E-05	0.00
NEA+KAERI (TRANSX, ENDF/B-VI.5)	–	–	–	–	–	–	1.117E-05	0.50
KAERI+NEA (MCNP-4B, JEF-2.2)	6.273E-06	-5.59	7.600E-07	-3.52	4.490E-06	21.90	1.152E-05	3.67
GRS (MCNP-4C, JEF-2.2)	6.378E-06	-4.01	7.586E-07	-3.69	4.497E-06	22.10	1.163E-05	4.67
SCK•CEN (MCNP-4C, JEF-2.2)	6.379E-06	-3.99	7.614E-07	-3.33	4.533E-06	23.07	1.167E-05	5.03
KAERI+NEA (MCNP-4B, JENDL-3.2)	6.479E-06	-2.49	7.002E-07	-11.11	3.502E-06	-4.91	1.068E-05	-3.90
GRS (MCNP-4C, JENDL-3.2)	6.472E-06	-2.59	7.014E-07	-10.95	3.488E-06	-5.31	1.066E-05	-4.08
JAERI (MVP, JENDL-3.2)	6.458E-06	-2.80	6.980E-07	-11.39	3.512E-06	-4.65	1.067E-05	-4.02
NEA+KAERI (TRANSX, JENDL-3.2)	–	–	–	–	–	–	1.071E-05	-3.60
JAERI (MVP, JENDL-3.3)	6.499E-06	-2.18	8.271E-07	5.00	3.855E-06	4.67	1.118E-05	0.60
KI (MCU-REA, MCUDAT)	6.941E-06	4.48	7.848E-07	-0.37	3.409E-06	-7.46	1.113E-05	0.17

Table 4.12. ^{235}U reaction rates in 3/0 UO_2 fuel pin (relative to the arbitrary reference GRS ENDF-VI.5 values)

Institution (code, library)	g=1	Dev. (%)	g=2	Dev. (%)	g=3	Dev. (%)	Total	Dev. (%)
Absorption rates								
KFKI (MCNP-4C, ENDF/B-VI.2)	1.634E-02	0.19	1.142E-01	-1.41	1.016E+00	-0.29	1.147E+00	-0.40
Purdue Univ. (HELIOS, ENDF/B-VI.3)	1.613E-02	-1.10	1.189E-01	2.68	1.018E+00	-0.11	1.153E+00	0.16
KAERI+NEA (MCNP-4B, ENDF/B-VI.5)	1.629E-02	-0.13	1.158E-01	0.02	1.019E+00	0.02	1.151E+00	0.01
SCK•CEN (MCNP-4C, ENDF/B-VI.5)	1.633E-02	0.10	1.140E-01	-1.58	1.016E+00	-0.27	1.147E+00	-0.40
KAERI (TRANSX, ENDF/B-VI.7)	1.640E-02	0.55	1.183E-01	2.16	1.018E+00	-0.07	1.153E+00	0.16
KAERI+NEA (MCNP-4B, ENDF60)	1.630E-02	-0.06	1.142E-01	-1.42	1.016E+00	-0.26	1.147E+00	-0.38
FRAMATOME-ANP (CASMO, ENDF/B-IV)	–	–	–	–	–	–	1.146E+00	-0.50
SEA (MCNP-4C, ENDF/B-VI)	1.877E-02	15.05	1.251E-01	8.02	9.973E-01	-2.15	1.141E+00	-0.91
GRS (MCNP-4C, ENDF/B-VI.5)	1.631E-02	0.00	1.158E-01	0.00	1.019E+00	0.00	1.151E+00	0.00
NEA+KAERI (TRANSX, ENDF/B-VI.5)	–	–	–	–	–	–	1.153E+00	0.16
KAERI+NEA (MCNP-4B, JEF-2.2)	1.617E-02	-0.85	1.133E-01	-2.18	1.018E+00	-0.13	1.147E+00	-0.34
GRS (MCNP-4C, JEF-2.2)	1.616E-02	-0.94	1.132E-01	-2.22	1.018E+00	-0.12	1.147E+00	-0.34
SCK•CEN (MCNP-4C, JEF-2.2)	1.614E-02	-1.07	1.133E-01	-2.18	1.018E+00	-0.09	1.148E+00	-0.32
KAERI+NEA (MCNP-4B, JENDL-3.2)	1.610E-02	-1.31	1.127E-01	-2.66	1.019E+00	0.00	1.148E+00	-0.29
GRS (MCNP-4C, JENDL-3.2)	1.608E-02	-1.43	1.125E-01	-2.89	1.019E+00	0.00	1.148E+00	-0.31
JAERI (MVP, JENDL-3.2)	1.606E-02	-1.54	1.129E-01	-2.49	1.020E+00	0.04	1.149E+00	-0.24
NEA+KAERI (TRANSX, JENDL-3.2)	–	–	–	–	–	–	1.150E+00	-0.13
JAERI (MVP, JENDL-3.3)	1.631E-02	0.02	1.158E-01	0.01	1.020E+00	0.09	1.152E+00	0.08
KI (MCU-REA, MCUDAT)	1.639E-02	0.47	1.150E-01	-0.73	1.017E+00	-0.19	1.149E+00	-0.23
Fission rates								
KFKI (MCNP-4C, ENDF/B-VI.2)	1.384E-02	0.18	7.343E-02	1.67	8.658E-01	-0.15	9.531E-01	-0.01
Purdue Univ. (HELIOS, ENDF/B-VI.3)	1.369E-02	-0.91	7.344E-02	1.68	8.673E-01	0.02	9.545E-01	0.14
KAERI+NEA (MCNP-4B, ENDF/B-VI.5)	1.380E-02	-0.13	7.219E-02	-0.04	8.673E-01	0.01	9.533E-01	0.01
SCK•CEN (MCNP-4C, ENDF/B-VI.5)	1.383E-02	0.09	7.335E-02	1.57	8.660E-01	-0.13	9.532E-01	0.00
KAERI (TRANSX, ENDF/B-VI.7)	1.388E-02	0.42	7.323E-02	1.39	8.665E-01	-0.08	9.536E-01	0.04
KAERI+NEA (MCNP-4B, ENDF60)	1.381E-02	-0.07	7.341E-02	1.64	8.661E-01	-0.12	9.533E-01	0.01
FRAMATOME-ANP (CASMO, ENDF/B-IV)	–	–	–	–	–	–	9.471E-01	-0.64
SEA (MCNP-4C, ENDF/B-VI)	1.592E-02	15.20	8.052E-02	11.49	8.493E-01	-2.05	9.458E-01	-0.77
GRS (MCNP-4C, ENDF/B-VI.5)	1.382E-02	0.00	7.222E-02	0.00	8.671E-01	0.00	9.532E-01	0.00
NEA+KAERI (TRANSX, ENDF/B-VI.5)	–	–	–	–	–	–	9.536E-01	0.04
KAERI+NEA (MCNP-4B, JEF-2.2)	1.369E-02	-0.93	7.312E-02	1.25	8.667E-01	-0.05	9.535E-01	0.03
GRS (MCNP-4C, JEF-2.2)	1.368E-02	-1.01	7.311E-02	1.23	8.668E-01	-0.04	9.536E-01	0.04
SCK•CEN (MCNP-4C, JEF-2.2)	1.366E-02	-1.15	7.311E-02	1.23	8.669E-01	-0.02	9.537E-01	0.06
KAERI+NEA (MCNP-4B, JENDL-3.2)	1.359E-02	-1.68	7.271E-02	0.67	8.685E-01	0.15	9.548E-01	0.17
GRS (MCNP-4C, JENDL-3.2)	1.358E-02	-1.76	7.247E-02	0.34	8.685E-01	0.16	9.546E-01	0.15
JAERI (MVP, JENDL-3.2)	1.355E-02	-1.93	7.262E-02	0.55	8.688E-01	0.19	9.550E-01	0.19
NEA+KAERI (TRANSX, JENDL-3.2)	–	–	–	–	–	–	9.553E-01	0.22
JAERI (MVP, JENDL-3.3)	1.371E-02	-0.79	7.221E-02	-0.02	8.678E-01	0.08	9.537E-01	0.06
KI (MCU-REA, MCUDAT)	1.386E-02	0.31	7.328E-02	1.46	8.657E-01	-0.16	9.530E-01	-0.02

Table 4.13. ^{238}U reaction rates in 3/0 UO_2 fuel pin (relative to the arbitrary reference GRS ENDF-VI.5 values)

Institution (code, library)	g=1	Dev. (%)	g=2	Dev. (%)	g=3	Dev. (%)	Total	Dev. (%)
Absorption rates								
KFKI (MCNP-4C, ENDF/B-VI.2)	9.159E-02	0.26	2.514E-01	2.64	1.323E-01	-0.36	4.753E-01	1.33
Purdue Univ. (HELIOS, ENDF/B-VI.3)	8.748E-02	-4.24	2.413E-01	-1.49	1.314E-01	-1.00	4.602E-01	-1.89
KAERI+NEA (MCNP-4B, ENDF/B-VI.5)	9.121E-02	-0.15	2.455E-01	0.22	1.328E-01	0.05	4.695E-01	0.10
SCK•CEN (MCNP-4C, ENDF/B-VI.5)	9.148E-02	0.13	2.516E-01	2.71	1.323E-01	-0.36	4.753E-01	1.34
KAERI (TRANSX, ENDF/B-VI.7)	9.082E-02	-0.58	2.605E-01	6.37	1.328E-01	0.04	4.841E-01	3.23
KAERI+NEA (MCNP-4B, ENDF60)	9.126E-02	-0.11	2.516E-01	2.72	1.323E-01	-0.33	4.751E-01	1.30
FRAMATOME-ANP (CASMO, ENDF/B-IV)	–	–	–	–	–	–	4.822E-01	2.82
SEA (MCNP-4C, ENDF/B-VI)	1.052E-01	15.17	2.772E-01	13.17	1.289E-01	-2.87	5.115E-01	9.06
GRS (MCNP-4C, ENDF/B-VI.5)	9.136E-02	0.00	2.449E-01	0.00	1.327E-01	0.00	4.690E-01	0.00
NEA+KAERI (TRANSX, ENDF/B-VI.5)	–	–	–	–	–	–	4.841E-01	3.23
KAERI+NEA (MCNP-4B, JEF-2.2)	9.062E-02	-0.80	2.447E-01	-0.10	1.326E-01	-0.06	4.680E-01	-0.22
GRS (MCNP-4C, JEF-2.2)	9.053E-02	-0.90	2.446E-01	-0.14	1.327E-01	0.01	4.679E-01	-0.25
SCK•CEN (MCNP-4C, JEF-2.2)	8.978E-02	-1.73	2.451E-01	0.06	1.328E-01	0.08	4.677E-01	-0.29
KAERI+NEA (MCNP-4B, JENDL-3.2)	8.873E-02	-2.87	2.454E-01	0.18	1.324E-01	-0.24	4.665E-01	-0.53
GRS (MCNP-4C, JENDL-3.2)	8.887E-02	-2.72	2.449E-01	-0.01	1.324E-01	-0.25	4.662E-01	-0.61
JAERI (MVP, JENDL-3.2)	8.796E-02	-3.71	2.445E-01	-0.16	1.325E-01	-0.18	4.650E-01	-0.86
NEA+KAERI (TRANSX, JENDL-3.2)	–	–	–	–	–	–	4.807E-01	2.50
JAERI (MVP, JENDL-3.3)	8.996E-02	-1.53	2.448E-01	-0.05	1.329E-01	0.15	4.677E-01	-0.28
KI (MCU-REA, MCUDAT)	9.226E-02	0.99	2.471E-01	0.89	1.312E-01	-1.13	4.707E-01	0.35
Fission rates								
KFKI (MCNP-4C, ENDF/B-VI.2)	4.690E-02	0.20	1.686E-05	-0.17	5.619E-07	-0.40	4.692E-02	0.20
Purdue Univ. (HELIOS, ENDF/B-VI.3)	4.552E-02	-2.74	0.000E+00	-100.00	5.463E-07	-3.16	4.552E-02	-2.78
KAERI+NEA (MCNP-4B, ENDF/B-VI.5)	4.673E-02	-0.17	1.692E-05	0.20	5.643E-07	0.04	4.675E-02	-0.17
SCK•CEN (MCNP-4C, ENDF/B-VI.5)	4.680E-02	-0.01	1.708E-05	1.17	5.619E-07	-0.39	4.682E-02	-0.01
KAERI (TRANSX, ENDF/B-VI.7)	4.640E-02	-0.86	1.689E-05	0.01	5.645E-07	0.08	4.642E-02	-0.86
KAERI+NEA (MCNP-4B, ENDF60)	4.670E-02	-0.23	1.714E-05	1.53	5.620E-07	-0.37	4.672E-02	-0.23
FRAMATOME-ANP (CASMO, ENDF/B-IV)	–	–	–	–	–	–	5.290E-02	12.97
SEA (MCNP-4C, ENDF/B-VI)	5.419E-02	15.78	1.888E-05	11.82	5.475E-07	-2.94	5.419E-02	15.74
GRS (MCNP-4C, ENDF/B-VI.5)	4.681E-02	0.00	1.689E-05	0.00	5.641E-07	0.00	4.682E-02	0.00
NEA+KAERI (TRANSX, ENDF/B-VI.5)	–	–	–	–	–	–	4.642E-02	-0.86
KAERI+NEA (MCNP-4B, JEF-2.2)	4.648E-02	-0.70	1.691E-05	0.13	5.637E-07	-0.08	4.650E-02	-0.70
GRS (MCNP-4C, JEF-2.2)	4.642E-02	-0.82	1.699E-05	0.60	5.641E-07	0.01	4.644E-02	-0.82
SCK•CEN (MCNP-4C, JEF-2.2)	4.627E-02	-1.14	1.784E-05	5.68	5.643E-07	0.04	4.629E-02	-1.14
KAERI+NEA (MCNP-4B, JENDL-3.2)	4.523E-02	-3.37	1.730E-05	2.47	5.627E-07	-0.26	4.525E-02	-3.37
GRS (MCNP-4C, JENDL-3.2)	4.541E-02	-2.99	1.680E-05	-0.51	5.626E-07	-0.26	4.542E-02	-2.99
JAERI (MVP, JENDL-3.2)	4.503E-02	-3.80	1.687E-05	-0.12	5.631E-07	-0.18	4.505E-02	-3.80
NEA+KAERI (TRANSX, JENDL-3.2)	–	–	–	–	–	–	4.474E-02	-4.45
JAERI (MVP, JENDL-3.3)	4.626E-02	-1.17	1.691E-05	0.13	5.650E-07	0.15	4.628E-02	-1.17
KI (MCU-REA, MCUDAT)	4.700E-02	0.41	–	–	–	–	4.700E-02	0.37

Table 4.14. ^{235}U reaction rates in 4/0 UO_2 fuel pin (relative to the arbitrary reference GRS ENDF-VI.5 values)

Institution (code, library)	g=1	Dev. (%)	g=2	Dev. (%)	g=3	Dev. (%)	Total	Dev. (%)
Absorption rates								
KFKI (MCNP-4C, ENDF/B-VI.2)	2.508E-02	0.23	1.663E-01	-1.82	9.578E-01	-0.43	1.149E+00	-0.60
Purdue Univ. (HELIOS, ENDF/B-VI.3)	2.475E-02	-1.08	1.730E-01	2.15	9.607E-01	-0.13	1.158E+00	0.19
KAERI+NEA (MCNP-4B, ENDF/B-VI.5)	2.507E-02	0.20	1.697E-01	0.18	9.617E-01	-0.02	1.156E+00	0.01
SCK•CEN (MCNP-4C, ENDF/B-VI.5)	2.499E-02	-0.10	1.663E-01	-1.85	9.586E-01	-0.34	1.150E+00	-0.56
KAERI (TRANSX, ENDF/B-VI.7)	2.520E-02	0.74	1.730E-01	2.12	9.606E-01	-0.14	1.159E+00	0.21
KAERI+NEA (MCNP-4B, ENDF60)	2.498E-02	-0.15	1.662E-01	-1.86	9.587E-01	-0.34	1.150E+00	-0.55
FRAMATOME-ANP (CASMO, ENDF/B-IV)	–	–	–	–	–	–	1.150E+00	-0.57
SEA (MCNP-4C, ENDF/B-VI)	2.661E-02	6.36	1.646E-01	-2.84	9.689E-01	0.73	1.160E+00	0.34
GRS (MCNP-4C, ENDF/B-VI.5)	2.502E-02	0.00	1.694E-01	0.00	9.619E-01	0.00	1.156E+00	0.00
NEA+KAERI (TRANSX, ENDF/B-VI.5)	–	–	–	–	–	–	1.159E+00	0.21
KAERI+NEA (MCNP-4B, JEF-2.2)	2.477E-02	-1.01	1.656E-01	-2.25	9.601E-01	-0.19	1.150E+00	-0.51
GRS (MCNP-4C, JEF-2.2)	2.475E-02	-1.09	1.652E-01	-2.49	9.605E-01	-0.14	1.150E+00	-0.51
SCK•CEN (MCNP-4C, JEF-2.2)	2.476E-02	-1.02	1.654E-01	-2.34	9.602E-01	-0.18	1.150E+00	-0.52
KAERI+NEA (MCNP-4B, JENDL-3.2)	2.478E-02	-0.97	1.648E-01	-2.74	9.611E-01	-0.09	1.151E+00	-0.50
GRS (MCNP-4C, JENDL-3.2)	2.466E-02	-1.45	1.640E-01	-3.21	9.621E-01	0.02	1.151E+00	-0.49
JAERI (MVP, JENDL-3.2)	2.460E-02	-1.68	1.645E-01	-2.88	9.624E-01	0.05	1.152E+00	-0.42
NEA+KAERI (TRANSX, JENDL-3.2)	–	–	–	–	–	–	1.153E+00	-0.29
JAERI (MVP, JENDL-3.3)	2.502E-02	-0.01	1.691E-01	-0.19	9.630E-01	0.11	1.157E+00	0.07
KI (MCU-REA, MCUDAT)	2.516E-02	0.56	1.681E-01	-0.76	9.589E-01	-0.31	1.152E+00	-0.35
Fission rates								
KFKI (MCNP-4C, ENDF/B-VI.2)	2.119E-02	0.23	1.075E-01	1.29	8.152E-01	-0.19	9.439E-01	-0.01
Purdue Univ. (HELIOS, ENDF/B-VI.3)	2.096E-02	-0.90	1.074E-01	1.27	8.170E-01	0.04	9.454E-01	0.16
KAERI+NEA (MCNP-4B, ENDF/B-VI.5)	2.119E-02	0.21	1.062E-01	0.11	8.165E-01	-0.03	9.439E-01	-0.01
SCK•CEN (MCNP-4C, ENDF/B-VI.5)	2.112E-02	-0.11	1.075E-01	1.34	8.155E-01	-0.15	9.441E-01	0.02
KAERI (TRANSX, ENDF/B-VI.7)	2.128E-02	0.62	1.076E-01	1.40	8.155E-01	-0.15	9.443E-01	0.04
KAERI+NEA (MCNP-4B, ENDF60)	2.111E-02	-0.15	1.074E-01	1.26	8.155E-01	-0.15	9.440E-01	0.01
FRAMATOME-ANP (CASMO, ENDF/B-IV)	–	–	–	–	–	–	9.373E-01	-0.70
SEA (MCNP-4C, ENDF/B-VI)	2.257E-02	6.73	1.064E-01	0.25	8.247E-01	0.98	9.534E-01	1.00
GRS (MCNP-4C, ENDF/B-VI.5)	2.115E-02	0.00	1.061E-01	0.00	8.167E-01	0.00	9.439E-01	0.00
NEA+KAERI (TRANSX, ENDF/B-VI.5)	–	–	–	–	–	–	9.443E-01	0.04
KAERI+NEA (MCNP-4B, JEF-2.2)	2.092E-02	-1.08	1.074E-01	1.24	8.160E-01	-0.08	9.443E-01	0.04
GRS (MCNP-4C, JEF-2.2)	2.090E-02	-1.16	1.071E-01	1.00	8.164E-01	-0.03	9.445E-01	0.05
SCK•CEN (MCNP-4C, JEF-2.2)	2.091E-02	-1.10	1.074E-01	1.21	8.160E-01	-0.08	9.443E-01	0.04
KAERI+NEA (MCNP-4B, JENDL-3.2)	2.086E-02	-1.33	1.067E-01	0.62	8.177E-01	0.12	9.453E-01	0.14
GRS (MCNP-4C, JENDL-3.2)	2.076E-02	-1.81	1.062E-01	0.15	8.186E-01	0.24	9.456E-01	0.18
JAERI (MVP, JENDL-3.2)	2.071E-02	-2.07	1.063E-01	0.23	8.188E-01	0.26	9.458E-01	0.20
NEA+KAERI (TRANSX, JENDL-3.2)	–	–	–	–	–	–	9.460E-01	0.22
JAERI (MVP, JENDL-3.3)	2.097E-02	-0.82	1.059E-01	-0.19	8.175E-01	0.10	9.444E-01	0.05
KI (MCU-REA, MCUDAT)	2.124E-02	0.47	1.076E-01	1.39	8.145E-01	-0.27	9.433E-01	-0.07

Table 4.15. ^{238}U reaction rates in 4/0 UO_2 fuel pin (relative to the arbitrary reference GRS ENDF-VI.5 values)

Institution (code, library)	g=1	Dev. (%)	g=2	Dev. (%)	g=3	Dev. (%)	Total	Dev. (%)
Absorption rates								
KFKI (MCNP-4C, ENDF/B-VI.2)	1.127E-01	0.25	2.945E-01	2.60	1.059E-01	-0.47	5.131E-01	1.44
Purdue Univ. (HELIOS, ENDF/B-VI.3)	1.077E-01	-4.17	2.791E-01	-2.76	1.050E-01	-1.29	4.918E-01	-2.77
KAERI+NEA (MCNP-4B, ENDF/B-VI.5)	1.126E-01	0.16	2.884E-01	0.50	1.064E-01	0.01	5.075E-01	0.32
SCK•CEN (MCNP-4C, ENDF/B-VI.5)	1.123E-01	-0.15	2.939E-01	2.40	1.059E-01	-0.44	5.121E-01	1.23
KAERI (TRANSX, ENDF/B-VI.7)	1.118E-01	-0.55	3.034E-01	5.70	1.063E-01	-0.11	5.215E-01	3.09
KAERI+NEA (MCNP-4B, ENDF60)	1.123E-01	-0.11	2.941E-01	2.47	1.060E-01	-0.40	5.124E-01	1.29
FRAMATOME-ANP (CASMO, ENDF/B-IV)	–	–	–	–	–	–	5.167E-01	2.15
SEA (MCNP-4C, ENDF/B-VI)	1.210E-01	7.67	2.920E-01	1.75	1.051E-01	-1.27	5.181E-01	2.42
GRS (MCNP-4C, ENDF/B-VI.5)	1.124E-01	0.00	2.870E-01	0.00	1.064E-01	0.00	5.058E-01	0.00
NEA+KAERI (TRANSX, ENDF/B-VI.5)	–	–	–	–	–	–	5.215E-01	3.09
KAERI+NEA (MCNP-4B, JEF-2.2)	1.114E-01	-0.90	2.879E-01	0.31	1.062E-01	-0.24	5.055E-01	-0.08
GRS (MCNP-4C, JEF-2.2)	1.113E-01	-1.02	2.871E-01	0.04	1.063E-01	-0.10	5.047E-01	-0.23
SCK•CEN (MCNP-4C, JEF-2.2)	1.107E-01	-1.51	2.876E-01	0.21	1.063E-01	-0.10	5.046E-01	-0.24
KAERI+NEA (MCNP-4B, JENDL-3.2)	1.100E-01	-2.17	2.878E-01	0.28	1.061E-01	-0.28	5.039E-01	-0.39
GRS (MCNP-4C, JENDL-3.2)	1.093E-01	-2.73	2.875E-01	0.17	1.062E-01	-0.24	5.030E-01	-0.56
JAERI (MVP, JENDL-3.2)	1.083E-01	-3.68	2.863E-01	-0.25	1.062E-01	-0.20	5.008E-01	-1.00
NEA+KAERI (TRANSX, JENDL-3.2)	–	–	–	–	–	–	5.186E-01	2.51
JAERI (MVP, JENDL-3.3)	1.108E-01	-1.46	2.870E-01	-0.02	1.066E-01	0.16	5.043E-01	-0.30
KI (MCU-REA, MCUDAT)	1.138E-01	1.21	2.906E-01	1.23	1.050E-01	-1.28	5.094E-01	0.71
Fission rates								
KFKI (MCNP-4C, ENDF/B-VI.2)	5.614E-02	0.17	2.111E-05	-0.36	4.465E-07	-0.47	5.615E-02	0.16
Purdue Univ. (HELIOS, ENDF/B-VI.3)	5.458E-02	-2.60	0.000E+00	-100.00	4.285E-07	-4.49	5.458E-02	-2.64
KAERI+NEA (MCNP-4B, ENDF/B-VI.5)	5.612E-02	0.15	2.145E-05	1.25	4.486E-07	0.00	5.614E-02	0.15
SCK•CEN (MCNP-4C, ENDF/B-VI.5)	5.588E-02	-0.28	2.103E-05	-0.74	4.464E-07	-0.48	5.590E-02	-0.28
KAERI (TRANSX, ENDF/B-VI.7)	5.566E-02	-0.67	2.099E-05	-0.92	4.484E-07	-0.04	5.568E-02	-0.67
KAERI+NEA (MCNP-4B, ENDF60)	5.594E-02	-0.18	2.067E-05	-2.43	4.466E-07	-0.45	5.596E-02	-0.18
FRAMATOME-ANP (CASMO, ENDF/B-IV)	–	–	–	–	–	–	6.271E-02	11.87
SEA (MCNP-4C, ENDF/B-VI)	4.656E-02	-16.91	2.116E-05	-0.13	4.438E-07	-1.06	4.658E-02	-16.90
GRS (MCNP-4C, ENDF/B-VI.5)	5.604E-02	0.00	2.118E-05	0.00	4.486E-07	0.00	5.606E-02	0.00
NEA+KAERI (TRANSX, ENDF/B-VI.5)	–	–	–	–	–	–	5.568E-02	-0.67
KAERI+NEA (MCNP-4B, JEF-2.2)	5.566E-02	-0.68	2.106E-05	-0.58	4.474E-07	-0.25	5.568E-02	-0.68
GRS (MCNP-4C, JEF-2.2)	5.552E-02	-0.92	2.086E-05	-1.51	4.481E-07	-0.11	5.554E-02	-0.92
SCK•CEN (MCNP-4C, JEF-2.2)	5.568E-02	-0.64	2.104E-05	-0.70	4.480E-07	-0.14	5.570E-02	-0.64
KAERI+NEA (MCNP-4B, JENDL-3.2)	5.471E-02	-2.37	2.147E-05	1.35	4.472E-07	-0.31	5.473E-02	-2.37
GRS (MCNP-4C, JENDL-3.2)	5.435E-02	-3.02	2.111E-05	-0.36	4.475E-07	-0.25	5.437E-02	-3.02
JAERI (MVP, JENDL-3.2)	5.414E-02	-3.38	2.099E-05	-0.94	4.477E-07	-0.20	5.416E-02	-3.38
NEA+KAERI (TRANSX, JENDL-3.2)	–	–	–	–	–	–	5.402E-02	-3.63
JAERI (MVP, JENDL-3.3)	5.561E-02	-0.77	2.105E-05	-0.64	4.493E-07	0.16	5.563E-02	-0.77
KI (MCU-REA, MCUDAT)	5.668E-02	1.14	–	–	–	–	5.668E-02	1.10

Table 4.16. k_{eff} values of core calculations

Institution	Code used	Library used	k_{eff}	Statistical error (1σ)	Deviation (%)	Comments
FRAMATOME-ANP	TORT-2.7.3	ENDF/B-IV	0.99719	–	-0.28	S_8P_0 (5 groups)
		ENDF/B-IV	0.99438	–	-0.56	S_2P_0 (5 groups)
KAERI	DANTSYS-3.0	ENDF/B-VI.7	0.99659	–	-0.34	S_8P_3 (35 groups)
NEA+KAERI	TORT-3.2	ENDF/B-VI.5	0.99549	–	-0.45	S_8P_3 (35 groups)
		JENDL-3.2	1.00511	–	0.51	S_8P_3 (35 groups)
Purdue Univ.	PARCS-2.1	ENDF/B-VI.3	1.00093	–	0.09	(8 groups)
FRAMATOME-ANP	MOCA	ENDF/B-IV	1.00110	0.00007	0.11	5 groups, histories?
JAERI	MVP	JENDL-3.2	1.00500	0.000055	0.50	Histories: 199 million
		JENDL-3.3	1.00056	0.000054	0.06	Histories: 199 million
SCK•CEN	MCNP-4C	ENDF/B-VI.5	1.00062	0.00004	0.06	Histories: 350 million
		JEF-2.2	1.00662	0.00004	0.66	Histories: 350 million
KAERI+NEA	MCNP-4B	ENDF60	1.00036	0.00014	0.04	Histories: 50 million
		ENDF60	1.00046	0.00007	0.05	Histories: 200 million
		ENDF60	1.00056	0.00006	0.06	Histories: 300 million
		ENDF/B-VI.5	1.00199	0.00007	0.20	Histories: 200 million
		JENDL-3.2	1.01014	0.00007	1.01	Histories: 200 million
		JEF-2.2	1.00747	0.00007	0.75	Histories: 200 million
KFKI	MCNP-4C	ENDF/B-VI.2	0.99880	0.00013	-0.12	Histories: 37 million
KI	MCU-REA	MCUDAT	0.99946	0.00015	-0.05	Histories: 40 million
GRS	MCNP-4C	ENDF/B-VI.5	0.99794	0.00012	-0.21	Histories: 40 million
		JENDL-3.2	1.00369	0.00012	0.37	Histories: 40 million
		JEF-2.2	1.00275	0.00012	0.28	Histories: 40 million
SEA	MCNP-4C	ENDF/B-VI	1.00028	0.00012	0.03	Histories: 40 million (60 million for MOX zone)

Table 4.17. Normalised experimental pin power values

Pin type	MOX		4/0 UO_2		3/0 UO_2	
Pin position	(-27,-12)	(-22,-2)	(-15,+2)	(-13,-12)	(-11,+2)	(-6,-6)
Pin number	325	240	131	115	74	30
Axial position (cm)	Measured fission rates (normalised to 1)					
110	0.0333	0.0322	0.0321	0.0323	0.0322	0.0324
112	0.0356	0.0366	0.0363	0.0358	0.0366	0.0364
114	0.0399	0.0395*	0.0404	0.0402	0.0399	0.0405
116	0.0438	0.0424	0.0441	0.0444	0.0441	0.0440
118	0.0466	0.0478	0.0477	0.0472	0.0481	0.0477
120	0.0500	0.0507	0.0504	0.0503	0.0500	0.0505
122	0.0527	0.0516	0.0531	0.0527	0.0528	0.0524
124	0.0548	0.0545	0.0542	0.0544	0.0550	0.0546
126	0.0558	0.0559	0.0564	0.0557	0.0563	0.0554
128	0.0557	0.0558	0.0572	0.0564	0.0563	0.0567
130	0.0574	0.0567	0.0568	0.0564	0.0571	0.0562
132	0.0567*	0.0578	0.0565	0.0572	0.0565	0.0569
134	0.0559	0.0564	0.0562	0.0561	0.0560	0.0559
136	0.0548	0.0560	0.0548	0.0555	0.0546	0.0545
138	0.0529	0.0533	0.0530	0.0524	0.0526	0.0524
140	0.0506	0.0508	0.0504	0.0506	0.0503	0.0504
142	0.0481	0.0477	0.0477	0.0476	0.0476	0.0474
144	0.0438	0.0445	0.0439	0.0446	0.0442	0.0446
146	0.0411	0.0412	0.0403	0.0413	0.0409	0.0407
148	0.0375	0.0366*	0.0365	0.0366	0.0366	0.0369
150	0.0331	0.0320	0.0321	0.0321	0.0325	0.0337

* Interpolated values.

Table 4.18. FRAMATOME-ANP axial pin power results and [C/E]-1 values (TORT, ENDF/B-IV)

Pin	MOX (-27,-12)		MOX (-22,-2)		4/0 UO_2 (-15,+2)		4/0 UO_2 (-13,-12)		3/0 UO_2 (-11,+2)		3/0 UO_2 (-6,-6)	
Axial position (cm)	Calculated fission rate	[C/E]-1 (%)	Calculated fission rate	[C/E]-1 (%)	Calculated fission rate	[C/E]-1 (%)	Calculated fission rate	[C/E]-1 (%)	Calculated fission rate	[C/E]-1 (%)	Calculated fission rate	[C/E]-1 (%)
110	0.0324	-2.67	0.0319	-0.97	0.0322	0.53	0.0323	-0.09	0.0324	0.62	0.0326	0.47
112	0.0362	1.81	0.0363	-0.66	0.0364	0.26	0.0363	1.44	0.0364	-0.54	0.0365	0.29
114	0.0404	1.34	0.0405	2.64	0.0406	0.51	0.0405	0.67	0.0406	1.61	0.0406	0.31
116	0.0441	0.71	0.0442	4.37	0.0442	0.31	0.0442	-0.45	0.0442	0.37	0.0442	0.57
118	0.0475	1.95	0.0476	-0.58	0.0476	-0.29	0.0475	0.69	0.0475	-1.07	0.0475	-0.33
120	0.0503	0.74	0.0504	-0.60	0.0504	-0.09	0.0504	0.03	0.0503	0.73	0.0503	-0.40
122	0.0527	0.07	0.0528	2.19	0.0527	-0.80	0.0527	0.10	0.0527	-0.23	0.0527	0.52
124	0.0546	-0.31	0.0546	0.22	0.0546	0.72	0.0546	0.25	0.0545	-0.82	0.0545	-0.20
126	0.0560	0.21	0.0560	0.06	0.0559	-0.88	0.0559	0.50	0.0559	-0.70	0.0558	0.85
128	0.0568	1.95	0.0568	1.78	0.0567	-0.82	0.0567	0.51	0.0567	0.68	0.0566	-0.18
130	0.0571	-0.66	0.0570	0.55	0.0570	0.40	0.0570	1.12	0.0570	-0.19	0.0569	1.33
132	0.0568	0.20	0.0568	-1.68	0.0567	0.37	0.0567	-0.75	0.0567	0.37	0.0566	-0.44
134	0.0560	0.21	0.0560	-0.73	0.0559	-0.50	0.0560	-0.30	0.0559	-0.12	0.0559	-0.07
136	0.0546	-0.28	0.0547	-2.36	0.0546	-0.37	0.0546	-1.66	0.0546	-0.14	0.0545	0.13
138	0.0528	-0.19	0.0528	-0.99	0.0528	-0.38	0.0528	0.67	0.0527	0.32	0.0527	0.51
140	0.0504	-0.49	0.0505	-0.65	0.0504	-0.02	0.0504	-0.31	0.0504	0.12	0.0504	-0.04
142	0.0476	-1.11	0.0476	-0.04	0.0476	-0.17	0.0476	-0.01	0.0476	-0.07	0.0476	0.27
144	0.0442	0.91	0.0443	-0.50	0.0443	0.90	0.0443	-0.79	0.0443	0.31	0.0443	-0.79
146	0.0405	-1.26	0.0406	-1.28	0.0406	0.75	0.0406	-1.71	0.0407	-0.56	0.0407	0.00
148	0.0363	-3.19	0.0365	-0.27	0.0365	0.02	0.0364	-0.54	0.0365	-0.36	0.0365	-0.85
150	0.0327	-1.34	0.0321	0.25	0.0323	0.68	0.0324	0.94	0.0325	-0.03	0.0326	-3.09

Table 4.19. KAERI axial pin power results and [C/E]-1 values (DANTSYS, ENDF/B-IV.7)

Pin	MOX (-27,-12)		MOX (-22,-2)		4/0 UO_2 (-15,+2)		4/0 UO_2 (-13,-12)		3/0 UO_2 (-11,+2)		3/0 UO_2 (-6,-6)	
Axial position (cm)	Calculated fission rate	[C/E]-1 (%)	Calculated fission rate	[C/E]-1 (%)	Calculated fission rate	[C/E]-1 (%)	Calculated fission rate	[C/E]-1 (%)	Calculated fission rate	[C/E]-1 (%)	Calculated fission rate	[C/E]-1 (%)
110	0.0334	0.27	0.0331	2.66	0.0330	2.94	0.0331	2.25	0.0329	2.35	0.0329	1.64
112	0.0361	1.49	0.0364	-0.40	0.0365	0.66	0.0363	1.59	0.0366	-0.14	0.0366	0.63
114	0.0408	2.33	0.0410	3.86	0.0410	1.49	0.0409	1.57	0.0409	2.41	0.0409	0.99
116	0.0440	0.46	0.0442	4.38	0.0443	0.48	0.0442	-0.40	0.0443	0.58	0.0443	0.79
118	0.0475	1.96	0.0476	-0.40	0.0477	-0.07	0.0476	0.84	0.0476	-0.85	0.0476	-0.10
120	0.0500	0.10	0.0502	-1.07	0.0502	-0.34	0.0502	-0.30	0.0503	0.58	0.0503	-0.50
122	0.0525	-0.49	0.0526	1.79	0.0526	-1.04	0.0526	-0.21	0.0526	-0.41	0.0526	0.39
124	0.0541	-1.24	0.0542	-0.58	0.0543	0.17	0.0543	-0.35	0.0543	-1.23	0.0543	-0.54
126	0.0555	-0.63	0.0556	-0.63	0.0556	-1.38	0.0556	-0.06	0.0556	-1.10	0.0557	0.52
128	0.0562	0.87	0.0562	0.82	0.0563	-1.49	0.0563	-0.22	0.0564	0.13	0.0564	-0.65
130	0.0565	-1.56	0.0566	-0.22	0.0567	-0.19	0.0567	0.49	0.0567	-0.67	0.0567	0.92
132	0.0562	-0.83	0.0563	-2.60	0.0563	-0.32	0.0563	-1.46	0.0564	-0.18	0.0564	-0.91
134	0.0556	-0.56	0.0556	-1.38	0.0556	-1.00	0.0557	-0.84	0.0557	-0.53	0.0557	-0.41
136	0.0542	-1.08	0.0542	-3.11	0.0543	-0.92	0.0543	-2.23	0.0543	-0.57	0.0543	-0.23
138	0.0526	-0.55	0.0526	-1.33	0.0526	-0.63	0.0526	0.40	0.0526	0.12	0.0526	0.36
140	0.0502	-0.86	0.0502	-1.05	0.0503	-0.30	0.0503	-0.58	0.0503	-0.07	0.0503	-0.17
142	0.0478	-0.68	0.0478	0.23	0.0477	0.02	0.0477	0.24	0.0477	0.09	0.0477	0.46
144	0.0444	1.26	0.0444	-0.38	0.0444	1.01	0.0443	-0.62	0.0444	0.44	0.0444	-0.64
146	0.0413	0.70	0.0412	0.04	0.0410	1.66	0.0411	-0.61	0.0409	0.11	0.0409	0.59
148	0.0367	-2.12	0.0366	0.13	0.0366	0.28	0.0366	-0.09	0.0366	-0.14	0.0366	-0.65
150	0.0345	4.13	0.0333	4.13	0.0330	2.87	0.0334	3.92	0.0329	1.44	0.0330	-2.14

Table 4.20. NEA+KAERI axial pin power results and [C/E]-1 values (TORT, ENDF/B-VI.5)

Pin	MOX (-27,-12)		MOX (-22,-2)		4/0 UO_2 (-15,+2)		4/0 UO_2 (-13,-12)		3/0 UO_2 (-11,+2)		3/0 UO_2 (-6,-6)	
Axial position (cm)	Calculated fission rate	[C/E]-1 (%)	Calculated fission rate	[C/E]-1 (%)	Calculated fission rate	[C/E]-1 (%)	Calculated fission rate	[C/E]-1 (%)	Calculated fission rate	[C/E]-1 (%)	Calculated fission rate	[C/E]-1 (%)
110	0.0333	-0.06	0.0331	2.68	0.0331	3.25	0.0331	2.53	0.0331	2.96	0.0331	2.28
112	0.0371	4.45	0.0372	1.72	0.0372	2.44	0.0371	3.64	0.0371	1.37	0.0371	2.00
114	0.0410	2.71	0.0411	4.04	0.0410	1.68	0.0410	1.77	0.0410	2.66	0.0410	1.22
116	0.0445	1.53	0.0446	5.11	0.0445	0.96	0.0445	0.18	0.0445	0.96	0.0445	1.13
118	0.0476	2.07	0.0476	-0.51	0.0476	-0.22	0.0476	0.74	0.0476	-1.00	0.0476	-0.24
120	0.0502	0.49	0.0502	-0.95	0.0502	-0.37	0.0502	-0.24	0.0502	0.49	0.0502	-0.59
122	0.0524	-0.59	0.0524	1.45	0.0524	-1.41	0.0524	-0.51	0.0524	-0.79	0.0524	0.04
124	0.0541	-1.17	0.0541	-0.77	0.0541	-0.11	0.0541	-0.54	0.0541	-1.56	0.0541	-0.85
126	0.0554	-0.88	0.0553	-1.09	0.0553	-1.88	0.0554	-0.47	0.0554	-1.60	0.0554	0.04
128	0.0561	0.78	0.0561	0.49	0.0561	-1.88	0.0561	-0.53	0.0561	-0.30	0.0561	-1.05
130	0.0564	-1.87	0.0563	-0.74	0.0564	-0.73	0.0564	0.03	0.0564	-1.20	0.0564	0.41
132	0.0561	-0.96	0.0561	-2.93	0.0561	-0.71	0.0562	-1.77	0.0561	-0.60	0.0562	-1.31
134	0.0554	-0.90	0.0553	-1.88	0.0554	-1.50	0.0554	-1.27	0.0554	-1.02	0.0554	-0.87
136	0.0541	-1.16	0.0541	-3.35	0.0541	-1.20	0.0542	-2.45	0.0542	-0.88	0.0542	-0.52
138	0.0524	-0.90	0.0524	-1.74	0.0524	-1.01	0.0525	0.05	0.0524	-0.24	0.0525	0.03
140	0.0502	-0.79	0.0503	-1.04	0.0503	-0.32	0.0503	-0.59	0.0503	-0.12	0.0503	-0.22
142	0.0476	-1.07	0.0476	-0.03	0.0476	-0.12	0.0476	0.02	0.0476	0.00	0.0476	0.38
144	0.0445	1.65	0.0446	0.14	0.0446	1.52	0.0445	-0.19	0.0446	0.90	0.0445	-0.23
146	0.0410	-0.07	0.0412	-0.02	0.0411	1.89	0.0410	-0.67	0.0411	0.47	0.0410	0.94
148	0.0372	-0.86	0.0373	2.00	0.0372	2.15	0.0372	1.56	0.0372	1.56	0.0372	0.88
150	0.0334	0.79	0.0332	3.80	0.0332	3.35	0.0332	3.43	0.0332	2.31	0.0332	-1.28

Table 4.21. NEA+KAERI axial pin power results and [C/E]-1 values (TORT, JENDL-3.2)

Pin	MOX (-27,-12)		MOX (-22,-2)		4/0 UO_2 (-15,+2)		4/0 UO_2 (-13,-12)		3/0 UO_2 (-11,+2)		3/0 UO_2 (-6,-6)	
Axial position (cm)	Calculated fission rate	[C/E]-1 (%)	Calculated fission rate	[C/E]-1 (%)	Calculated fission rate	[C/E]-1 (%)	Calculated fission rate	[C/E]-1 (%)	Calculated fission rate	[C/E]-1 (%)	Calculated fission rate	[C/E]-1 (%)
110	0.0331	-0.82	0.0330	2.35	0.0330	3.04	0.0330	2.10	0.0330	2.77	0.0331	2.07
112	0.0370	4.05	0.0371	1.53	0.0371	2.31	0.0370	3.42	0.0371	1.26	0.0370	1.87
114	0.0409	2.54	0.0410	3.93	0.0410	1.61	0.0409	1.68	0.0410	2.59	0.0409	1.15
116	0.0445	1.49	0.0445	5.07	0.0445	0.92	0.0445	0.15	0.0445	0.93	0.0445	1.09
118	0.0476	2.12	0.0476	-0.51	0.0476	-0.22	0.0476	0.76	0.0476	-1.00	0.0476	-0.24
120	0.0503	0.59	0.0502	-0.92	0.0502	-0.35	0.0502	-0.19	0.0502	0.51	0.0502	-0.57
122	0.0525	-0.46	0.0524	1.51	0.0524	-1.38	0.0525	-0.44	0.0524	-0.75	0.0524	0.07
124	0.0542	-1.02	0.0541	-0.69	0.0541	-0.07	0.0542	-0.46	0.0542	-1.52	0.0542	-0.80
126	0.0554	-0.71	0.0554	-1.01	0.0554	-1.82	0.0554	-0.38	0.0554	-1.55	0.0554	0.10
128	0.0562	0.96	0.0561	0.59	0.0561	-1.82	0.0562	-0.43	0.0562	-0.24	0.0562	-0.99
130	0.0565	-1.70	0.0564	-0.64	0.0564	-0.66	0.0565	0.14	0.0564	-1.14	0.0564	0.48
132	0.0562	-0.78	0.0561	-2.84	0.0561	-0.65	0.0562	-1.67	0.0562	-0.55	0.0562	-1.24
134	0.0555	-0.73	0.0554	-1.79	0.0554	-1.45	0.0555	-1.17	0.0554	-0.97	0.0554	-0.81
136	0.0542	-1.01	0.0542	-3.27	0.0542	-1.15	0.0542	-2.36	0.0542	-0.83	0.0542	-0.47
138	0.0525	-0.76	0.0524	-1.68	0.0525	-0.97	0.0525	0.12	0.0525	-0.20	0.0525	0.07
140	0.0503	-0.69	0.0503	-1.00	0.0503	-0.30	0.0503	-0.54	0.0503	-0.10	0.0503	-0.20
142	0.0476	-1.02	0.0477	-0.02	0.0476	-0.12	0.0476	0.05	0.0476	0.00	0.0476	0.39
144	0.0445	1.62	0.0446	0.11	0.0446	1.50	0.0445	-0.21	0.0446	0.88	0.0445	-0.25
146	0.0410	-0.21	0.0411	-0.12	0.0411	1.84	0.0410	-0.76	0.0410	0.41	0.0410	0.88
148	0.0371	-1.22	0.0372	1.82	0.0372	2.05	0.0371	1.36	0.0372	1.46	0.0371	0.77
150	0.0331	0.03	0.0331	3.48	0.0331	3.16	0.0331	3.01	0.0332	2.13	0.0332	-1.46

Table 4.22. Purdue University axial pin power results and [C/E]-1 values (PARCS, ENDF/B-VI.3)

Pin	MOX (-27,-12)		MOX (-22,-2)		4/0 UO_2 (-15,+2)		4/0 UO_2 (-13,-12)		3/0 UO_2 (-11,+2)		3/0 UO_2 (-6,-6)	
Axial position (cm)	Calculated fission rate	[C/E]-1 (%)	Calculated fission rate	[C/E]-1 (%)	Calculated fission rate	[C/E]-1 (%)	Calculated fission rate	[C/E]-1 (%)	Calculated fission rate	[C/E]-1 (%)	Calculated fission rate	[C/E]-1 (%)
110	0.0347	4.18	0.0322	-0.06	0.0322	0.53	0.0324	0.24	0.0323	0.35	0.0323	-0.16
112	0.0378	6.22	0.0363	-0.80	0.0363	-0.05	0.0363	1.36	0.0363	-1.02	0.0363	-0.27
114	0.0410	2.87	0.0404	2.24	0.0403	-0.08	0.0403	0.12	0.0403	0.91	0.0403	-0.43
116	0.0442	0.93	0.0441	4.07	0.0441	-0.06	0.0440	-0.79	0.0441	-0.05	0.0440	0.14
118	0.0471	1.19	0.0474	-0.86	0.0474	-0.58	0.0474	0.36	0.0474	-1.37	0.0474	-0.62
120	0.0498	-0.42	0.0503	-0.78	0.0503	-0.21	0.0503	-0.13	0.0503	0.63	0.0503	-0.47
122	0.0520	-1.43	0.0527	2.04	0.0527	-0.84	0.0527	-0.01	0.0527	-0.23	0.0527	0.56
124	0.0537	-1.90	0.0546	0.11	0.0546	0.78	0.0546	0.25	0.0546	-0.70	0.0546	-0.03
126	0.0550	-1.51	0.0559	0.00	0.0560	-0.78	0.0560	0.53	0.0560	-0.52	0.0560	1.09
128	0.0558	0.20	0.0568	1.74	0.0568	-0.65	0.0568	0.60	0.0568	0.93	0.0568	0.12
130	0.0561	-2.40	0.0570	0.55	0.0571	0.57	0.0571	1.22	0.0571	0.07	0.0571	1.65
132	0.0558	-1.48	0.0568	-1.69	0.0568	0.57	0.0568	-0.61	0.0568	0.66	0.0568	-0.11
134	0.0551	-1.45	0.0560	-0.71	0.0560	-0.33	0.0560	-0.20	0.0560	0.14	0.0560	0.24
136	0.0538	-1.76	0.0547	-2.36	0.0547	-0.20	0.0547	-1.55	0.0547	0.10	0.0547	0.42
138	0.0521	-1.55	0.0528	-1.00	0.0528	-0.27	0.0528	0.71	0.0528	0.48	0.0528	0.71
140	0.0499	-1.45	0.0505	-0.65	0.0505	0.05	0.0504	-0.28	0.0504	0.23	0.0504	0.10
142	0.0473	-1.62	0.0476	-0.10	0.0476	-0.22	0.0476	-0.10	0.0476	-0.12	0.0476	0.25
144	0.0444	1.44	0.0443	-0.51	0.0443	0.83	0.0442	-0.84	0.0443	0.21	0.0442	-0.89
146	0.0413	0.58	0.0406	-1.35	0.0406	0.52	0.0405	-1.91	0.0405	-0.87	0.0405	-0.34
148	0.0381	1.43	0.0366	-0.04	0.0365	0.14	0.0365	-0.21	0.0365	-0.39	0.0365	-0.93
150	0.0351	5.89	0.0325	1.64	0.0325	1.20	0.0327	1.73	0.0325	0.27	0.0326	-3.11

Table 4.23. FRAMATOME-ANP axial pin power results and [C/E]-1 values (MOCA, ENDF/B-IV)

Pin	MOX (-27,-12)		MOX (-22,-2)		4/0 UO_2 (-15,+2)		4/0 UO_2 (-13,-12)		3/0 UO_2 (-11,+2)		3/0 UO_2 (-6,-6)	
Axial position (cm)	Calculated fission rate	[C/E]-1 (%)	Calculated fission rate	[C/E]-1 (%)	Calculated fission rate	[C/E]-1 (%)	Calculated fission rate	[C/E]-1 (%)	Calculated fission rate	[C/E]-1 (%)	Calculated fission rate	[C/E]-1 (%)
110	0.0357	7.05	0.0349	8.23	0.0344	7.40	0.0352	8.79	0.0349	8.56	0.0348	7.53
112	0.0377	6.03	0.0374	2.24	0.0373	2.69	0.0378	5.70	0.0377	2.89	0.0377	3.54
114	0.0404	1.14	0.0404	2.21	0.0404	0.09	0.0407	1.22	0.0407	1.92	0.0407	0.64
116	0.0434	-0.97	0.0435	2.70	0.0437	-0.97	0.0438	-1.42	0.0438	-0.60	0.0439	-0.19
118	0.0465	-0.14	0.0467	-2.35	0.0469	-1.64	0.0468	-0.96	0.0469	-2.49	0.0470	-1.45
120	0.0496	-0.80	0.0497	-1.93	0.0499	-1.00	0.0496	-1.55	0.0497	-0.55	0.0498	-1.34
122	0.0522	-0.93	0.0523	1.35	0.0525	-1.28	0.0520	-1.23	0.0522	-1.23	0.0523	-0.20
124	0.0543	-0.89	0.0544	-0.25	0.0544	0.49	0.0540	-0.76	0.0541	-1.57	0.0542	-0.84
126	0.0556	-0.39	0.0558	-0.32	0.0557	-1.18	0.0555	-0.34	0.0555	-1.38	0.0554	0.04
128	0.0564	1.26	0.0565	1.35	0.0565	-1.25	0.0563	-0.19	0.0563	0.00	0.0561	-1.16
130	0.0566	-1.44	0.0568	0.10	0.0567	-0.15	0.0566	0.43	0.0566	-0.90	0.0563	0.22
132	0.0564	-0.49	0.0565	-2.12	0.0565	-0.09	0.0563	-1.47	0.0563	-0.32	0.0561	-1.44
134	0.0556	-0.45	0.0558	-1.14	0.0557	-0.84	0.0555	-1.17	0.0555	-0.84	0.0554	-0.90
136	0.0543	-0.92	0.0544	-2.88	0.0544	-0.66	0.0540	-2.71	0.0541	-0.95	0.0542	-0.56
138	0.0522	-1.28	0.0523	-1.90	0.0525	-0.94	0.0520	-0.75	0.0522	-0.76	0.0523	-0.28
140	0.0496	-2.13	0.0497	-2.10	0.0499	-1.04	0.0496	-2.00	0.0497	-1.25	0.0498	-1.07
142	0.0465	-3.30	0.0467	-1.98	0.0469	-1.66	0.0468	-1.79	0.0469	-1.63	0.0470	-0.95
144	0.0434	-0.96	0.0435	-2.28	0.0437	-0.56	0.0438	-1.92	0.0438	-0.80	0.0439	-1.67
146	0.0404	-1.71	0.0404	-1.95	0.0404	0.12	0.0407	-1.39	0.0407	-0.44	0.0407	0.17
148	0.0377	0.49	0.0374	2.31	0.0373	2.17	0.0378	3.35	0.0377	2.84	0.0377	2.15
150	0.0357	7.80	0.0349	9.10	0.0344	7.21	0.0352	9.45	0.0349	7.54	0.0348	3.46

Table 4.24. JAERI axial pin power results and [C/E]-1 values (MVP, JENDL-3.2)

Pin	MOX (-27,-12)		MOX (-22,-2)		4/0 UO_2 (-15,+2)		4/0 UO_2 (-13,-12)		3/0 UO_2 (-11,+2)		3/0 UO_2 (-6,-6)	
Axial position (cm)	Calculated fission rate	[C/E]-1 (%)	Calculated fission rate	[C/E]-1 (%)	Calculated fission rate	[C/E]-1 (%)	Calculated fission rate	[C/E]-1 (%)	Calculated fission rate	[C/E]-1 (%)	Calculated fission rate	[C/E]-1 (%)
110	0.0324	-2.72	0.0320	-0.81	0.0319	-0.58	0.0323	-0.13	0.0325	1.14	0.0320	-1.35
112	0.0359	1.02	0.0364	-0.57	0.0363	-0.06	0.0362	1.24	0.0365	-0.47	0.0368	1.23
114	0.0406	1.85	0.0405	2.65	0.0403	-0.01	0.0404	0.33	0.0404	1.17	0.0402	-0.59
116	0.0444	1.30	0.0442	4.33	0.0442	0.24	0.0440	-0.78	0.0439	-0.48	0.0447	1.66
118	0.0467	0.17	0.0471	-1.65	0.0474	-0.58	0.0471	-0.31	0.0474	-1.29	0.0474	-0.66
120	0.0511	2.33	0.0508	0.30	0.0501	-0.53	0.0506	0.53	0.0505	1.10	0.0499	-1.26
122	0.0527	0.00	0.0526	1.83	0.0526	-1.10	0.0526	-0.25	0.0526	-0.43	0.0529	0.90
124	0.0541	-1.24	0.0546	0.26	0.0549	1.36	0.0547	0.54	0.0547	-0.55	0.0547	0.23
126	0.0552	-1.17	0.0565	1.00	0.0563	-0.24	0.0560	0.54	0.0562	-0.18	0.0561	1.28
128	0.0572	2.75	0.0574	2.85	0.0569	-0.53	0.0563	-0.31	0.0567	0.73	0.0569	0.27
130	0.0571	-0.52	0.0568	0.11	0.0569	0.31	0.0571	1.27	0.0573	0.45	0.0567	0.95
132	0.0569	0.46	0.0564	-2.37	0.0566	0.19	0.0570	-0.27	0.0568	0.50	0.0570	0.20
134	0.0554	-0.77	0.0561	-0.44	0.0564	0.36	0.0559	-0.31	0.0560	0.08	0.0558	-0.15
136	0.0539	-1.63	0.0547	-2.23	0.0553	0.96	0.0550	-0.94	0.0544	-0.43	0.0544	-0.05
138	0.0538	1.76	0.0521	-2.37	0.0528	-0.34	0.0531	1.19	0.0524	-0.35	0.0529	0.80
140	0.0506	-0.06	0.0504	-0.80	0.0504	-0.09	0.0507	0.29	0.0505	0.42	0.0504	-0.01
142	0.0479	-0.39	0.0477	0.16	0.0477	0.05	0.0473	-0.62	0.0476	-0.07	0.0480	1.17
144	0.0439	0.19	0.0444	-0.37	0.0442	0.69	0.0444	-0.45	0.0448	1.39	0.0446	-0.16
146	0.0402	-1.96	0.0408	-0.99	0.0405	0.40	0.0407	-1.38	0.0401	-1.94	0.0403	-0.85
148	0.0367	-2.24	0.0365	-0.31	0.0363	-0.52	0.0366	0.01	0.0364	-0.56	0.0361	-2.13
150	0.0331	-0.01	0.0320	0.23	0.0320	-0.49	0.0320	-0.52	0.0323	-0.39	0.0324	-3.90

Table 4.25. JAERI axial pin power results and [C/E]-1 values (MVP, JENDL-3.3)

Pin	MOX (-27,-12)		MOX (-22,-2)		4/0 UO_2 (-15,+2)		4/0 UO_2 (-13,-12)		3/0 UO_2 (-11,+2)		3/0 UO_2 (-6,-6)	
Axial position (cm)	Calculated fission rate	[C/E]-1 (%)	Calculated fission rate	[C/E]-1 (%)	Calculated fission rate	[C/E]-1 (%)	Calculated fission rate	[C/E]-1 (%)	Calculated fission rate	[C/E]-1 (%)	Calculated fission rate	[C/E]-1 (%)
110	0.0330	-1.12	0.0320	-0.66	0.0323	0.68	0.0323	-0.01	0.0322	0.15	0.0320	-1.24
112	0.0365	2.56	0.0363	-0.74	0.0360	-0.75	0.0363	1.40	0.0365	-0.23	0.0365	0.29
114	0.0409	2.64	0.0405	2.49	0.0405	0.34	0.0401	-0.31	0.0404	1.13	0.0407	0.59
116	0.0446	1.81	0.0441	4.13	0.0448	1.52	0.0445	0.16	0.0447	1.43	0.0439	-0.17
118	0.0483	3.71	0.0477	-0.34	0.0479	0.39	0.0475	0.60	0.0475	-1.07	0.0478	0.33
120	0.0512	2.43	0.0502	-0.92	0.0503	-0.27	0.0508	0.98	0.0505	0.99	0.0503	-0.42
122	0.0523	-0.87	0.0530	2.68	0.0529	-0.55	0.0531	0.76	0.0528	-0.03	0.0528	0.68
124	0.0549	0.24	0.0546	0.14	0.0546	0.72	0.0544	-0.14	0.0547	-0.54	0.0547	0.14
126	0.0555	-0.67	0.0564	0.85	0.0558	-1.01	0.0557	0.13	0.0561	-0.25	0.0563	1.69
128	0.0569	2.19	0.0566	1.45	0.0565	-1.22	0.0568	0.57	0.0568	0.96	0.0564	-0.63
130	0.0568	-1.02	0.0574	1.25	0.0573	0.89	0.0569	0.98	0.0572	0.17	0.0569	1.28
132	0.0579	2.28	0.0573	-0.81	0.0567	0.41	0.0569	-0.52	0.0569	0.85	0.0568	-0.14
134	0.0554	-0.83	0.0558	-1.04	0.0560	-0.45	0.0561	0.01	0.0559	-0.11	0.0555	-0.69
136	0.0542	-1.11	0.0541	-3.42	0.0549	0.14	0.0548	-1.26	0.0549	0.47	0.0542	-0.47
138	0.0519	-1.89	0.0527	-1.15	0.0524	-1.11	0.0526	0.28	0.0526	0.13	0.0531	1.21
140	0.0501	-1.06	0.0503	-0.93	0.0503	-0.17	0.0502	-0.76	0.0497	-1.32	0.0509	0.98
142	0.0469	-2.63	0.0471	-1.20	0.0475	-0.47	0.0472	-0.94	0.0474	-0.52	0.0481	1.40
144	0.0441	0.58	0.0445	-0.12	0.0439	0.08	0.0443	-0.76	0.0441	-0.23	0.0443	-0.75
146	0.0401	-2.31	0.0410	-0.44	0.0407	0.80	0.0411	-0.39	0.0403	-1.53	0.0403	-0.91
148	0.0366	-2.48	0.0366	0.03	0.0367	0.74	0.0362	-1.04	0.0362	-1.17	0.0364	-1.29
150	0.0321	-3.19	0.0318	-0.69	0.0322	0.21	0.0322	0.22	0.0326	0.36	0.0322	-4.26

Table 4.26. SCK•CEN axial pin power results and [C/E]-1 values (MCNP-4C, ENDF/B-VI.5)

Pin	MOX (-27,-12)		MOX (-22,-2)		4/0 UO_2 (-15,+2)		4/0 UO_2 (-13,-12)		3/0 UO_2 (-11,+2)		3/0 UO_2 (-6,-6)	
Axial position (cm)	Calculated fission rate	[C/E]-1 (%)	Calculated fission rate	[C/E]-1 (%)	Calculated fission rate	[C/E]-1 (%)	Calculated fission rate	[C/E]-1 (%)	Calculated fission rate	[C/E]-1 (%)	Calculated fission rate	[C/E]-1 (%)
110	0.0324	-2.84	0.0326	1.23	0.0330	2.87	0.0330	2.14	0.0335	4.25	0.0332	2.37
112	0.0371	4.28	0.0372	1.74	0.0372	2.46	0.0370	3.29	0.0372	1.60	0.0369	1.43
114	0.0410	2.79	0.0406	2.93	0.0410	1.54	0.0412	2.33	0.0413	3.51	0.0406	0.33
116	0.0445	1.66	0.0438	3.40	0.0443	0.56	0.0450	1.27	0.0442	0.33	0.0447	1.57
118	0.0472	1.38	0.0477	-0.20	0.0474	-0.61	0.0475	0.51	0.0476	-0.90	0.0475	-0.36
120	0.0504	0.97	0.0503	-0.78	0.0502	-0.50	0.0507	0.79	0.0503	0.59	0.0503	-0.39
122	0.0527	-0.04	0.0525	1.58	0.0525	-1.30	0.0529	0.31	0.0524	-0.89	0.0528	0.72
124	0.0548	0.10	0.0542	-0.65	0.0543	0.26	0.0541	-0.68	0.0542	-1.47	0.0542	-0.78
126	0.0559	0.06	0.0557	-0.44	0.0555	-1.56	0.0556	-0.10	0.0553	-1.66	0.0556	0.46
128	0.0562	1.03	0.0565	1.29	0.0562	-1.73	0.0560	-0.82	0.0563	0.08	0.0567	-0.03
130	0.0576	0.29	0.0563	-0.69	0.0567	-0.16	0.0563	-0.10	0.0564	-1.09	0.0564	0.44
132	0.0578	2.10	0.0560	-3.03	0.0563	-0.33	0.0557	-2.53	0.0560	-0.81	0.0555	-2.41
134	0.0559	0.14	0.0551	-2.37	0.0554	-1.47	0.0547	-2.46	0.0551	-1.52	0.0553	-1.00
136	0.0515	-5.89	0.0546	-2.55	0.0540	-1.43	0.0539	-2.91	0.0544	-0.41	0.0543	-0.30
138	0.0531	0.44	0.0527	-1.20	0.0524	-1.14	0.0524	-0.12	0.0529	0.65	0.0528	0.61
140	0.0510	0.63	0.0500	-1.59	0.0503	-0.21	0.0505	-0.11	0.0500	-0.62	0.0503	-0.25
142	0.0469	-2.48	0.0471	-1.25	0.0472	-0.99	0.0478	0.37	0.0477	0.07	0.0474	-0.15
144	0.0440	0.57	0.0452	1.36	0.0449	2.24	0.0447	0.26	0.0443	0.23	0.0445	-0.34
146	0.0402	-2.19	0.0411	-0.05	0.0407	0.93	0.0406	-1.61	0.0408	-0.09	0.0407	0.21
148	0.0365	-2.67	0.0376	2.96	0.0373	2.33	0.0371	1.51	0.0370	1.08	0.0370	0.52
150	0.0330	-0.29	0.0332	3.76	0.0333	3.55	0.0333	3.58	0.0329	1.38	0.0333	-1.01

Table 4.27. SCK•CEN axial pin power results and [C/E]-1 values (MCNP-4C, JEF-2.2)

Pin	MOX (-27,-12)		MOX (-22,-2)		4/0 UO_2 (-15,+2)		4/0 UO_2 (-13,-12)		3/0 UO_2 (-11,+2)		3/0 UO_2 (-6,-6)	
Axial position (cm)	Calculated fission rate	[C/E]-1 (%)	Calculated fission rate	[C/E]-1 (%)	Calculated fission rate	[C/E]-1 (%)	Calculated fission rate	[C/E]-1 (%)	Calculated fission rate	[C/E]-1 (%)	Calculated fission rate	[C/E]-1 (%)
110	0.0331	-0.72	0.0328	1.87	0.0331	3.22	0.0332	2.55	0.0329	2.36	0.0331	2.10
112	0.0369	3.74	0.0371	1.34	0.0374	3.07	0.0363	1.43	0.0369	0.62	0.0373	2.58
114	0.0416	4.37	0.0412	4.27	0.0413	2.30	0.0404	0.34	0.0406	1.55	0.0411	1.64
116	0.0453	3.43	0.0446	5.23	0.0448	1.55	0.0448	0.88	0.0447	1.49	0.0440	0.07
118	0.0469	0.64	0.0465	-2.91	0.0476	-0.19	0.0480	1.64	0.0478	-0.58	0.0477	-0.04
120	0.0499	-0.15	0.0500	-1.36	0.0499	-1.09	0.0503	-0.01	0.0501	0.22	0.0501	-0.80
122	0.0525	-0.47	0.0520	0.78	0.0517	-2.80	0.0525	-0.28	0.0527	-0.30	0.0526	0.31
124	0.0542	-1.04	0.0543	-0.35	0.0542	-0.03	0.0543	-0.18	0.0539	-1.93	0.0547	0.20
126	0.0561	0.51	0.0549	-1.88	0.0555	-1.53	0.0559	0.36	0.0551	-2.08	0.0555	0.30
128	0.0560	0.56	0.0566	1.49	0.0560	-1.99	0.0566	0.26	0.0562	-0.22	0.0563	-0.85
130	0.0566	-1.42	0.0569	0.32	0.0565	-0.48	0.0568	0.71	0.0568	-0.50	0.0560	-0.35
132	0.0568	0.19	0.0570	-1.34	0.0563	-0.35	0.0558	-2.47	0.0556	-1.54	0.0562	-1.25
134	0.0554	-0.93	0.0556	-1.37	0.0552	-1.75	0.0555	-1.13	0.0558	-0.21	0.0553	-1.00
136	0.0532	-2.79	0.0547	-2.29	0.0546	-0.45	0.0541	-2.57	0.0541	-0.91	0.0545	0.09
138	0.0529	0.03	0.0526	-1.33	0.0524	-1.03	0.0521	-0.64	0.0524	-0.37	0.0524	-0.07
140	0.0495	-2.19	0.0506	-0.34	0.0505	0.08	0.0507	0.27	0.0502	-0.35	0.0506	0.38
142	0.0478	-0.71	0.0478	0.38	0.0475	-0.41	0.0473	-0.61	0.0480	0.84	0.0475	0.04
144	0.0445	1.66	0.0444	-0.43	0.0443	0.84	0.0445	-0.21	0.0445	0.85	0.0444	-0.53
146	0.0401	-2.37	0.0405	-1.67	0.0411	1.97	0.0410	-0.82	0.0411	0.63	0.0406	-0.08
148	0.0380	1.23	0.0374	2.26	0.0372	2.08	0.0368	0.57	0.0370	0.93	0.0370	0.46
150	0.0328	-1.08	0.0325	1.55	0.0330	2.70	0.0332	3.26	0.0337	3.69	0.0332	-1.45

Table 4.28. KAERI+NEA axial pin power results and [C/E]-1 values (MCNP-4B, ENDF60)

Pin	MOX (-27,-12)		MOX (-22,-2)		4/0 UO_2 (-15,+2)		4/0 UO_2 (-13,-12)		3/0 UO_2 (-11,+2)		3/0 UO_2 (-6,-6)	
Axial position (cm)	Calculated fission rate	[C/E]-1 (%)	Calculated fission rate	[C/E]-1 (%)	Calculated fission rate	[C/E]-1 (%)	Calculated fission rate	[C/E]-1 (%)	Calculated fission rate	[C/E]-1 (%)	Calculated fission rate	[C/E]-1 (%)
110	0.0328	-1.76	0.0335	3.80	0.0333	3.83	0.0330	2.04	0.0329	2.32	0.0330	1.70
112	0.0358	0.65	0.0368	0.44	0.0371	2.37	0.0371	3.77	0.0372	1.53	0.0370	1.67
114	0.0406	1.86	0.0403	1.93	0.0408	1.01	0.0403	0.27	0.0409	2.46	0.0407	0.59
116	0.0436	-0.43	0.0443	4.44	0.0440	-0.11	0.0445	0.34	0.0443	0.51	0.0443	0.69
118	0.0479	2.70	0.0469	-2.01	0.0482	0.98	0.0477	1.04	0.0474	-1.39	0.0478	0.20
120	0.0503	0.61	0.0509	0.41	0.0503	-0.25	0.0501	-0.38	0.0497	-0.56	0.0502	-0.72
122	0.0528	0.24	0.0522	1.14	0.0527	-0.80	0.0520	-1.21	0.0528	-0.09	0.0524	0.08
124	0.0535	-2.36	0.0544	-0.21	0.0541	-0.21	0.0546	0.25	0.0542	-1.37	0.0542	-0.66
126	0.0542	-2.88	0.0553	-1.08	0.0553	-2.00	0.0555	-0.22	0.0562	-0.12	0.0550	-0.67
128	0.0564	1.25	0.0561	0.55	0.0560	-2.03	0.0569	0.85	0.0559	-0.74	0.0563	-0.71
130	0.0576	0.23	0.0574	1.21	0.0558	-1.73	0.0564	0.03	0.0564	-1.08	0.0564	0.36
132	0.0564	-0.49	0.0555	-3.85	0.0566	0.10	0.0560	-2.03	0.0564	-0.12	0.0562	-1.18
134	0.0554	-0.82	0.0553	-1.91	0.0552	-1.88	0.0554	-1.27	0.0549	-1.82	0.0547	-2.22
136	0.0538	-1.70	0.0547	-2.27	0.0538	-1.91	0.0538	-3.14	0.0544	-0.41	0.0543	-0.27
138	0.0534	0.93	0.0532	-0.29	0.0529	-0.21	0.0532	1.41	0.0524	-0.33	0.0524	-0.16
140	0.0494	-2.54	0.0499	-1.69	0.0506	0.26	0.0505	-0.14	0.0503	0.00	0.0509	1.00
142	0.0480	-0.22	0.0476	-0.07	0.0476	-0.26	0.0469	-1.50	0.0480	0.79	0.0476	0.42
144	0.0452	3.09	0.0446	0.04	0.0442	0.54	0.0445	-0.38	0.0442	0.14	0.0444	-0.44
146	0.0414	0.96	0.0413	0.25	0.0411	1.86	0.0407	-1.56	0.0406	-0.78	0.0413	1.67
148	0.0376	0.15	0.0374	2.16	0.0372	2.06	0.0374	2.21	0.0370	1.04	0.0375	1.84
150	0.0341	2.86	0.0325	1.76	0.0336	4.48	0.0334	3.86	0.0338	4.07	0.0334	-0.77

Table 4.29. KAERI+NEA axial pin power results and [C/E]-1 values (MCNP-4B, ENDF/B-VI.5)

Pin	MOX (-27,-12)		MOX (-22,-2)		4/0 UO_2 (-15,+2)		4/0 UO_2 (-13,-12)		3/0 UO_2 (-11,+2)		3/0 UO_2 (-6,-6)	
Axial position (cm)	Calculated fission rate	[C/E]-1 (%)	Calculated fission rate	[C/E]-1 (%)	Calculated fission rate	[C/E]-1 (%)	Calculated fission rate	[C/E]-1 (%)	Calculated fission rate	[C/E]-1 (%)	Calculated fission rate	[C/E]-1 (%)
110	0.0327	-1.89	0.0330	2.49	0.0334	4.34	0.0334	3.38	0.0337	4.72	0.0331	2.14
112	0.0377	5.95	0.0368	0.57	0.0373	2.72	0.0366	2.19	0.0371	1.34	0.0370	1.86
114	0.0425	6.55	0.0408	3.26	0.0405	0.30	0.0404	0.51	0.0406	1.78	0.0409	1.21
116	0.0444	1.34	0.0445	5.04	0.0444	0.79	0.0447	0.77	0.0437	-0.96	0.0438	-0.35
118	0.0465	-0.14	0.0482	0.67	0.0469	-1.58	0.0480	1.61	0.0478	-0.51	0.0473	-0.82
120	0.0503	0.63	0.0505	-0.33	0.0503	-0.17	0.0503	-0.01	0.0502	0.46	0.0499	-1.27
122	0.0517	-1.86	0.0527	2.00	0.0526	-0.95	0.0526	-0.09	0.0521	-1.34	0.0526	0.35
124	0.0544	-0.57	0.0543	-0.45	0.0542	0.10	0.0551	1.14	0.0540	-1.72	0.0544	-0.37
126	0.0558	-0.11	0.0556	-0.63	0.0555	-1.66	0.0560	0.65	0.0552	-1.92	0.0558	0.86
128	0.0556	-0.08	0.0558	-0.02	0.0557	-2.50	0.0561	-0.53	0.0561	-0.33	0.0561	-1.08
130	0.0562	-2.16	0.0568	0.05	0.0566	-0.36	0.0559	-0.82	0.0561	-1.66	0.0564	0.48
132	0.0559	-1.28	0.0563	-2.50	0.0559	-1.01	0.0563	-1.59	0.0564	-0.21	0.0559	-1.78
134	0.0549	-1.65	0.0552	-2.06	0.0555	-1.35	0.0552	-1.61	0.0555	-0.91	0.0558	-0.25
136	0.0554	1.12	0.0551	-1.61	0.0541	-1.19	0.0539	-2.95	0.0545	-0.16	0.0541	-0.62
138	0.0530	0.14	0.0518	-2.94	0.0520	-1.79	0.0528	0.69	0.0524	-0.38	0.0525	0.03
140	0.0497	-1.77	0.0499	-1.76	0.0503	-0.25	0.0503	-0.60	0.0504	0.23	0.0506	0.37
142	0.0482	0.12	0.0468	-1.72	0.0480	0.53	0.0477	0.10	0.0475	-0.38	0.0480	1.16
144	0.0436	-0.53	0.0442	-0.68	0.0447	1.75	0.0448	0.39	0.0444	0.55	0.0448	0.32
146	0.0419	2.13	0.0409	-0.67	0.0413	2.34	0.0408	-1.16	0.0410	0.21	0.0410	0.97
148	0.0368	-1.83	0.0374	2.28	0.0377	3.30	0.0366	0.15	0.0380	3.66	0.0371	0.62
150	0.0327	-1.37	0.0335	4.68	0.0330	2.80	0.0324	0.73	0.0334	2.75	0.0329	-2.43

Table 4.30. KAERI+NEA axial pin power results and [C/E]-1 values (MCNP-4B, JENDL-3.2)

Pin	MOX (-27,-12)		MOX (-22,-2)		4/0 UO_2 (-15,+2)		4/0 UO_2 (-13,-12)		3/0 UO_2 (-11,+2)		3/0 UO_2 (-6,-6)	
Axial position (cm)	Calculated fission rate	[C/E]-1 (%)	Calculated fission rate	[C/E]-1 (%)	Calculated fission rate	[C/E]-1 (%)	Calculated fission rate	[C/E]-1 (%)	Calculated fission rate	[C/E]-1 (%)	Calculated fission rate	[C/E]-1 (%)
110	0.0329	-1.29	0.0331	2.71	0.0329	2.51	0.0330	2.23	0.0327	1.56	0.0332	2.41
112	0.0359	0.95	0.0366	-0.06	0.0369	1.82	0.0367	2.64	0.0369	0.71	0.0372	2.17
114	0.0414	3.66	0.0414	4.78	0.0406	0.59	0.0406	0.87	0.0404	1.09	0.0413	2.13
116	0.0441	0.74	0.0449	5.94	0.0443	0.46	0.0444	-0.08	0.0445	0.95	0.0445	1.16
118	0.0469	0.70	0.0468	-2.27	0.0471	-1.32	0.0471	-0.19	0.0477	-0.73	0.0472	-0.91
120	0.0513	2.63	0.0505	-0.45	0.0503	-0.23	0.0504	0.14	0.0504	0.77	0.0500	-0.96
122	0.0520	-1.30	0.0523	1.24	0.0530	-0.25	0.0520	-1.32	0.0531	0.45	0.0522	-0.43
124	0.0543	-0.78	0.0544	-0.28	0.0541	-0.21	0.0538	-1.09	0.0544	-1.05	0.0544	-0.42
126	0.0563	0.84	0.0556	-0.67	0.0557	-1.30	0.0562	1.02	0.0558	-0.90	0.0561	1.34
128	0.0565	1.48	0.0564	1.12	0.0567	-0.88	0.0567	0.52	0.0568	0.82	0.0563	-0.83
130	0.0563	-1.99	0.0559	-1.40	0.0557	-1.91	0.0566	0.41	0.0562	-1.43	0.0564	0.49
132	0.0569	0.37	0.0565	-2.14	0.0561	-0.71	0.0566	-1.00	0.0559	-1.09	0.0555	-2.40
134	0.0549	-1.81	0.0553	-1.99	0.0546	-2.92	0.0554	-1.38	0.0548	-1.99	0.0555	-0.74
136	0.0544	-0.70	0.0532	-5.00	0.0554	1.05	0.0540	-2.68	0.0540	-1.19	0.0543	-0.24
138	0.0536	1.37	0.0525	-1.54	0.0531	0.16	0.0525	0.10	0.0527	0.34	0.0523	-0.32
140	0.0503	-0.72	0.0502	-1.24	0.0506	0.28	0.0504	-0.36	0.0500	-0.64	0.0503	-0.20
142	0.0473	-1.61	0.0485	1.68	0.0473	-0.85	0.0477	0.24	0.0474	-0.46	0.0477	0.53
144	0.0434	-0.94	0.0444	-0.29	0.0443	0.81	0.0444	-0.40	0.0446	0.95	0.0445	-0.21
146	0.0409	-0.43	0.0414	0.66	0.0409	1.49	0.0409	-0.96	0.0414	1.26	0.0406	-0.17
148	0.0373	-0.58	0.0370	1.26	0.0372	2.04	0.0370	1.01	0.0371	1.20	0.0371	0.58
150	0.0331	0.07	0.0333	4.15	0.0335	4.21	0.0334	4.01	0.0334	2.82	0.0334	-0.68

Table 4.31. KAERI+NEA axial pin power results and [C/E]-1 values (MCNP-4B, JEF-2.2)

Pin	MOX (-27,-12)		MOX (-22,-2)		4/0 UO_2 (-15,+2)		4/0 UO_2 (-13,-12)		3/0 UO_2 (-11,+2)		3/0 UO_2 (-6,-6)	
Axial position (cm)	Calculated fission rate	[C/E]-1 (%)	Calculated fission rate	[C/E]-1 (%)	Calculated fission rate	[C/E]-1 (%)	Calculated fission rate	[C/E]-1 (%)	Calculated fission rate	[C/E]-1 (%)	Calculated fission rate	[C/E]-1 (%)
110	0.0329	-1.18	0.0333	3.32	0.0326	1.68	0.0329	1.83	0.0331	2.86	0.0336	3.76
112	0.0371	4.40	0.0372	1.70	0.0374	3.04	0.0372	3.93	0.0367	0.07	0.0369	1.50
114	0.0403	1.06	0.0420	6.42	0.0411	1.86	0.0408	1.44	0.0407	1.87	0.0413	2.13
116	0.0431	-1.59	0.0444	4.87	0.0447	1.25	0.0444	0.02	0.0436	-1.02	0.0445	1.26
118	0.0469	0.67	0.0477	-0.23	0.0482	1.01	0.0475	0.53	0.0475	-1.06	0.0475	-0.48
120	0.0526	5.21	0.0506	-0.19	0.0500	-0.71	0.0505	0.33	0.0503	0.73	0.0501	-0.76
122	0.0534	1.28	0.0526	1.97	0.0524	-1.41	0.0527	0.01	0.0525	-0.68	0.0522	-0.32
124	0.0534	-2.50	0.0542	-0.52	0.0544	0.37	0.0538	-1.17	0.0545	-0.95	0.0544	-0.34
126	0.0577	3.34	0.0547	-2.12	0.0550	-2.51	0.0549	-1.32	0.0561	-0.27	0.0547	-1.12
128	0.0563	1.22	0.0553	-0.81	0.0561	-1.85	0.0567	0.51	0.0564	0.22	0.0559	-1.42
130	0.0570	-0.70	0.0564	-0.65	0.0564	-0.72	0.0566	0.35	0.0566	-0.89	0.0568	1.05
132	0.0567	0.04	0.0567	-1.83	0.0566	0.08	0.0559	-2.27	0.0564	-0.15	0.0562	-1.24
134	0.0545	-2.38	0.0557	-1.30	0.0554	-1.52	0.0561	0.02	0.0546	-2.45	0.0553	-1.09
136	0.0518	-5.43	0.0534	-4.66	0.0538	-1.76	0.0538	-3.09	0.0540	-1.17	0.0543	-0.30
138	0.0527	-0.34	0.0524	-1.76	0.0519	-1.94	0.0523	-0.23	0.0524	-0.36	0.0528	0.71
140	0.0514	1.50	0.0497	-2.08	0.0497	-1.35	0.0509	0.56	0.0503	-0.03	0.0504	0.11
142	0.0472	-1.97	0.0477	0.06	0.0482	0.99	0.0478	0.46	0.0480	0.67	0.0471	-0.76
144	0.0447	2.03	0.0448	0.63	0.0446	1.51	0.0441	-1.09	0.0447	1.32	0.0447	0.25
146	0.0410	-0.16	0.0411	-0.10	0.0417	3.27	0.0408	-1.29	0.0414	1.36	0.0410	0.77
148	0.0363	-3.17	0.0371	1.47	0.0369	1.33	0.0373	2.01	0.0372	1.62	0.0368	-0.03
150	0.0329	-0.76	0.0327	2.43	0.0330	2.83	0.0329	2.45	0.0330	1.74	0.0333	-1.13

Table 4.32. KFKI axial pin power results and [C/E]-1 values (MCNP-4C, ENDF/B-VI.2)

Pin	MOX (-27,-12)		MOX (-22,-2)		4/0 UO_2 (-15,+2)		4/0 UO_2 (-13,-12)		3/0 UO_2 (-11,+2)		3/0 UO_2 (-6,-6)	
Axial position (cm)	Calculated fission rate	[C/E]-1 (%)	Calculated fission rate	[C/E]-1 (%)	Calculated fission rate	[C/E]-1 (%)	Calculated fission rate	[C/E]-1 (%)	Calculated fission rate	[C/E]-1 (%)	Calculated fission rate	[C/E]-1 (%)
110	0.0354	6.18	0.0339	5.09	0.0321	0.26	0.0327	1.06	0.0333	3.52	0.0331	2.10
112	0.0356	0.07	0.0379	3.50	0.0368	1.56	0.0370	3.30	0.0373	1.85	0.0361	-0.84
114	0.0422	5.81	0.0414	4.89	0.0415	2.82	0.0404	0.28	0.0409	2.52	0.0414	2.32
116	0.0461	5.28	0.0442	4.35	0.0454	3.00	0.0449	1.20	0.0438	-0.74	0.0438	-0.40
118	0.0477	2.37	0.0448	-6.46	0.0482	1.11	0.0470	-0.56	0.0483	0.48	0.0472	-1.11
120	0.0487	-2.55	0.0510	0.62	0.0502	-0.39	0.0494	-1.89	0.0508	1.63	0.0507	0.30
122	0.0519	-1.55	0.0525	1.68	0.0526	-1.03	0.0512	-2.84	0.0534	1.17	0.0528	0.79
124	0.0495	-9.53	0.0532	-2.45	0.0534	-1.43	0.0538	-1.18	0.0542	-1.45	0.0552	1.05
126	0.0550	-1.47	0.0551	-1.57	0.0561	-0.49	0.0567	1.89	0.0544	-3.30	0.0552	-0.32
128	0.0557	0.13	0.0565	1.19	0.0555	-2.95	0.0576	2.03	0.0559	-0.71	0.0566	-0.23
130	0.0544	-5.26	0.0566	-0.23	0.0569	0.19	0.0578	2.51	0.0585	2.45	0.0576	2.55
132	0.0573	1.15	0.0560	-2.99	0.0572	1.19	0.0560	-2.06	0.0570	0.88	0.0554	-2.70
134	0.0550	-1.59	0.0545	-3.41	0.0556	-1.14	0.0554	-1.22	0.0548	-2.09	0.0550	-1.53
136	0.0560	2.22	0.0534	-4.69	0.0540	-1.50	0.0547	-1.52	0.0537	-1.70	0.0556	2.01
138	0.0516	-2.42	0.0529	-0.87	0.0520	-1.81	0.0525	0.09	0.0531	0.95	0.0525	0.16
140	0.0512	1.14	0.0497	-2.13	0.0502	-0.37	0.0505	-0.12	0.0496	-1.55	0.0503	-0.25
142	0.0499	3.74	0.0476	-0.13	0.0479	0.31	0.0472	-0.91	0.0483	1.37	0.0468	-1.27
144	0.0440	0.44	0.0461	3.40	0.0441	0.49	0.0454	1.66	0.0444	0.42	0.0445	-0.42
146	0.0399	-2.85	0.0419	1.72	0.0402	-0.42	0.0412	-0.25	0.0399	-2.50	0.0409	0.51
148	0.0374	-0.39	0.0373	2.01	0.0378	3.67	0.0373	1.87	0.0363	-0.82	0.0367	-0.51
150	0.0354	6.96	0.0338	5.72	0.0323	0.43	0.0316	-1.81	0.0323	-0.43	0.0329	-2.21

Table 4.33. KI axial pin power results and [C/E]-1 values (MCU-REA, MCUDAT)

Pin	MOX (-27,-12)		MOX (-22,-2)		4/0 UO_2 (-15,+2)		4/0 UO_2 (-13,-12)		3/0 UO_2 (-11,+2)		3/0 UO_2 (-6,-6)	
Axial position (cm)	Calculated fission rate	[C/E]-1 (%)	Calculated fission rate	[C/E]-1 (%)	Calculated fission rate	[C/E]-1 (%)	Calculated fission rate	[C/E]-1 (%)	Calculated fission rate	[C/E]-1 (%)	Calculated fission rate	[C/E]-1 (%)
110	0.0330	-1.02	0.0320	-0.71	0.0330	2.94	0.0320	-1.01	0.0330	2.62	0.0340	4.94
112	0.0350	-1.59	0.0370	1.12	0.0370	2.00	0.0360	0.62	0.0370	1.03	0.0380	4.50
114	0.0390	-2.24	0.0410	3.83	0.0410	1.60	0.0400	-0.59	0.0410	2.67	0.0410	1.33
116	0.0460	5.01	0.0450	6.17	0.0430	-2.49	0.0450	1.38	0.0440	-0.17	0.0450	2.33
118	0.0480	3.01	0.0470	-1.76	0.0470	-1.45	0.0490	3.78	0.0460	-4.28	0.0480	0.67
120	0.0510	2.08	0.0500	-1.37	0.0500	-0.80	0.0500	-0.68	0.0500	0.05	0.0500	-1.03
122	0.0510	-3.24	0.0520	0.71	0.0530	-0.28	0.0520	-1.30	0.0520	-1.56	0.0530	1.15
124	0.0540	-1.38	0.0540	-0.93	0.0550	1.53	0.0540	-0.81	0.0540	-1.79	0.0540	-1.12
126	0.0560	0.29	0.0560	0.13	0.0550	-2.49	0.0560	0.62	0.0570	1.30	0.0550	-0.66
128	0.0550	-1.20	0.0580	3.97	0.0560	-2.05	0.0570	0.98	0.0570	1.26	0.0580	2.22
130	0.0580	0.99	0.0580	2.23	0.0570	0.42	0.0570	1.09	0.0570	-0.11	0.0560	-0.30
132	0.0560	-1.15	0.0560	-3.06	0.0560	-0.90	0.0560	-2.04	0.0570	0.94	0.0560	-1.58
134	0.0570	2.02	0.0550	-2.47	0.0560	-0.38	0.0560	-0.22	0.0570	1.86	0.0550	-1.60
136	0.0540	-1.41	0.0540	-3.55	0.0540	-1.46	0.0550	-0.96	0.0540	-1.17	0.0540	-0.84
138	0.0520	-1.70	0.0530	-0.65	0.0530	0.06	0.0520	-0.82	0.0530	0.82	0.0520	-0.83
140	0.0520	2.68	0.0520	2.39	0.0510	1.14	0.0500	-1.12	0.0500	-0.65	0.0500	-0.75
142	0.0470	-2.32	0.0470	-1.39	0.0480	0.63	0.0470	-1.29	0.0480	0.77	0.0480	1.18
144	0.0460	5.02	0.0450	1.02	0.0450	2.47	0.0450	0.85	0.0440	-0.37	0.0440	-1.43
146	0.0410	-0.13	0.0400	-2.82	0.0410	1.63	0.0410	-0.73	0.0410	0.29	0.0400	-1.60
148	0.0370	-1.40	0.0360	-1.55	0.0380	4.22	0.0370	1.11	0.0360	-1.75	0.0370	0.39
150	0.0310	-6.36	0.0320	0.09	0.0330	2.73	0.0320	-0.41	0.0330	1.66	0.0330	-2.00

Table 4.34. GRS axial pin power results and [C/E]-1 values (MCNP-4C, ENDF/B-VI.5)

Pin	MOX (-27,-12)		MOX (-22,-2)		4/0 UO_2 (-15,+2)		4/0 UO_2 (-13,-12)		3/0 UO_2 (-11,+2)		3/0 UO_2 (-6,-6)	
Axial position (cm)	Calculated fission rate	[C/E]-1 (%)	Calculated fission rate	[C/E]-1 (%)	Calculated fission rate	[C/E]-1 (%)	Calculated fission rate	[C/E]-1 (%)	Calculated fission rate	[C/E]-1 (%)	Calculated fission rate	[C/E]-1 (%)
110	0.0334	0.16	0.0322	-0.17	0.0333	3.80	0.0324	0.24	0.0324	0.67	0.0325	0.20
112	0.0376	5.67	0.0359	-1.82	0.0364	0.36	0.0363	1.41	0.0358	-2.24	0.0369	1.36
114	0.0399	0.12	0.0408	3.37	0.0397	-1.54	0.0402	-0.07	0.0409	2.30	0.0402	-0.70
116	0.0437	-0.15	0.0437	3.20	0.0445	0.86	0.0444	-0.02	0.0439	-0.33	0.0439	-0.22
118	0.0481	3.21	0.0471	-1.64	0.0473	-0.86	0.0480	1.57	0.0473	-1.53	0.0475	-0.32
120	0.0517	3.48	0.0510	0.63	0.0499	-1.03	0.0511	1.43	0.0507	1.50	0.0500	-1.07
122	0.0541	2.55	0.0524	1.40	0.0526	-0.98	0.0534	1.27	0.0528	-0.05	0.0525	0.16
124	0.0562	2.58	0.0540	-1.00	0.0549	1.38	0.0542	-0.37	0.0553	0.49	0.0555	1.56
126	0.0550	-1.54	0.0556	-0.50	0.0559	-0.92	0.0567	1.90	0.0558	-0.75	0.0562	1.57
128	0.0550	-1.28	0.0579	3.71	0.0564	-1.31	0.0568	0.69	0.0567	0.69	0.0576	1.52
130	0.0565	-1.67	0.0584	2.91	0.0575	1.29	0.0569	0.98	0.0573	0.46	0.0575	2.40
132	0.0548	-3.18	0.0565	-2.13	0.0576	1.91	0.0569	-0.47	0.0556	-1.58	0.0566	-0.59
134	0.0542	-3.03	0.0558	-1.13	0.0559	-0.61	0.0565	0.64	0.0558	-0.25	0.0555	-0.71
136	0.0565	3.15	0.0551	-1.60	0.0532	-2.91	0.0548	-1.30	0.0540	-1.11	0.0542	-0.41
138	0.0528	-0.23	0.0538	0.94	0.0525	-0.82	0.0516	-1.64	0.0527	0.25	0.0533	1.66
140	0.0489	-3.42	0.0497	-2.20	0.0499	-1.13	0.0497	-1.77	0.0496	-1.41	0.0507	0.55
142	0.0475	-1.23	0.0472	-0.98	0.0475	-0.41	0.0477	0.09	0.0484	1.66	0.0479	0.87
144	0.0440	0.37	0.0449	0.84	0.0444	1.07	0.0444	-0.52	0.0453	2.50	0.0439	-1.72
146	0.0411	0.08	0.0393	-4.57	0.0404	0.19	0.0400	-3.13	0.0404	-1.06	0.0403	-0.76
148	0.0370	-1.42	0.0367	0.27	0.0366	0.41	0.0363	-0.85	0.0368	0.31	0.0363	-1.50
150	0.0321	-2.91	0.0321	0.42	0.0336	4.65	0.0318	-0.90	0.0324	-0.05	0.0312	-7.35

Table 4.35. GRS axial pin power results and [C/E]-1 values (MCNP-4C, JENDL-3.2)

Pin	MOX (-27,-12)		MOX (-22,-2)		4/0 UO_2 (-15,+2)		4/0 UO_2 (-13,-12)		3/0 UO_2 (-11,+2)		3/0 UO_2 (-6,-6)	
Axial position (cm)	Calculated fission rate	[C/E]-1 (%)	Calculated fission rate	[C/E]-1 (%)	Calculated fission rate	[C/E]-1 (%)	Calculated fission rate	[C/E]-1 (%)	Calculated fission rate	[C/E]-1 (%)	Calculated fission rate	[C/E]-1 (%)
110	0.0312	-6.30	0.0325	0.99	0.0326	1.66	0.0320	-0.95	0.0320	-0.48	0.0323	-0.19
112	0.0371	4.23	0.0357	-2.34	0.0366	0.92	0.0358	0.03	0.0365	-0.36	0.0360	-1.03
114	0.0397	-0.52	0.0406	2.87	0.0409	1.27	0.0407	1.12	0.0399	-0.14	0.0397	-2.00
116	0.0463	5.63	0.0444	4.65	0.0446	1.18	0.0438	-1.35	0.0445	0.92	0.0436	-0.74
118	0.0477	2.44	0.0482	0.70	0.0477	-0.04	0.0479	1.50	0.0479	-0.31	0.0469	-1.63
120	0.0483	-3.35	0.0503	-0.72	0.0506	0.40	0.0504	0.15	0.0497	-0.49	0.0507	0.30
122	0.0540	2.36	0.0526	1.81	0.0528	-0.62	0.0540	2.53	0.0532	0.71	0.0522	-0.34
124	0.0545	-0.53	0.0540	-0.84	0.0539	-0.43	0.0551	1.14	0.0548	-0.26	0.0541	-0.94
126	0.0567	1.52	0.0570	1.86	0.0556	-1.37	0.0559	0.48	0.0565	0.48	0.0549	-0.85
128	0.0583	4.79	0.0573	2.66	0.0562	-1.77	0.0560	-0.83	0.0563	0.10	0.0570	0.42
130	0.0582	1.41	0.0568	0.07	0.0575	1.23	0.0572	1.41	0.0578	1.28	0.0577	2.67
132	0.0544	-3.98	0.0568	-1.76	0.0566	0.14	0.0560	-2.06	0.0574	1.64	0.0573	0.74
134	0.0545	-2.44	0.0566	0.40	0.0559	-0.52	0.0559	-0.43	0.0557	-0.48	0.0558	-0.11
136	0.0543	-0.81	0.0540	-3.55	0.0538	-1.80	0.0548	-1.25	0.0536	-1.85	0.0554	1.82
138	0.0508	-3.99	0.0528	-1.01	0.0535	0.99	0.0536	2.21	0.0528	0.49	0.0538	2.53
140	0.0532	5.11	0.0498	-2.00	0.0505	0.05	0.0504	-0.34	0.0507	0.83	0.0515	2.16
142	0.0490	1.73	0.0477	0.17	0.0471	-1.27	0.0475	-0.23	0.0481	0.95	0.0474	-0.07
144	0.0431	-1.70	0.0443	-0.57	0.0437	-0.59	0.0439	-1.68	0.0440	-0.48	0.0448	0.39
146	0.0413	0.56	0.0401	-2.70	0.0405	0.44	0.0403	-2.45	0.0404	-1.11	0.0396	-2.58
148	0.0358	-4.57	0.0367	0.37	0.0369	1.18	0.0367	0.29	0.0362	-1.31	0.0368	-0.19
150	0.0317	-4.31	0.0319	-0.31	0.0326	1.51	0.0321	0.01	0.0319	-1.82	0.0325	-3.47

Table 4.36. GRS axial pin power results and [C/E]-1 values (MCNP-4C, JEF-2.2)

Pin	MOX (-27,-12)		MOX (-22,-2)		4/0 UO_2 (-15,+2)		4/0 UO_2 (-13,-12)		3/0 UO_2 (-11,+2)		3/0 UO_2 (-6,-6)	
Axial position (cm)	Calculated fission rate	[C/E]-1 (%)	Calculated fission rate	[C/E]-1 (%)	Calculated fission rate	[C/E]-1 (%)	Calculated fission rate	[C/E]-1 (%)	Calculated fission rate	[C/E]-1 (%)	Calculated fission rate	[C/E]-1 (%)
110	0.0318	-4.64	0.0322	-0.05	0.0331	3.39	0.0323	0.01	0.0323	0.44	0.0326	0.52
112	0.0368	3.40	0.0368	0.56	0.0372	2.58	0.0357	-0.19	0.0369	0.81	0.0358	-1.57
114	0.0399	-0.05	0.0395	-0.07	0.0404	0.09	0.0405	0.68	0.0403	0.86	0.0405	0.15
116	0.0457	4.23	0.0444	4.82	0.0439	-0.46	0.0439	-1.20	0.0442	0.31	0.0439	-0.10
118	0.0484	3.82	0.0473	-1.13	0.0471	-1.17	0.0476	0.88	0.0476	-0.87	0.0474	-0.68
120	0.0492	-1.59	0.0511	0.70	0.0512	1.66	0.0498	-1.12	0.0511	2.15	0.0503	-0.33
122	0.0522	-0.97	0.0526	1.91	0.0524	-1.36	0.0525	-0.31	0.0528	-0.07	0.0528	0.78
124	0.0575	5.05	0.0544	-0.18	0.0541	-0.17	0.0542	-0.46	0.0540	-1.77	0.0554	1.41
126	0.0563	0.91	0.0553	-1.13	0.0561	-0.50	0.0564	1.25	0.0560	-0.49	0.0556	0.40
128	0.0572	2.75	0.0564	1.14	0.0571	-0.08	0.0566	0.35	0.0573	1.71	0.0568	0.07
130	0.0577	0.55	0.0575	1.29	0.0572	0.84	0.0580	2.82	0.0568	-0.41	0.0576	2.63
132	0.0568	0.34	0.0557	-3.54	0.0578	2.30	0.0570	-0.25	0.0577	2.26	0.0565	-0.69
134	0.0552	-1.27	0.0573	1.62	0.0556	-1.11	0.0565	0.61	0.0559	-0.19	0.0554	-0.95
136	0.0541	-1.17	0.0555	-0.94	0.0538	-1.81	0.0545	-1.85	0.0537	-1.63	0.0541	-0.68
138	0.0517	-2.31	0.0534	0.02	0.0521	-1.71	0.0518	-1.14	0.0523	-0.59	0.0527	0.59
140	0.0496	-2.14	0.0503	-0.91	0.0506	0.37	0.0504	-0.43	0.0509	1.10	0.0509	0.96
142	0.0475	-1.19	0.0482	1.04	0.0475	-0.43	0.0471	-1.17	0.0474	-0.59	0.0475	0.12
144	0.0440	0.35	0.0443	-0.59	0.0442	0.62	0.0442	-1.05	0.0446	1.05	0.0449	0.57
146	0.0403	-1.95	0.0399	-2.97	0.0405	0.29	0.0409	-0.86	0.0402	-1.65	0.0404	-0.73
148	0.0358	-4.60	0.0364	-0.53	0.0362	-0.69	0.0374	2.14	0.0357	-2.64	0.0367	-0.53
150	0.0324	-2.09	0.0316	-1.11	0.0318	-1.15	0.0328	1.99	0.0324	-0.26	0.0323	-4.03

Table 4.37. SEA axial pin power results and [C/E]-1 values (MCNP-4C, ENDF/B-VI)

Pin	MOX (-27,-12)		MOX (-22,-2)		4/0 UO_2 (-15,+2)		4/0 UO_2 (-13,-12)		3/0 UO_2 (-11,+2)		3/0 UO_2 (-6,-6)	
Axial position (cm)	Calculated fission rate	[C/E]-1 (%)	Calculated fission rate	[C/E]-1 (%)	Calculated fission rate	[C/E]-1 (%)	Calculated fission rate	[C/E]-1 (%)	Calculated fission rate	[C/E]-1 (%)	Calculated fission rate	[C/E]-1 (%)
110	0.0331	-0.72	0.0330	2.33	0.0344	7.43	0.0342	5.74	0.0332	3.33	0.0345	6.39
112	0.0345	-3.00	0.0379	3.71	0.0378	4.09	0.0382	6.84	0.0365	-0.43	0.0379	4.32
114	0.0411	3.02	0.0404	2.41	0.0416	3.03	0.0419	4.02	0.0408	2.09	0.0404	-0.14
116	0.0453	3.41	0.0448	5.70	0.0428	-2.99	0.0423	-4.81	0.0443	0.62	0.0456	3.74
118	0.0486	4.30	0.0484	1.21	0.0470	-1.43	0.0468	-0.98	0.0454	-5.45	0.0464	-2.61
120	0.0492	-1.53	0.0491	-3.06	0.0491	-2.68	0.0496	-1.52	0.0504	0.83	0.0523	3.50
122	0.0501	-4.95	0.0532	2.94	0.0537	1.07	0.0520	-1.29	0.0520	-1.52	0.0521	-0.57
124	0.0548	0.08	0.0535	-1.78	0.0521	-3.81	0.0548	0.69	0.0525	-4.47	0.0525	-3.89
126	0.0570	2.08	0.0550	-1.66	0.0554	-1.86	0.0556	-0.10	0.0555	-1.28	0.0549	-0.79
128	0.0558	0.24	0.0577	3.42	0.0539	-5.66	0.0546	-3.33	0.0548	-2.64	0.0564	-0.66
130	0.0563	-1.97	0.0568	0.08	0.0548	-3.50	0.0555	-1.63	0.0548	-3.94	0.0579	3.13
132	0.0576	1.68	0.0561	-2.89	0.0561	-0.67	0.0551	-3.69	0.0556	-1.61	0.0559	-1.77
134	0.0561	0.41	0.0550	-2.54	0.0553	-1.58	0.0543	-3.22	0.0568	1.46	0.0531	-5.02
136	0.0539	-1.59	0.0520	-7.13	0.0532	-2.92	0.0552	-0.59	0.0564	3.29	0.0522	-4.18
138	0.0519	-1.89	0.0527	-1.14	0.0520	-1.74	0.0519	-1.06	0.0528	0.45	0.0526	0.33
140	0.0495	-2.25	0.0481	-5.34	0.0502	-0.54	0.0499	-1.26	0.0493	-2.03	0.0486	-3.45
142	0.0478	-0.66	0.0476	-0.06	0.0492	3.21	0.0480	0.76	0.0464	-2.61	0.0476	0.36
144	0.0433	-1.14	0.0451	1.33	0.0487	10.95	0.0455	1.98	0.0466	5.50	0.0450	0.89
146	0.0388	-5.48	0.0425	3.20	0.0419	3.97	0.0424	2.67	0.0432	5.70	0.0429	5.44
148	0.0369	-1.67	0.0367	0.25	0.0374	2.46	0.0396	8.19	0.0374	2.07	0.0360	-2.30
150	0.0366	10.55	0.0341	6.56	0.0336	4.69	0.0333	3.67	0.0349	7.39	0.0338	0.47

FIGURES

Figure 2.1. VENUS-2 core geometry

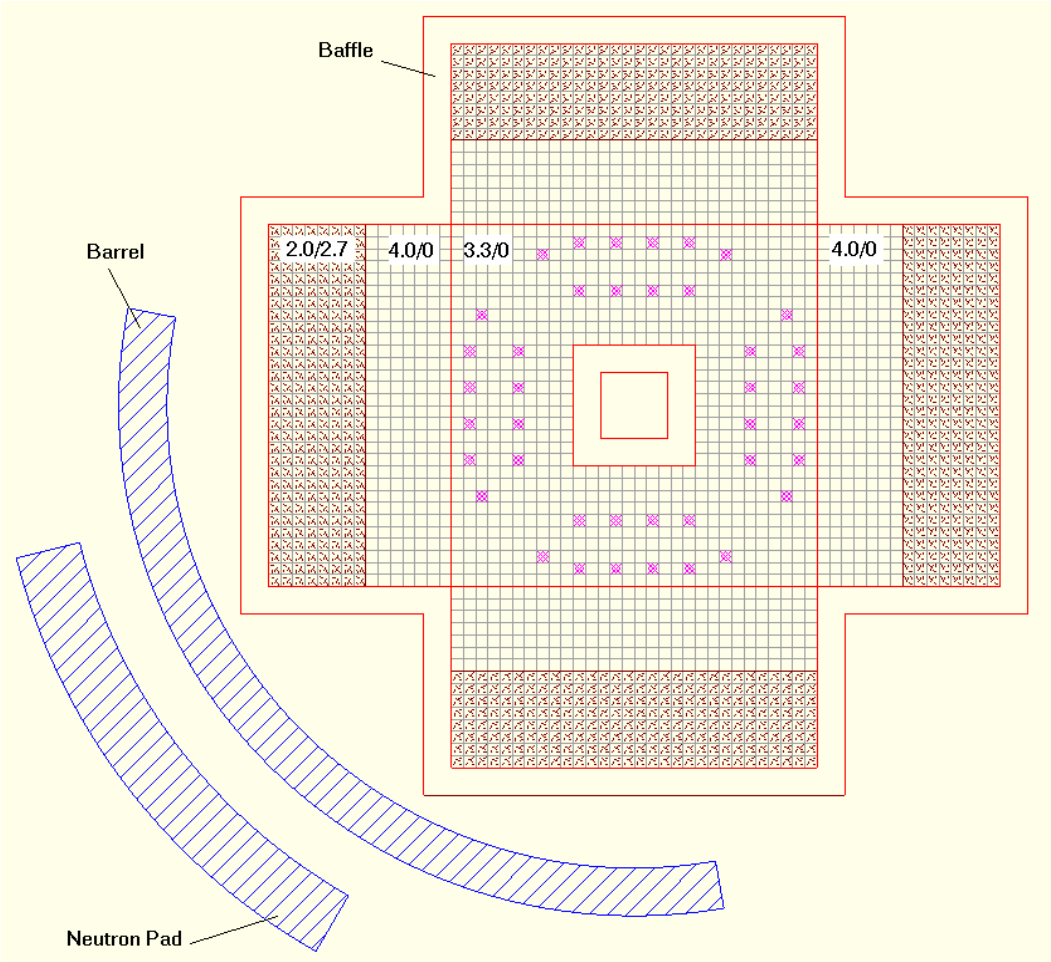

Figure 2.2. Measured and interpolated pin power positions in VENUS-2

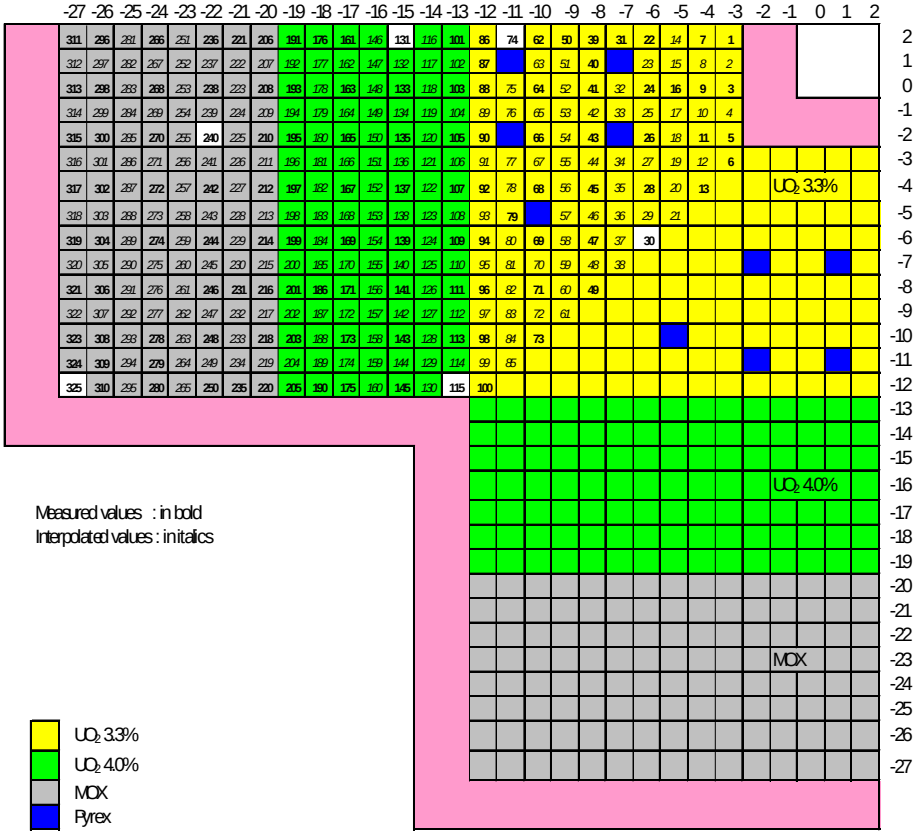

Figure 2.3. Vertical cross-section of the VENUS-2 reactor configuration

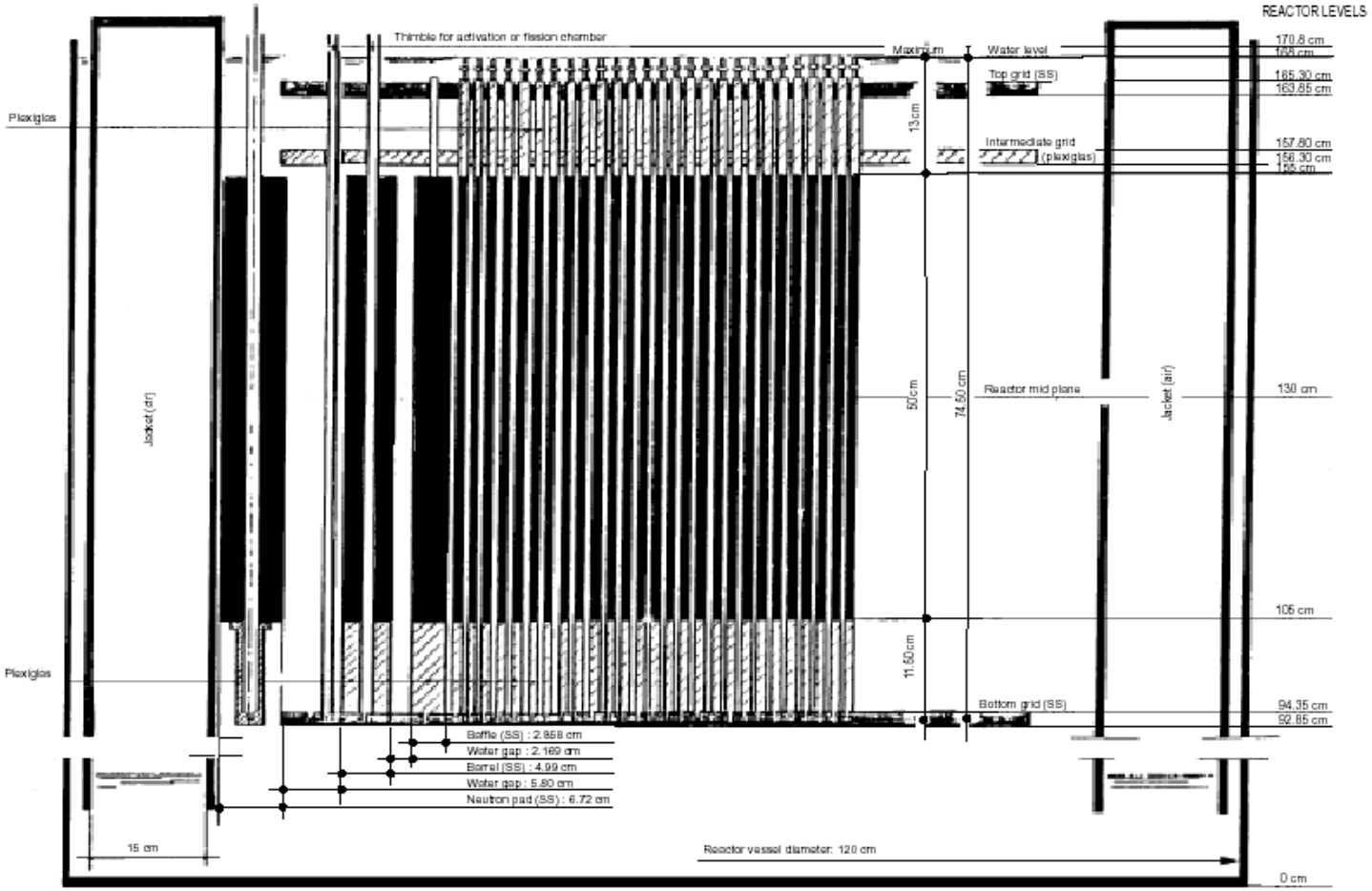

Figure 4.1. Calculated k_∞ values in 3/0 UO_2 fuel pin

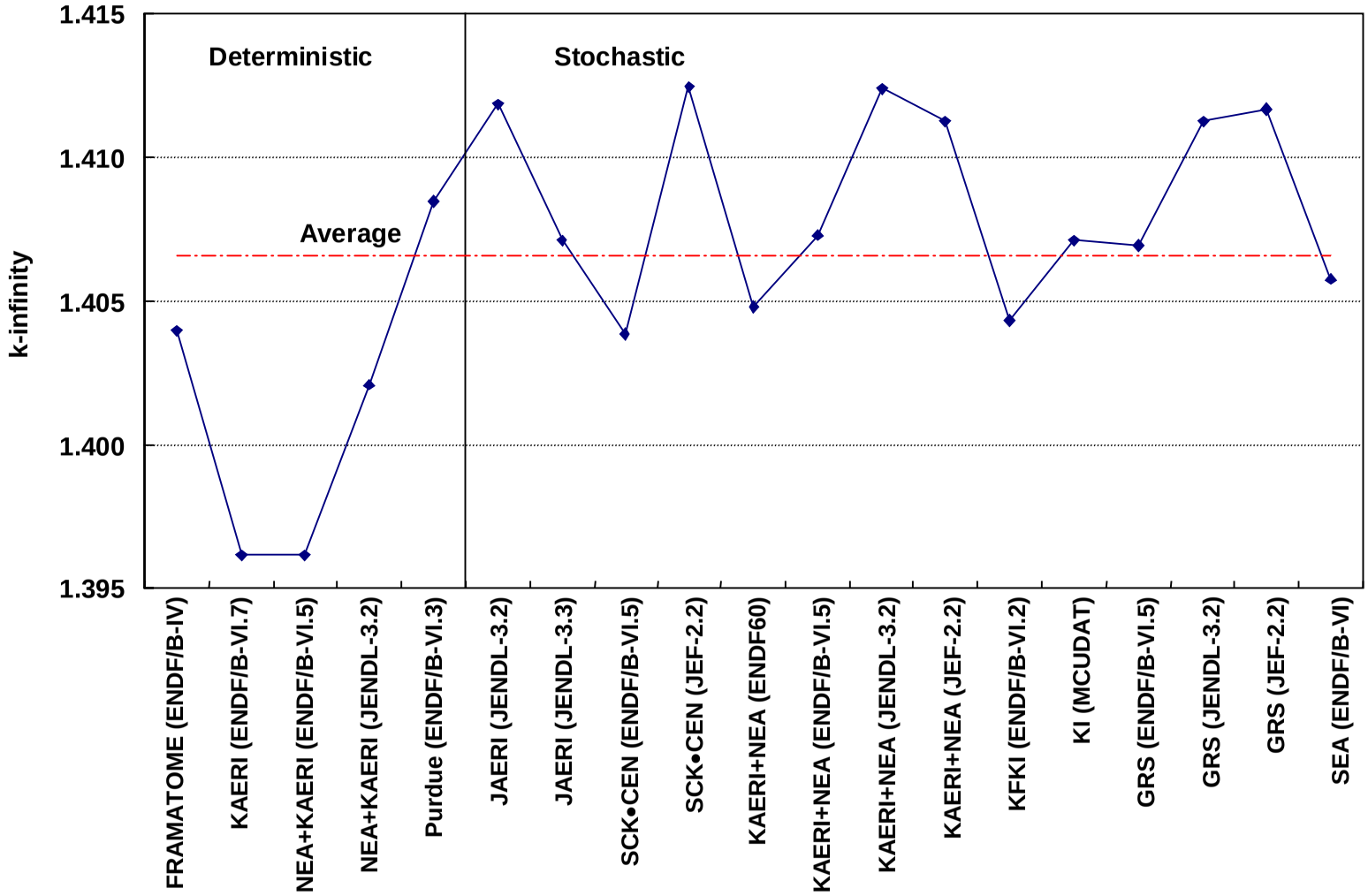

Figure 4.2. Calculated k_∞ values in 4/0 UO_2 fuel pin

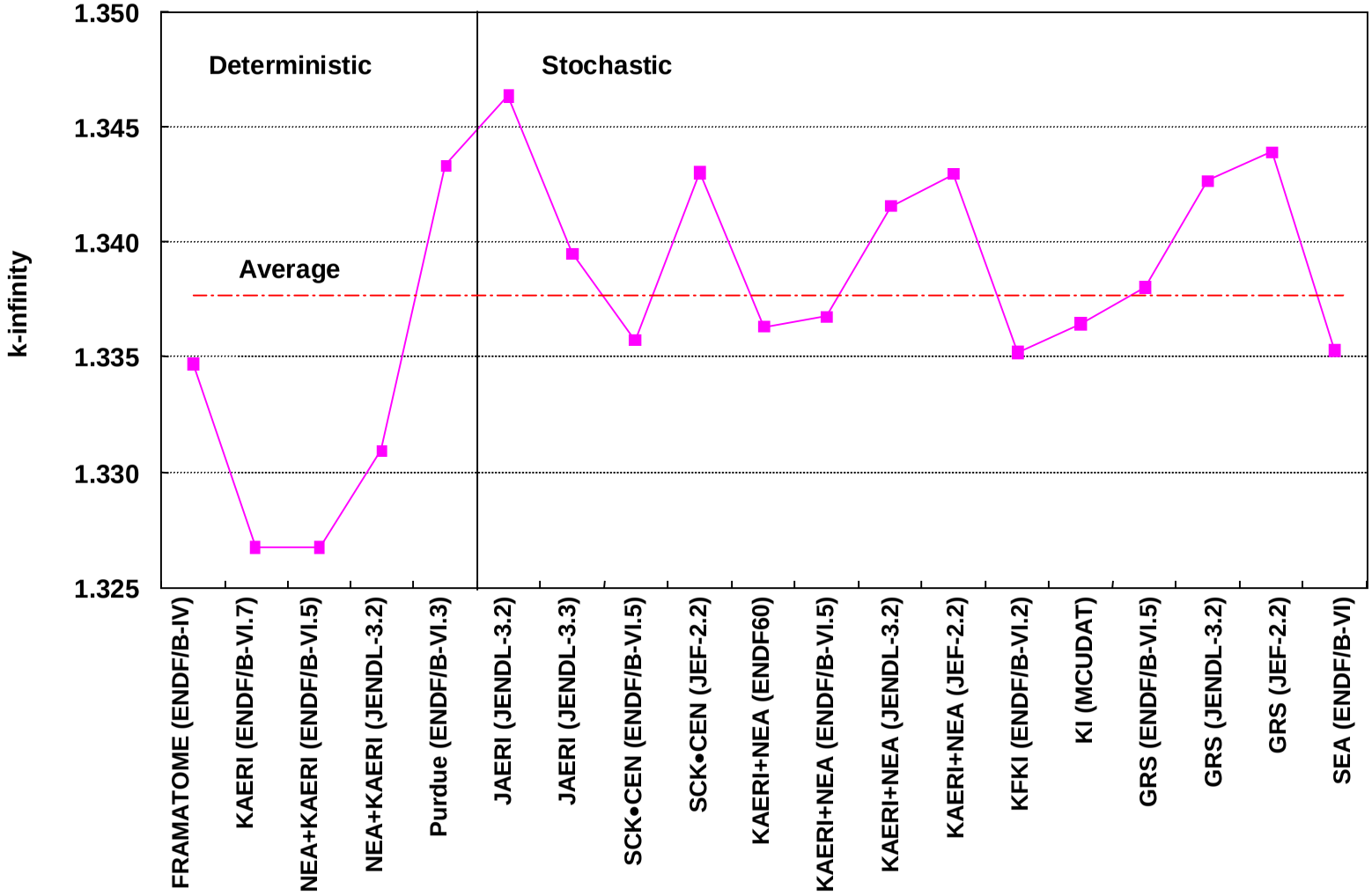

Figure 4.3. Calculated k_∞ values in MOX fuel pin

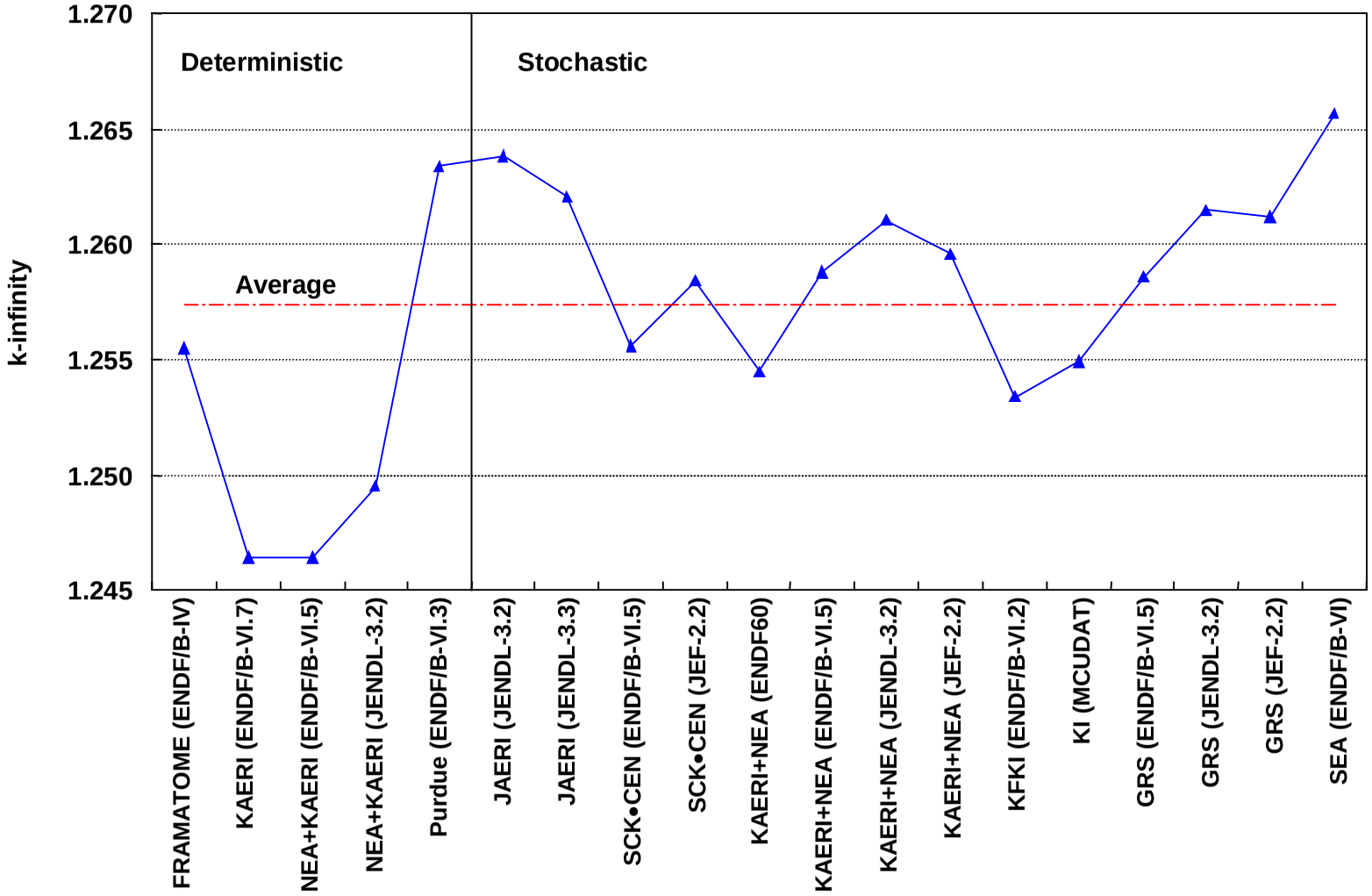

Figure 4.4(a). Comparison of ^{234}U total absorption reaction rates in MOX fuel pin (relative to the arbitrary reference GRS ENDF-VI.5 values)

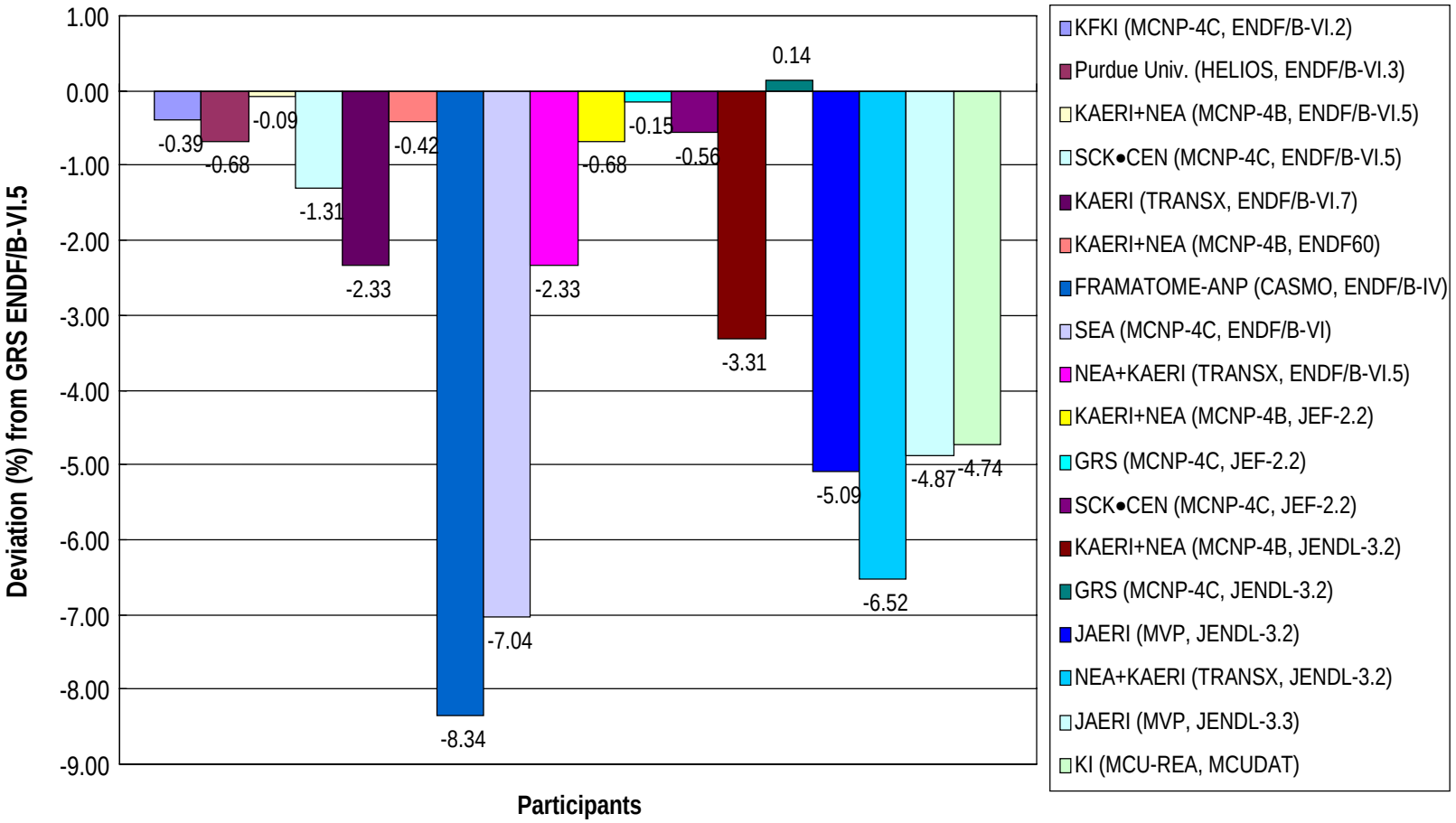

Figure 4.4(b). Comparison of ^{234}U total fission reaction rates in MOX fuel pin (relative to the arbitrary reference GRS ENDF-VI.5 values)

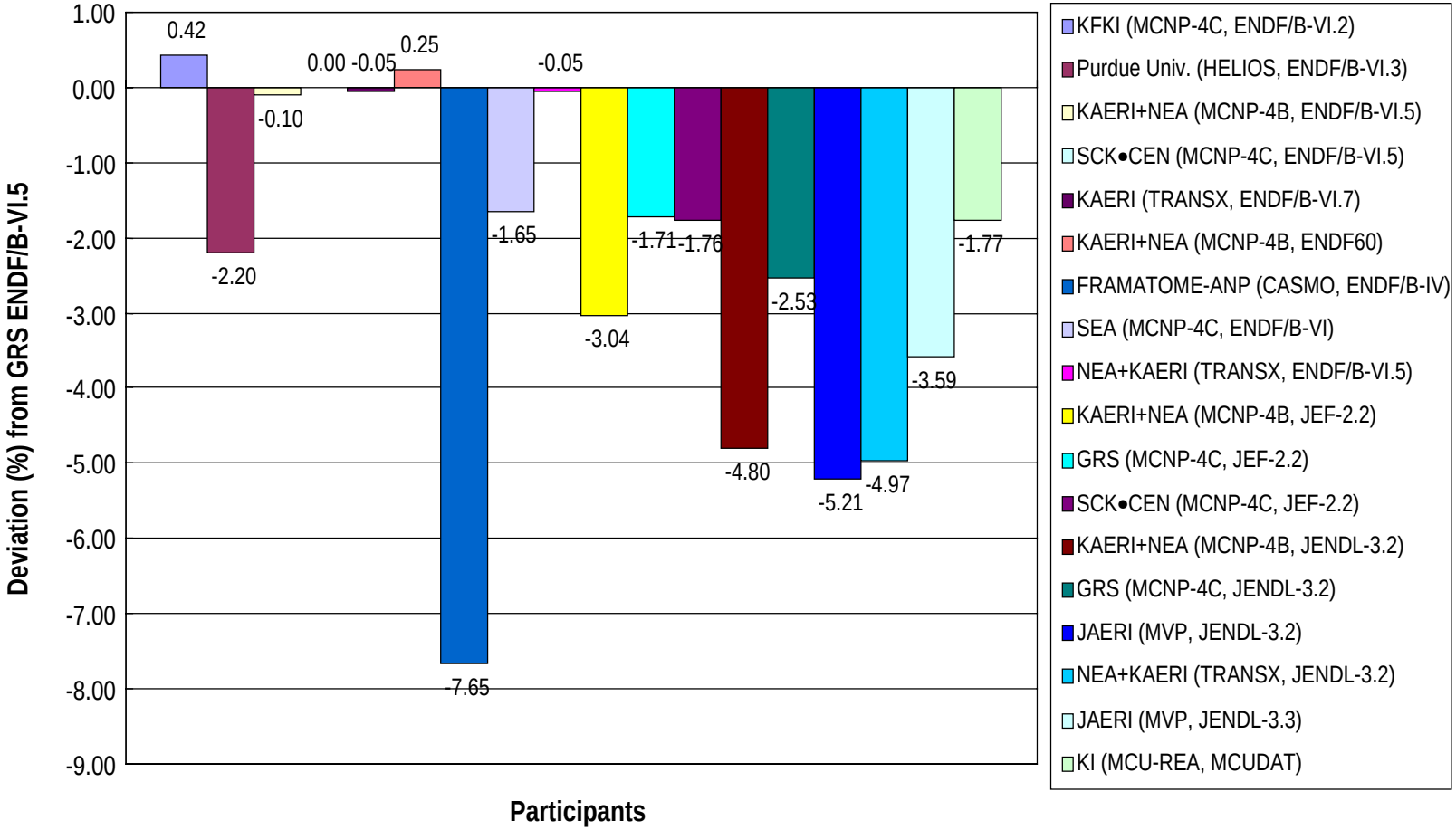

Figure 4.5(a). Comparison of ^{235}U total absorption reaction rates in MOX fuel pin (relative to the arbitrary reference GRS ENDF-VI.5 values)

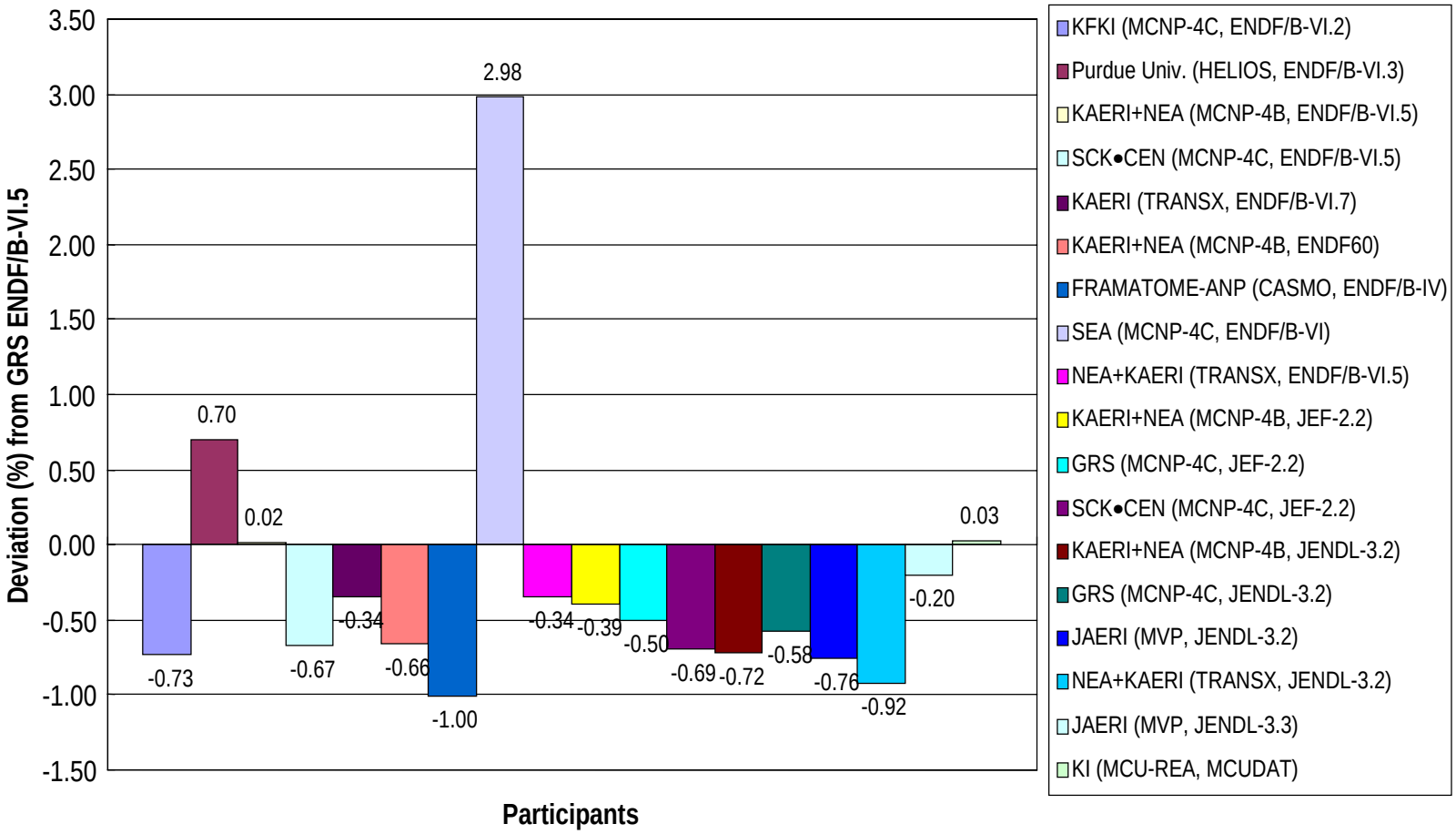

Figure 4.5(b). Comparison of ^{235}U total fission reaction rates in MOX fuel pin (relative to the arbitrary reference GRS ENDF-VI.5 values)

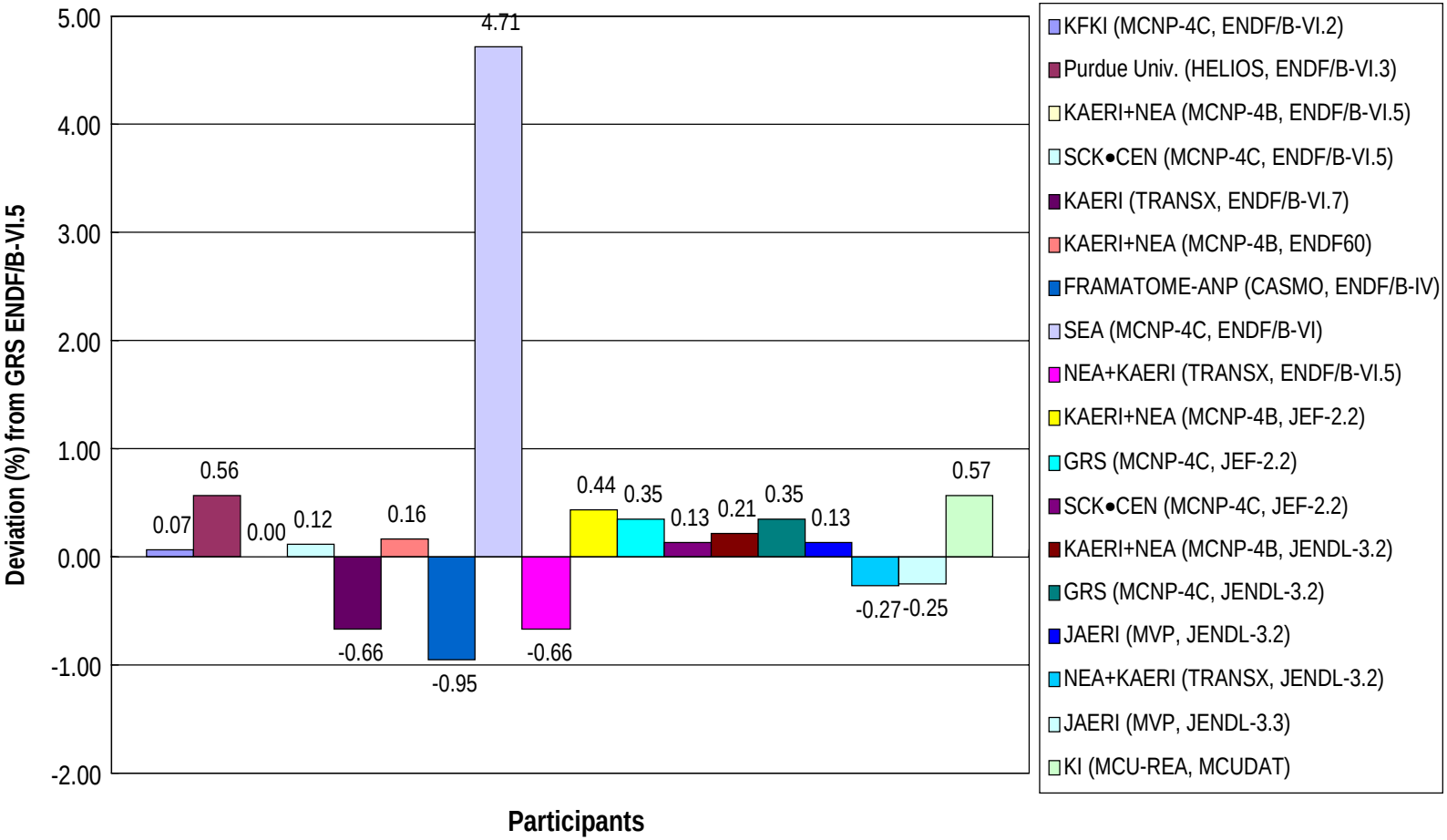

Figure 4.6(a). Comparison of ^{236}U total absorption reaction rates in MOX fuel pin (relative to the arbitrary reference GRS ENDF-VI.5 values)

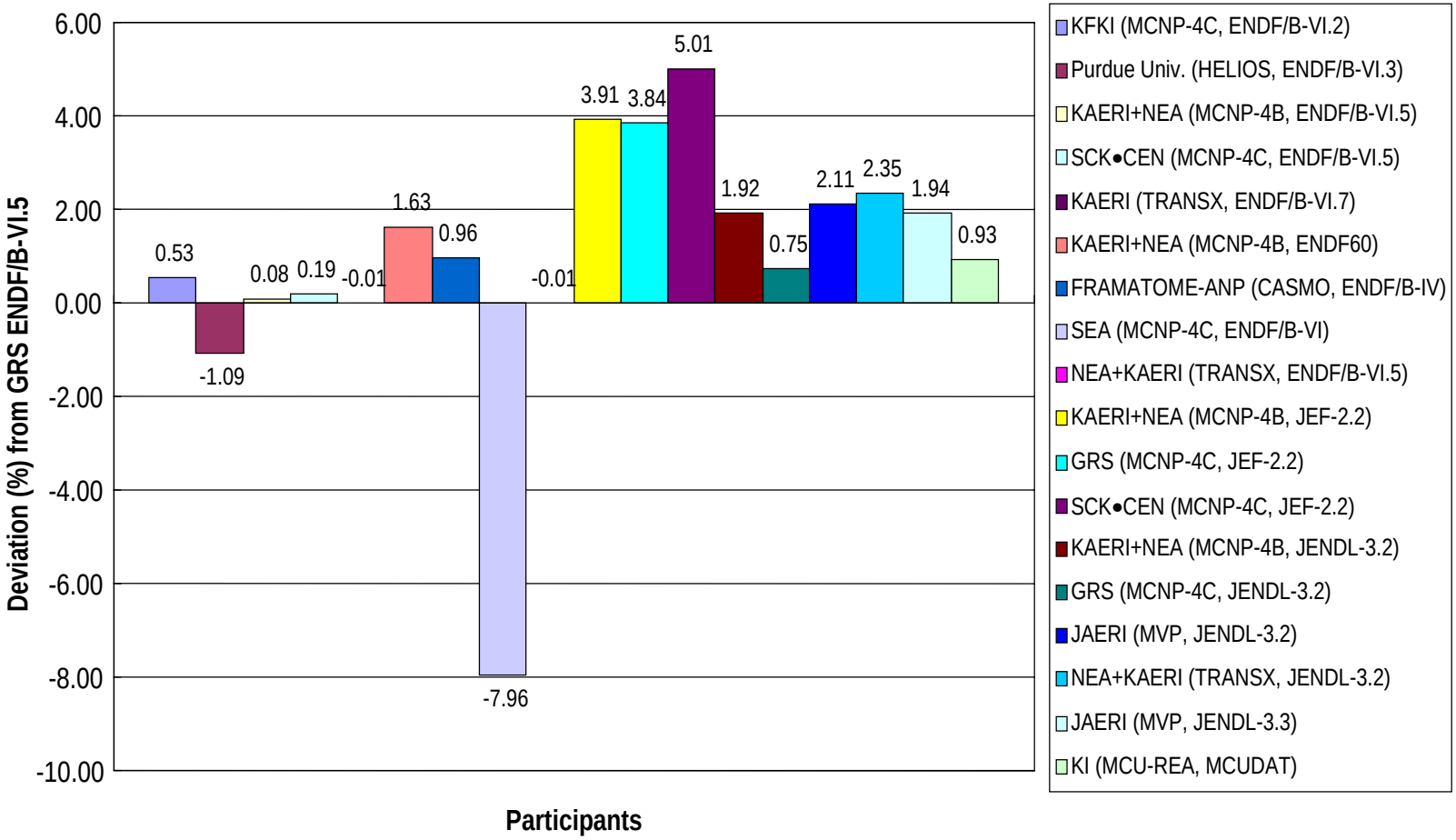

Figure 4.6(b). Comparison of ^{236}U total fission reaction rates in MOX fuel pin (relative to the arbitrary reference GRS ENDF-VI.5 values)

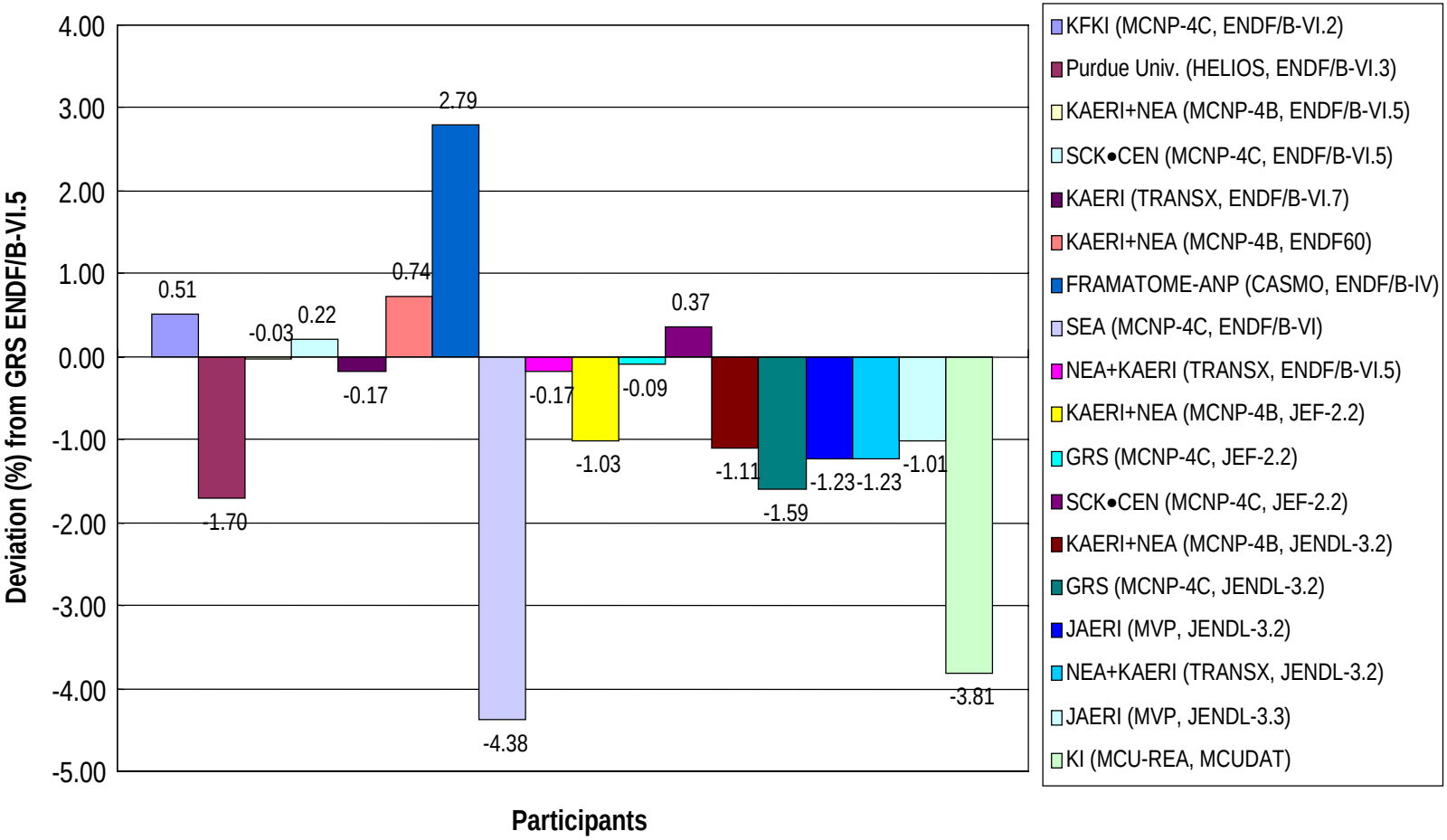

Figure 4.7(a). Comparison of ^{238}U total absorption reaction rates in MOX fuel pin (relative to the arbitrary reference GRS ENDF-VI.5 values)

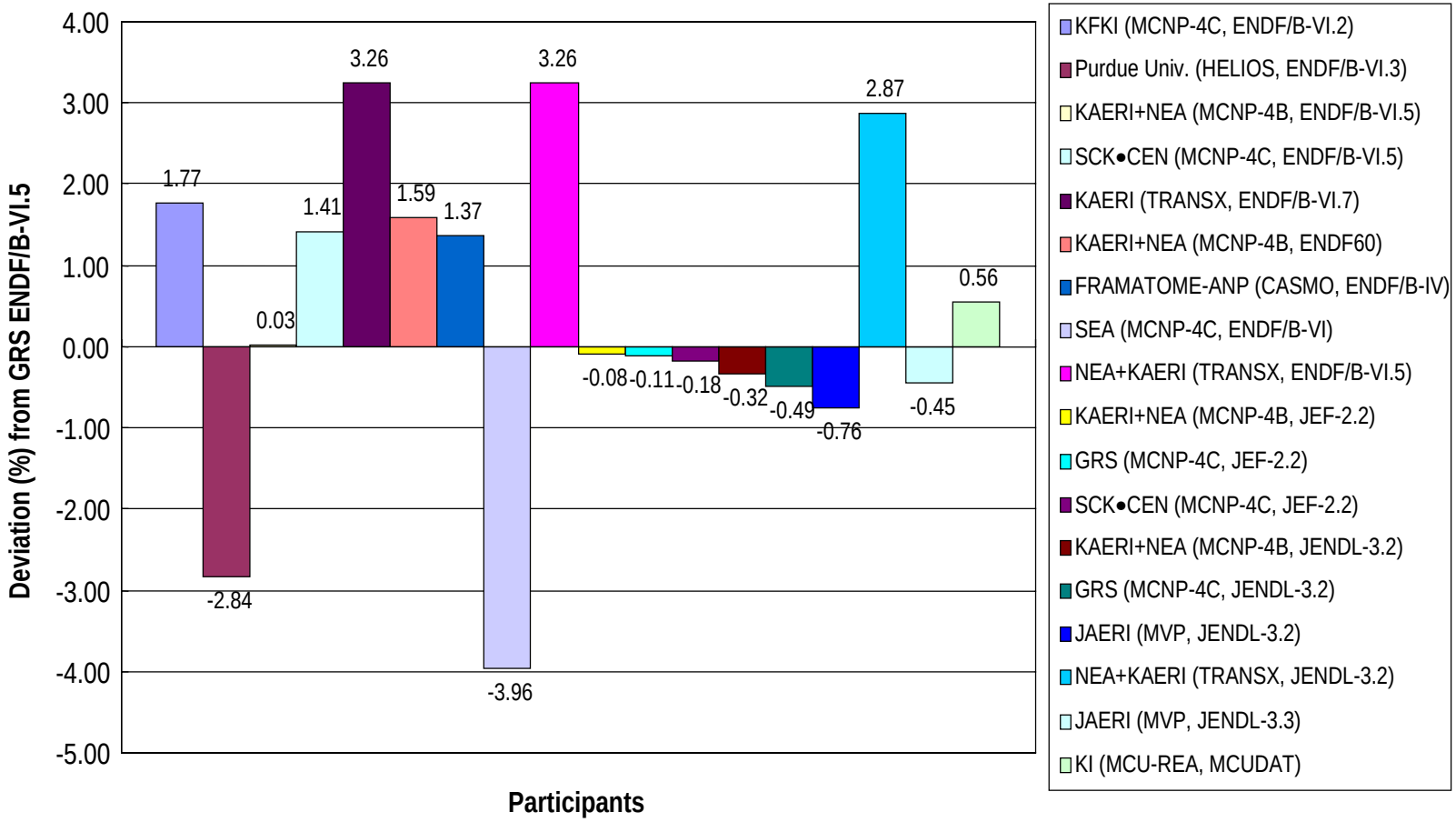

Figure 4.7(b). Comparison of ^{238}U total fission reaction rates in MOX fuel pin (relative to the arbitrary reference GRS ENDF-VI.5 values)

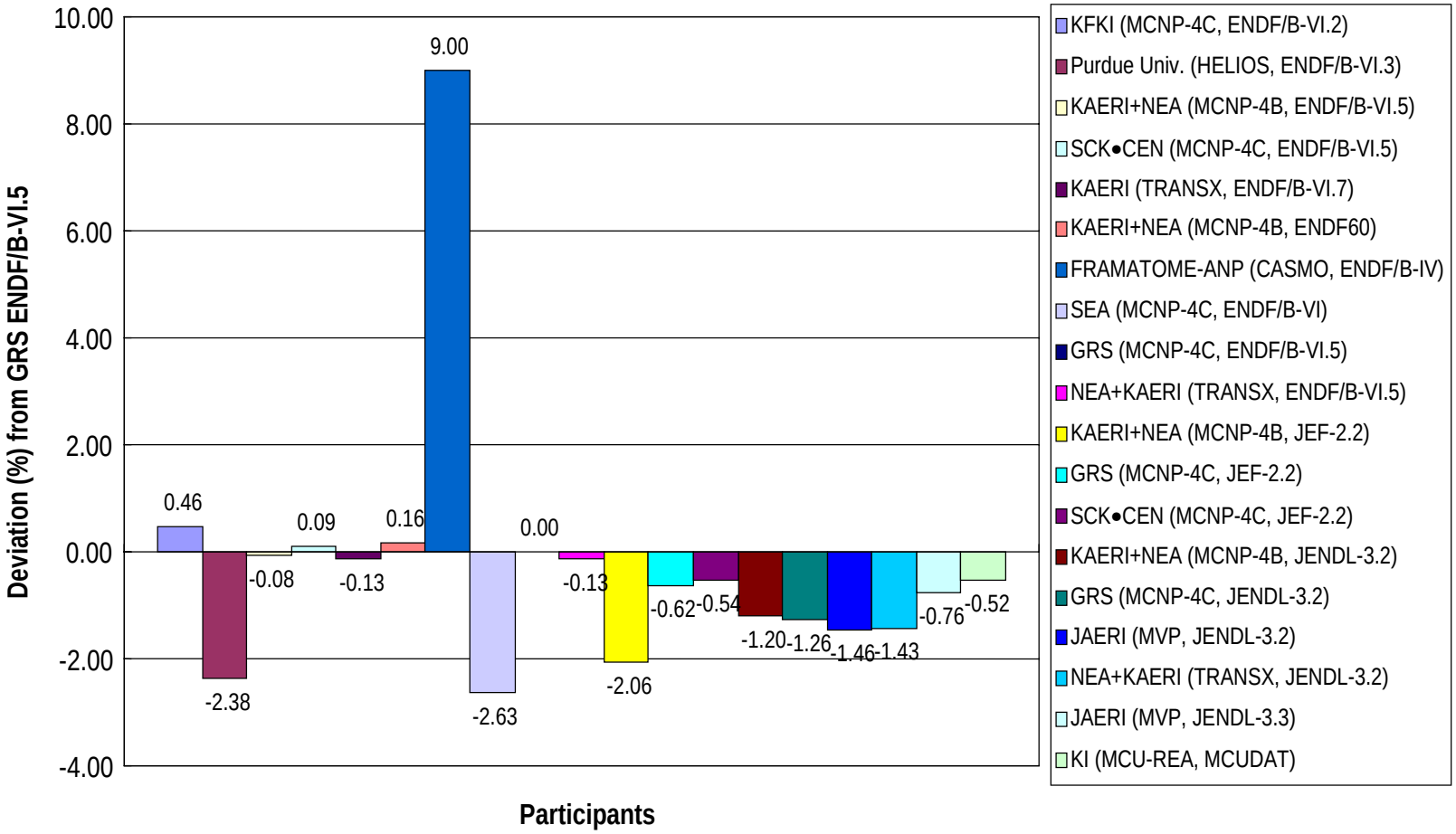

Figure 4.8(a). Comparison of ^{239}Pu total absorption reaction rates in MOX fuel pin (relative to the arbitrary reference GRS ENDF-VI.5 values)

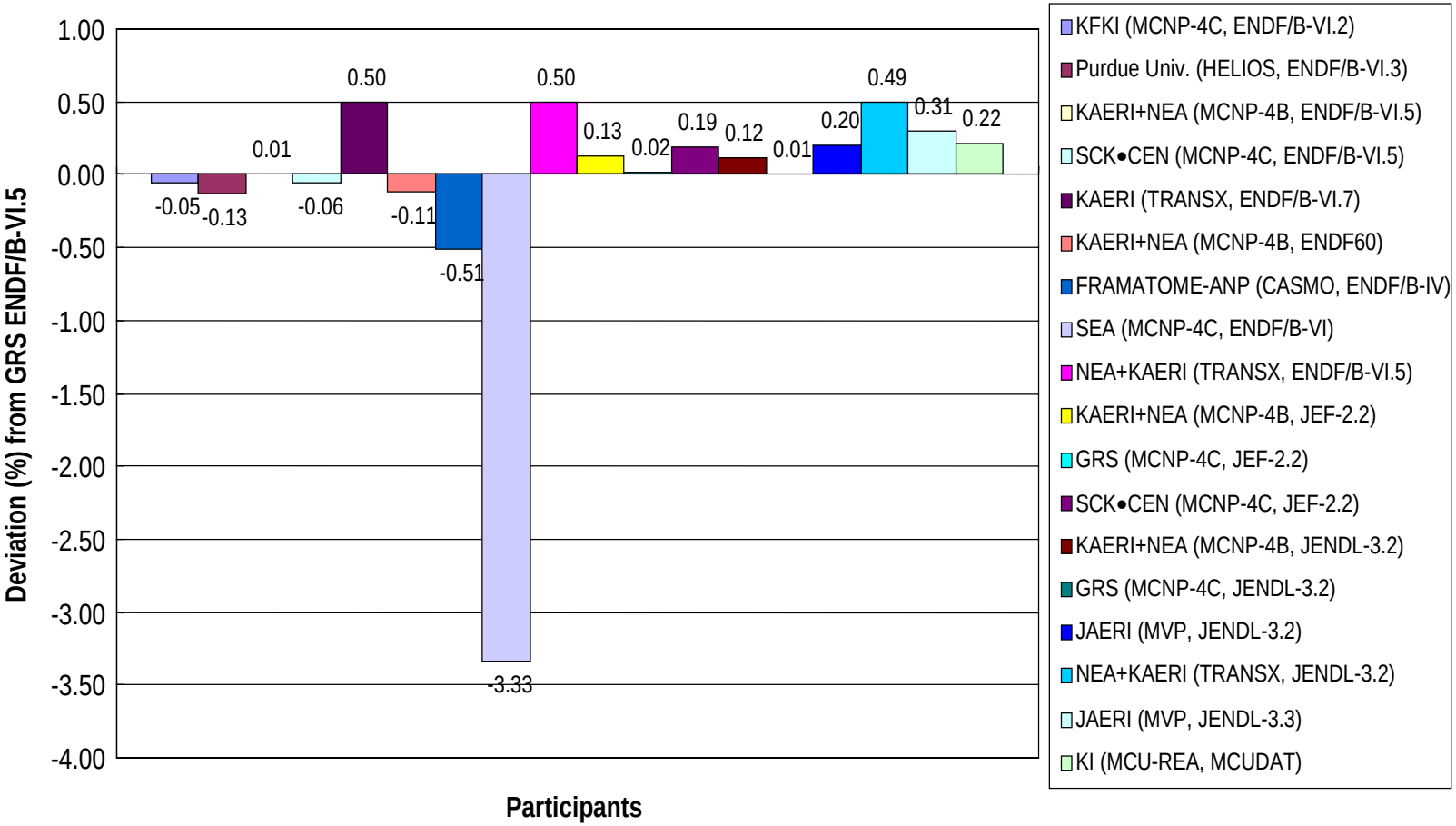

Figure 4.8(b). Comparison of ^{239}Pu total fission reaction rates in MOX fuel pin (relative to the arbitrary reference GRS ENDF-VI.5 values)

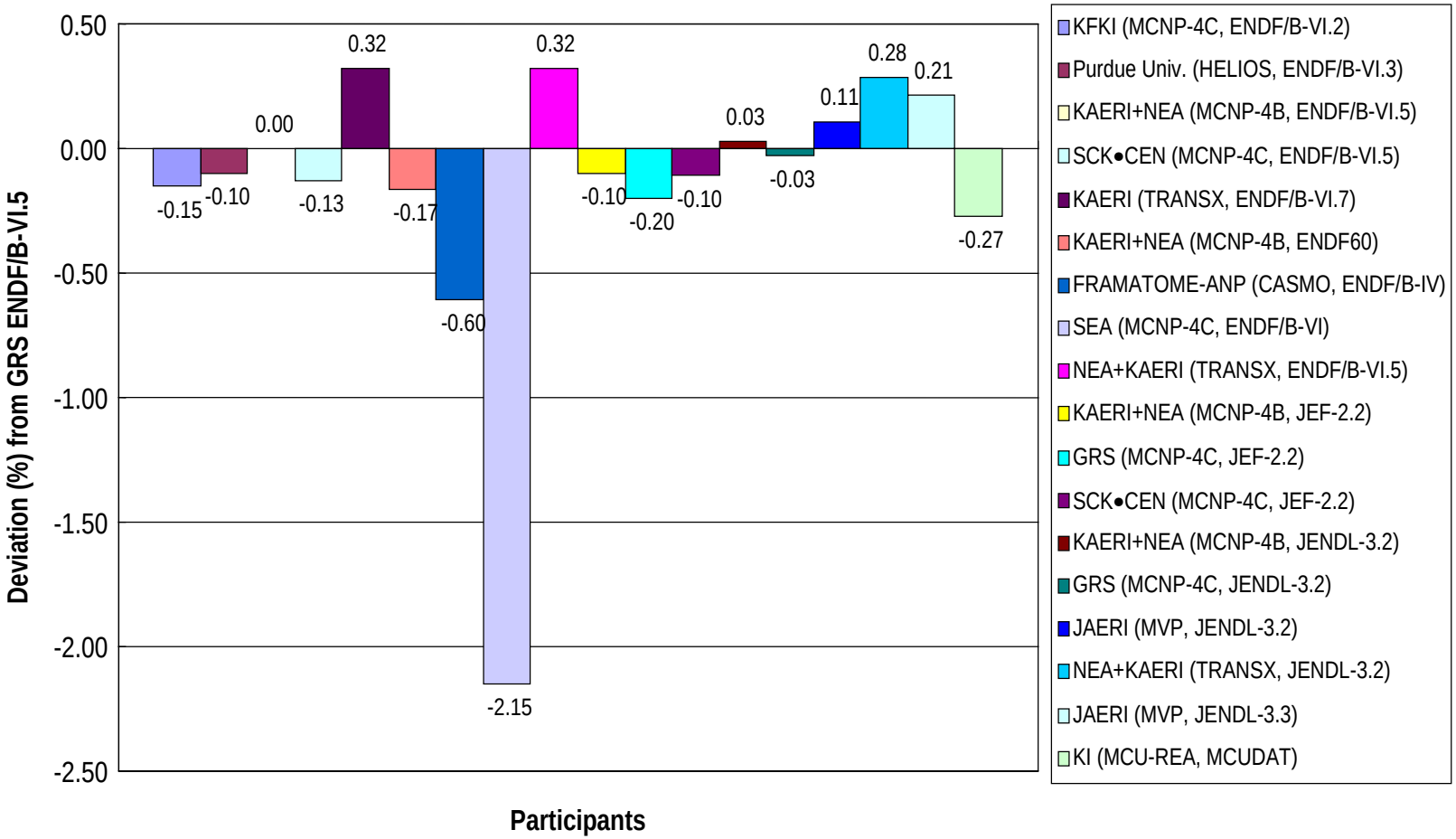

Figure 4.9(a). Comparison of ^{240}Pu total absorption reaction rates in MOX fuel pin (relative to the arbitrary reference GRS ENDF-VI.5 values)

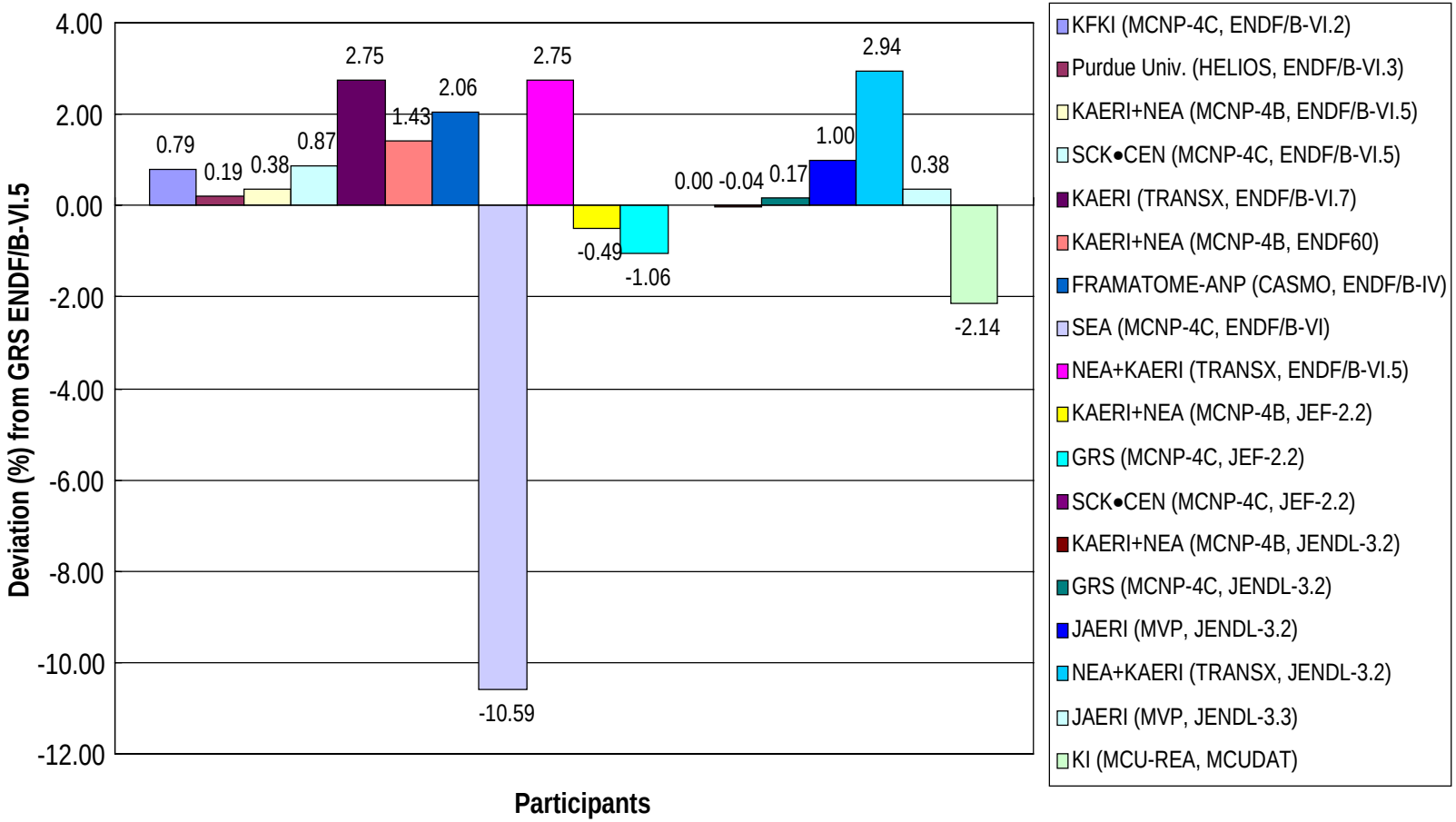

Figure 4.9(b). Comparison of ^{240}Pu total fission reaction rates in MOX fuel pin (relative to the arbitrary reference GRS ENDF-VI.5 values)

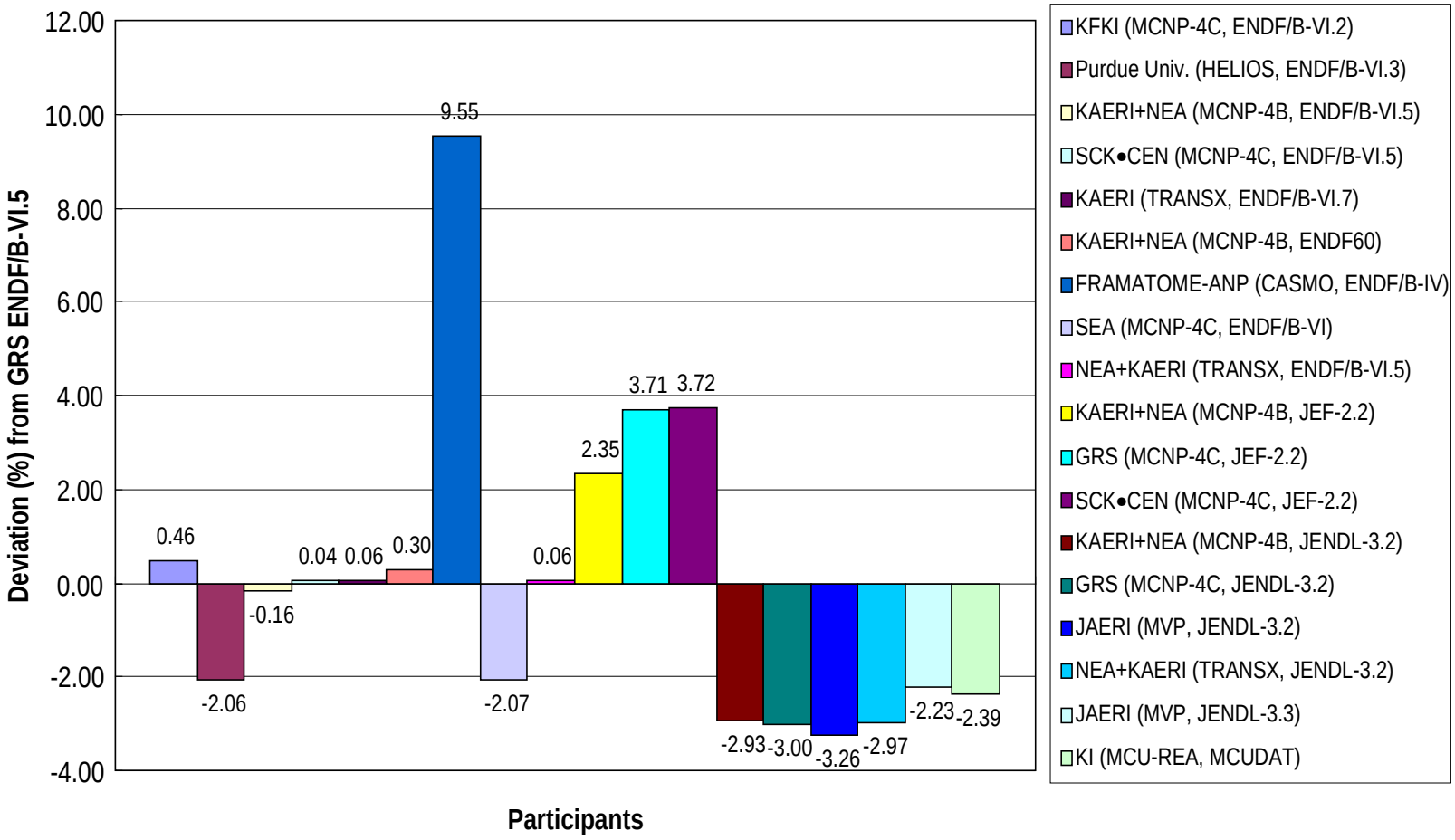

Figure 4.10(a). Comparison of ^{241}Pu total absorption reaction rates in MOX fuel pin (relative to the arbitrary reference GRS ENDF-VI.5 values)

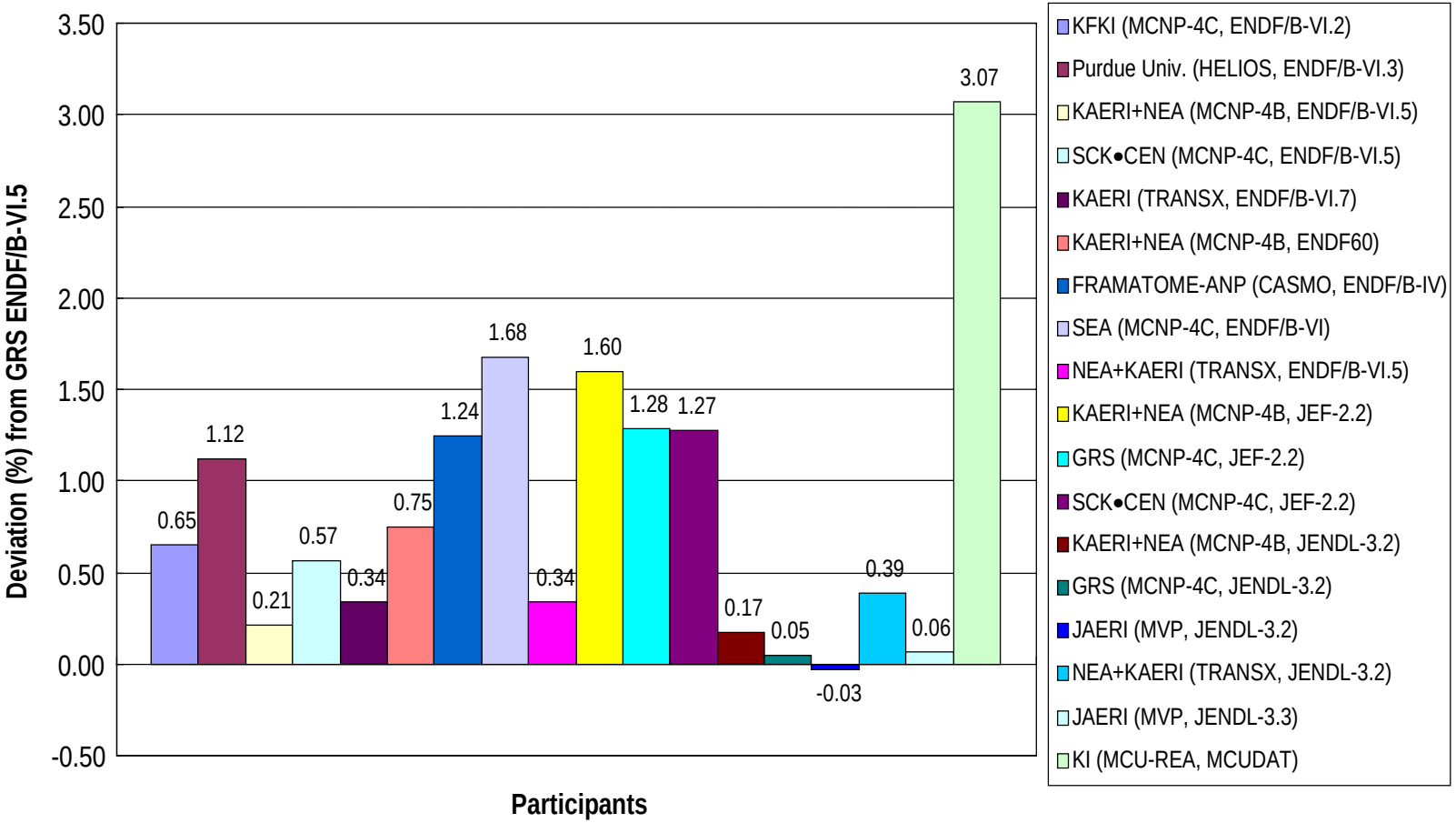

Figure 4.10(b). Comparison of ^{241}Pu total fission reaction rates in MOX fuel pin (relative to the arbitrary reference GRS ENDF-VI.5 values)

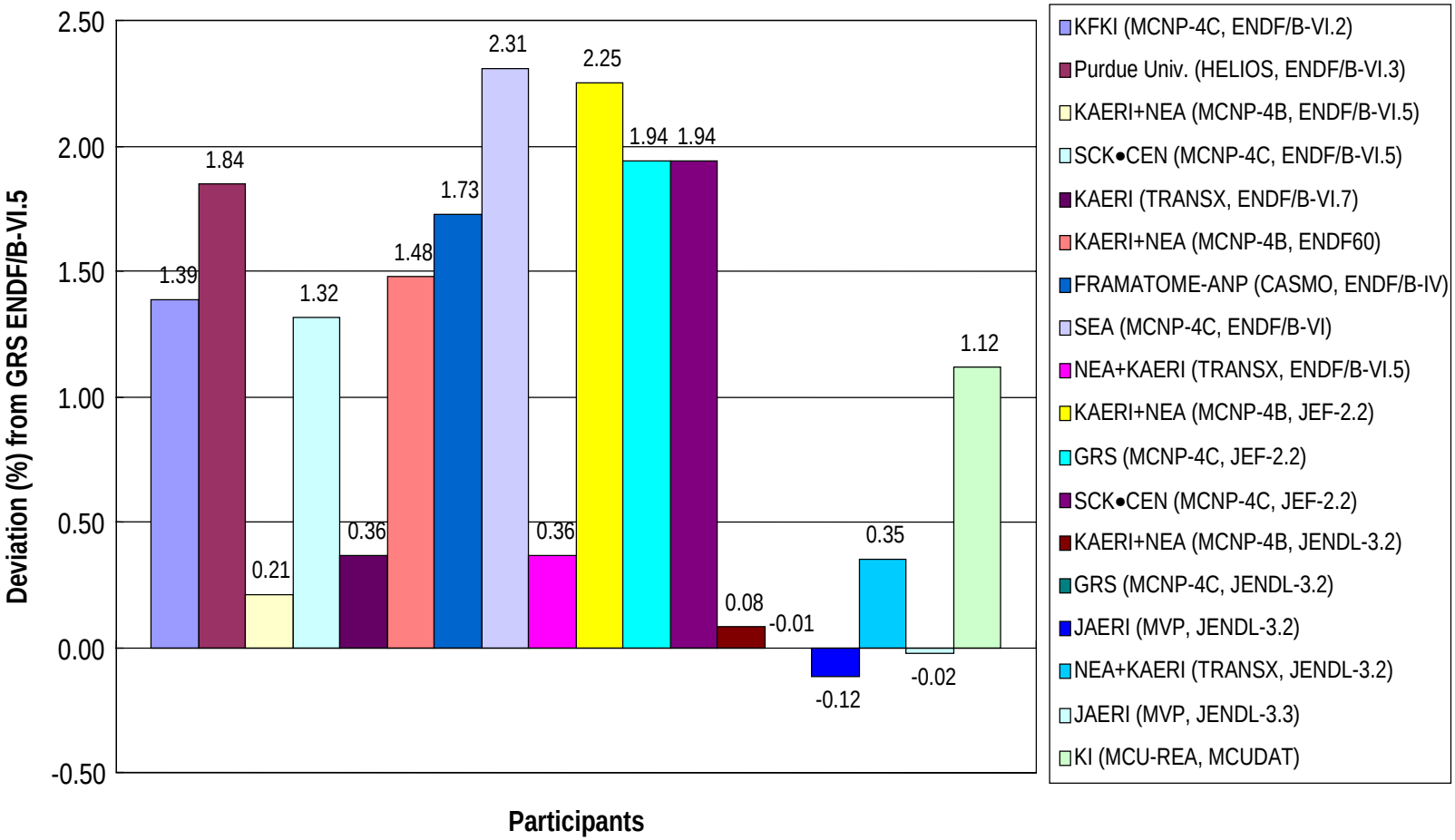

Figure 4.11(a). Comparison of ^{242}Pu total absorption reaction rates in MOX fuel pin (relative to the arbitrary reference GRS ENDF-VI.5 values)

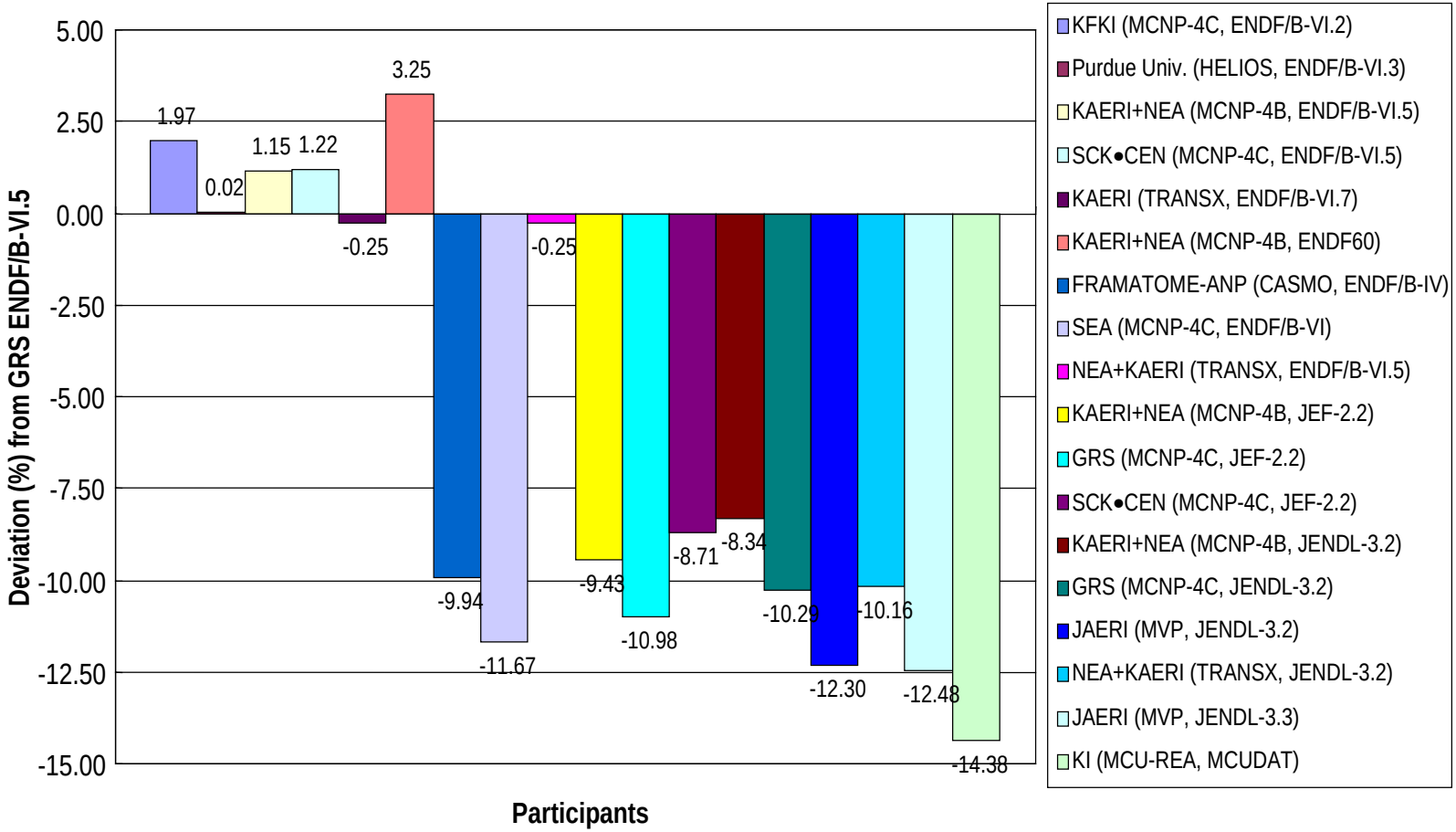

Figure 4.11(b). Comparison of ^{242}Pu total fission reaction rates in MOX fuel pin (relative to the arbitrary reference GRS ENDF-VI.5 values)

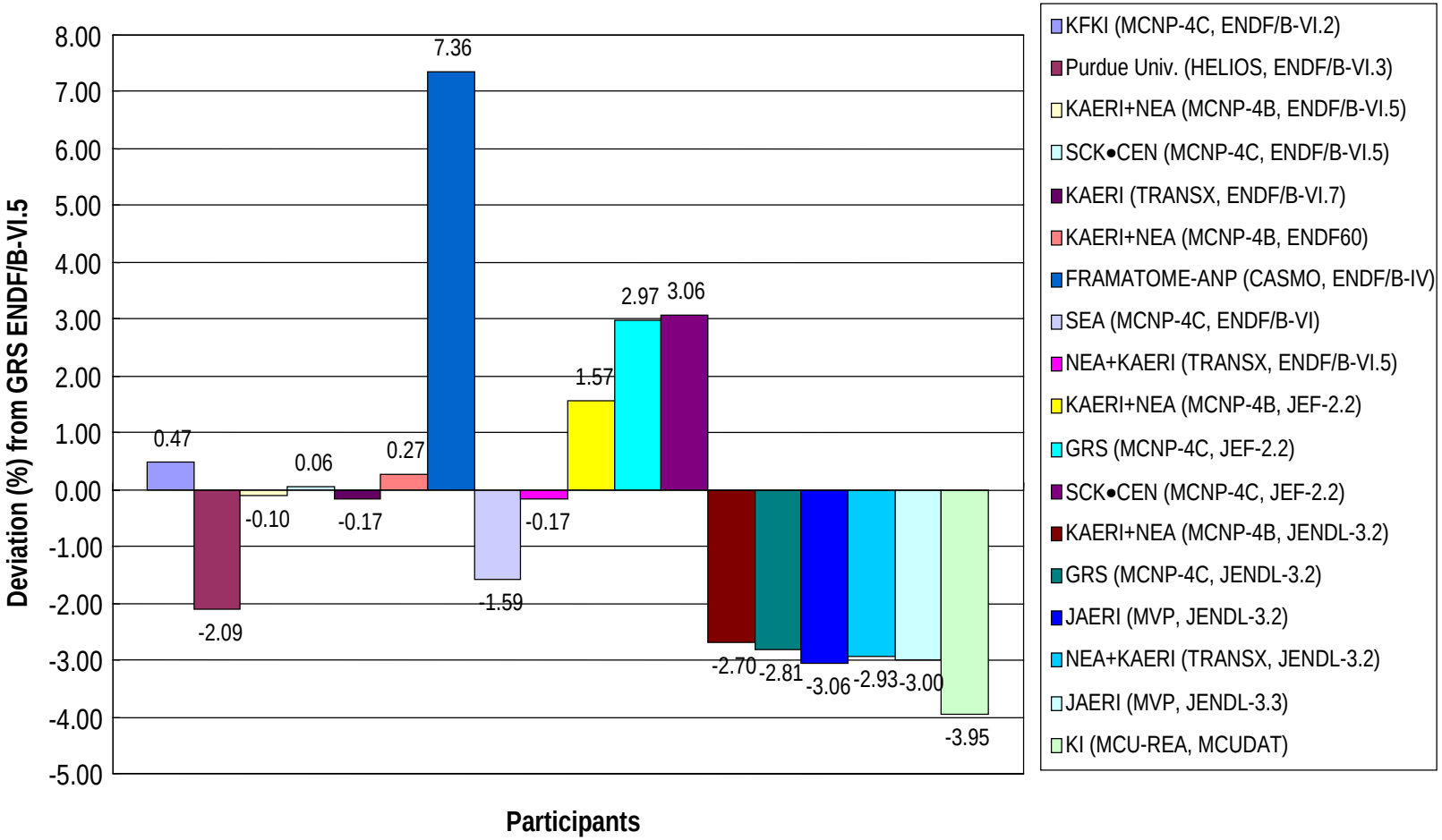

Figure 4.12(a). Comparison of ^{241}Am total absorption reaction rates in MOX fuel pin (relative to the arbitrary reference GRS ENDF-VI.5 values)

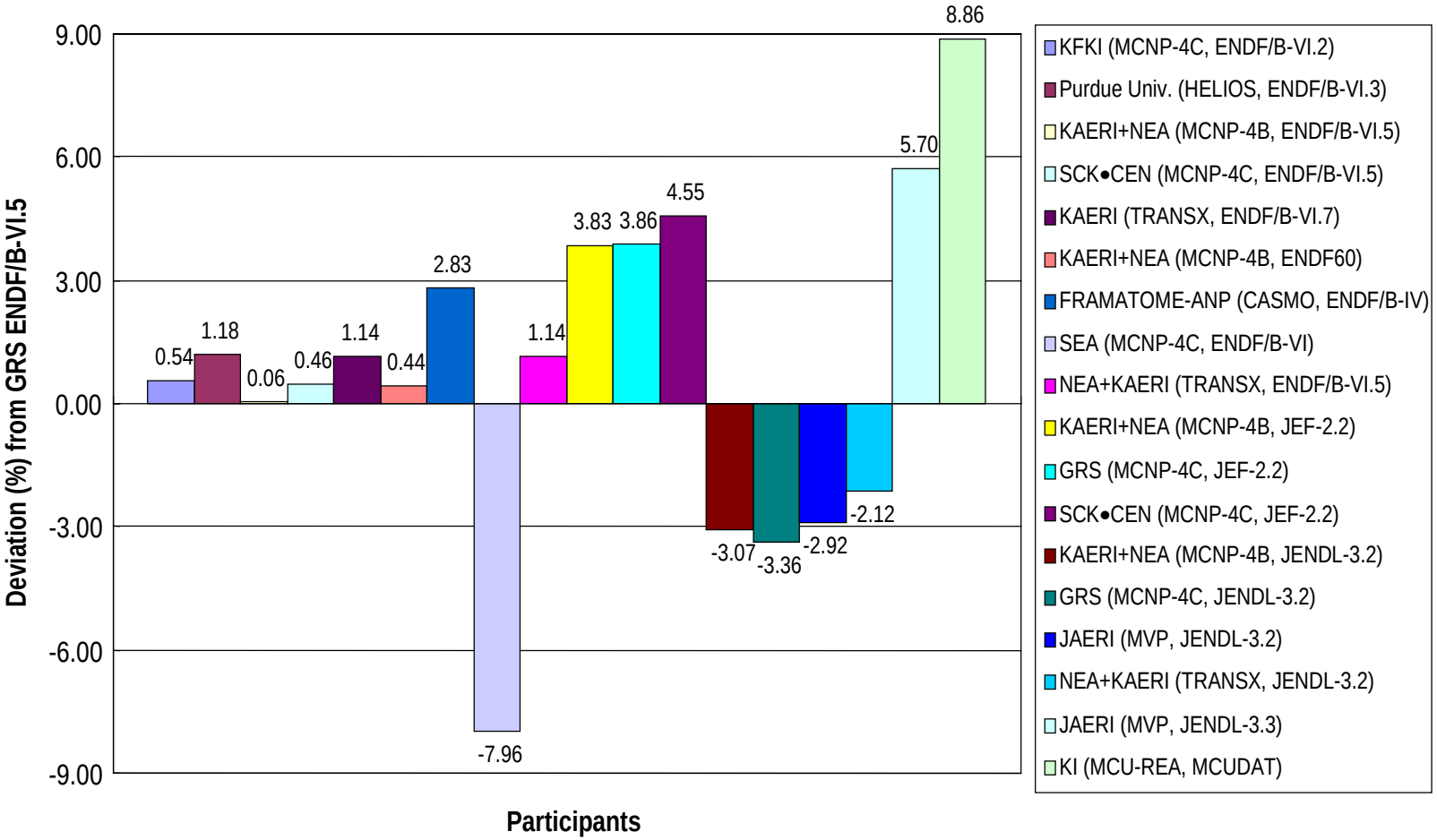

Figure 4.12(b). Comparison of ^{241}Am total fission reaction rates in MOX fuel pin (relative to the arbitrary reference GRS ENDF-VI.5 values)

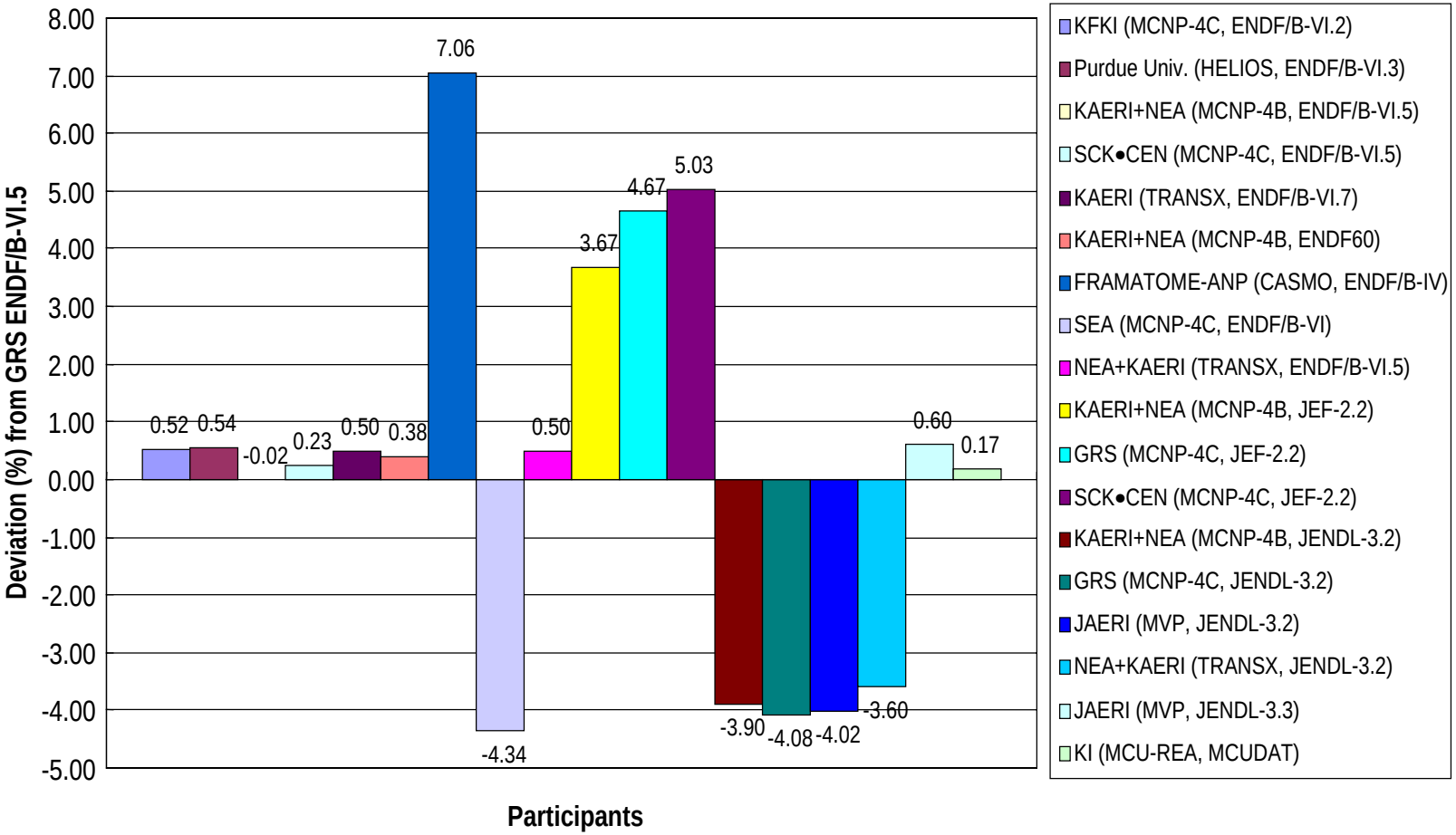

Figure 4.13(a). Comparison of ^{235}U total absorption reaction rates in 3/0 UO_2 fuel pin (relative to the arbitrary reference GRS ENDF-VI.5 values)

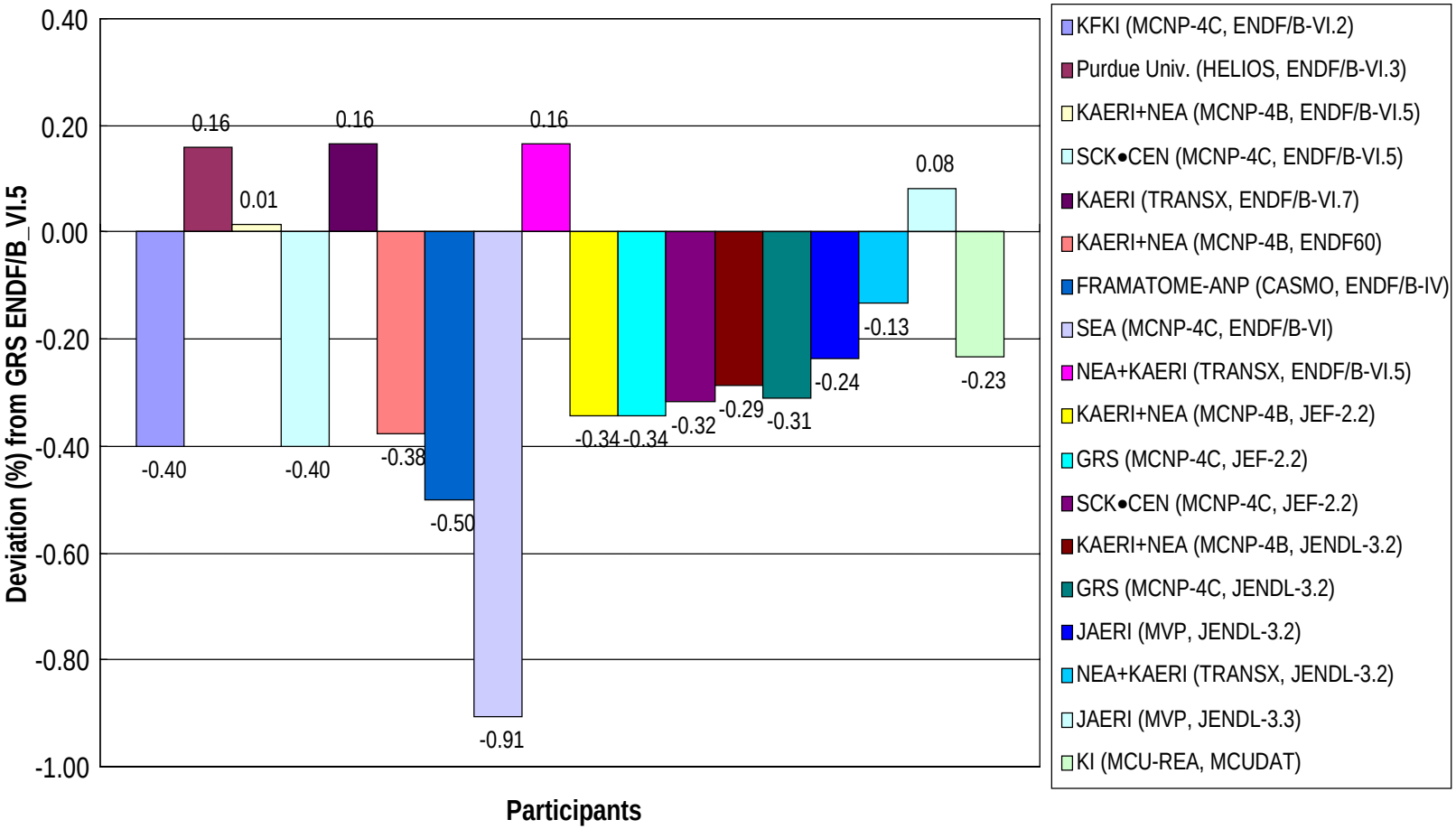

Figure 4.13(b). Comparison of ^{235}U total fission reaction rates in 3/0 UO_2 fuel pin (relative to the arbitrary reference GRS ENDF-VI.5 values)

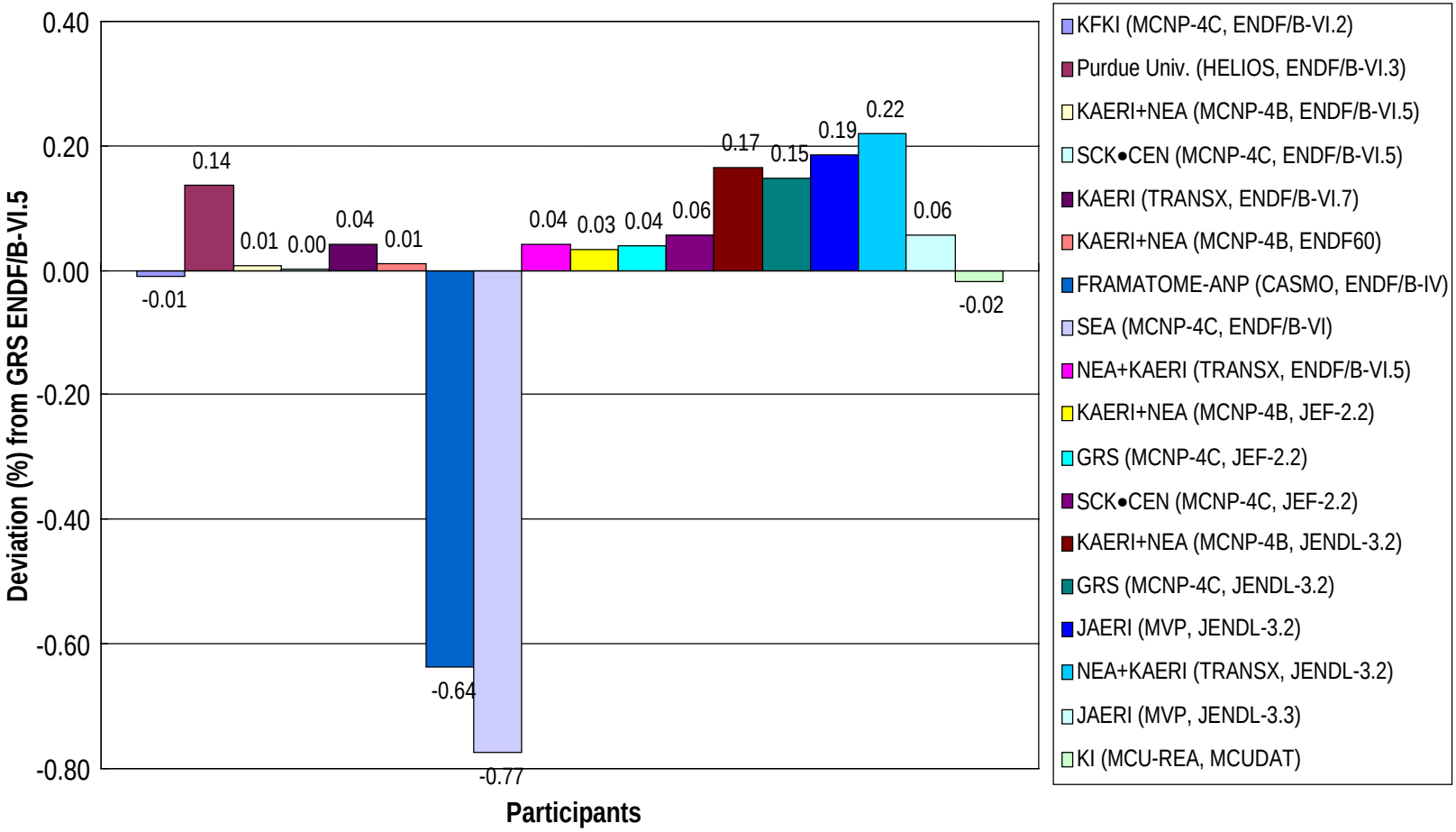

Figure 4.14(a). Comparison of ^{238}U total absorption reaction rates in 3/0 UO_2 fuel pin (relative to the arbitrary reference GRS ENDF-VI.5 values)

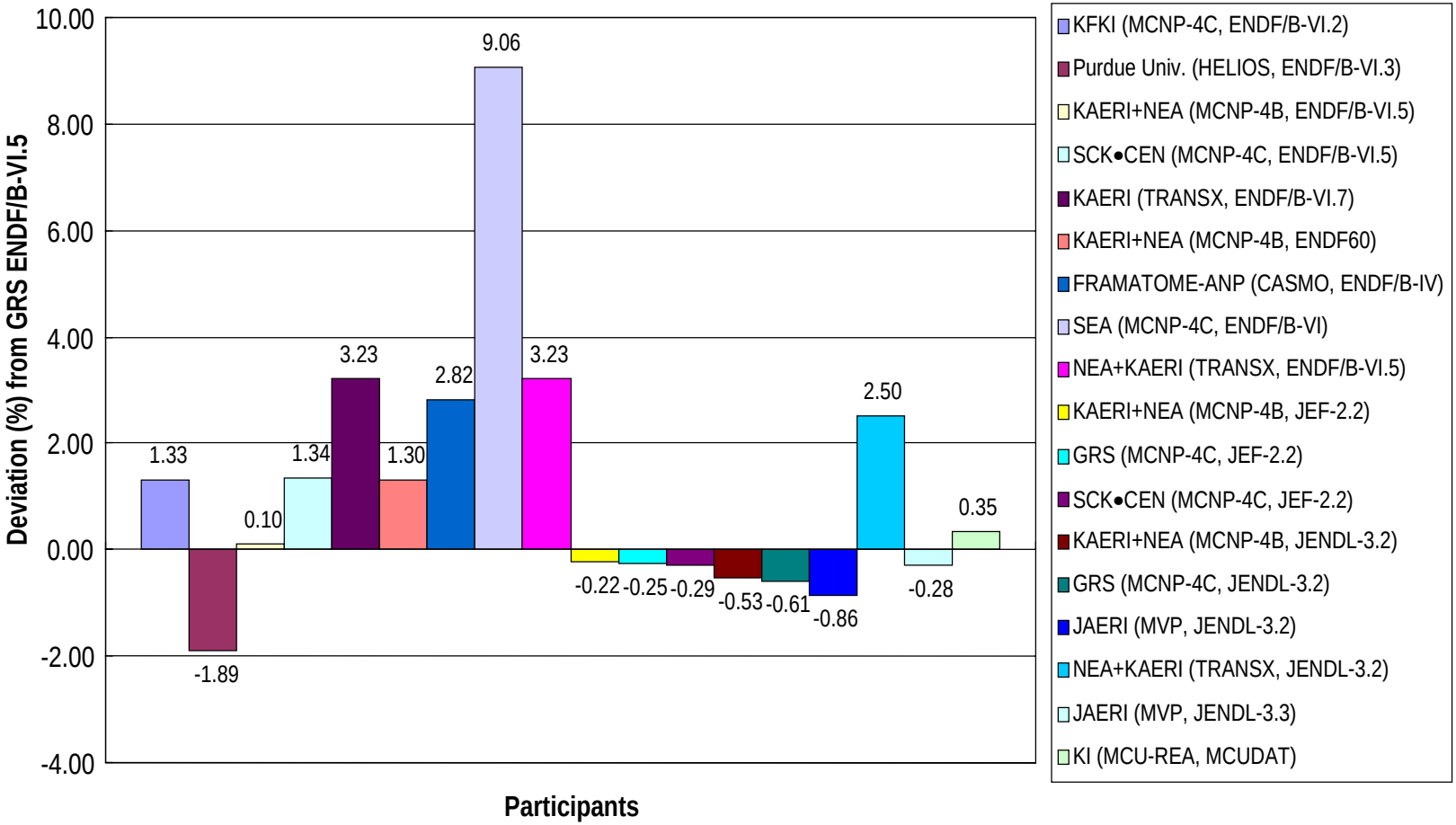

Figure 4.14(b). Comparison of ^{238}U total fission reaction rates in 3/0 UO_2 fuel pin (relative to the arbitrary reference GRS ENDF-VI.5 values)

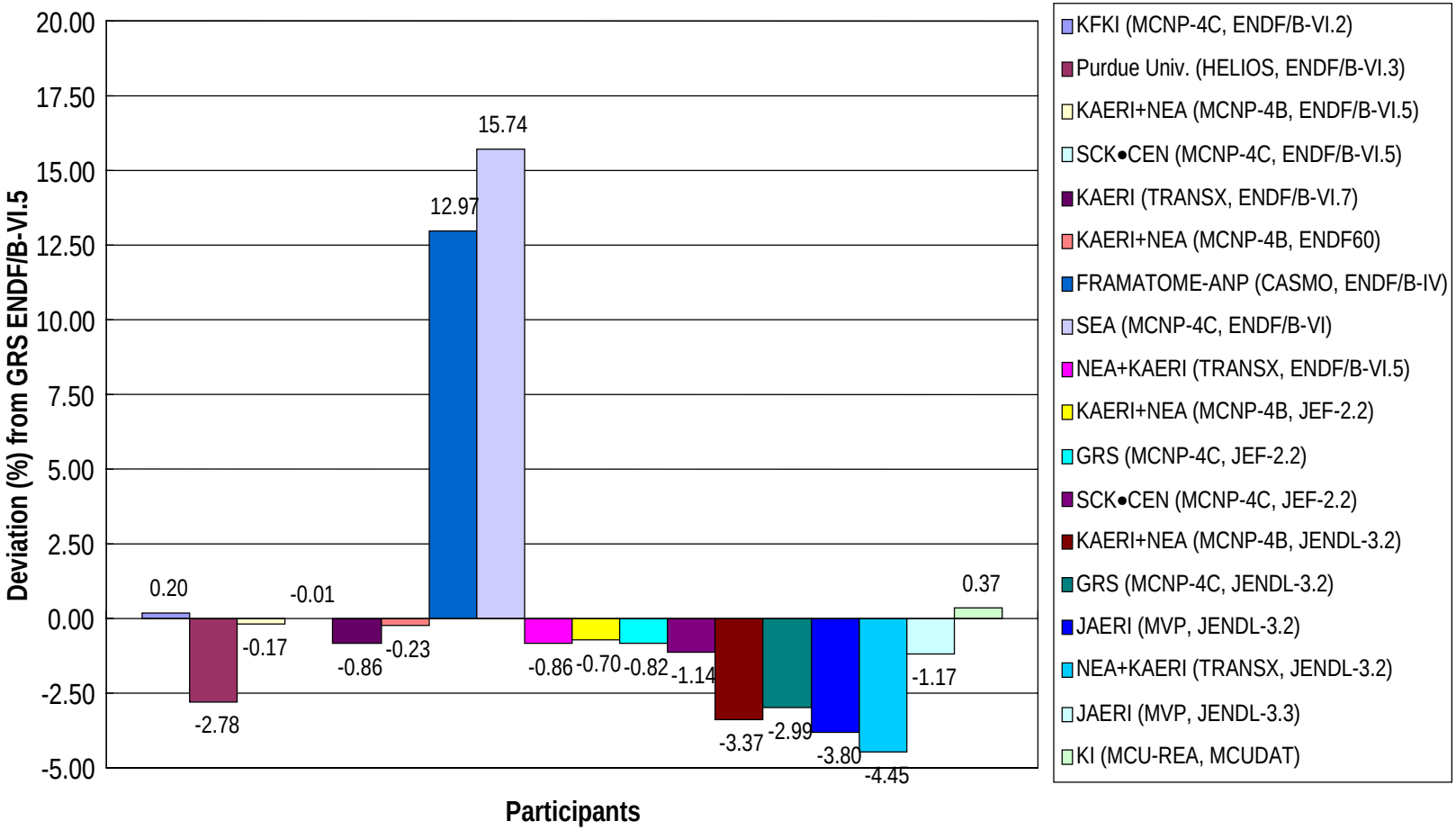

Figure 4.15(a). Comparison of ^{235}U total absorption reaction rates in 4/0 UO_2 fuel pin (relative to the arbitrary reference GRS ENDF-VI.5 values)

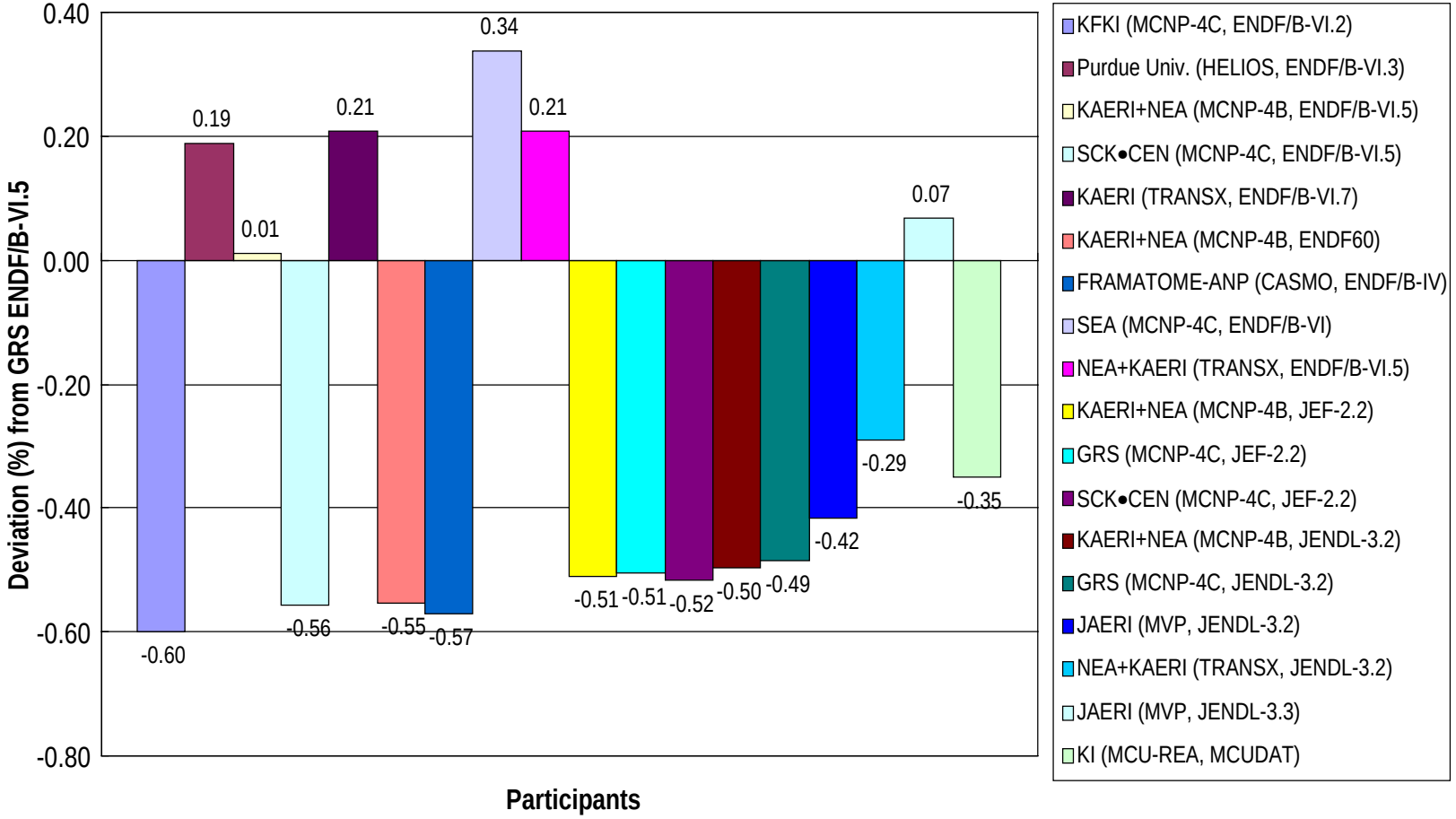

Figure 4.15(b). Comparison of ^{235}U total fission reaction rates in 4/0 UO_2 fuel pin (relative to the arbitrary reference GRS ENDF-VI.5 values)

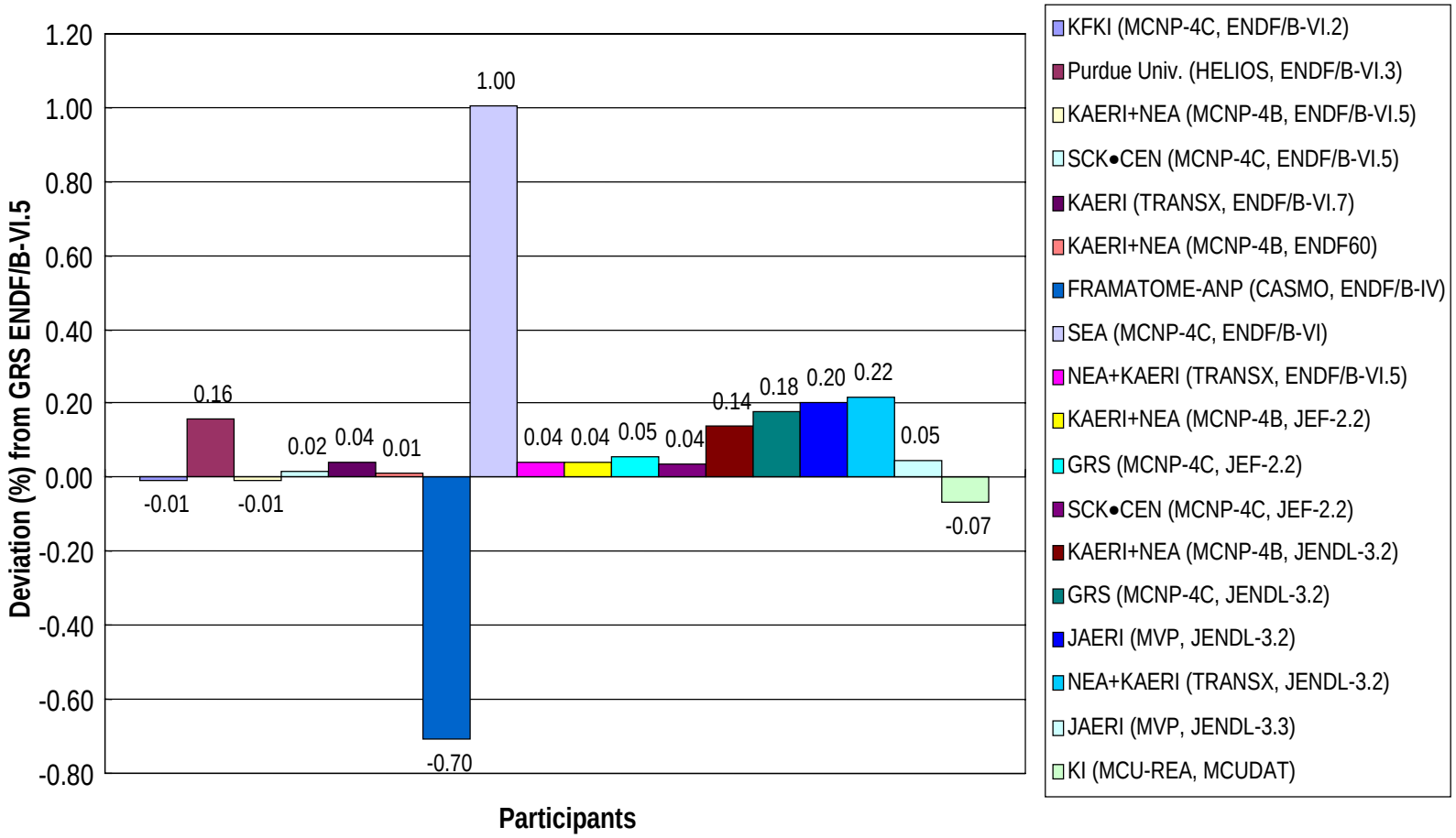

Figure 4.16(a). Comparison of ^{238}U total absorption reaction rates in 4/0 UO_2 fuel pin (relative to the arbitrary reference GRS ENDF-VI.5 values)

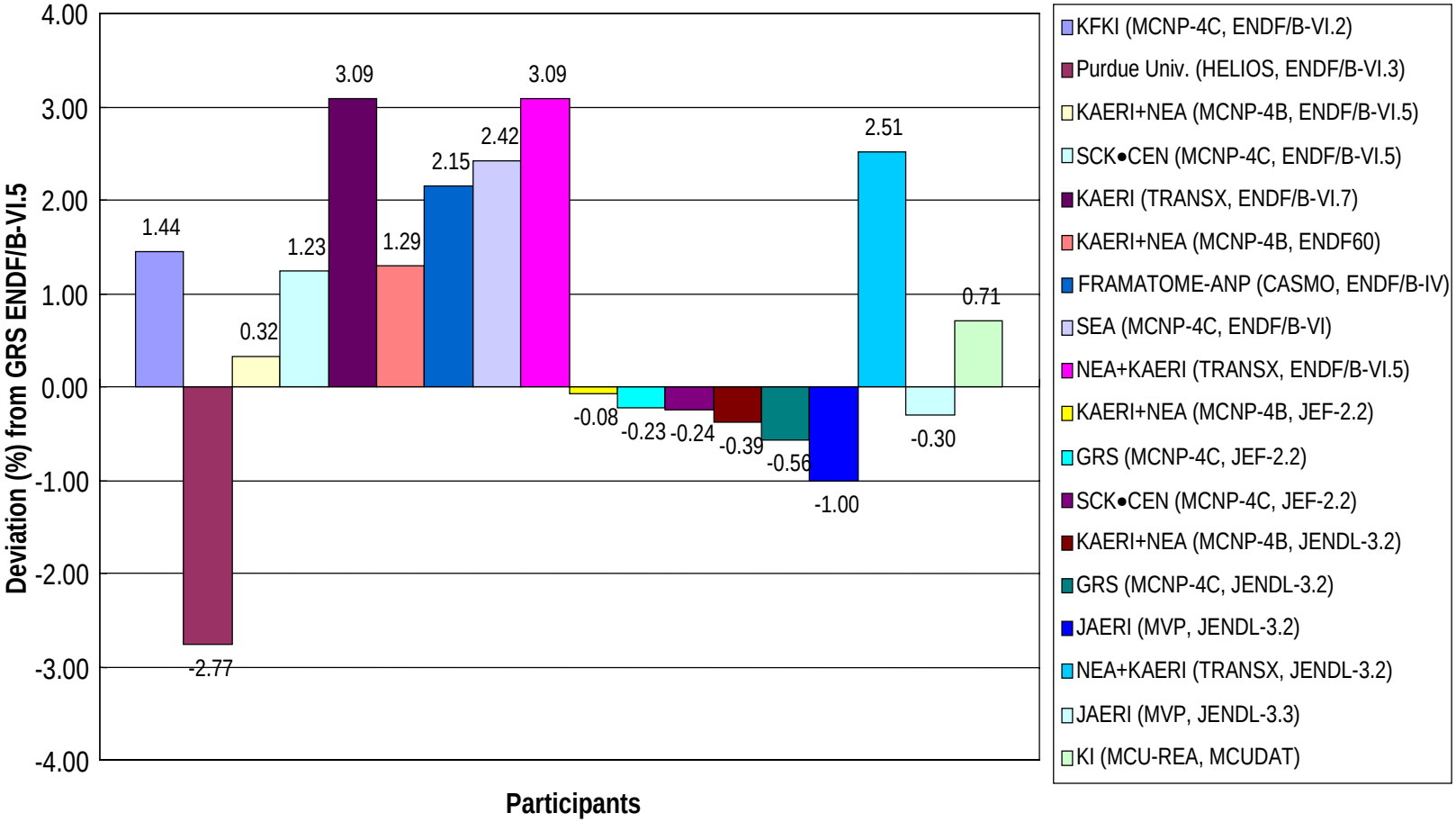

Figure 4.16(b). Comparison of ^{238}U total fission reaction rates in 4/0 UO_2 fuel pin (relative to the arbitrary reference GRS ENDF-VI.5 values)

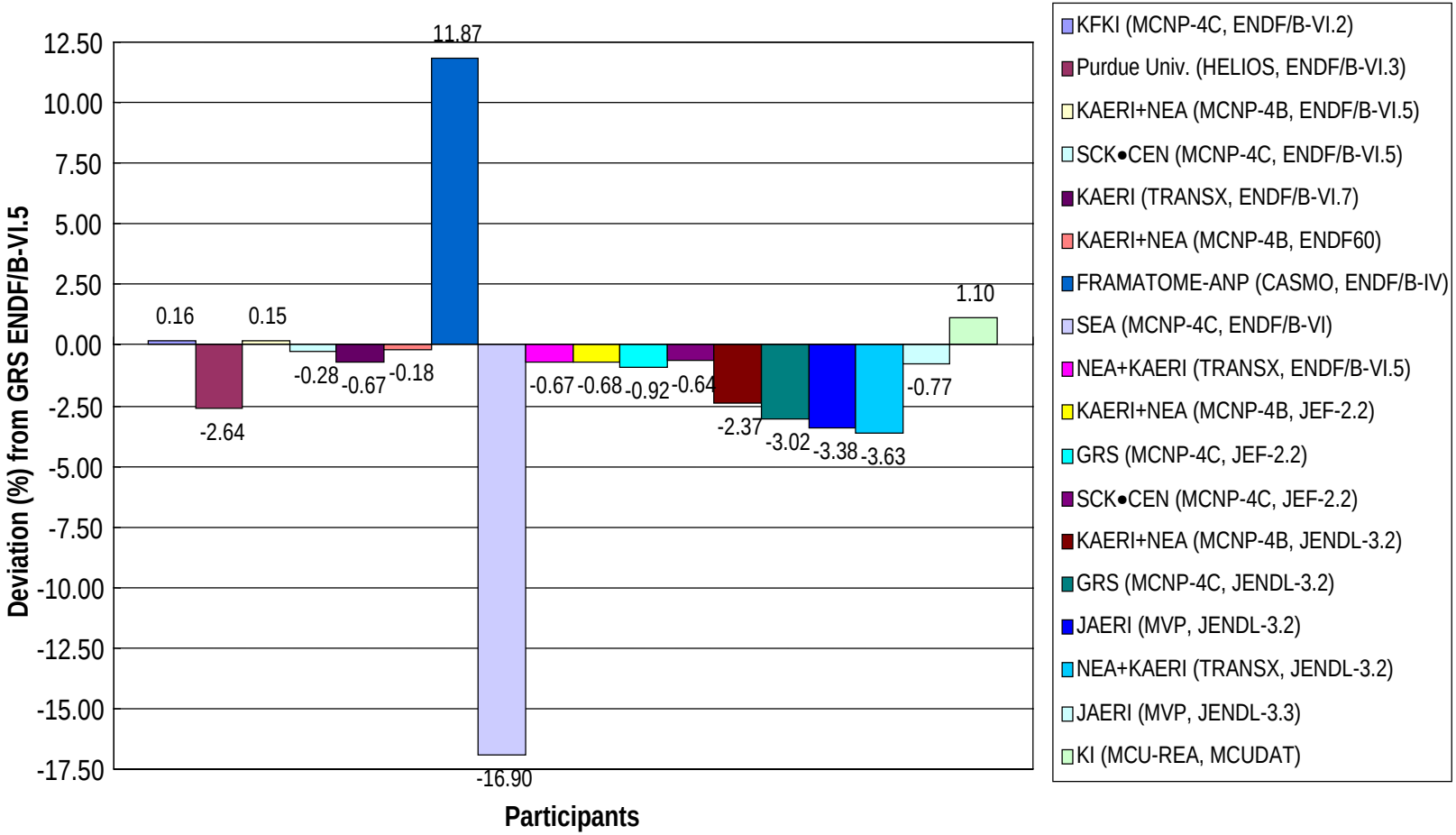

Figure 4.17. Deterministic calculations: Comparison of axial power distributions in MOX pin (-27,-12)

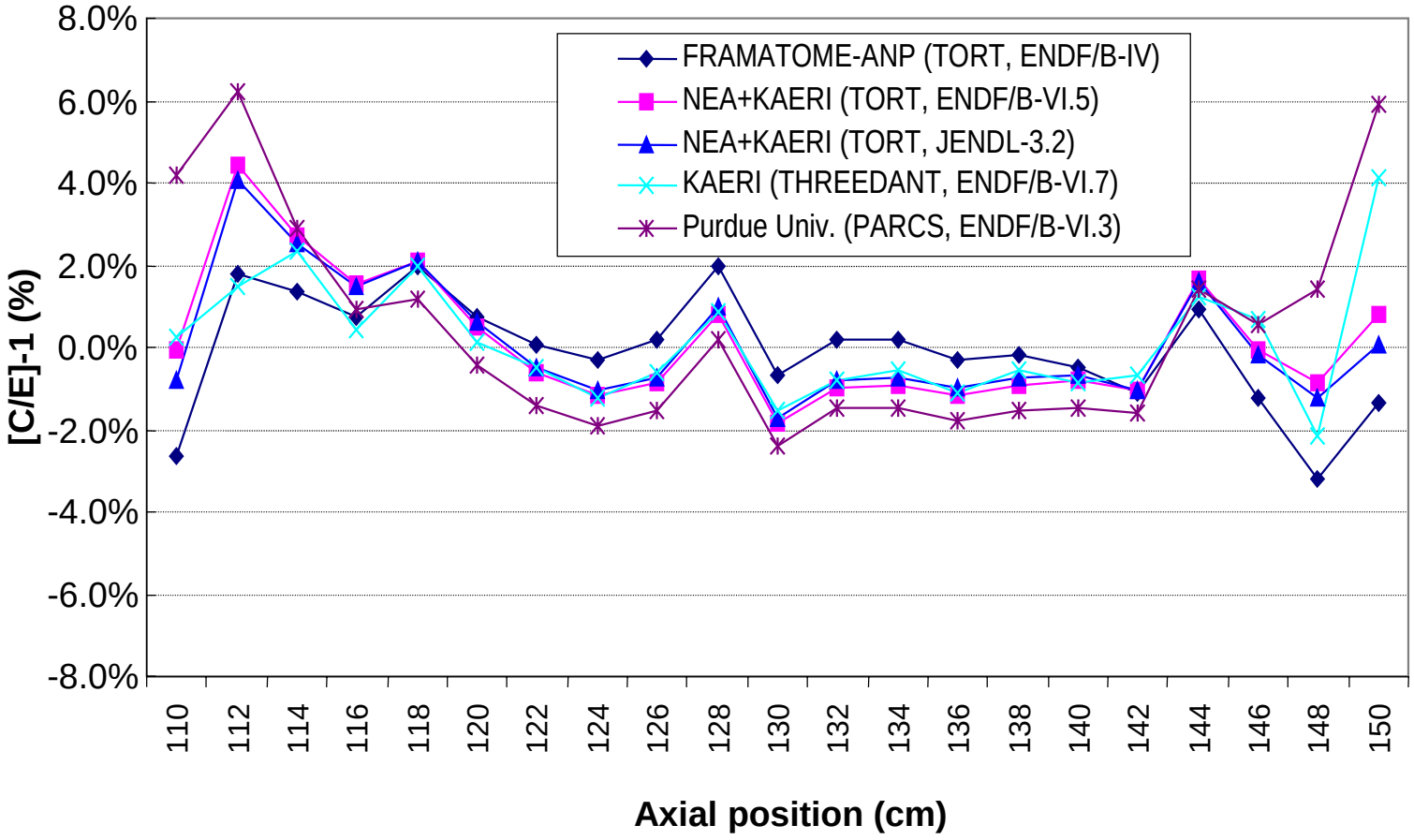

Figure 4.18. Deterministic calculations: Comparison of axial power distributions in MOX pin (-22,-2)

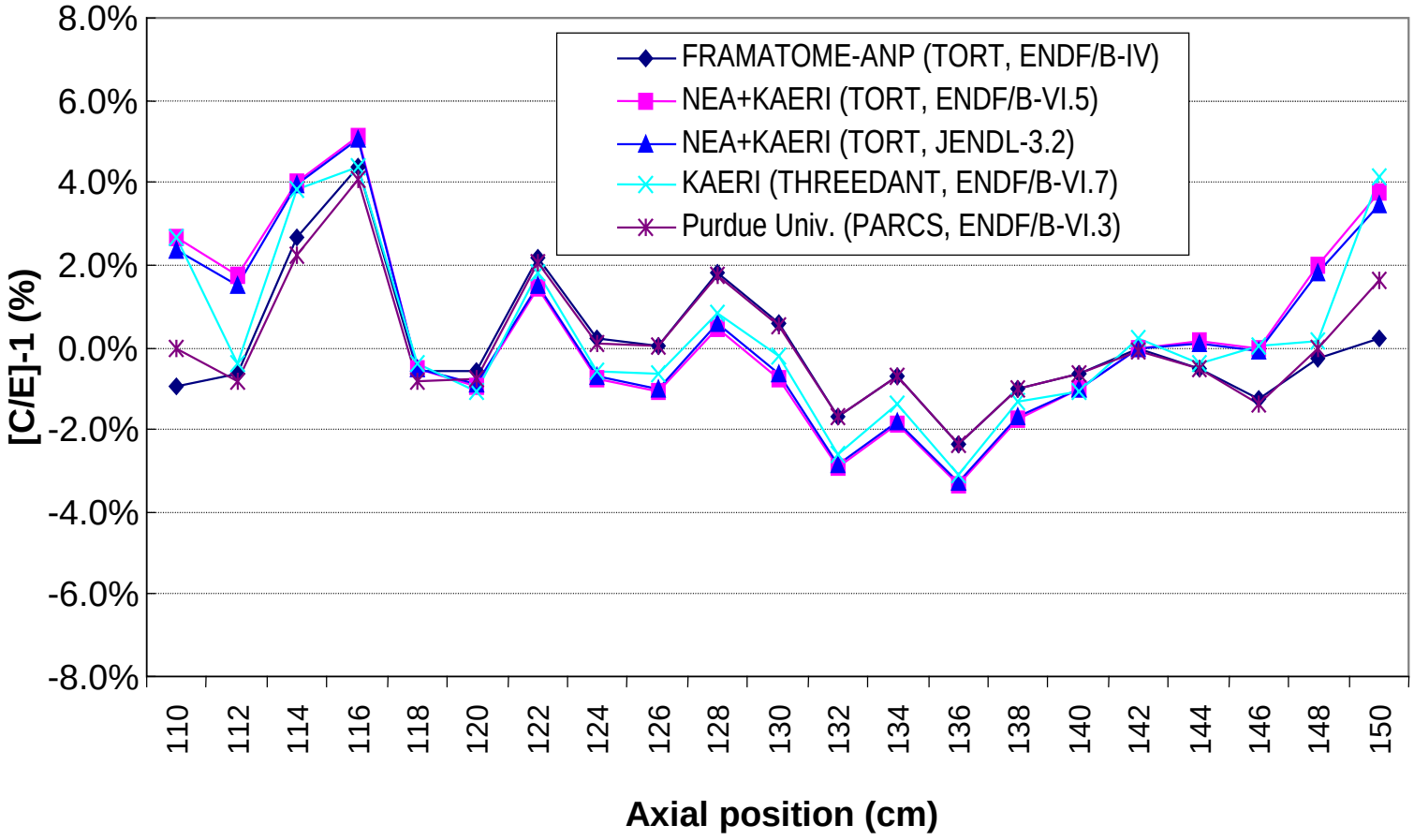

Figure 4.19. Deterministic calculations: Comparison of axial power distributions in 4/0 UO_2 pin (-15,+2)

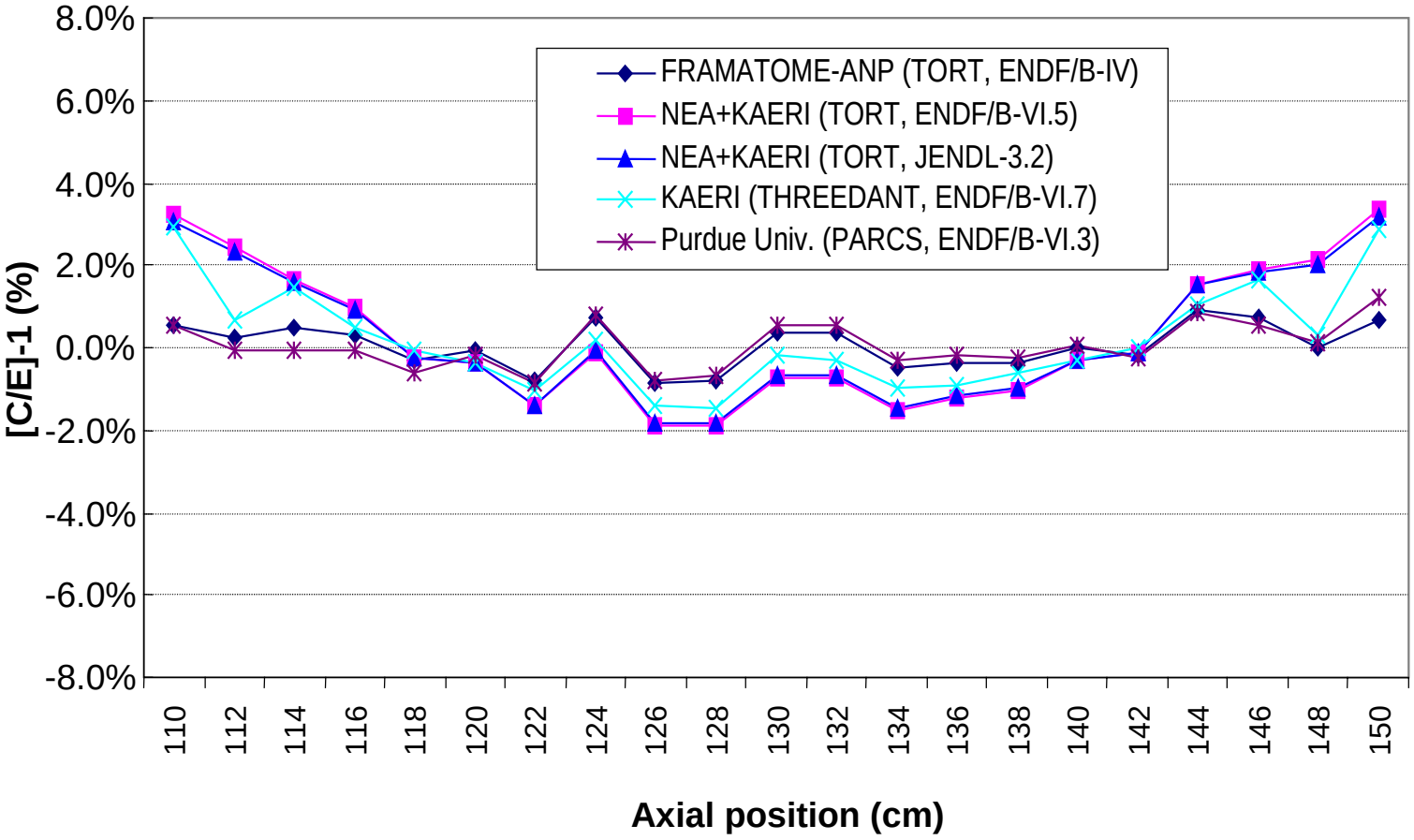

Figure 4.20. Deterministic calculations: Comparison of axial power distributions in 4/0 UO_2 pin (-13,-12)

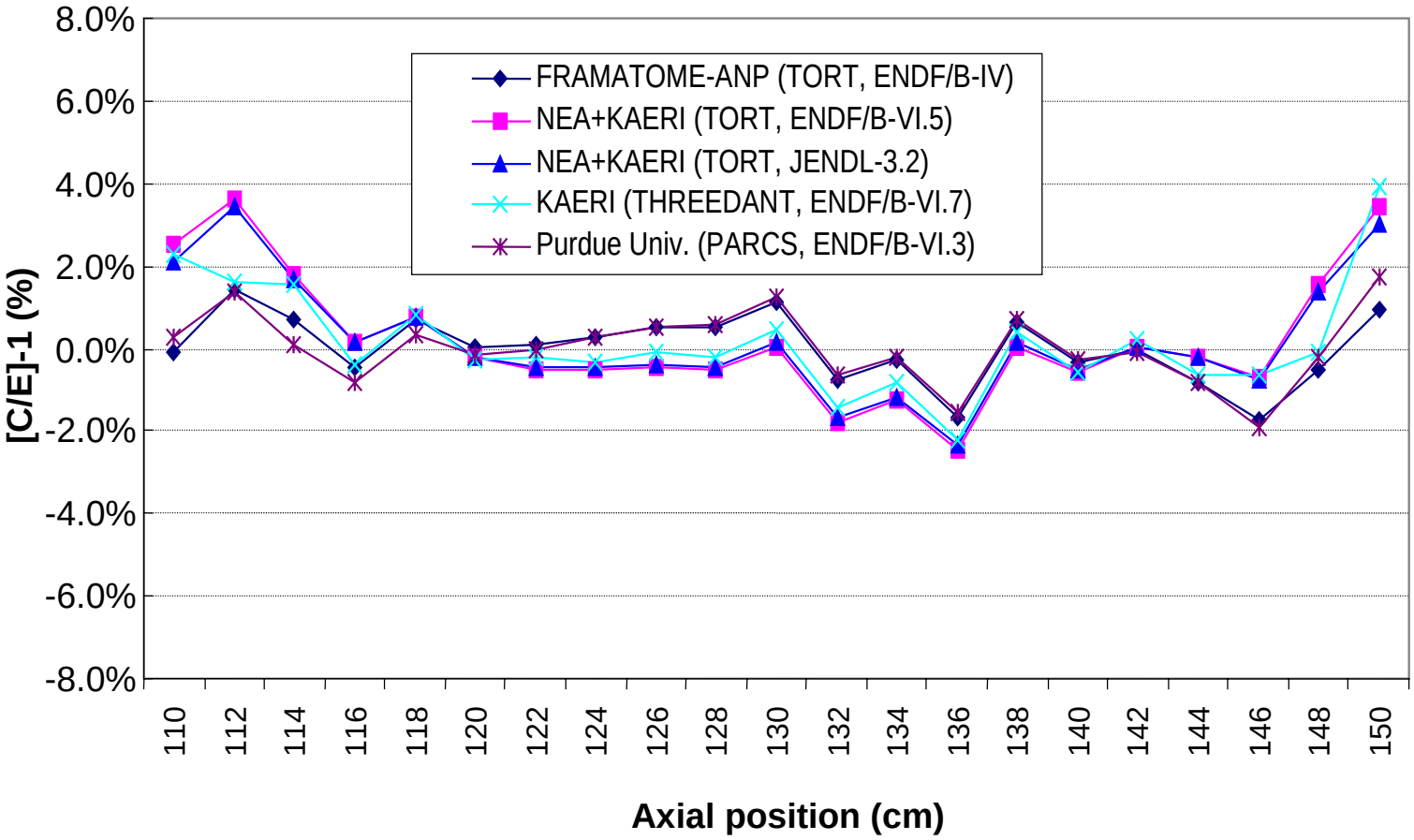

Figure 4.21. Deterministic calculations: Comparison of axial power distributions in 3/0 UO_2 pin (-11,+2)

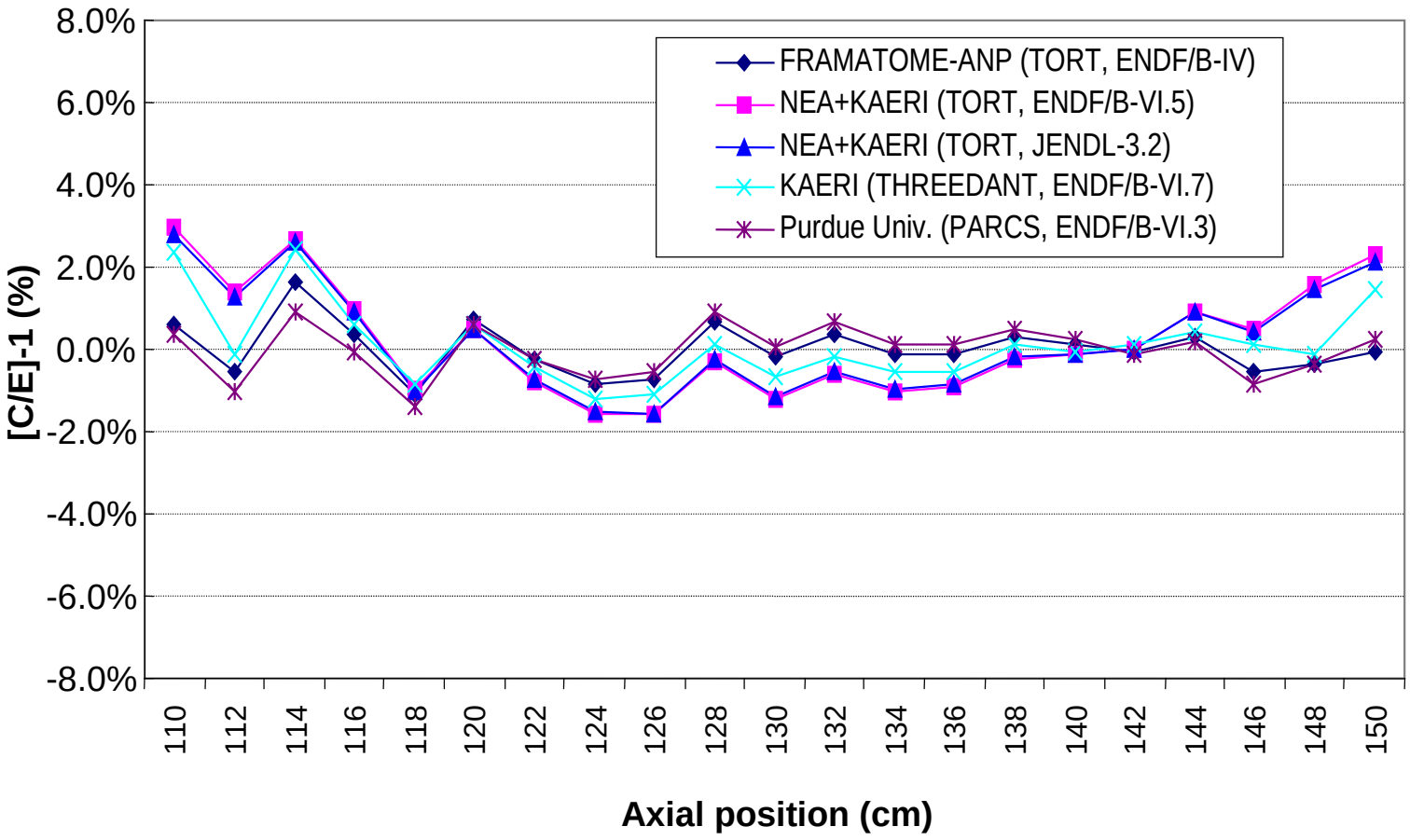

Figure 4.22. Deterministic calculations: Comparison of axial power distributions in 3/0 UO_2 pin (-6,-6)

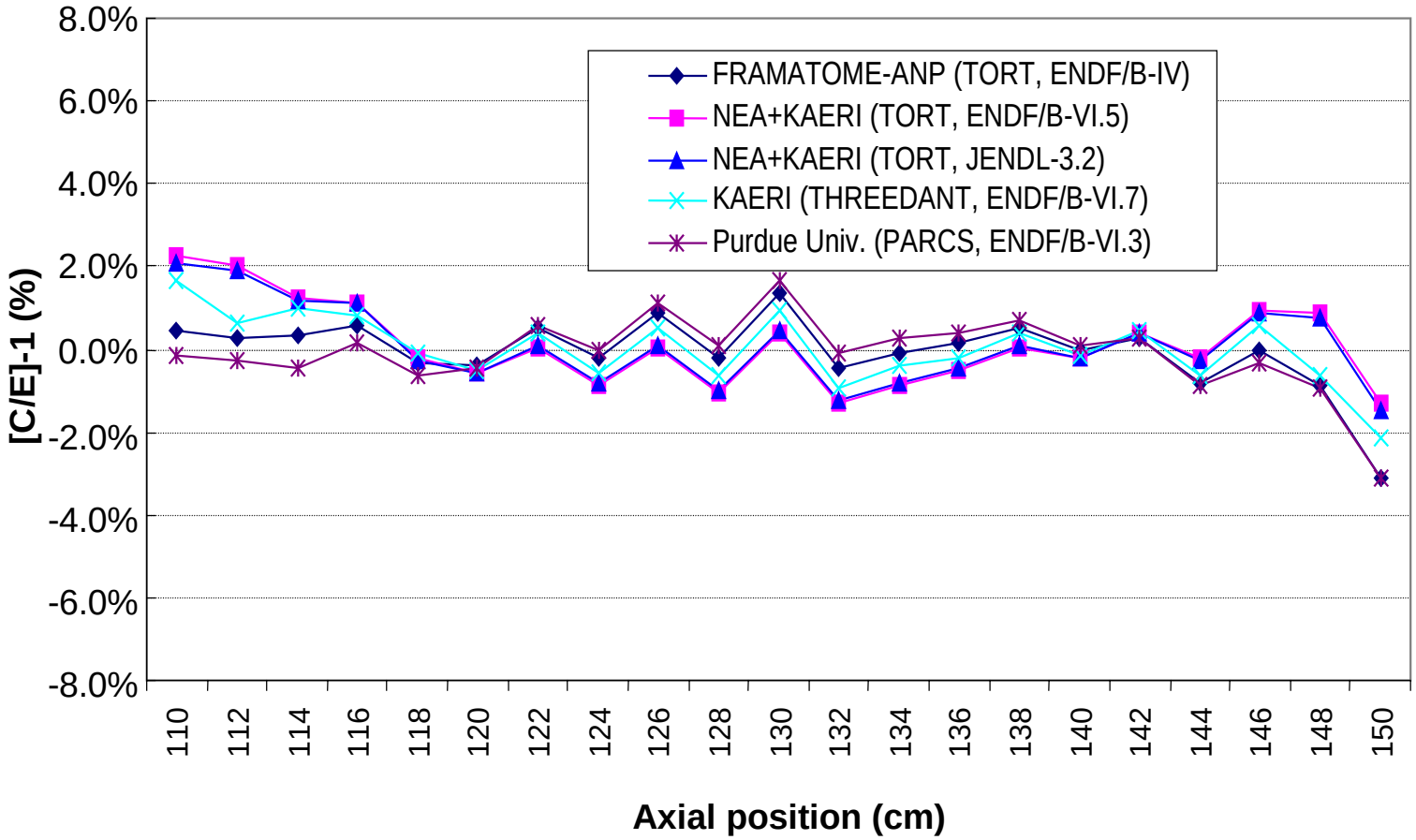

Figure 4.23. Monte Carlo calculations: Comparison of axial power distributions in MOX pin (-27,-12)

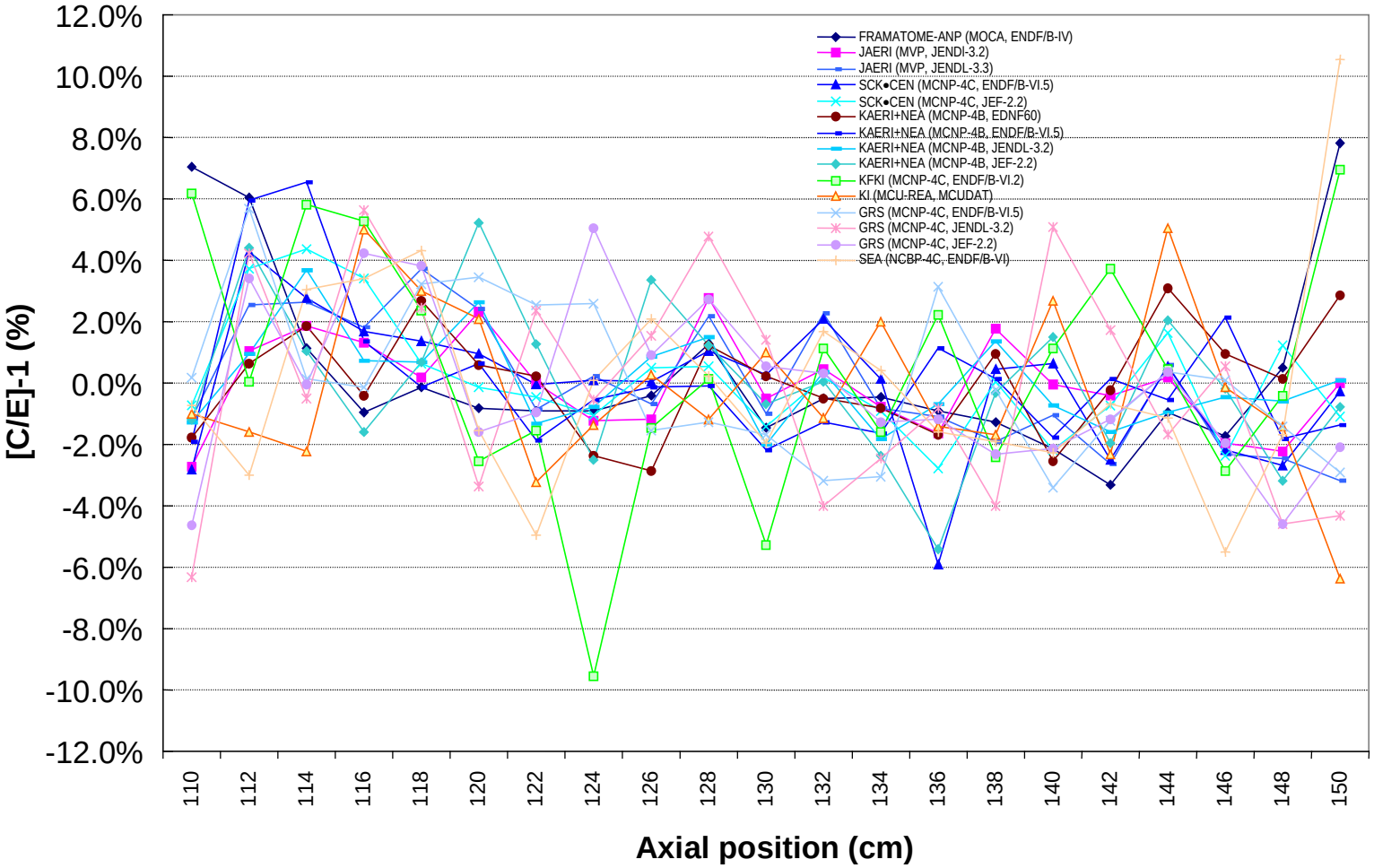

Figure 4.24. Monte Carlo calculations: Comparison of axial power distributions in MOX pin (-22,-2)

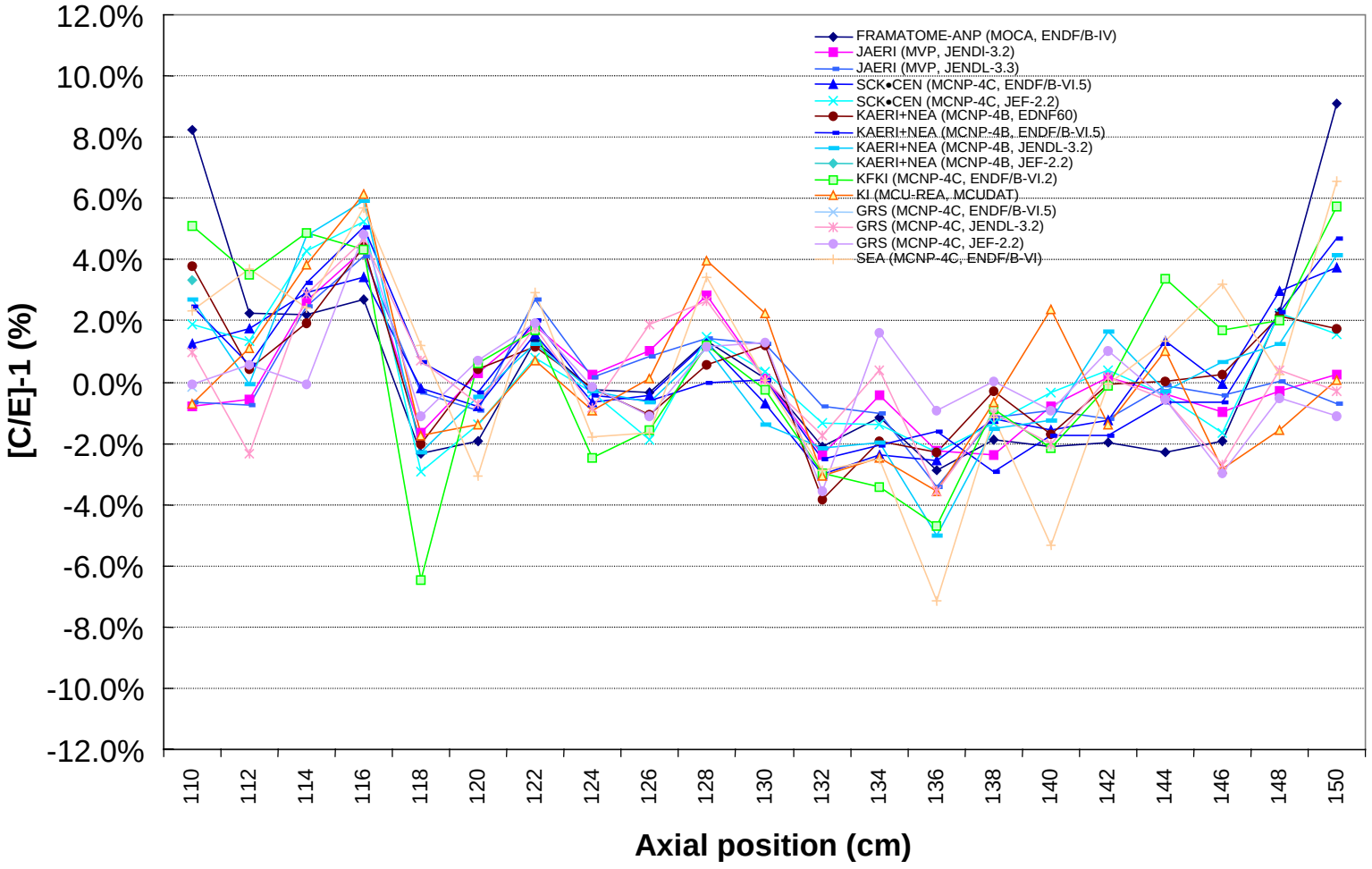

Figure 4.25. Monte Carlo calculations: Comparison of axial power distributions in 4/0 UO_2 pin (-15,+2)

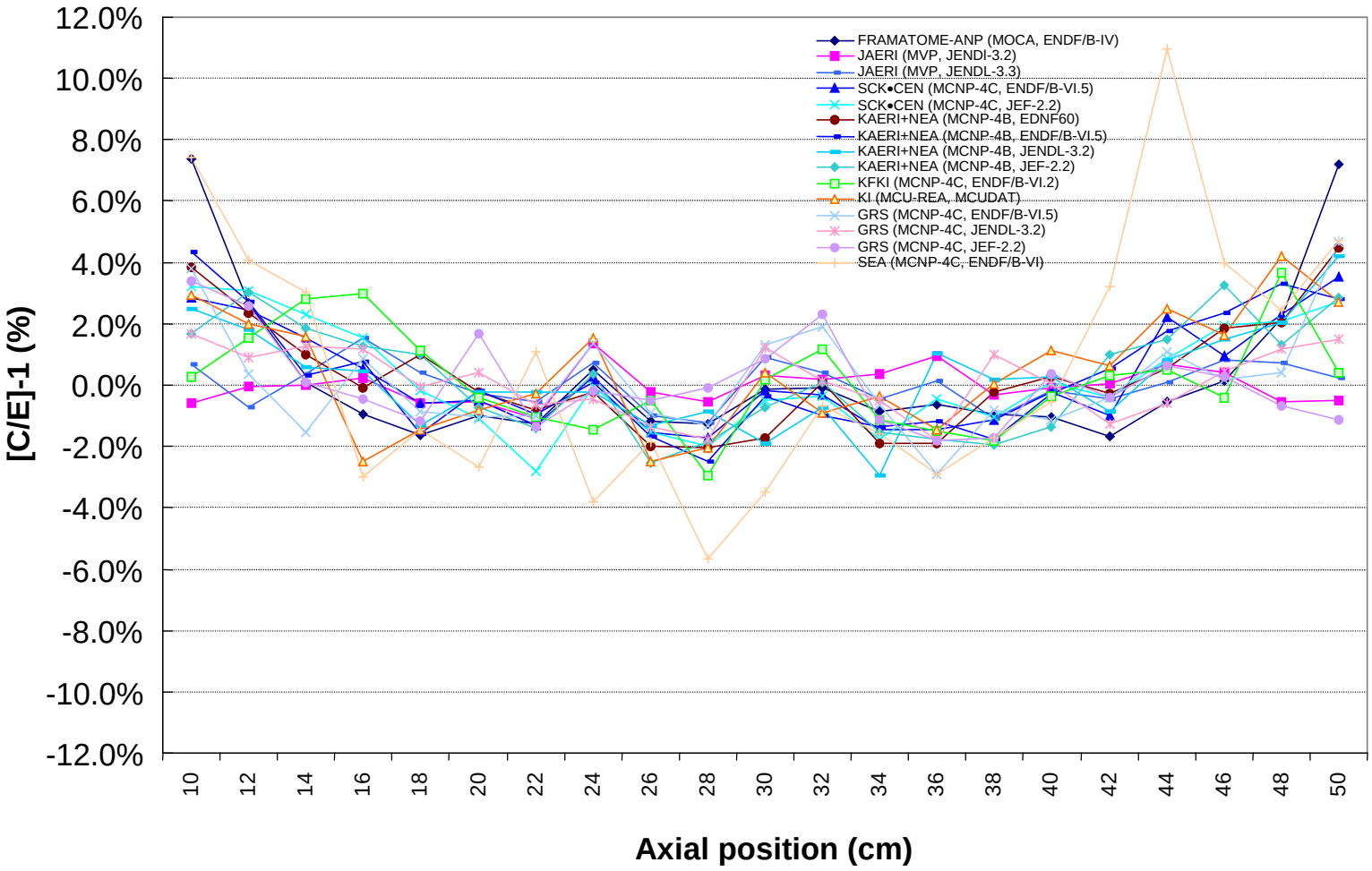

Figure 4.26. Monte Carlo calculations: Comparison of axial power distributions in 4/0 UO_2 pin (-13,-12)

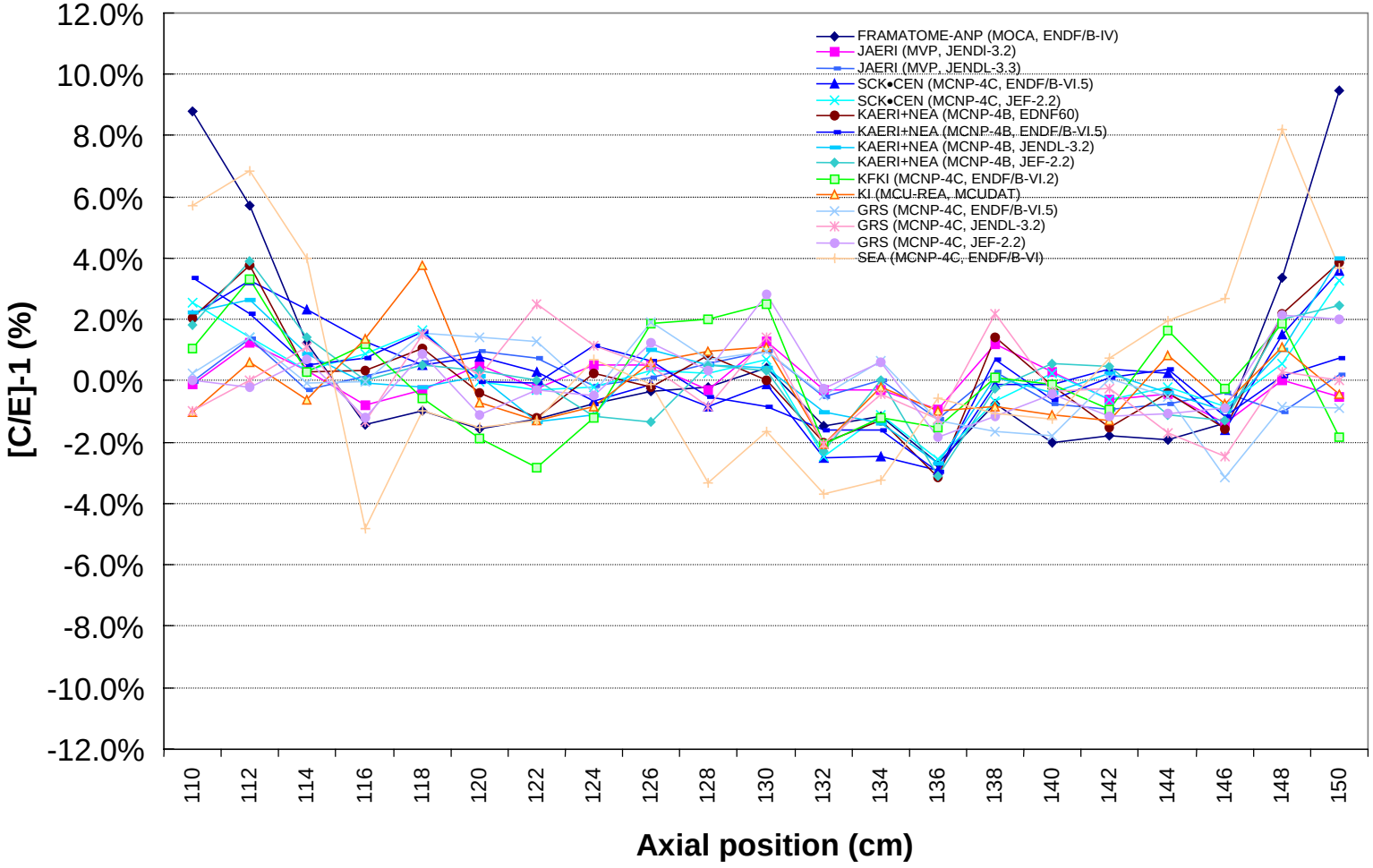

Figure 4.27. Monte Carlo calculations: Comparison of axial power distributions in 3/0 UO_2 pin (-11,+2)

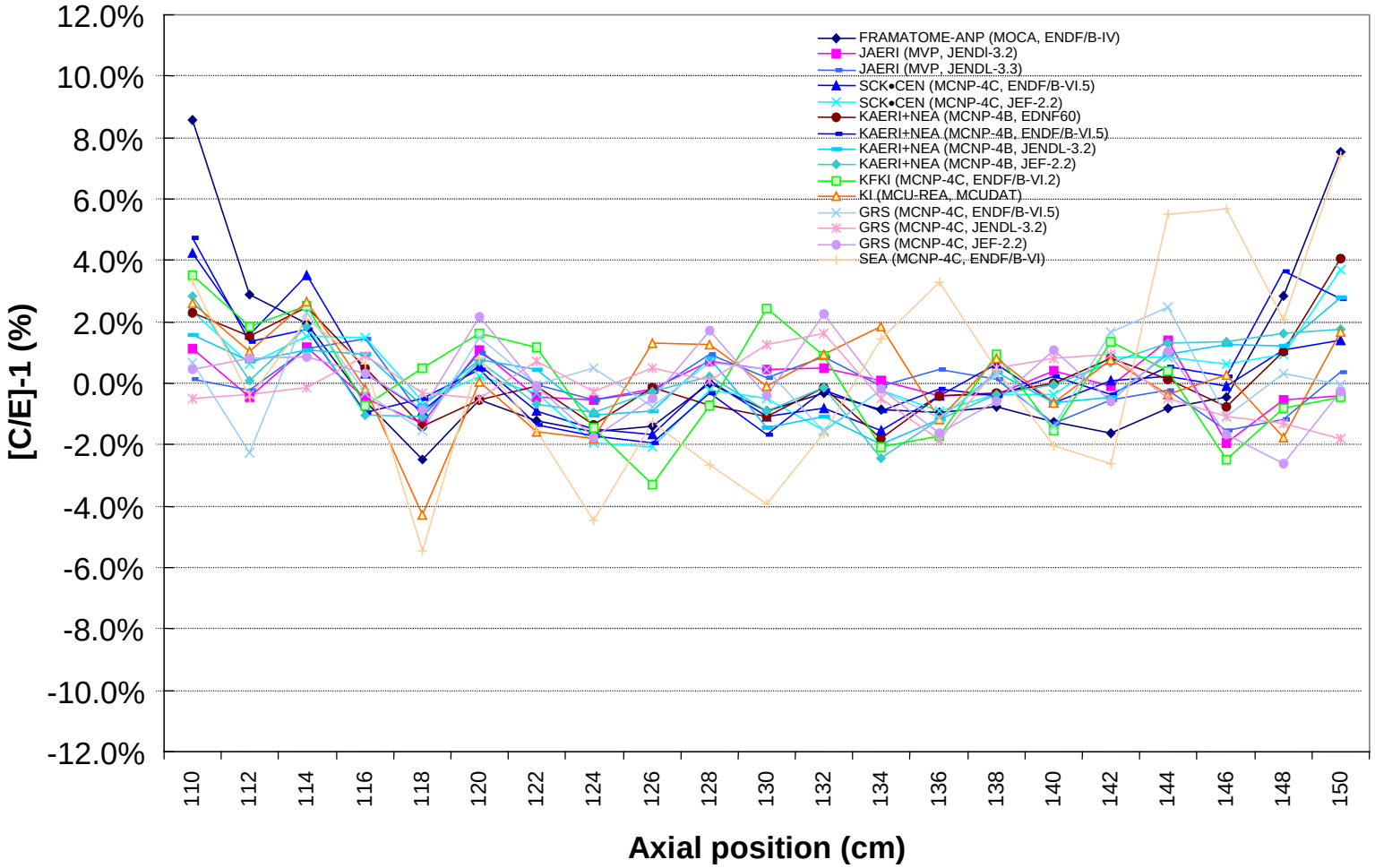

Figure 4.28. Monte Carlo calculations: Comparison of axial power distributions in 3/0 UO_2 pin (-6,-6)

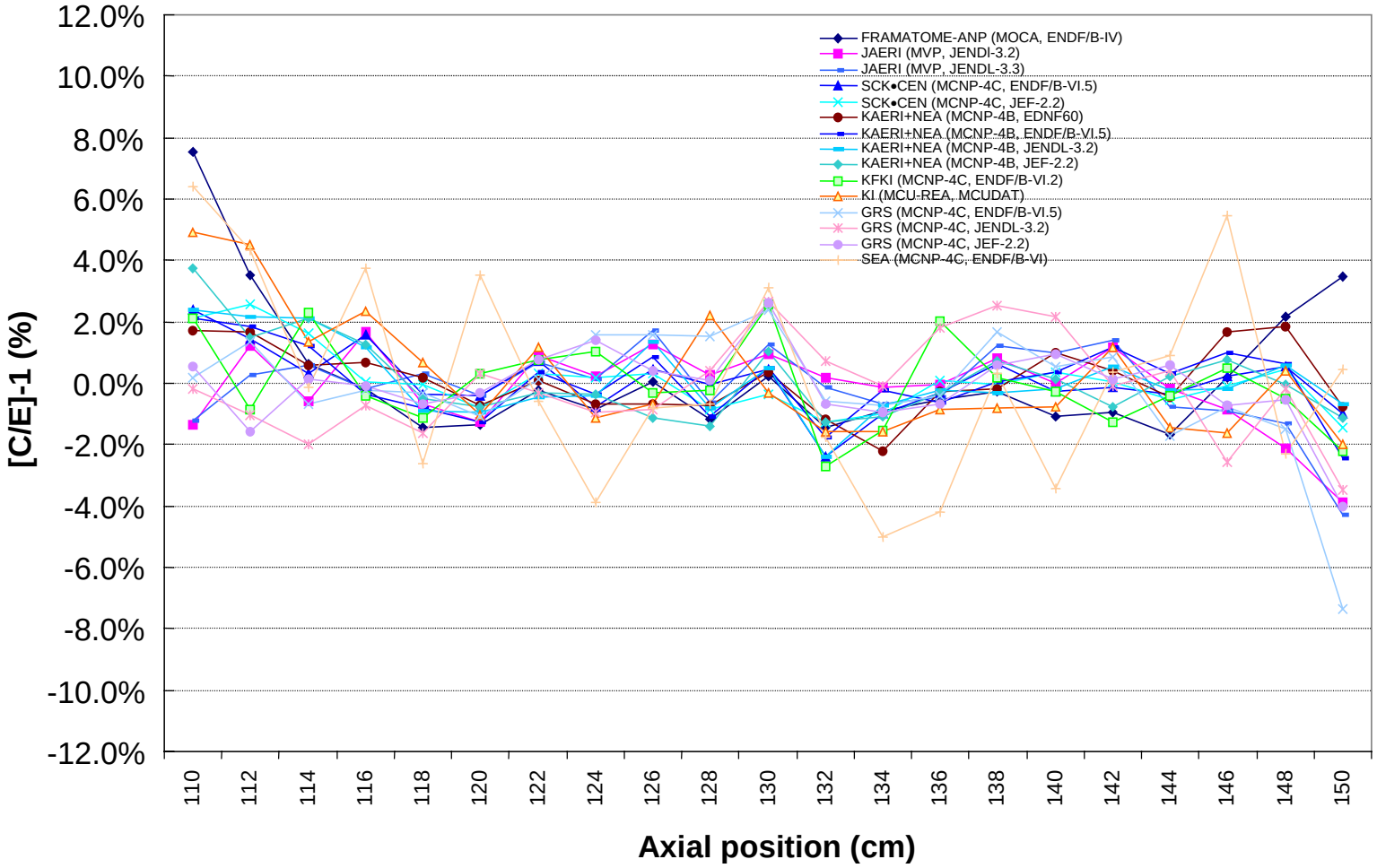

Figure 4.29. Comparison of deterministic and Monte Carlo (MC) results for MOX pins

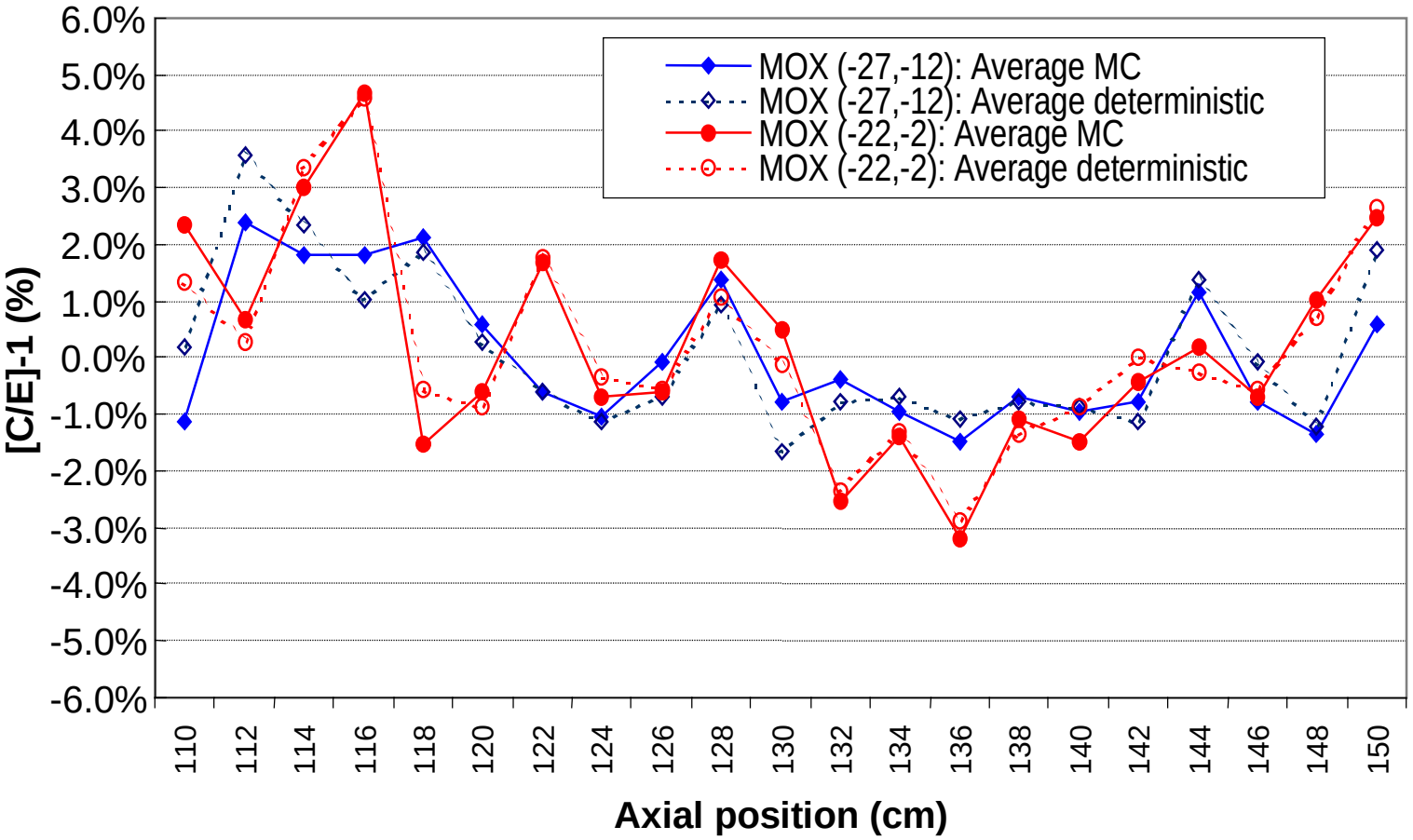

Figure 4.30. Comparison of deterministic and Monte Carlo (MC) results for 4/0 UO_2 pins

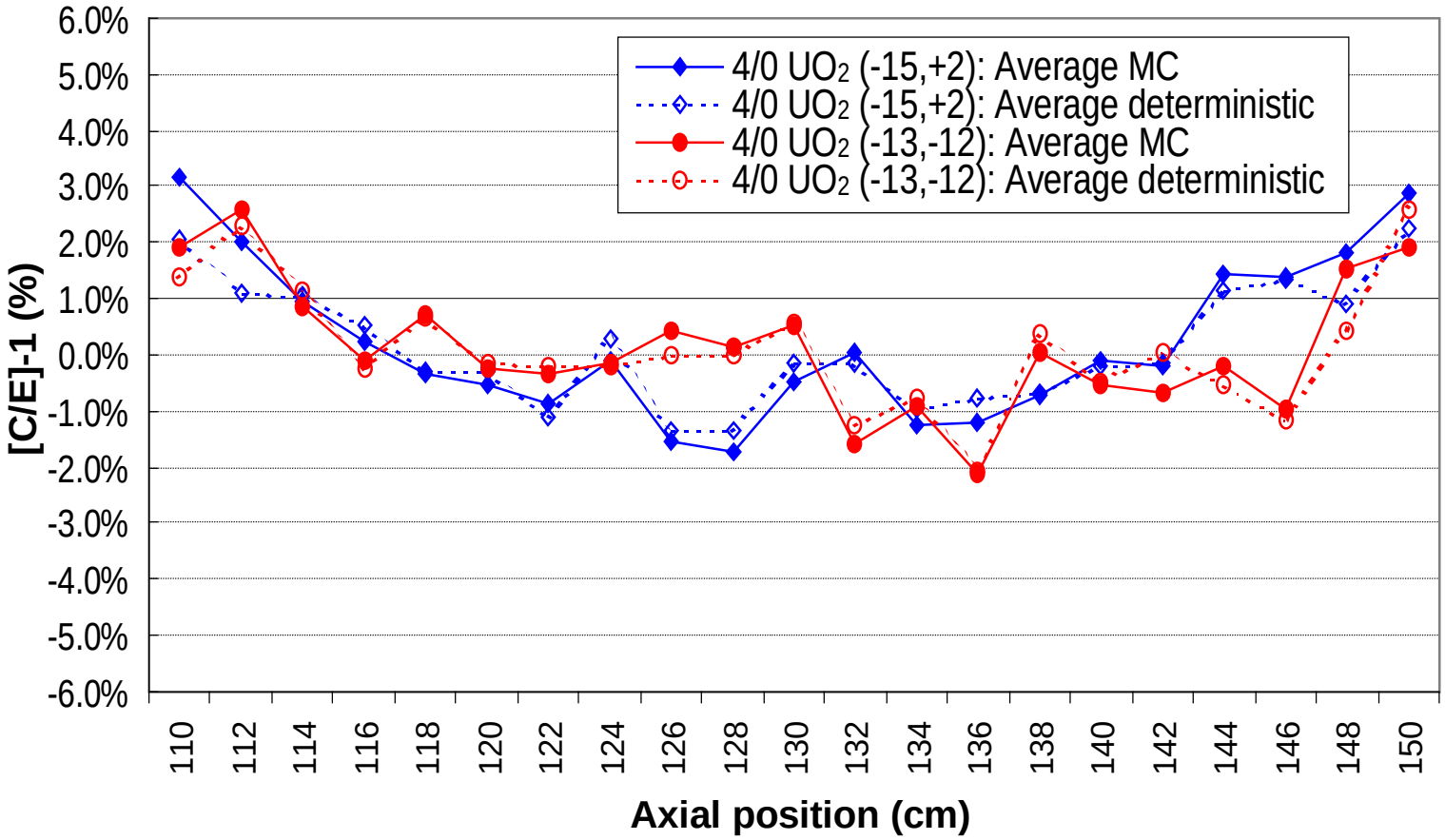

Figure 4.31. Comparison of deterministic and Monte Carlo (MC) results for 3/0 UO_2 pins

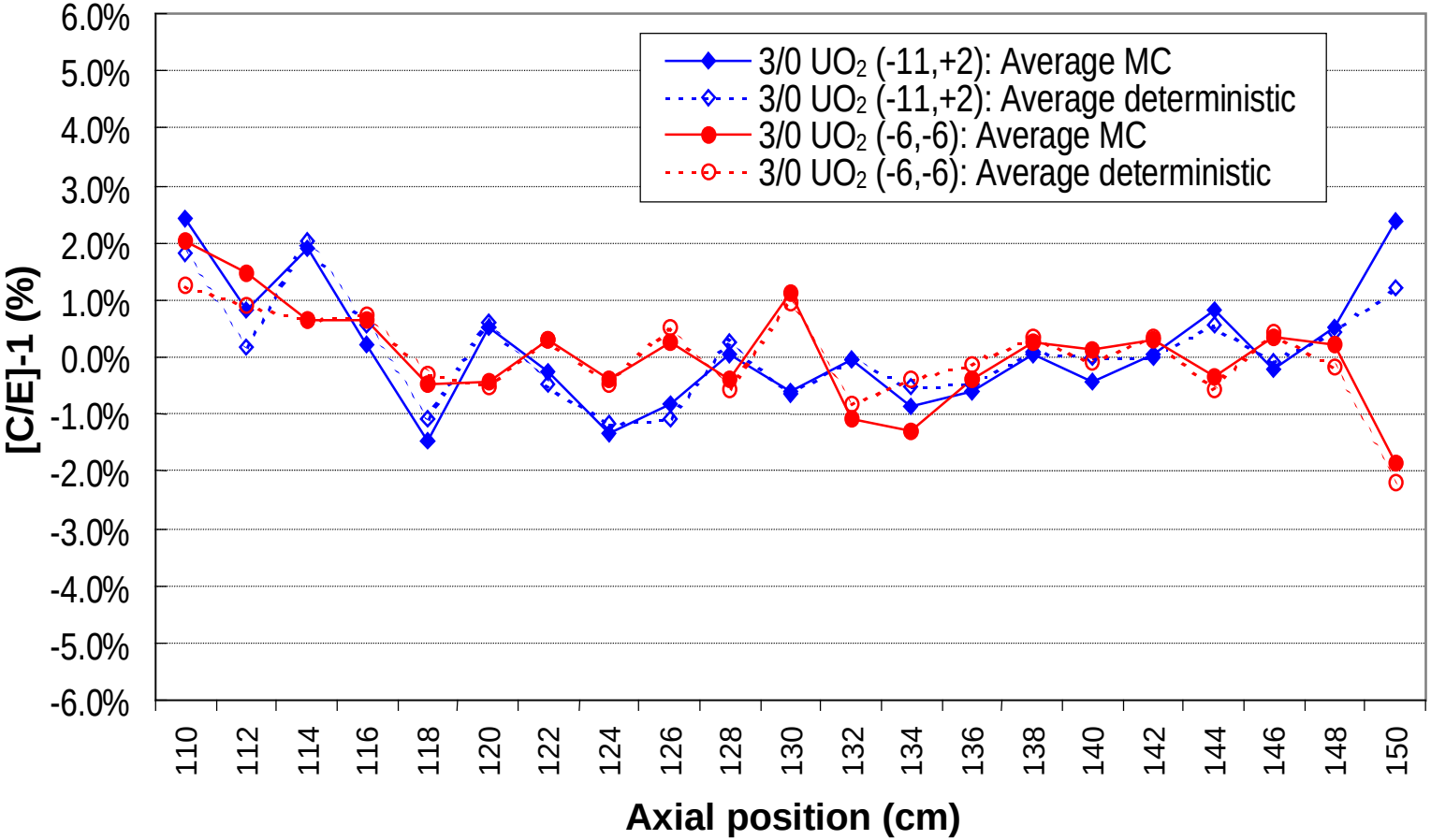

Figure 4.32. Comparison of axial pin power results with different libraries for MOX pin (-27,-12)

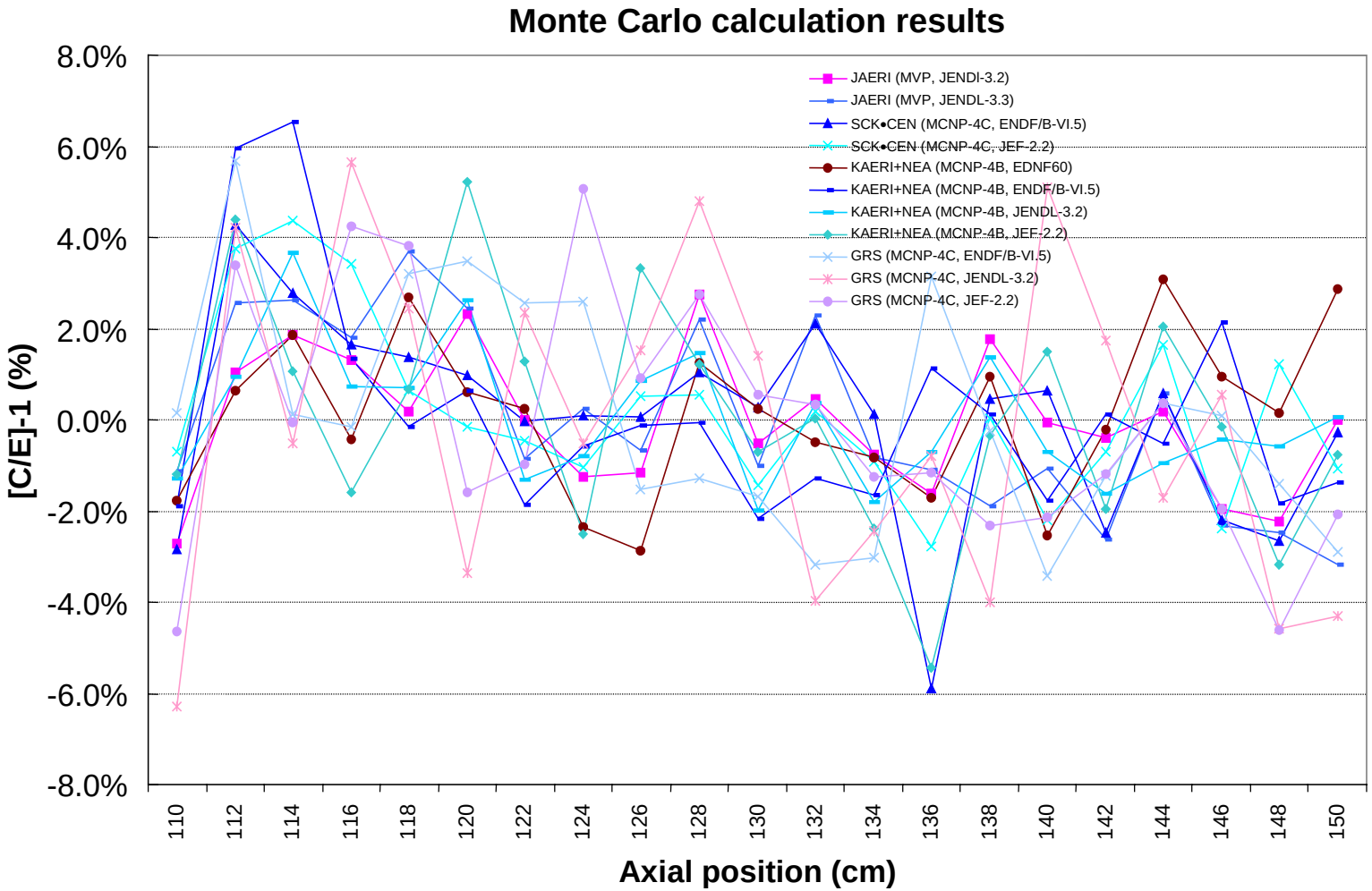

Figure 4.33. Comparison of axial pin power results with different libraries for MOX pin (-22,-2)

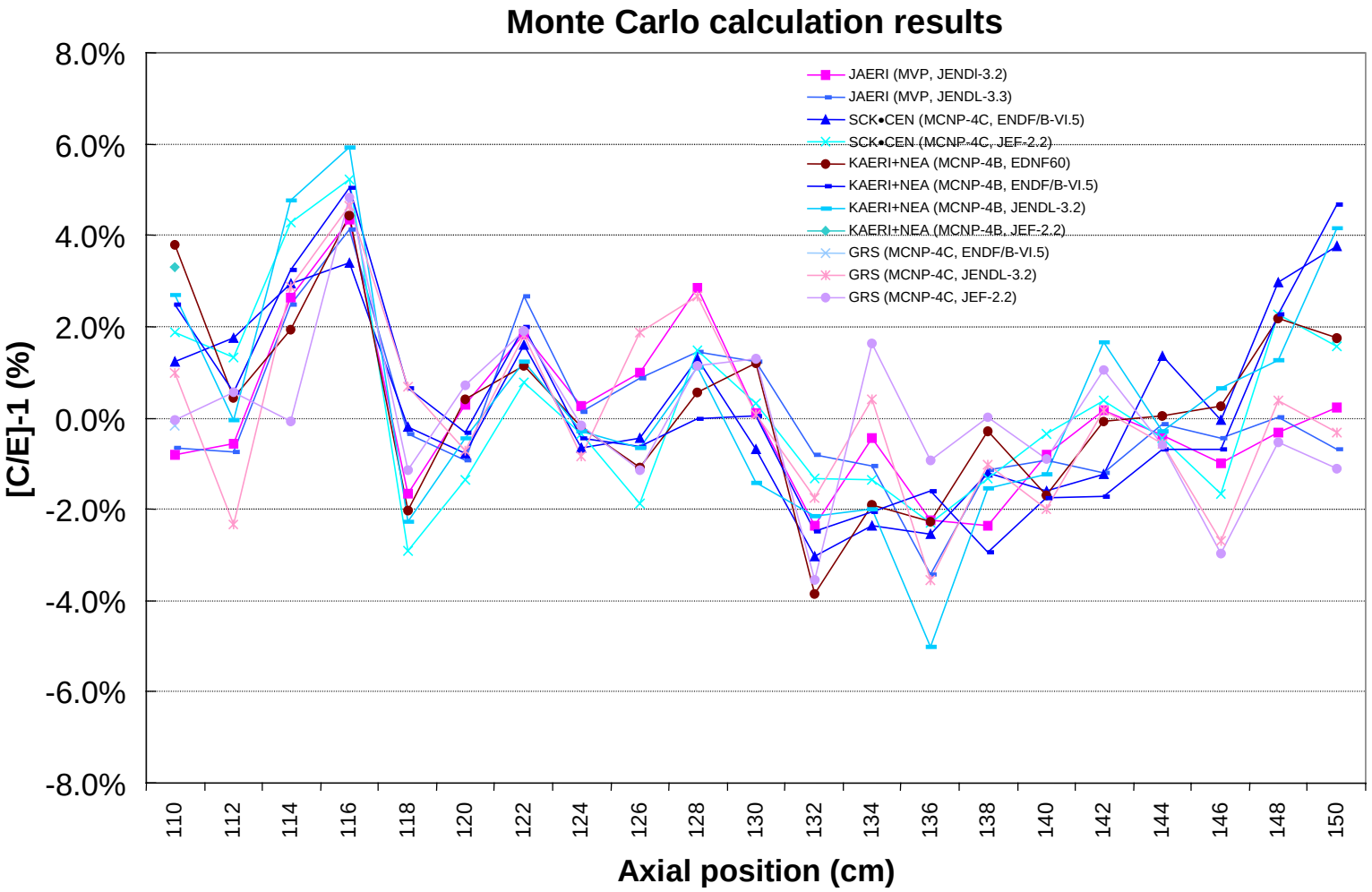

Figure 4.34. Comparison of axial pin power results with different libraries for 4/0 UO_2 pin (-15,+2)

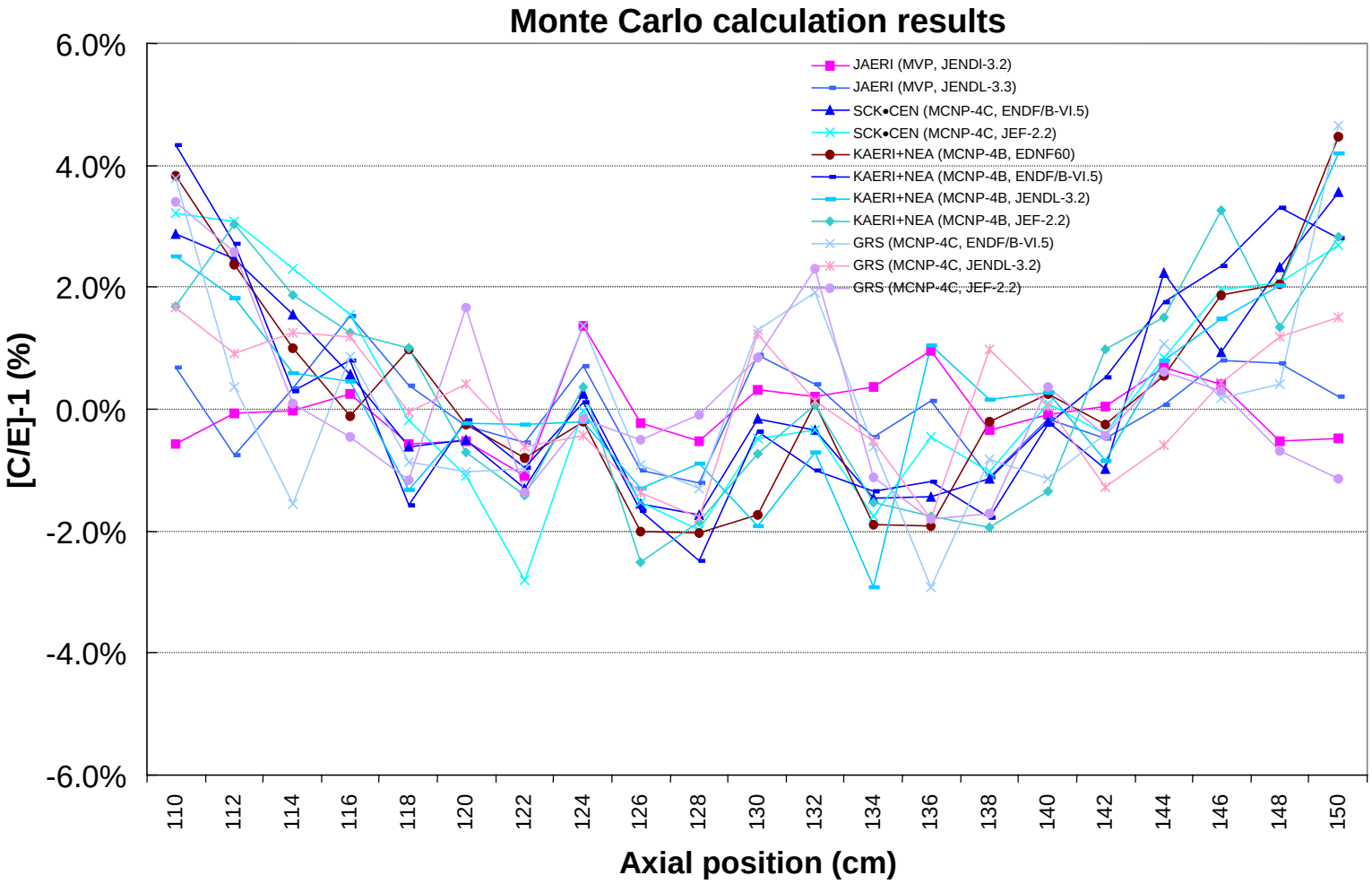

Figure 4.35. Comparison of axial pin power results with different libraries for 4/0 UO_2 pin (-13,-12)

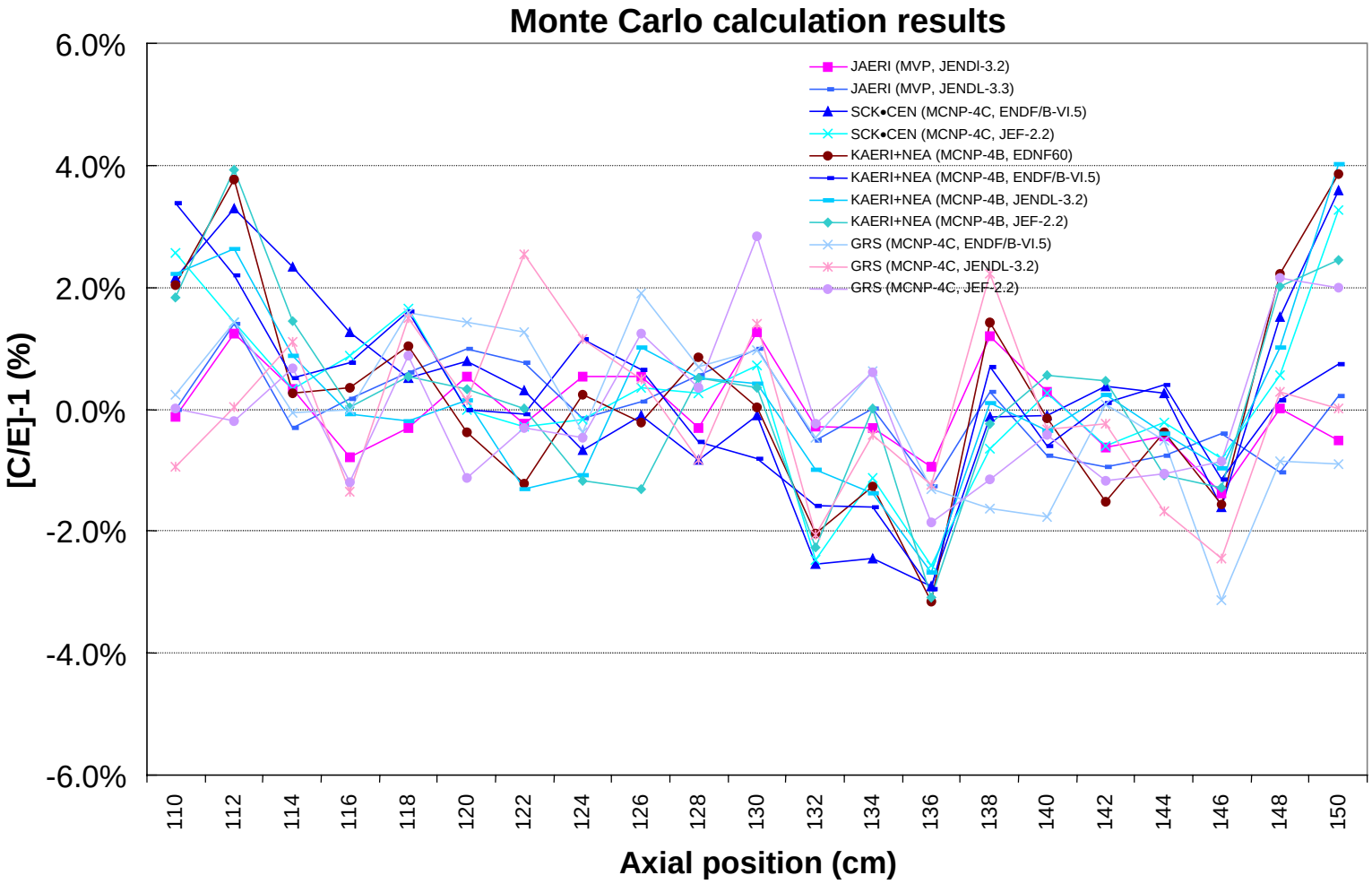

Figure 4.36. Comparison of axial pin power results with different libraries for 3/0 UO_2 pin (-11,+2)

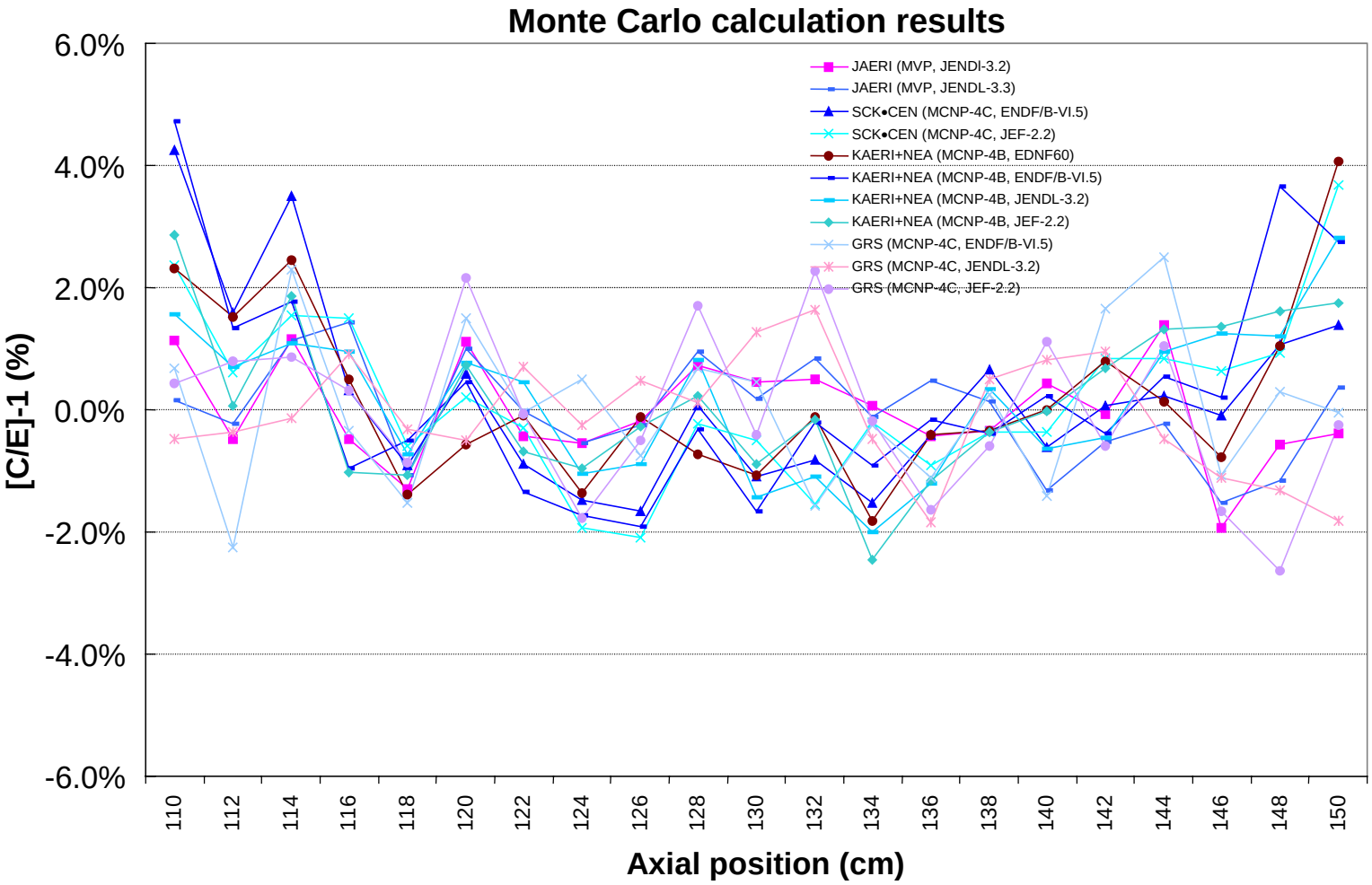

Figure 4.37. Comparison of axial pin power results with different libraries for 3/0 UO_2 pin (-6,-6)

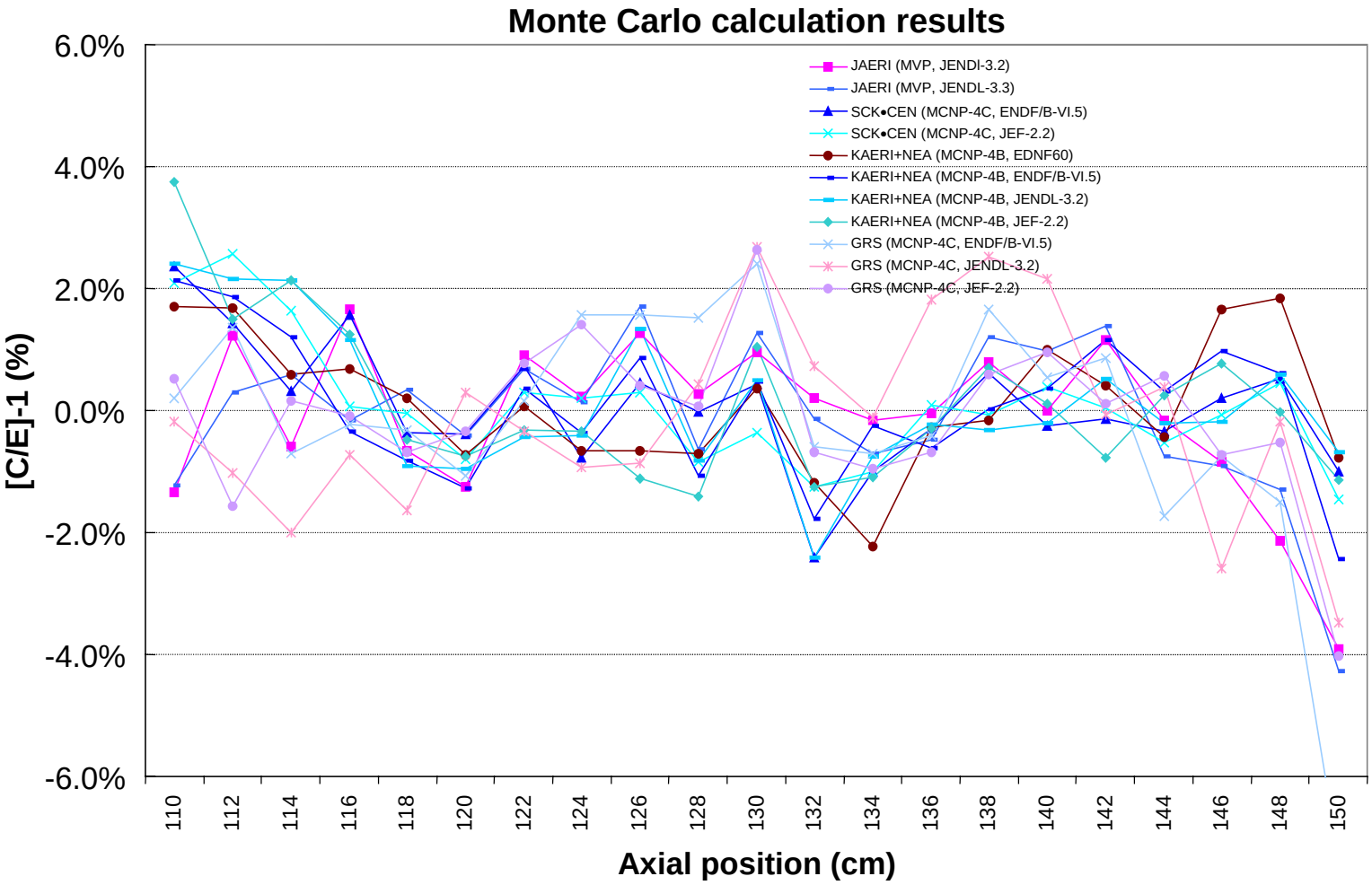

Figure 4.38. Comparison of number of particle histories for MOX pin (-27,-12)

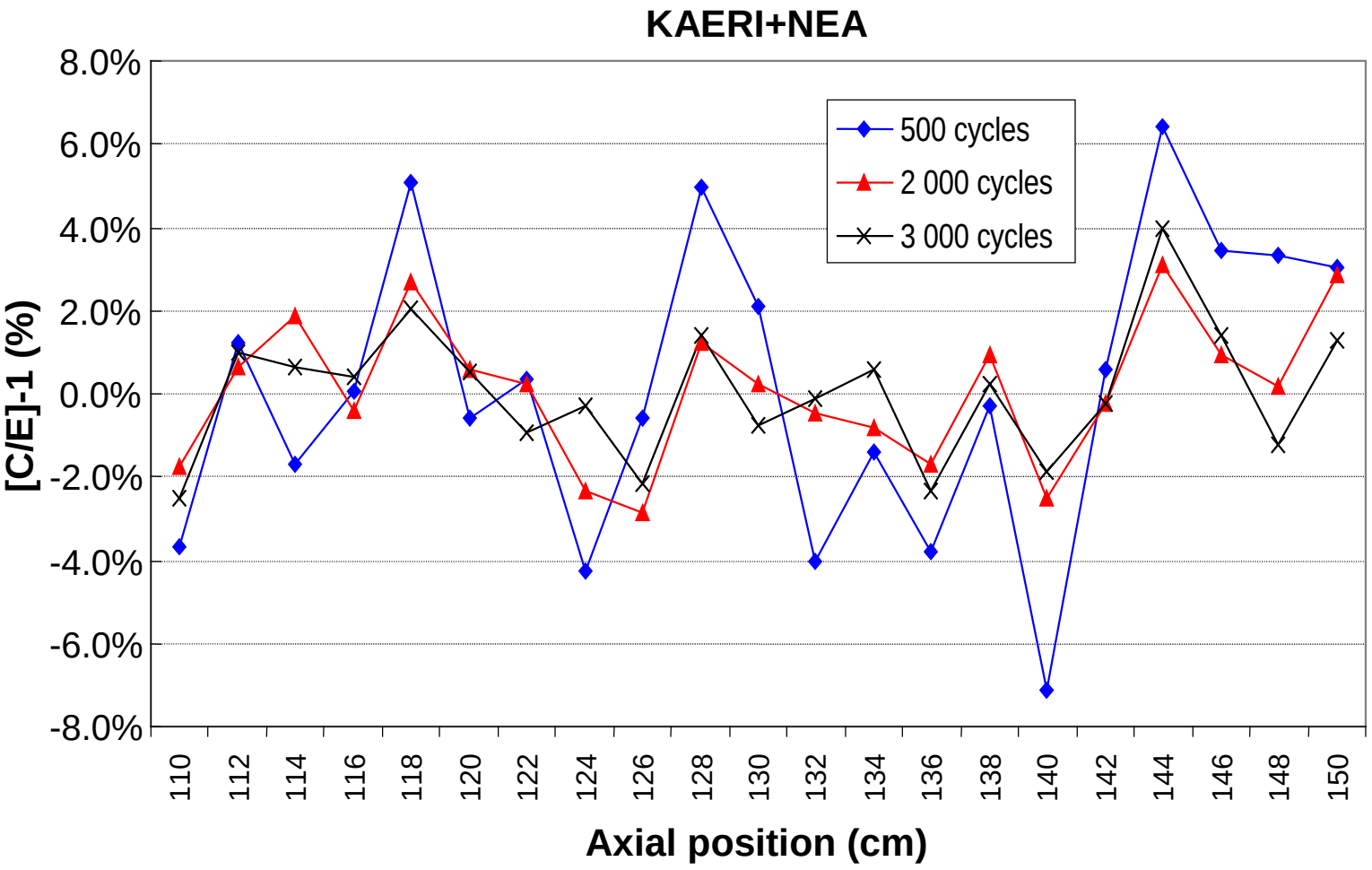

Figure 4.39. Comparison of number of particle histories for MOX pin (-22,-2)

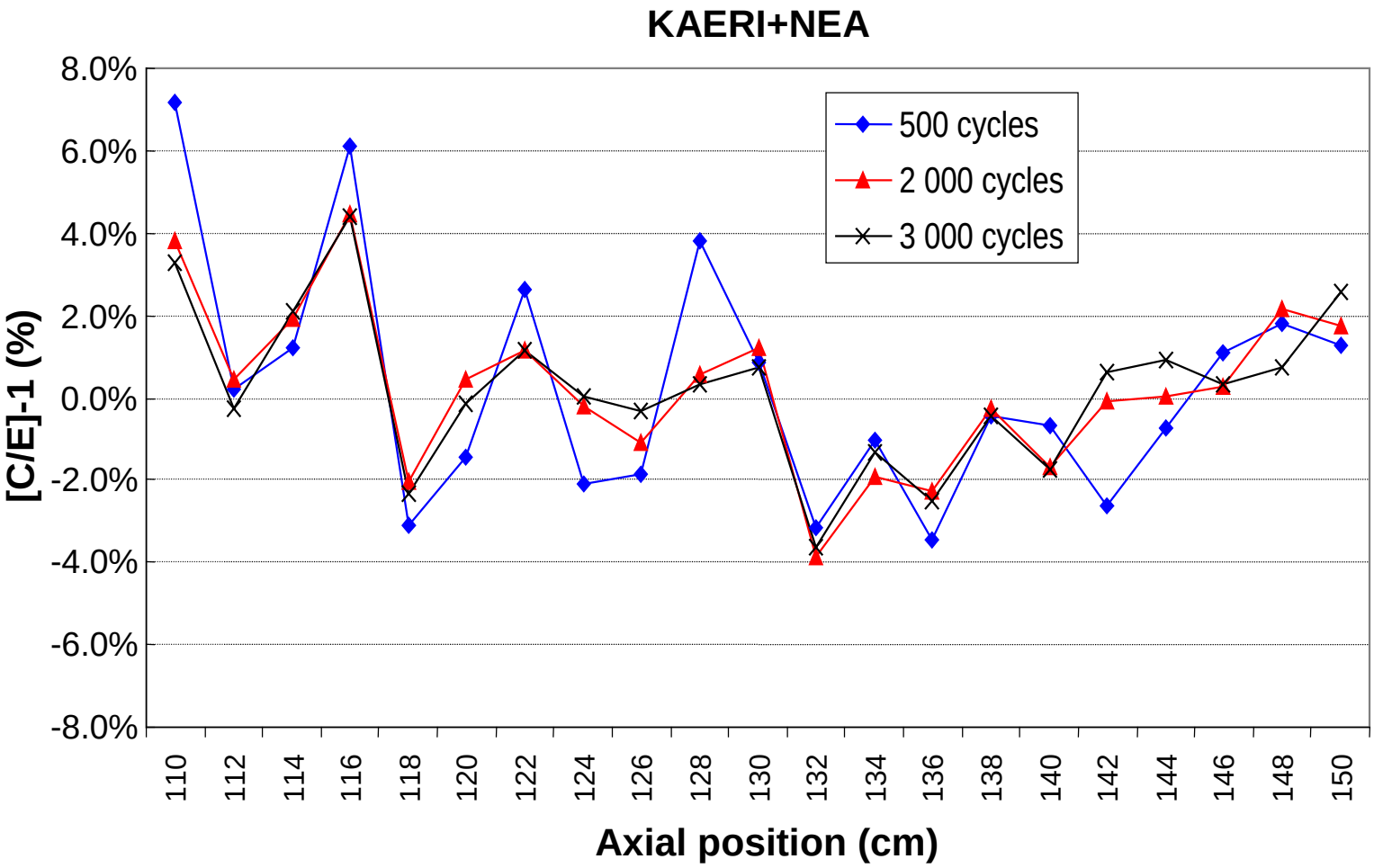

Figure 4.40. Comparison of number of particle histories for 4/0 UO_2 pin (-15,+2)

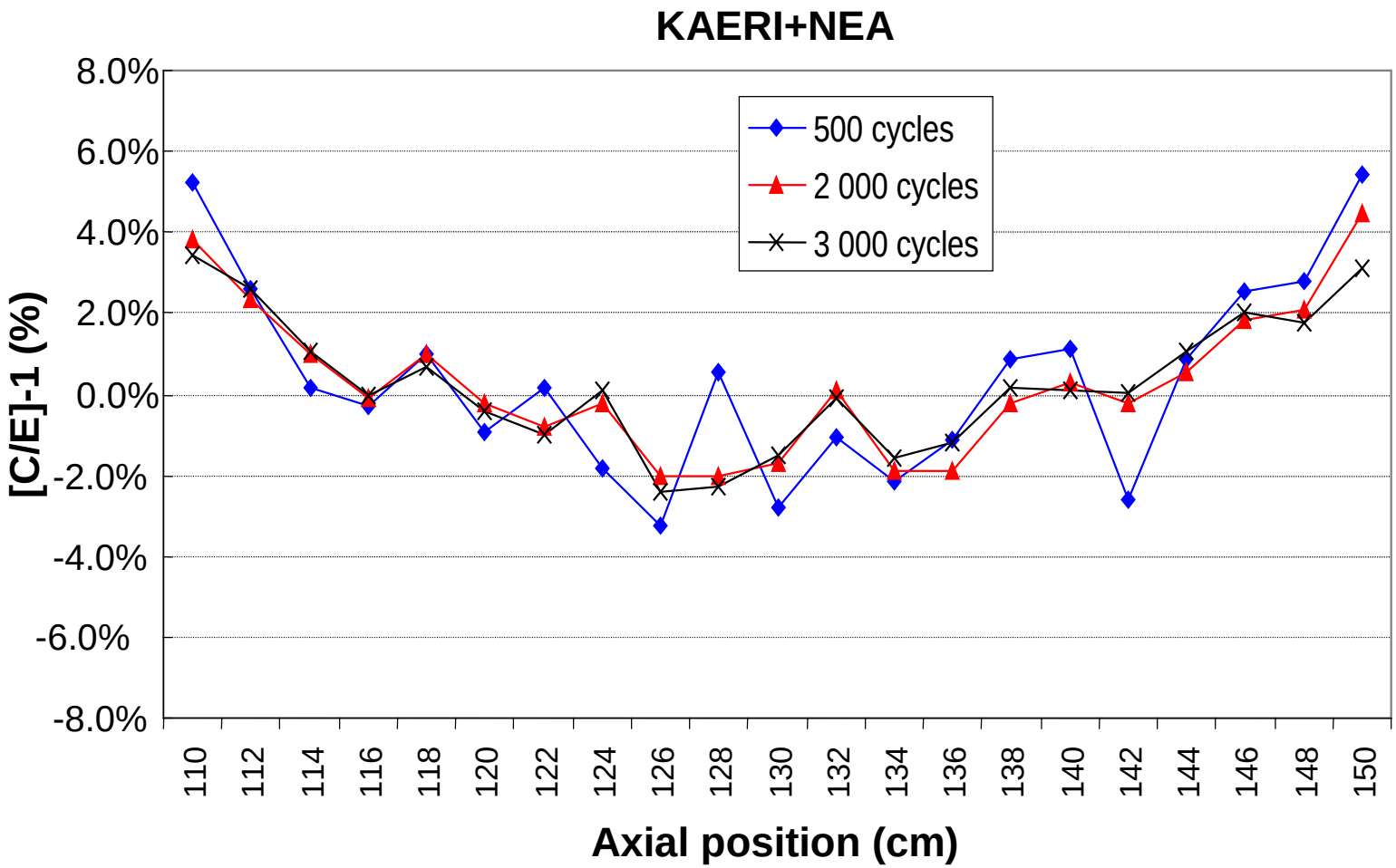

Figure 4.41. Comparison of number of particle histories for 4/0 UO_2 pin (-13,-12)

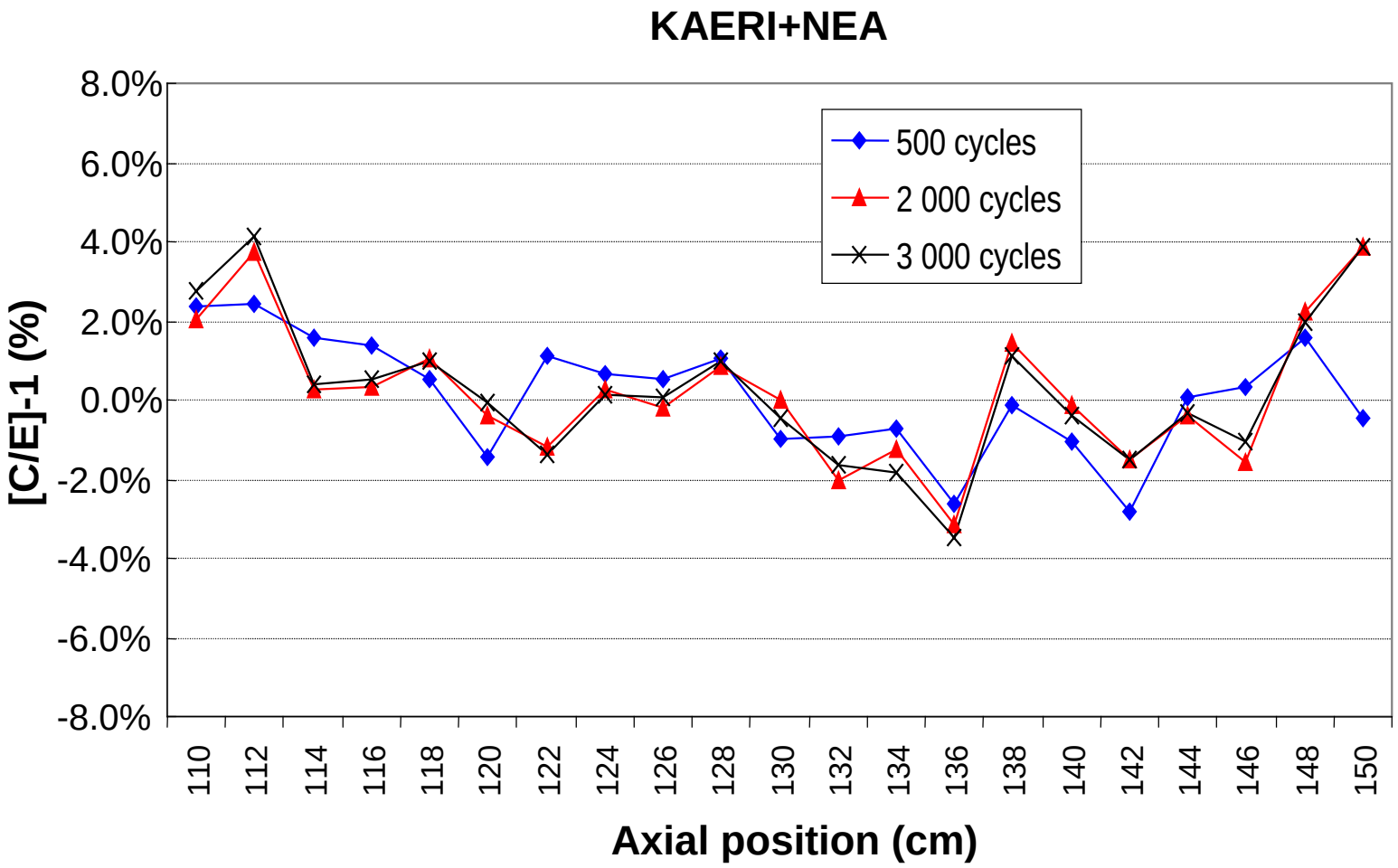

Figure 4.42. Comparison of number of particle histories for 3/0 UO_2 pin (-11,+2)

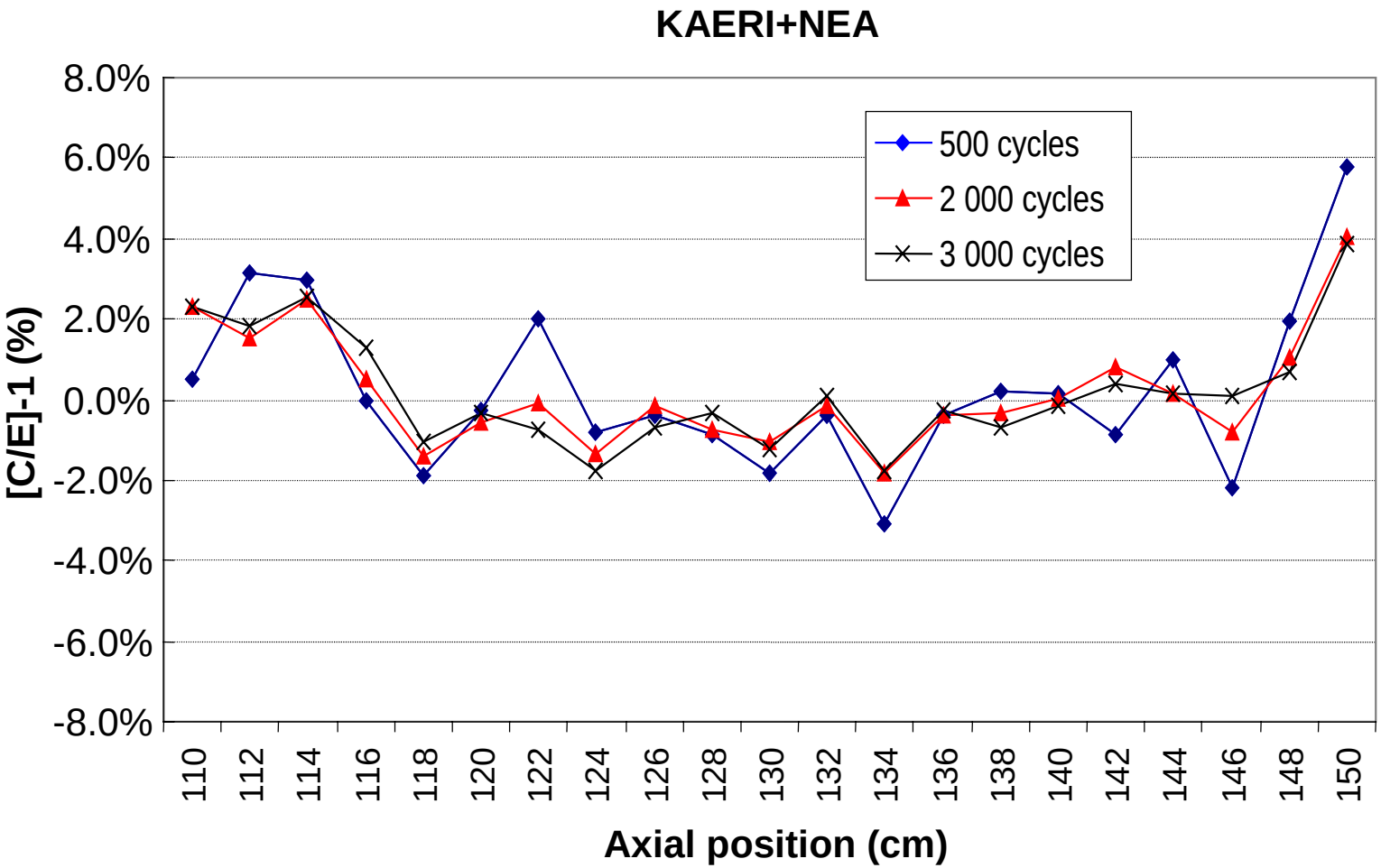

Figure 4.43. Comparison of number of particle histories for 3/0 UO_2 pin (-6,-6)

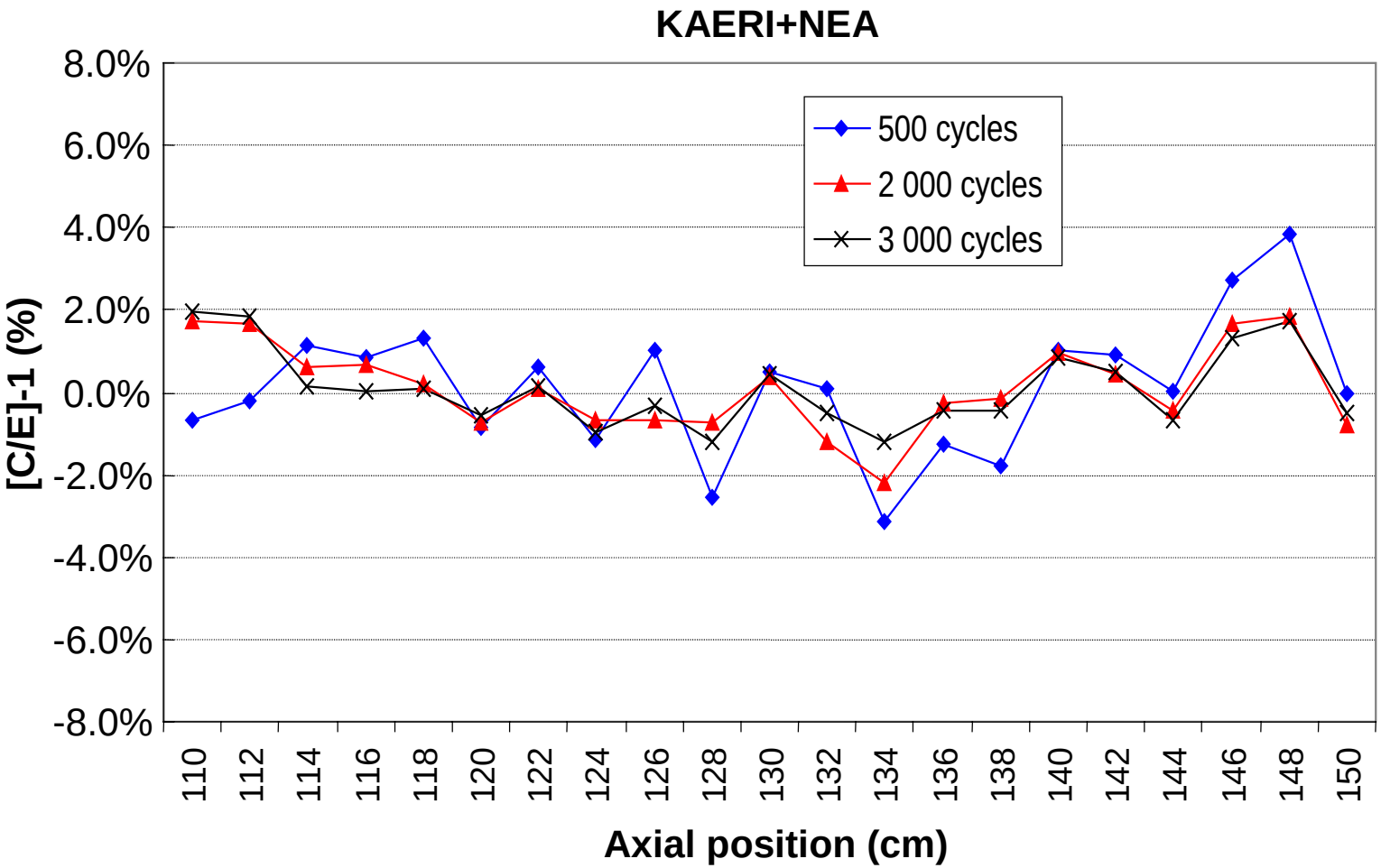

Appendix A

BENCHMARK SPECIFICATION

BLIND BENCHMARK ON THE 3-D VENUS-2 MOX CORE MEASUREMENTS

Byung-Chan Na[*] and Nadia Messaoudi[**]
[*]OECD Nuclear Energy Agency, France
[**]SCK•CEN, Mol, Belgium

Outline

Summary specification

Appendix A.1: VENUS-2 PWR core source and azimuthal lead factor experiments – Description of the composition of different materials

Appendix A.2: Details to be provided about the calculation scheme used

Appendix A.3: Results to be reported

1. Motivations

In the framework of joint activities carried out by the WPPR and TFRPD, the benchmark exercise for the prediction of power distribution in the two-dimensional VENUS-2 MOX core experiment has been completed [1,2]. Twelve participants from ten countries participated in this first experiment-based benchmark. Overall, the results were very encouraging and confirmed that present methods using the latest nuclear data sets can adequately calculate MOX-fuelled systems. However, the calculations overestimate the MOX fission rates and slightly underestimate the UO_2 fission rates. This is reflected in all combinations of codes and methods. A three-dimensional benchmark will therefore allow a more thorough investigation into the calculation methods used for MOX-fuelled systems. For this purpose, the three-dimensional VENUS-2 MOX core experiment data have been released by SCK•CEN, Mol. The three-dimensional VENUS-2 MOX core experimental results consist of the measured fission rate distributions of six fuel rods in 21 axial points [3]. This document specifies all geometry and material data required in developing the detailed three-dimensional computation model of the 1/4 fraction of the VENUS-2 reactor core [4-9].

2. VENUS-2 facility

The VENUS Critical Facility is a zero power reactor located at SCK•CEN, Mol (Belgium). This facility was built in 1963-1964, as a nuclear mock-up of a projected marine reactor called VULCAIN; hence the name VENUS, which means VULCAIN Experimental NUclear Study.

In 1967, this facility was adapted and improved in order to study LWR core designs and to provide experimental data for nuclear code validation. A great flexibility was sought after, as well as an easy handling of the fuel pins, one by one, while a great precision of the results had to be achieved.

In 1980, additional material was purchased with a view to studying typical 17×17 PWR fuel assemblies. Such an adaptation was easy: only new reactor grids and small devices adapted to the new fuel geometry were necessary. In 1982, special stainless steel pieces were manufactured in order to build a mock-up of the pressure vessel internals representative of a three-loop Westinghouse power plant.

The VENUS facility comprises a reactor-shielded room and several associated facilities: the control room, fuel storage area, gamma-scanning device, counting room and plutonium laboratory. The shielded room is partly illustrated in Figure 1. Under the floor are contained (1) the reactor vessel [~2.6 m^3], (2) the reactor grids [1 m diameter], (3) the safety neutron detectors, (4) the safety system [moderator fast dump] and (5) the water and compressed air circuitries (not shown in the figure).

The working room [(6), above the floor] gives direct access to the reactor core for loading and unloading fuel pins or experimental thimbles. This room contains the start-up neutron source, the reactor and health physics controls, the regulating rod or fission chamber mechanisms and the handling tools.

Due to the direct access to the fuel, the reactor is shut down when the shielded room is open. The neutron flux level in operation is limited to 10^9 neutrons/cm^2sec, with a view to limiting the irradiation level of the core and the radioactivity of unloaded fuel pins.

Figure 1. Vertical cross-section of the facility

SCK/CEN-Mol

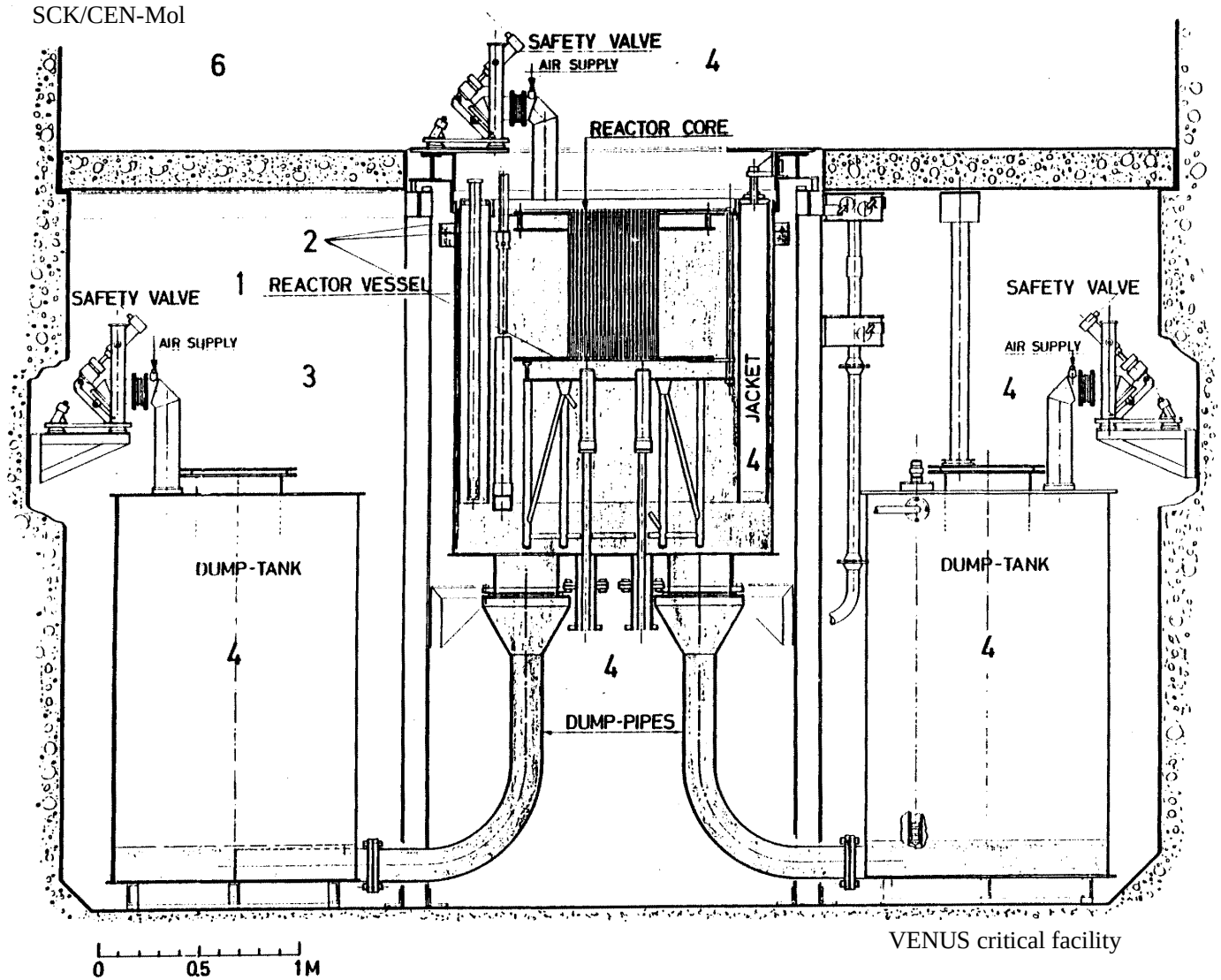

VENUS critical facility

3. VENUS-2 core configuration (geometry and materials)

The horizontal cross-section of the core is shown in Figure 2 and its dimensions are given in Table 1. For experimental and analytical purposes, it should be regarded as a perfect symmetrical core reproducing four times the quadrant between 0° and 90°. The other quadrants are loaded with fuel pins "quasi" identical to the fuel pins of the first quadrant (due to fuel inventory limitations) and with some absorbing rods for criticality balance adjustment. Starting from the centre, the core may be divided into 10 regions as follows:

1. the *4/0 fuel and 2/2.7 fuel region*, containing stainless steel clad UO_2 rods, with 4.0 wt.% enriched the *central hole* (water);

2. the *inner baffle* (stainless steel: 2.858 cm thick);

3. the *3/0 fuel region*, containing zircaloy-clad UO_2 rods, with 3.3 wt.% enriched uranium, in a "17 × 17" type lattice; 10 Pyrex rods, typical of PWR poison clusters are loaded per quadrant (in VENUS language: 3/0 means 3.3 wt.% ^{235}U and 0 wt.% PuO_2);

4. uranium, the rods are typical of a "15 × 15" lattice (first generation of Westinghouse plants), and are loaded with the same pin-to-pin pitch typical of the "17 × 17" type lattice; eight rows of the most external fuel pins have been replaced by mixed-oxide fuel pins (UO_2-PuO_2) enriched 2.0 wt.% in ^{235}U and 2.7 wt.% in Pu;

5. the *outer baffle* (stainless steel: 2.858 cm thick);

6. the *reflector* (minimum thickness: 2.169 cm);

7. the *barrel* (stainless steel: 4.99 cm thick);

8. the *water gap* (water: 5.80 cm thick);

9. the *neutron pad* (stainless steel, average thickness: 6.72 cm);

10. the VENUS environment, i.e. the *jacket* (air filled), the *reactor vessel* (stainless steel) and the reactor room (air).

Regarding its external structures (baffles, barrel, thermal pad, etc.), the configuration of VENUS-2 presents no changes from VENUS-1 (Figure 3), with the exception of core loading. The central part of the core (four assemblies 15 × 15), consisting of fuel pins 3.3 wt.% enriched in ^{235}U, is the same as that for VENUS-1.

However, of the eight assemblies on the periphery of the core, all of which contain fuel pins 4.0 wt.% enriched in ^{235}U, eight rows of the most external fuel pins have been replaced by mixed-oxide fuel pins (UO_2-PuO_2) enriched 2.0 wt.% in ^{235}U and 2.7 wt.% in Pu. The cladding of MOX pins is fabricated in stainless steel. Another significant change compared with VENUS-1 is the modification of the number and positions of Pyrex pins in the central part of the core loading. There are five Pyrex pins in 1/8 of the core rather than six. The VENUS-2 core loading configuration is shown in Figure 4. The descriptions of fuel and Pyrex cells are given in Table 2.

Figure 2. Core model (horizontal cross-section)

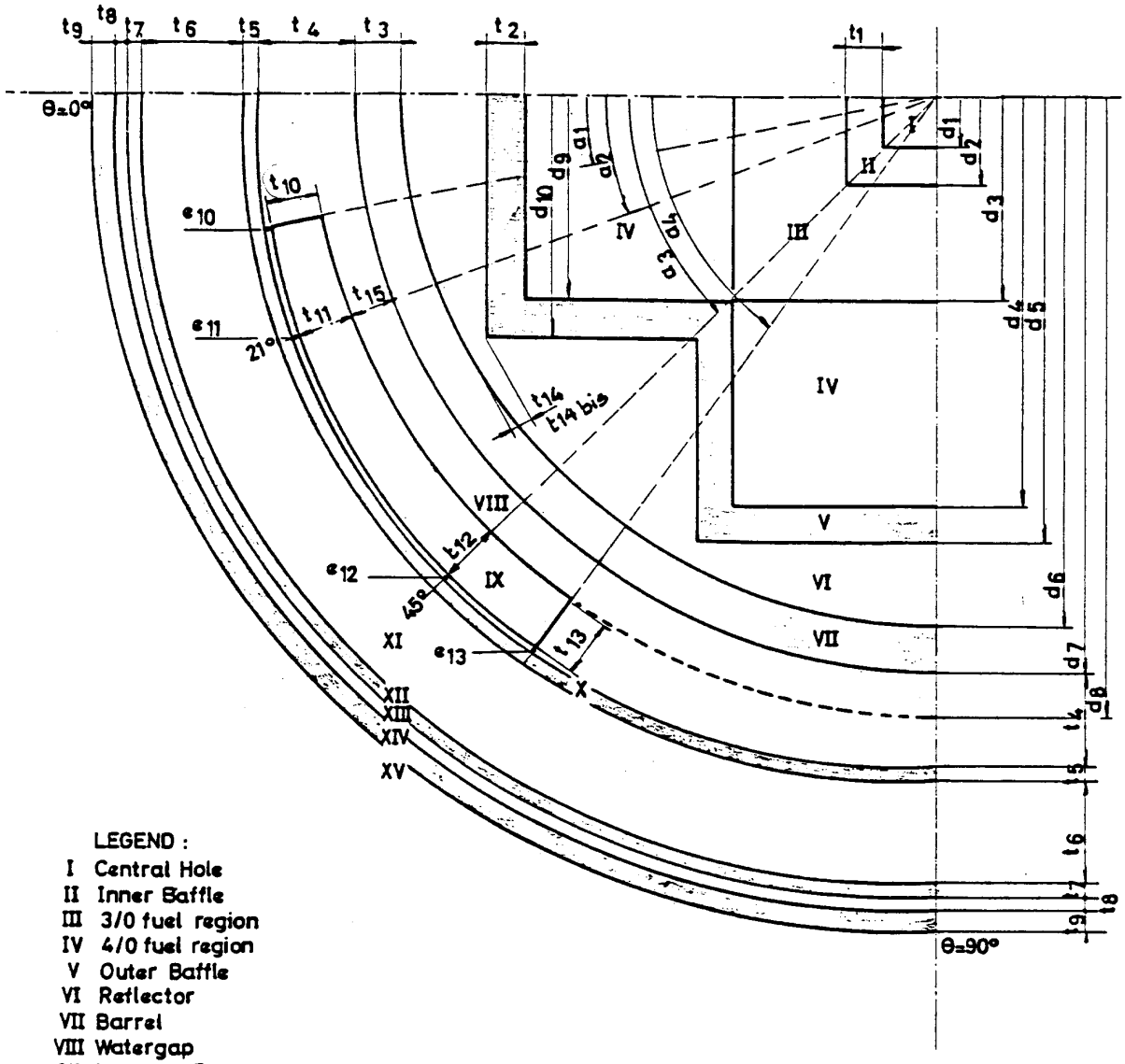

Table 1. Dimensions of the VENUS-2 core

Region	Notation	Dimensions
Central hole (I)	d1	(3.442 ± .021) cm
Inner baffle (II)	d2 t1 LL[a] II UL[b] II h II	(6.300 ± .013) cm (2.858 ± .003) cm (104.849 ± .032) cm (154.856 ± .036) cm (50.006 ± .004) cm
3/0 fuel region (III)	d3 LL III UL III h III	(18.900 ± .005) cm (105.00 ± .05) cm (155.00 ± .15) cm (50.0 ± .1) cm
4/0 fuel and 2/2.7 fuel region (IV)	d4 d9 LL IV UL IV h IV	(37.800 ± .013) cm (18.900 ± .013) cm (105.00 ± .05) cm (155.00 ± .55) cm (50.0 ± .5) cm
Outer baffle (V)	d5 d10 t2 LL V UL V h V	(40.658 ± .021) cm (21.758 ± .021) cm (2.858 ± .003) cm (104.850 ± .033) cm (154.850 ± .039) cm (50.000 ± .006) cm
Reflector (VI)	t14* t14 bis** d6 ***	(2.169 ± .080) cm (2.251 ± .080) cm (48.283 ± 0.050) cm
Barrel (VII)	d6 d7 t3 LL VII UL VII h VII	(48.283 ± 0.050) cm (53.273 ± .060) cm (4.99 ± .01) cm (105.00 ± .06) cm (155.00 ± .16) cm (50.0 ± .1) cm
Water gap (VIII)	t15	(5.800 ± .060) cm

[a] LL: Lower level.
[b] UL: Upper level.
* Distance between baffle corner and barrel.
** Distance between baffle corner and barrel, but taking account of broken corners.
*** Barrel inner radius.

Table 1. Dimensions of the VENUS-2 core (*cont.*)

Region	Notation	Dimensions
Neutron pad (IX)	d8 t10 t11 t12 t13 a1 a2 a3 a4 LL IX UL IX h IX	(59.073 ± .120) cm (6.300 ± .030) cm (6.690 ± .030) cm (7.050 ± .030) cm (6.900 ± .030) cm (11.25 ± .25)° (21.10 ± .10)° 45° (54.75 ± .25)° (105.00 ± .26) cm (155.00 ± .16) cm (50.0 ± .1) cm
Space between neutron pad and jacket	e10 e11 e12 e13	(.3 ± .3) cm at 11.25° (.3 ± .3) cm at 21.10° (.332 ± .310) cm at 45° (.3 ± .3) cm at 54.75°
Jacket inner wall (X)	t4 t5	(11.80 ± .21) cm 0.5 cm
Jacket volume	t6	(15.0 ± .3) cm
Jacket outer wall (XII)****	t7	0.5 cm
Space between jacket and reactor vessel (XIII)	t8	(2.0 ± .3) cm
Reactor vessel wall (XIV)	t9	0.4 cm
Reactor room (XV)		Infinite medium filled by air

**** The inner radius of the jacket inner wall is (62.0 ± .15) cm with respect to a centre being at (X′ = -3.15 cm, Y′ = -3.15 cm) from the core centre, all the next internals are concentric with this jacket inner wall

Figure 3. Core description: VENUS-1 configuration

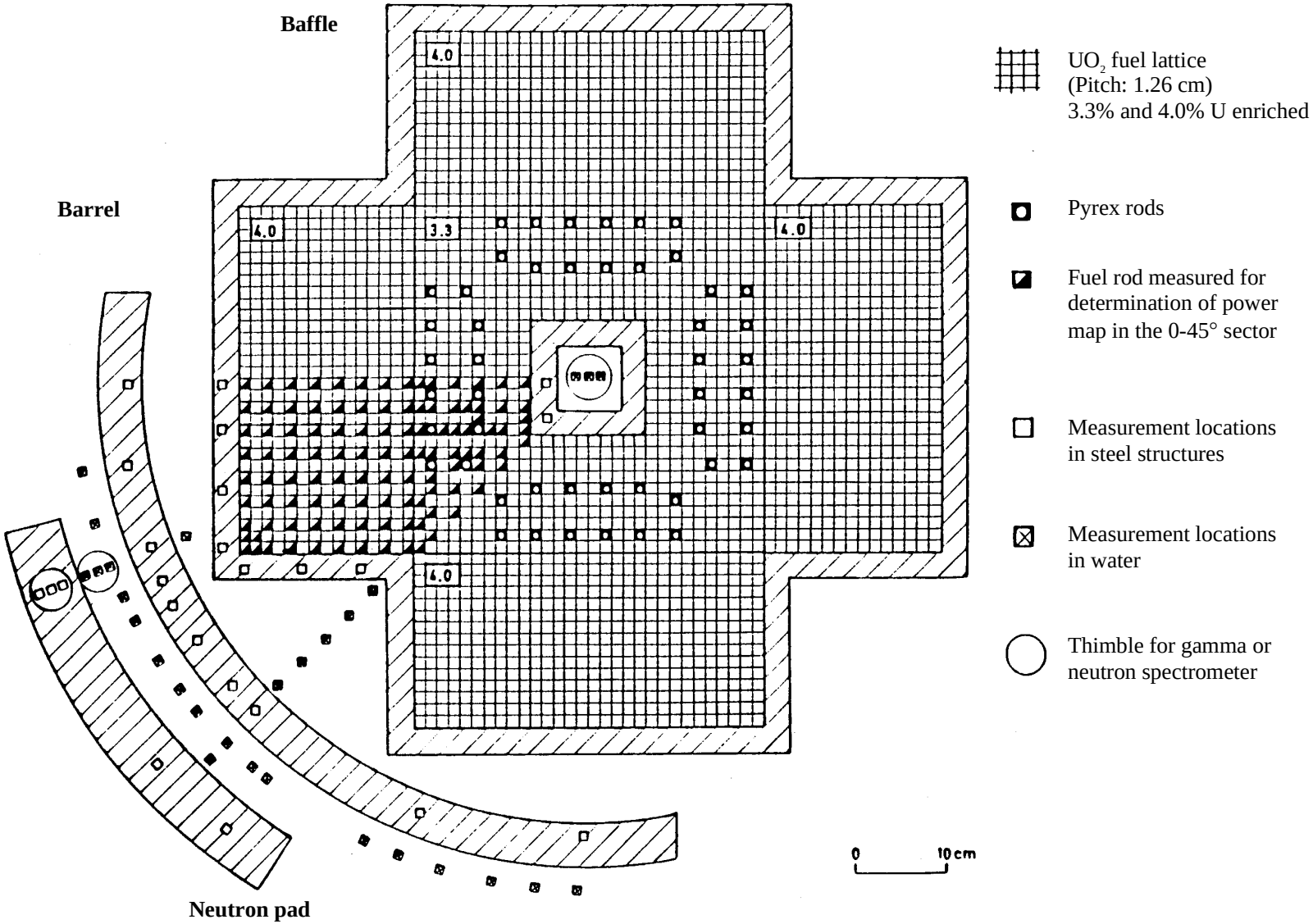

Figure 4. VENUS-2 core loading configuration

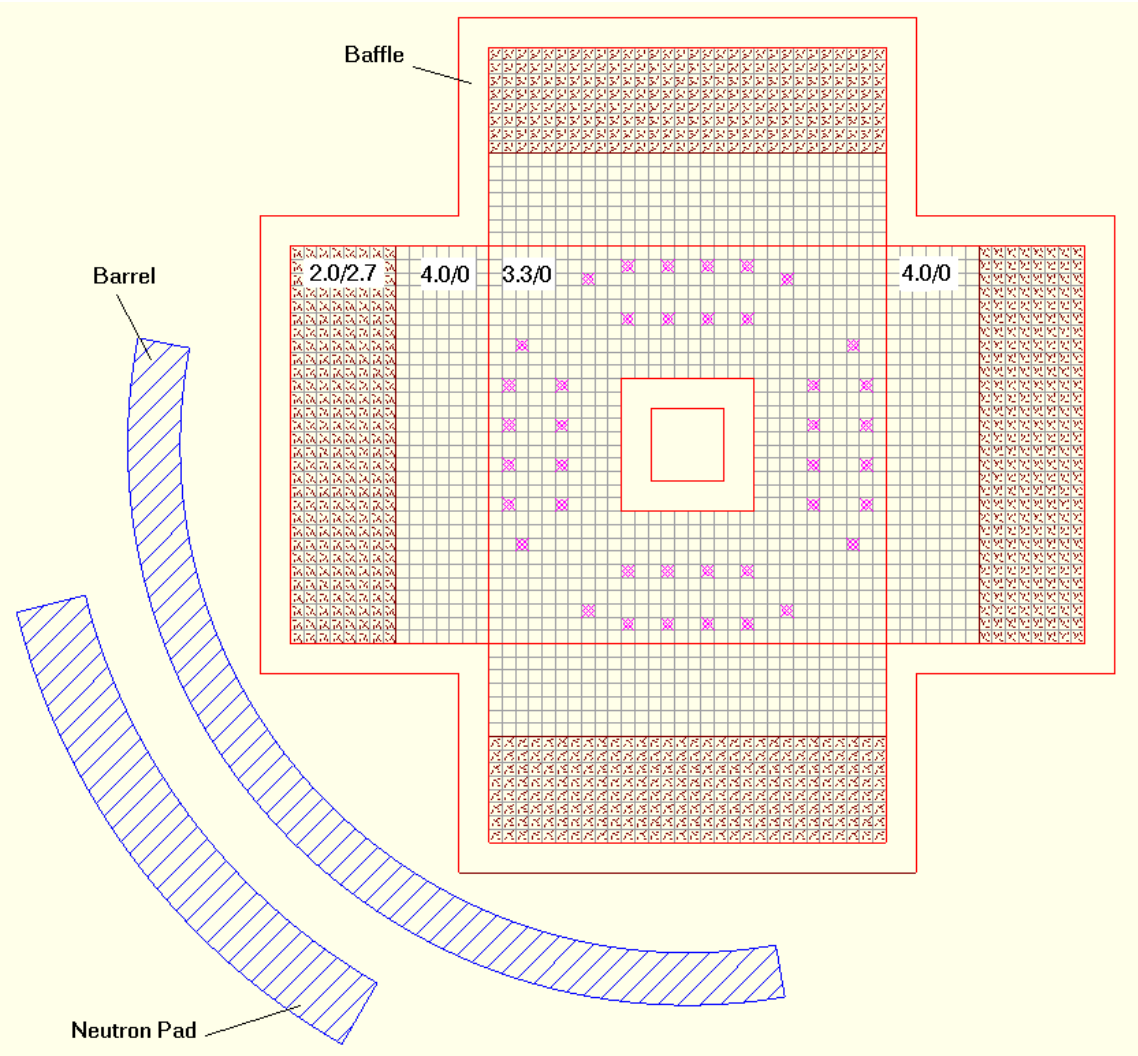

Table 2. Descriptions of fuel and Pyrex cells

(1) 3/0 fuel cell

Fuel type	UO_2
Fuel diameter, cm	0.819 ± .002
Fuel pellet length, cm	0.992 ± .040
Fuel length, cm	50.0 ± .1
Cladding material	Zircaloy 4
Cladding outer diameter, cm	0.950 ± .001
Cladding inner diameter, cm	0.836 ± .001
Fuel cell pitch, cm	1.260 ± .001

Note: The gap between fuel and cladding is *void*.

(2) 4/0 fuel cell

Fuel type	UO_2
Fuel diameter, cm	0.8926 ± .0005
Fuel pellet length, cm	1.114 ± .115
Fuel length, cm	50.0 ± .5
Cladding material	AISI 304 stainless steel
Cladding outer diameter, cm	0.978 ± .002
Cladding inner diameter, cm	0.902 ± .004
Fuel cell pitch, cm	1.260 ± .001

Note: The gap between fuel and cladding is *void*.

(3) 2/2.7 fuel cell (MOX)

Fuel type	UO_2+PuO_2
Fuel diameter, cm	0.902
Cladding material	Stainless steel
Cladding outer diameter, cm	0.978
Cladding inner diameter, cm	0.902
Fuel cell pitch, cm	1.260 ± .001

(4) Pyrex cell

Pyrex material	Corning glass code 7740
Pyrex outer diameter, cm	0.9048 ± .0043
Pyrex inner diameter, cm	0.6058 ± .0031
Cladding material	AISI 304 stainless steel
Cladding outer diameter, cm	0.978 ± .005
Cladding inner diameter, cm	0.940 ± .003
Pyrex cell pitch, cm	1.260 ± .001

Note: The inner hole of the Pyrex cell and the gap between Pyrex cell and cladding are *void*.

Figure 5 shows a vertical cross-section of the core with corresponding axial co-ordinates. Vertically the core may be divided, from bottom to top, as follows:

1. the *reactor vessel* (stainless steel);
2. the *lower filling* (water);
3. the *reactor support* (water and stainless steel, not shown in the figure);
4. the *bottom grid* (32.8 vol.% water and 67.2 vol.% stainless steel*);
5. the *lower reflector* (mainly water and Plexiglas); the reflector composition changes a little from one fuel region to another, depending on the structure of the corresponding fuel pins;
6. the *active height* (fuel and stainless steel);
7. the *upper reflector* (mainly water and Plexiglas), including the *intermediate grid* (63.4 vol.% water and 36.6 vol.% Plexiglas*); the reflector composition changes a little from one fuel region to another, depending on the structure of the corresponding fuel pins;
8. the *upper grid* (63.4 vol.% water and 36.6 vol.% stainless steel*);
9. the *upper filling* (water);
10. the VENUS room environment (air).

The figure shows that the material of interest (i.e. fuel or stainless steel) is located from level 105 cm to level 155 cm (50 cm length). To ensure proper axial buckling conditions, both lower and upper axial reflectors are "quasi" infinite for all the regions (the effective extrapolation length is about 7 cm); where necessary water is replaced by Plexiglas. It can be assumed that neglecting the reactor support in calculation models would not affect the results very much. Although the co-ordinates given in Figure 5 are supposed to be sufficient for three-dimensional modelling, more detailed information on the axial structure of the VENUS core can be found in Refs. [10,11] on the VENUS-3 experiment. It is believed that the use of any additional information would not affect results. However, if the participants use any additional information that is not provided in this specification, it should be described in Section 9 of Appendix B.

The isotopic concentrations of each medium (in units of 10^{24}) in the core are provided in Table 3 and the participants are encouraged to use these values for their calculations. Nevertheless, the detailed compositions of the materials are given in Appendix A.1. As for the stainless steel of top and bottom grids, the isotopic concentrations of the jacket inner wall, given in Table 3, can be used. The theoretical composition of Plexiglas is $[C_5H_8O_2]_n$ and its density is 1.19 g/cm^3.

The criticality was attained by adjusting the water level. The operating temperature is 23.0°C.

* The given composition values assume that no pin is loaded.

Figure 5. Core description (vertical cross-section)

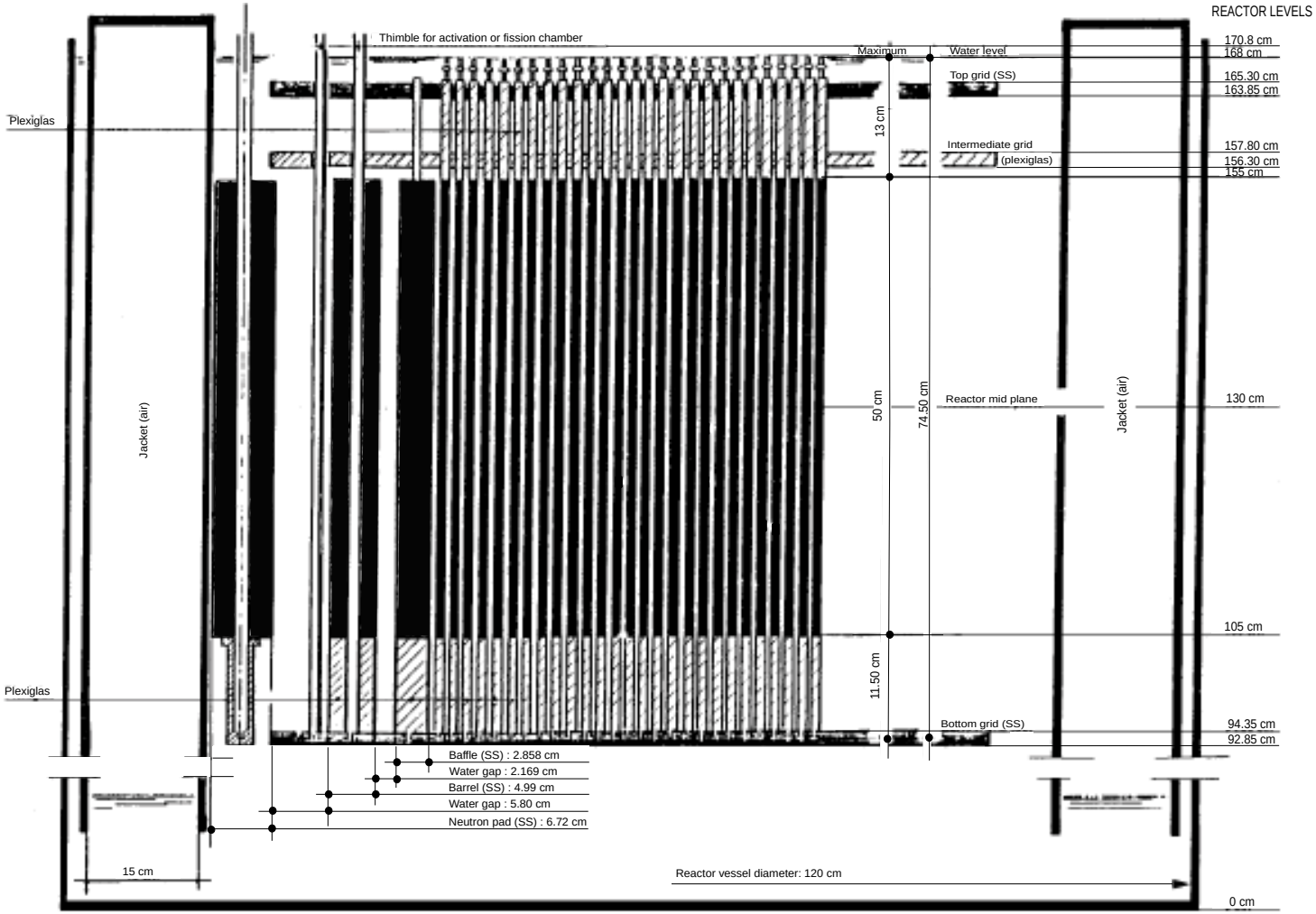

Table 3. Isotopic concentrations of each medium (10^{24} atoms/cm^3)

	3/0 fuel	4/0 fuel	2/2.7 MOX fuel	Pyrex
In the fuel zone				***In the Pyrex zone***
^{234}U	6.74213E-06	7.17988E-06	3.31550E-06	
^{235}U	7.65322E-04	9.27556E-04	4.13082E-04	
^{236}U	3.68820E-06	5.28177E-06	2.67097E-06	
^{238}U	2.20912E-02	2.18426E-02	1.99605E-02	
^{239}Pu			4.47077E-04	
^{240}Pu			9.61437E-05	
^{241}Pu			1.70372E-05	
^{242}Pu			2.44766E-06	
^{241}Am			4.18948E-07	
O	4.57338E-02	4.55653E-02	4.18853E-02	4.52326E-02
Si				1.74973E-02
^{10}B	3.64042E-09			1.12120E-03
^{11}B	1.46531E-08			4.51296E-03
Al				5.80342E-04
Fe				8.38326E-06
Na				1.48608E-03
K				3.21198E-04
In the cladding zone				
C		1.58254E-04	1.58254E-04	1.18827E-04
Mn		1.11582E-03	1.11582E-03	7.53397E-04
P		3.06841E-05	3.06841E-05	
S		2.22292E-05	2.22292E-05	
Si		2.28418E-04	2.28418E-04	4.91240E-04
Cr	7.69688E-05	1.67247E-02	1.67247E-02	1.68355E-02
Ni		8.12063E-03	8.12063E-03	7.70038E-03
Mo		6.53811E-05	6.53811E-05	3.47117E-05
Fe	1.43323E-04	5.95953E-02	5.95953E-02	6.03471E-02
Sn	4.75354E-04			
O	3.00167E-04			
Zr	4.30680E-02			
In the water zone				
H	6.68559E-02	6.68559E-02	6.68559E-02	6.6856E-02
O	3.34279E-02	3.34279E-02	3.34279E-02	3.3428E-02

Avogadro's number used: 0.60221367E+24 (nuclei/mol).
Atomic weights of isotopes are taken from the *CRC Handbook of Chemistry and Physics*, 73rd Edition (1992-1993).

Table 3. Isotopic concentrations of each medium (10^{24} atoms/cm^3) (*cont.*)

	Water	Baffle	Barrel	Neutron pad	Jacket inner wall
C		2.33752E-04	5.94134E-05	6.33743E-05	9.50614E-05
Mn		1.43008E-03	1.12836E-03	7.18758E-04	1.01146E-03
P		4.60909E-05	4.30073E-05	3.99353E-05	3.83993E-05
S		1.92924E-05	7.41827E-06	5.93462E-06	1.18692E-05
Si		4.82892E-04	8.68986E-04	6.69103E-04	6.33530E-04
Cr		1.49819E-02	1.68940E-02	1.64896E-02	1.61209E-02
Ni		7.06993E-03	8.26696E-03	8.58227E-03	7.97273E-03
Mo		2.25187E-04	2.35048E-04	2.10750E-04	2.24138E-04
Co		1.11431E-04	7.83050E-05	1.58225E-04	9.12213E-05
Fe		6.15902E-02	5.86255E-02	5.92039E-02	5.99331E-02
N			2.71726E-04		9.17074E-05
H	6.68559E-02				
O	3.34279E-02				

Avogadro's number used: 0.60221367E+24 (nuclei/mol).
Atomic weights of isotopes are taken from the *CRC Handbook of Chemistry and Physics*, 73rd Edition (1992-1993).

4. VENUS-2 measurements

Concerning the experimental fission rate measurements, the average fission rate in the core corresponding to absolute reference irradiation is 1.87E+08 fissions/cm/sec at the mid-plane. This average fission rate corresponds to a power of 595 Watts. The 1/8 of the core comprises 325 fuel rods in which the fission rates of 121 fuel rods (41 3/0 UO_2, 35 4/0 UO_2 and 45 2/2.7 MOX pins) were directly measured after an irradiation of 13.5 h at 90% of the VENUS maximum power. The experimental data were taken from the gamma activity of the ^{140}La (fission yields ~6.3% for ^{235}U and ~5.5% for ^{239}Pu, energy ~1.6 MeV, effective half-life ~12.8 d). The fission rates of 204 fuel rods were interpolated from the measured values. Seven additional fuel pins measured were located in symmetric positions out of 1/8 of the core. The measured fission rate values were normalised to a core averaged fission rate = 1 fission/sec/fuel cell (or to a total core fission rate of 2 560 fissions/sec). The measured fuel pin positions can be found in Figure 6. The reported uncertainty of the measured data (1σ) is ±1.0% in UO_2 and ±1.5% in MOX pins and that of the interpolated data (1σ) is ±2%.

In addition, the fission rate distributions of six fuel pins (two 3/0 UO_2, two 4/0 UO_2 and two 2/2.7 MOX pins) were measured *axially* by γ-scanning after an irradiation of 8 h at 90% of the VENUS maximum power. It originally was in order to obtain vertical buckling representative of the core.

The co-ordinates of the measurement points can be expressed in two different co-ordinate systems:

- (x,y) co-ordinates with respect to the reactor grid;
- (x,y) or (r,θ) co-ordinates with respect to the core centre.

The origin of the (x,y) co-ordinates with respect to the reactor grid is located in the inner baffle at a point 2.5 pitches (1 pitch = 1.26 cm) to the left and 2.5 pitches below the geometric centre of the core. Therefore, the origin of the (x,y) co-ordinates with respect to the reactor grid are at $X' = -3.15$ cm and $Y' = -3.15$ cm from the geometric centre of the core. The south-west quadrant of the core to be considered in the calculations is thus defined by the ranges $-27 < x < +2$ and $-27 < y < +2$, where the limits represent cell centre-to-centre distances in units of pitches.

Figure 6. Schematic view of the core lattice

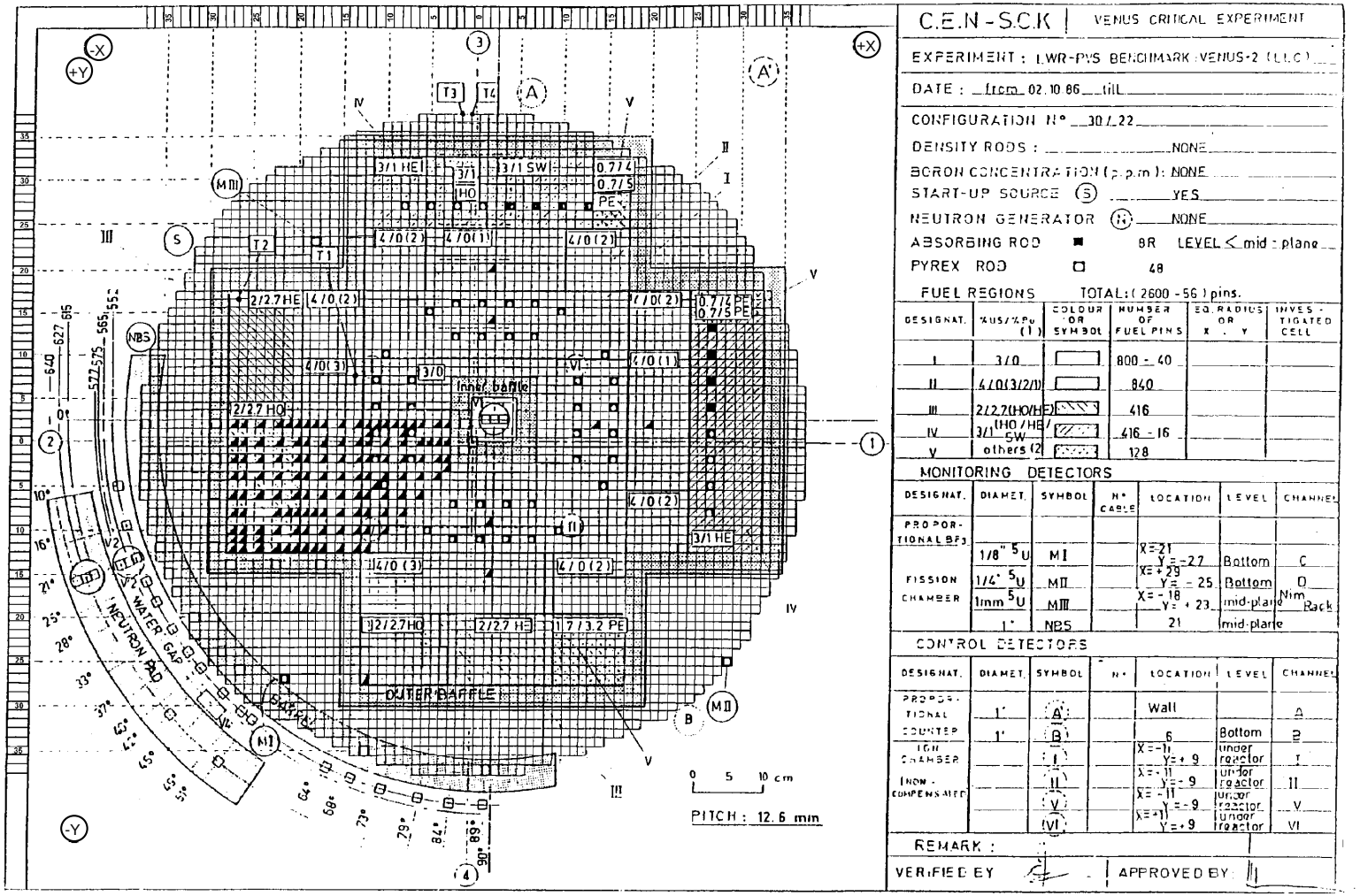

REMARKS: (1) between brackets: – or supply order
– or fabrication mode: HO = Homogeneous vibrated
HE = Heterogeneous vibrated
SW = Heterogeneous swaged
PE = Pelletised

(2) Other means: – or 1.7/3.2 PE
– or a mixture of 0.7/5 PE + some 0.7/4 PE & 2/2.7 PE

86/66053 A – Issued 18/09/86
– Updated 15/10/86

According to the (x,y) co-ordinates with respect to the reactor grid, the axially measured pin points are (-27,-12), (-22,-2), (-15,+2), (-13,-12), (-11,+2) and (-6,-6). If the (x,y) co-ordinates with respect to the core centre are used, they are in the points (-37.17, +18.27), (-30.87, +5.67), (-22.05, +0.63), (-19.53,+18.27), (-17.01,+0.63) and (-10.71,+10.71) in cm. The axial measurements were carried out at 21 different vertical planes along 50 cm of the fuel pin length (from 105 cm to 155 cm): starting from 110 cm, and at every 2 cm upwards to 150 cm.

5. Calculations and results

Results should be provided both on paper and a computer-processable medium with a short report describing the information requested in Appendix A.2.

5.1. Cell calculations

For each fuel cell (3/0 UO_2, 4/0 UO_2, 2/2.7 MOX), participants should provide the following results:

- k_∞;
- reaction rates (absorption and fission) per isotope (one group and three groups involving the 5 keV and 4 eV boundaries).

Results to be reported as demonstrated in Tables 1 and 2 in Appendix A.3.

For reaction rates, no normalisation is required. An appropriate normalisation will be made for the analysis of results afterwards. For libraries not having energy group boundaries that match the required three-group neutron energy boundaries (5 keV and 4 eV), an appropriate interpolation can be used by participants. If not, different energy boundaries used should be reported in Section 8.d of Appendix A.2.

5.2. Core calculations

- k_{eff};
- normalised radial fission rate distribution at 325 fuel pin positions (315 pins on 1/8 of the core, plus 10 diagonal pins);
- normalised axial fission rate distribution of six fuel pins.

Results to be reported as demonstrated in Tables 3 to 5 in Appendix A.3.

With regard to the normalisation of fission rate distributions, the radial fission rate distribution obtained for each axial level is first axially integrated and then normalised to an average value of unity so that the sum of the fission rate over the 640 pins on the 1/4 core is equal to 640. The axial fission rate distribution of the six fuel rods is each individually normalised to an average value of unity.

6. General comments

This benchmark exercise is a “blind” test, hence the measured values at specified VENUS locations are not revealed to the participants in this specification but will be provided when benchmark results are analysed.

REFERENCES

[1] Na, B-C., *Benchmark on the VENUS-2 MOX Core Measurements*, OECD/NEA report, NEA/NSC/DOC(2000)7, ISBN 92-64-18276-4, December 2000.

[2] Na, B-C. and E. Sartori, "OECD/NEA International Benchmark on the VENUS-2 MOX Core Measurements", *M&C 2001*, Salt Lake City, Utah, USA, 9-13 September 2001.

[3] van der Meer, K., *et al*., *Additional Data for the 3-D VENUS-2 Benchmark*, SCK•CEN report, TN-0008, September 2000.

[4] *VENUS-2 PWR Core Source and Azimuthal Lead Factor Experiments and Calculational Tests*, SCK•CEN report.

[5] LWR Pressure Vessel Surveillance Dosimetry Improvement Program Review Meeting, NBS, Maryland, 26-30 Oct. 1981: Exploratory Calculations Carried out at Westinghouse, S. Anderson in co-operation with G. Guthrie (HEDL).

[6] LWR Pressure Vessel Surveillance Dosimetry Improvement Program Review Meeting, NBS, Maryland, 11-15 Oct. 1982: Design Study of the Core Loading for the VENUS PWR Pressure Vessel Benchmark Facility, G. Minsart (SCK•CEN).

[7] LWR Pressure Vessel Surveillance Dosimetry Program, *Activities, Status and Scheduling*, 29 March-2 April 1982.

[8] Letters to Dr. Kam and Dr. Williams (ORNL), dated 22 June 1983 and 7 September 1983: *VENUS Core: Definition and Qualifications of the Materials, and Up-dating*, L. Leenders.

[9] Letters to Dr. Kam and Dr. Williams (ORNL), dated 7 July 1983: *VENUS LWR-PVS Benchmark: Definition and Qualifications of the Geometry*, L. Leenders.

[10] Leenders, L., *LWR-PVS Benchmark Experiment VENUS-3 (With Partial Length Shielded Assemblies)*, FCP/VEN/01, SCK•CEN report, September 1988.

[11] Hehn, G. and B-C. Na, *Prediction of Neutron Embrittlement in the Reactor Pressure Vessel: VENUS-1 and VENUS-3 Benchmarks*, OECD/NEA report, NEA/NSC/DOC(2000)5, ISBN 92-64-17637-3.

Appendix A.1

VENUS-2 PWR CORE SOURCE AND AZIMUTHAL LEAD FACTOR EXPERIMENTS

Description of the composition of different materials

The compositions of all the materials in the VENUS-2 core are given in Tables A.1 to A.11. All the data are extracted from the SCK•CEN report *VENUS-2 PWR Core Source and Azimuthal Lead Factor Experiments and Calculational Tests*.

Table A.1. Compositions of the 3/0 fuel cell

Fuel composition	UO_2
Fuel stoichiometry [O/U]	1.997 ± .005
Fuel linear specific weight, g/cm	(5.40 ± .05)
Fuel isotopic composition of U, wt.%	^{234}U (.029 ± .001) ^{235}U (3.306 ± .010) ^{236}U (.016 ± .001) ^{238}U (96.649 ± .012)
Total impurities	8 ppm B equivalent in U
Cladding composition	Zircaloy 4
Cladding linear specific weight, g/cm	(1.0627 ± .0004)
Cladding isotopic composition, wt.%	Sn (1.41 ± .06) Fe (.20 ± .01) Cr (.10 ± .01) O (.12 ± .01) Zr (98.17 ± .06)
Detected impurities in the cladding	– < 1 ppm: B, Cd, U – < 10 ppm: C1, Co, Cu, H, Mg, Mn, Ti, Zn – < 50 ppm: Al, Hf, N, Nb, Ni, V, W, Au, Ir, Mo, Pb – < 100 ppm: Ta, Si, Sm, Eu, Dy, Gd, Lu – 146 ppm: C
Moderator	Water

Table A.2. Compositions of the 4/0 fuel cell

Fuel composition	UO_2
Fuel stoichiometry [O/U]	2.00 ± .01
Fuel linear specific weight, g/cm	(6.39 ± .70)
Fuel isotopic composition of U, wt.%	^{234}U (.031 ± .009) ^{235}U (4.022 ± .008) ^{236}U (.023 ± .006) ^{238}U (95.924 ± .010)
Total impurities	Not available
Cladding composition	AISI 304 stainless steel
Cladding linear specific weight, g/cm	(.8855 ± .0007)
Cladding isotopic composition, wt.%	C (.040 ± .040) Mn (1.290 ± .030) P (.020 ± .020) S (.015 ± .015) Si (.135 ± .003) Cr (18.300 ± .400) Ni (10.030 ± .200) Mo (.132 ± .003) Fe (70.038 ± .711)
Detected impurities:	– < 10 ppm: Cd, Ta, Au, B, Co – < 100 ppm: Sm, Eu, Dy, Ir, Gd
Moderator	Water

Table A.3. Compositions of the 2/2.7 MOX fuel cell

Stoichiometry [O/(U+Pu)]	2.046	
Linear density, g/cm	6.000	
Chemical composition, wt.% $UO_2/[UO_2+PuO_2)]$ $PuO_2/[UO_2+PuO_2)]$	 97.3 2.70	
Fuel isotopic composition, wt.%	$^{233}U/U$ $^{234}U/U$ $^{235}U/U$ $^{236}U/U$ $^{238}U/U$ $^{238}Pu/Pu$ $^{239}Pu/Pu$ $^{240}Pu/Pu$ $^{241}Pu/Pu$ $^{242}Pu/Pu$ $^{241}Am/Pu$	0.0000 0.0160 2.0020 0.0130 97.976 0.0000 79.370 17.140 3.0500 0.4400 0.0750
Specific weight of components, g/cm^3	Mixture (UO_2+PuO_2) UO_2 in mixture PuO_2 in mixture U metal Pu metal ^{16}O total	9.389633 9.136113 0.253520 8.031689 0.2229926 1.134957
Cladding	Stainless steel	
Cladding linear specific weight, g/cm	0.8855	
Cladding isotopic composition, wt.%	C ^{55}Mn P S ^{28}Si Cr Ni Mo Fe	0.0400 1.2900 0.0200 0.0150 0.1350 18.300 10.030 0.1320 70.038
Moderator	Water	

Table A.4. Compositions of the Pyrex cell

Pyrex material	Corning glass code 7740
Pyrex linear specific weight, g/cm	(.7886 ± .0052)
Pyrex isotopic composition, wt.%	SiO_2 78.53 B_2O_3 (14.65 ± .15) Al_2O_3 2.21 Fe_2O_3 .05 Na_2O 3.44 K_2O 1.13
Isotopic composition of B, at.%	^{10}B: (19.775 ± .005) ^{11}B: (80.225 ± .005)
Cladding material	AISI 304 stainless steel
Cladding specific weight, g/cm^3	(7.9 ± .1)
Cladding isotopic composition, wt.%	C (.03 ± .03) Mn (.87 ± .42) Si (.29 ± .16) Cr (18.40 ± .10) Ni (9.50 ± .50) Mo (.07 ± .07) Fe (70.84 ± 1.28)
Moderator	Water

Table A.5. Compositions of the central hole/reflector/water gap/space between neutron pad and jacket/space between jacket and reactor vessel

Chemical composition	Water (H_2O)
Diluted oxygen	O 8.6 ppm (saturation for air-water contact)
Detected impurities	B 12 ppb (1.E-9 g/l) ~ ppm (weight) Si 46 Mn 2.5 Fe 0.7 Mg 5 Cu 5 Ca 75 Al 8 Sr .5 Zn 25 V 5 Ag 2 Ba 15
Non-detected impurities	Li, Zr, Ti, Be, Nb, Ga, Hf, Co, In, Bi, Ni, Pb, Cd, Te, P, Ge, W, Sb, Cr, Mo, Hg, As, Tl, Sn
Temperature, °C	(23.0 ± 1.5)

Table A.6. Compositions of the inner and outer baffles

Chemical composition	AISI 304 stainless steel
Isotopic composition, wt.%	C (.059 ± .020) Mn (1.651 ± .053) P (.030 ± .015) S (.013 ± .013) Si (.285 ± .129) Cr (16.370 ± .327) Ni (8.720 ± .185) Mo (.454 ± .075) Co (.138 ± .070) Fe (72.281 ± .231)
Detected impurities	– < 10 ppm: Cd, Ta, Au, B – < 100 ppm: Sm, Eu, Dy, Ir, Gd
Non-detected impurity	Cu
Specific weight, g/cm^3	(7.902 ± .002)

Table A.7. Compositions of the barrel

Chemical composition	AISI 304 stainless steel
Isotopic composition, wt.%	C .015 Mn (1.303 ± .430) P .028 S .005 Si .513 Cr (18.464 ± .200) Ni (10.199 ± .380) Mo .474 Co .097 Fe (68.819 ± 1.010) N .080
Non-detected impurity	Cd, Sm, Eu, Dy, Ir, Gd, Ta, Cu, Au, B
Specific weight, g/cm^3	(7.9 ± .1)

Table A.8. Compositions of the neutron pad

Chemical composition	AISI 304 stainless steel
Isotopic composition, wt.%	C .016 Mn (.830 ± .280) P .026 S .004 Si .395 Cr (18.022 ± .030) Ni (10.588 ± .360) Mo .425 Co .196 Fe (69.498 ± .670)
Non-detected impurity	Cd, Sm, Eu, Dy, Ir, Gd, Ta, Cu, Au, B
Specific weight, g/cm^3	(7.9 ± .1)

Table A.10. Compositions of the jacket inner wall/jacket outer wall/reactor vessel wall

Chemical composition	AISI 304 stainless steel
Isotopic composition, wt.%	C (.024 ± .012) Mn (1.168 ± .270) P (.025 ± .003) S (.008 ± .005) Si (.374 ± .150) Ce (17.619 ± 1.047) Ni (9.836 ± .934) Mo (.452 ± .024) Co (.113 ± .074) Fe (70.354 ± 1.963) N (.027 ± .040)
Specific weight, g/cm^3	(7.9 ± .1)

Table A.11. Compositions of the jacket volume and around the reactor vessel

Jacket volume	Air with 100% relative humidity
Around the reactor vessel	Dry air

Appendix A.2

DETAILS TO BE PROVIDED ABOUT THE CALCULATION SCHEME USED

1. Name of participant(s).

2. Establishment.

3. Name of code system(s) used.

4. Bibliographic references for the codes used.

5. Origin of cross-section data (e.g. ENDF/B-VI, JEF-2.2, JENDL-3.2, etc.) (describe deviations of standard libraries, e.g. mix from different libraries, details).

6. Spectral calculations and data reduction methods used (please describe your scheme, and through a graph and explanatory text provide details about the assumptions made):
   a) resonance shielding: specify method(s) and specify energy range, and the nuclides (actinides, clad, fission products, oxygen, unresolved resonance treatment);
   b) mutual shielding (overlapping of resonances);
   c) fission spectra: specify whether only a single spectrum was used or a weighted mix from all fissile nuclides, explain procedure;
   d) describe how the (n,2n) reaction was treated;
   e) weighting spectrum for scattering matrices, e.g. correction of the out-scatter and self-scatter terms considering the differences between the original weighting spectrum and realistic cell spectrum.

7. Number of energy groups used in the different phases.

8. Cell calculation:
   a) type of calculation (i.e. heterogeneous, homogeneous);
   b) theory used (diffusion, transport);
   c) method used (finite difference, finite elements, nodal, S_N (order), collision probability, Monte Carlo, $J_{\pm}$, etc.);
   d) calculation characteristics (meshes, elements/assembly, meshes/pin, number of histories, multi-group, continuous energy, etc.).

9. Other assumptions and characteristics.

10. Comments useful for interpreting correctly the results.

Appendix A.3

RESULTS TO BE REPORTED

1. Cell calculations

Table 1. k_∞

Fuel cell	k_∞
3/0 UO_2	
4/0 UO_2	
2/2.7 MOX	

Table 2.1. Energy integrated reaction rates in 2/2.7 MOX (reactions/cm^3/sec)

	Absorption*	Fission
^{234}U		
^{235}U		
^{236}U		
^{238}U		
^{239}Pu		
^{240}Pu		
^{241}Pu		
^{242}Pu		
^{241}Am		

* Absorption = fission + capture

Tables 2.2 and 2.3. Energy integrated reaction rates in 3/0 and 4/0 UO_2, respectively

	Absorption	Fission
^{235}U		
^{238}U		

Tables 2.4, 2.5 and 2.6** Group 1 (E > 5 keV) reaction rates in 2/2.7 MOX, 3/0 and 4/0 UO_2, respectively.

Tables 2.7, 2.8 and 2.9** Group 2 (4 eV < E < 5 keV) reaction rates in 2/2.7 MOX, 3/0 and 4/0 UO_2, respectively.

Tables 2.10, 2.11 and 2.12** Group 3 (E < 4 eV) reaction rates in 2/2.7 MOX, 3/0 and 4/0 UO_2, respectively.

** Table format as Tables 2.1, 2.2 and 2.3.

2. Core calculations

Table 3. Main characteristics from core calculations

k_{eff}	

Table 4. Normalised radial fission rate distribution at 325 fuel pin positions

This table should contain normalised fission rate values in the format as follows:

do iy=1,15
Axially integrated fission rate (ix,iy), ix = 1,25
enddo

where iy is 15 pin positions in the y-axis and ix is 25 pin positions in the x-axis. The pin positions given *with respect to the core centre* (see table below) can be used in the calculation model. The pin positions are given also with respect to the reactor grid used in the experiments. The origin of the (x,y) co-ordinate system with respect to the core centre is the geometric centre of the core (see Figure 6).

Co-ordinates of pin positions

X co-ordinate			Y co-ordinate		
ix	**Core centre (cm)**	**Reactor grid**	**iy**	**Core centre (cm)**	**Reactor grid**
1	-37.17	-27	1	0.63	+2
2	-35.91	-26	2	1.89	+1
3	-34.65	-25	3	3.15	0
4	-33.39	-24	4	4.41	-1
5	-32.13	-23	5	5.67	-2
6	-30.87	-22	6	6.93	-3
7	-29.61	-21	7	8.19	-4
8	-28.35	-20	8	9.45	-5
9	-27.09	-19	9	10.71	-6
10	-25.83	-18	10	11.97	-7
11	-24.57	-17	11	13.23	-8
12	-23.31	-16	12	14.49	-9
13	-22.05	-15	13	15.75	-10
14	-20.79	-14	14	17.01	-11
15	-19.53	-13	15	18.27	-12
16	-18.27	-12			
17	-17.01	-11			
18	-15.75	-10			
19	-14.49	-9			
20	-13.23	-8			
21	-11.97	-7			
22	-10.71	-6			
23	-9.45	-5			
24	-8.19	-4			
25	-6.93	-3			

Table 5. Normalised axial fission rate distribution of six fuel rods

Axial position (cm)	Fuel rod positions					
	2/2.7 MOX		4/0 UO_2		3/0 UO_2	
	(-27, -12)*	(-22, -2)*	(-15, +2)*	(-13, -12)*	(-11, +2)*	(-6, -6)*
110						
112						
114						
116						
118						
120						
122						
124						
126						
128						
130						
132						
134						
136						
138						
140						
142						
144						
146						
148						
150						
Sum	**1.0**	**1.0**	**1.0**	**1.0**	**1.0**	**1.0**

* The corresponding (x,y) co-ordinates with respect to the core centre are (-37.17,+18.27), (-30.87,+5.67), (-22.05,+0.63), (-19.53,+18.27), (-17.01,+0.63) and (-10.71,+10.71) in cm, respectively.

Appendix B

CALCULATION DETAILS PROVIDED BY THE PARTICIPANTS

FRAMATOME-ANP GmhH (Germany)

1. **Name of participant(s).**

   W. Hofmann, J. Koban, W.Timm

2. **Establishment.**

   FRAMATOME-ANP GmbH (Erlangen, Germany)

3. **Name of code system(s) used.**

   TORT 2.7.3

4. **Bibliographic references for the codes used.**

   TORT-DORT Two- and Three-dimensional Discrete Ordinates Transport, Version 2.7.3 [4].
   CASMO-4, a fuel assembly burn-up code: Studsvik SOA [3] (preparation of cross-section data).

5. **Origin of cross-section data.**

   Condensed cross-section library [5] based on Studsvik's own "L"-library in 70 energy groups [3], the cross-section data are mainly based on ENDF/B-IV.

6. **Spectral calculations and data reduction methods used.**

   See Ref. [5].

7. **Number of energy groups used in the different phases.**

   A condensation scheme with five energy groups has been chosen. The energy boundaries of the cross-sections for the 3-D calculations are as seen in Table 1.

Table 1. Energy group condensation structure

Group upper bounds		Fission spectrum
1	10.00 MeV	0.785
2	821.0 keV	0.215
3	5.53 keV	0.0
4	4.00 eV	0.0
5	0.625 eV	0.0

   The fission spectrum is taken from [5]. More detailed discussions about the cross-sections are given in [5].

8. **Cell calculation.**

   Information on cell calculations is given in [5].

9. Other assumptions and characteristics.

The geometry data were taken from [2].

In the 3-D core calculations the uniform grid with a pitch of 1.26 cm in x-y direction has been preserved also in all regions outside the fissile zones, i.e. baffle, water, barrel. Therefore baffle and barrel/neutron pad have been modelled only approximately in this uniform grid, i.e. in such a way that the masses (areas) of these materials are approximately preserved. In the geometrical model a size of 55×55 "meshes" has been assumed in the x-y direction. The geometrical model was limited to a core quadrant.

Axially, only two additional materials were introduced as in [5]:

- rods with Plexiglas (surrounded by water) above and below the 3/0 UO_2 zone;
- rods with Plexiglas (surrounded by water) above and below the 4/0 UO_2 zone and the 2/2.7 MOX zone.

For the upper axial reflector a thickness of 13 cm was assumed and for the lower a thickness of 21.5 cm. For these regions a combination of Plexiglas and water zones has been used.

The 3-D calculations with TORT were performed in x-y-z geometry with P_0S_8 approximation. For comparison with the S_8 calculation an extra S_2 calculation was performed.

10. Comments useful for interpreting correctly the results.

In order to get an accurate axial power profile in the specified fuel rods the rods were split axially into 25 equidistant regions (2 cm per region).

All results have been obtained by assuming quarter core symmetry.

Main results and comments

Cell calculations

No cell calculations were performed, see [5].

Core calculations

The 3-D core calculations were performed with the S_N code TORT 2.7.3 [4].

The k-effective of the core is:

$$\mathbf{k_{eff} = 0.99719} \qquad \text{(TORT S8)}$$

(For comparison: k_{eff} = 0.99438 for TORT S2.)

The radial fission rate distribution is given in a separate MS EXCEL file (see attachment). As the measured (and partially interpolated) normalised radial pin power (fission rate) distribution has been published in [1], the TORT pin power results can directly be compared to the measured values, see MS EXCEL attachment. Table 2 gives an overview of the main results, both for the individual fuel zones and for the total core.

Table 2. Overview of main results

Zone	Power calc.	Power exp.	Power (C/E)	Peaking calc.	Peaking exp.	Peaking (C/E)	1 sigma [%]
UOX 3.3	1.29143	1.33151	0.96990	1.15531	1.14381	1.01006	2.35
UOX 4.0	1.16296	1.16831	0.99542	1.29755	1.33611	0.97114	2.57
MOX 2/2.7	0.62912	0.59258	1.06166	1.77709	1.79722	0.98880	2.38
Total	1.00538	1.00595	0.99943	1.50900	1.56100	0.96669	4.99

The calculated normalised axial power profiles are almost identical for all six specified rods. For the central 40 cm of the core the calculated axial power peaking factor is around 1.20 (measured values are not yet available). The detailed axial fission rate distributions of all six specified rods are given in a separate MS EXCEL file (see attachment).

For comparison with the results of the TORT S_8 calculation the results of an additional S_2 calculation are given in the MS EXCEL attachment.

REFERENCES

[1] *Benchmark of the VENUS-2 MOX Core Measurements*, NEA/NSC/DOC(2000)7

[2] *Blind Benchmark on the 3-D VENUS-2 MOX Core Measurements: Final Specification*, NEA/SEN/NSC/WPPR(2001)1.

[3] *CASMO-4, A Fuel Assembly Burn-up Code*, Studsvik SOA.

[4] Rhoades, Childs, TORT-DORT Two- and *Three-dimensional Discrete Ordinates Transport Version 2.7.3*, RSIC CODE PACKAGE CCC-543, Oak Ridge National Laboratory, Oak Ridge, Tennessee (1993).

[5] W. Timm, S. Misu, D. Porsch, *VENUS-2 3-D MOX Core Benchmark*, FRAMATOME-ANP GmbH results.

KAERI (Korea)

1. **Name of participant(s).**

   Do Heon Kim, Jung-Do Kim, Choong-Sub Gil, Jonghwa Chang

2. **Establishment.**

   Nuclear Data Evaluation Laboratory
   Korea Atomic Energy Research Institute
   P.O. Box 105, Yuseong, Daejeon, 305-600, Korea

3. **Name of code system(s) used.**

   DANTSYS 3.0

4. **Bibliographic references for the codes used.**

   Alcouffe, R.E., *et al*., *DANTSYS: A Diffusion Accelerated Neutral Particle Transport Code System*, LA-12969-M, Los Alamos National Laboratory (1995).

5. **Origin of cross-section data.**

   The latest version of ENDF/B-VI (ENDF/B-VI Release 7) for all isotopes except natural tin (from ENDL-84 library) is used.

   The MATXS-formatted master library in the HELIOS neutron group structure of 190 groups is generated by NJOY99.50 code.

6. **Spectral calculations and data reduction methods used.**

   a) *Resonance shielding*: Bondarenko method or Background Cross-section Method (TRANSX).

   b) *Mutual shielding*: Overlapping of resonances is not considered.

   c) *Fission spectra*: Flux-, mixture-, and region-dependent fission spectra are used.

   d) *Describe how the (n,2n) reaction was treated*: The (n,2n) reaction is not treated.

   e) *Weighting spectrum for scattering matrices*: None.

7. **Number of energy groups used in the different phases.**

   - 190 groups for cell calculations.
   - 35 groups for core calculations.

8. **Cell calculation.**

   a) *Type of calculation*: Heterogeneous calculation.

   b) *Theory used*: Transport theory.

c) *Method used*: Discrete ordinates (S_N) method.

d) *Calculation characteristics*: S_8P_3, the mesh sizes are less than ~0.03 cm for three fuel cells.

9. Other assumptions and characteristics.

The VENUS-2 core was modelled explicitly from bottom to top with the proper use of homogenisation for the grid regions.

The VENUS-2 core was modelled up to the barrel in the x- and y- direction. The regions beyond the barrel were filled with water and the neutron pad was not taken into account.

10. Comments useful for interpreting correctly the results.

In preparing Tables 2.4 to 2.12 for the results of cell calculations, somewhat different energy bounds for Groups 1 to 3 were used because there were not appropriate energy groups with the exact energy bounds (i.e. 4 eV and 5 keV) in the HELIOS neutron group structure of 190 groups. Thus, we adopted the energy ranges of $E > 4.881$ keV for Group 1, 3.9279 eV $< E < 4.881$ keV for Group 2 and $E < 3.9279$ eV for Group 3.

NEA+KAERI (Korea)

1. **Name of participant(s).**

*Byung-Chan Na (e-mail: na@nea.fr), **Gyu-Hong Roh (e-mail: ghroh@kaeri.re.kr)

2. **Establishment.**

*OECD/NEA, Le Seine St-Germain, 12 Bd des Iles, 92130 Issy-les-Moulineaux, France
**Korea Atomic Energy Research Institute, P.O. Box 105, Yuseong, Daejeon, 305-600, Korea

3. **Name of code system(s) used.**

TRANSX-2.15 (cell calculations)
TORT-3.2 (core calculations)

4. **Bibliographic references for the codes used.**

TORT-DORT: Two- and Three-dimensional Discrete Ordinates Transport, Version 2.7.3, RISCC code package CCC-543, Oak Ridge National Laboratory, May 1993.

5. **Origin of cross-section data.**

For the cross-section generations, NJOY and TRANSX codes were used. The MATXS-format 190-group neutron libraries based on ENDF/B-VI release 5 and JENDL-3.2 were generated using MATXSR module of NJOY except for the natural S_N, which was obtained from the ENDL84 library. Using 190-group neutron libraries, ONEDANT calculations for three fuel pin-cell types and a Pyrex super-cell were undertaken to obtain weight flux for generating the region-wise homogenised cross-sections collapsed to 35 groups. The TORT core calculations were carried out using the collapsed 35-group libraries.

6. **Spectral calculations and data reduction methods used**

a) *Resonance shielding*: Bondarenko method or Background Cross-section Method (TRANSX).

b) *Mutual shielding*: None.

c) *Fission spectra*: Flux-, mixture- and region-dependent fission spectra are used.

d) *Describe how the (n,2n) reaction was treated*: The (n,2n) reaction was not treated.

e) *Weighting spectrum for scattering matrices*: None.

7. **Number of energy groups used in the different phases**

- 190 groups for cell calculations.
- 35 groups for core calculations.

8. Cell calculation

a) *Type of calculation*: Heterogeneous calculation.

b) *Theory used*: Transport theory.

c) *Method used*: Discrete ordinates (S_N) method.

d) *Calculation characteristics*: For the preparation of geometrical model in TORT inputs, the pre- and post-processing code BOT3P was used. One quarter of the full 3-D VENUS-2 core was modelled in the (x,y,z) geometry with the S_8P_3 approximation in all TORT calculations. Fully symmetrical quadrature sets were introduced. The spatial meshes used were $100 \times 102 \times 72$ in (x,y,z). The point-wise flux convergence criterion used was 1.0E-4 and the eigenvalue convergence criterion applied was 1.0E-5.

9. Other assumptions and characteristics.

10. Comments useful for interpreting correctly the results.

Purdue University (USA)

1. **Name of participant(s).**

Tomasz Kozlowski (tomasz@ecn.purdue.edu)
Chang-Ho Lee (changho@ecn.purdue.edu)
Thomas J. Downar (downar@ecn.purdue.edu)

2. **Establishment.**

Purdue University
School of Nuclear Engineering
1290 Nuclear Engineering Building
West Lafayette, IN 47907-1290
USA

3. **Name of code system(s) used.**

HELIOS 1.7 – pin cell calculation and few group cross-section generation for PARCS.
PARCS 2.1 – core calculation.

4. **Bibliographic references for the codes used.**

Stamm'ler, R.J.J., M.J. Abbate, *Methods of Steady-state Reactor Physics in Nuclear Design*, Academic Press, London (1983).

Casal, J.J., R.J.J. Stamm'ler, A.A. Ferri, E.A. Villarino, "HELIOS: Geometric Capabilities of a New Fuel-assembly Program", *Int. Topical Meeting on Advances in Mathematics, Computations, and Reactor Physics*, Pittsburgh, Pennsylvania, 28 April-2 May 1991,Vol. 2, p. 10.2.1 1-13.

Villarino, E.A., R.J.J. Stamm'ler, A.A. Ferri, J.J. Casal, "HELIOS: Angular Dependent Collisions Probabilities", *Nuclear Science and Engineering*, Vol. 112, 16 (1992).

Giust, F.D., R.J.J. Stamm'ler, A.A. Ferri, *HELIOS 1.7 User Guide and Manual*, Studsvik Scandpower (2001).

Downar, T.J., *et al*., "PARCS: Purdue Advanced Reactor Core Simulator", accepted for publication, *PHYSOR2002*, Seoul, Korea.

5. **Origin of cross-section data.**

ENDF/B-VI rev. 3.

6. Spectral calculations and data reduction methods used.

a) *Resonance shielding*:

The subgroup method is used to evaluate the following expression for $\hat{\sigma}_a$:

$$\hat{\sigma}_a = \frac{\int_{\Delta u} (u)\phi(u)\mathrm{d}u}{\int_{\Delta u} \phi(u)\mathrm{d}u} \cong \frac{\sum_n w_n \sigma_n \phi_n}{\sum_n w_n \phi_n} \tag{1}$$

where $\phi_n = \phi(\sigma_n)$ are the fluxes at discrete values of σ_a, σ_n which represents the seven subgroups into which the σ_a range has been subdivided. Sets of weights and cross-sections are stored in the nuclear-data library for each resonance isotope, in each resonance group, for about five different temperatures.

To evaluate $\hat{\sigma}_a$ it suffices to find the seven fluxes ϕ_n in each region of the system. First, four flux calculations with four different cross-sections σ_m of the resonance absorber yield four fluxes ϕ_m in each region, from which an effective background cross-section $\sigma_{b,m}$ is found according to the relation:

$$\phi_m = \frac{\sigma_{b,m}}{\sigma_m + \sigma_{b,m}} \Rightarrow \sigma_{b,m} = \frac{\sigma_m \phi_m}{1 - \phi_m} \tag{2}$$

Next, for each region, interpolation in these four $\sigma_{b,m}$ gives seven $\sigma_{b,n}$. Using Eq. (2), they yield the seven subgroup fluxes for use in the quadratures of Eq. (1).

b) Mutual shielding:

To describe interaction between resonance isotopes, they are grouped into categories inside which the resonances are assumed to overlap, while there is no overlap between the different categories. For each category the process outlined above is repeated.

Finally, $\hat{\sigma}_{ai}$ of a given resonance isotope *i* in a mixture of resonance isotopes is found by assuming that the effective cross-sections of the other resonance isotopes *j* act as a background cross-section. Using Eqs. (1) and (2), this assumption leads to the following expression for $\hat{\sigma}_{ai}$:

$$\hat{\sigma}_{ai} = \frac{\sum_n w_{ni} \dfrac{\sigma_{ni}\sigma_{b,ni}}{\sigma_{ni} + \sigma_{xi} + \sigma_{b,ni}}}{\sum_n w_{ni} \dfrac{\sigma_{b,ni}}{\sigma_{ni} + \sigma_{xi} + \sigma_{b,ni}}} \tag{3}$$

where:

$$\sigma_{xi} = \frac{1}{N_i} \sum_{j \neq i} N_j \hat{\sigma}_{aj} \tag{4}$$

c) *Fission spectra:*

The fission spectrum of a mixture of isotopes is evaluated from:

$$\chi_g = \sum_i \left(\chi_{ig} \frac{N_i w_i}{\sum_{i'} N_{i'} w_{i'}} \right) \text{ with } w_i = \sum_g \nu\sigma_{fi,g}\phi_g \tag{5}$$

where the w_i of the thirteen most important fissionable isotopes – other isotopes get the w_i of ^{235}U – have been obtained from a calculation of an infinite square UO_2 lattice at 20 MWd/kg, defined as:

Fuel: 920 Kelvin, radius 0.46 cm, 10 g/cm^3, 3 wt.% enriched UO_2.
Clad: 570 Kelvin, radius 0.54 cm, 6 g/cm^3, zircaloy.
Coolant: 560 Kelvin, pitch 1.43 cm, 0.74 g/cm^3, H_2O.

d) *Describe how the (n,2n) reaction was treated:*

In the transport calculations the (n,2n) and (n,3n) reactions are included by adjusting absorption cross-sections and scattering matrices. To obtain the true loss and capture rates in the depletion calculations, the absorption cross-sections are re-adjusted.

e) *Weighting spectrum for scattering matrices:*

The scattering data in the 190-group "master" library have been obtained from hyper-fine group calculations in a typical PWR pin cell at a number of different temperatures and, depending on the isotope, in either the fuel, clad or coolant. When collapsing to fewer-group libraries, not one collapsing spectrum is used but, depending on the isotope and its temperature tabulation, spectra are used that are chosen from a selection of 190-group HELIOS-generated spectra at a variety of temperatures, burn-ups and regions (e.g. fuel, clad, H_2O, D_2O or graphite moderator and control pin).

7. Number of energy groups used in the different phases.

The HELIOS 190 neutron group library with 3.4% adjustment in ^{238}U resonance capture "hy190n48g17a.dat" was used for cell calculation and to generate few group cell homogeneous cross-sections for PARCS. PARCS core calculation was performed in eight groups (energy cut-offs: 2.23130E+06, 8.20850E+05, 4.88100E+03, 1.30070E+02, 3.92790E+00, 6.25062E-01, 1.45720E-01, 0.00000E+00).

8. Cell calculation.

a) *Type of calculation*: Heterogeneous.

b) *Theory used*: Transport.

c) *Method used*: CCCP.

d) *Calculation characteristics*: "Wind-mill" mesh in the coolant of the pin cells; this mesh divides the sides of a cell into three flat-current segments, thus allowing to represent the dip in the thermal currents caused by the fuel in the middle of the side. The mesh must be described by

the user in the input since HELIOS has no pre-set cell mesh. The energy cut-offs for cell calculation reaction rates are 4.881 keV and 3.9279 eV. These correspond to the closest energy groups on lethargy scale available in HELIOS.

9. Other assumptions and characteristics.

The core calculation performed with PARCS core simulator was done using fine mesh finite difference (FMFD) SP3 kernel with one mesh per pin cell and SPH factors [1]. Fuel and radial reflector cross-sections and corresponding SPH factors were generated from VENUS-2 2-D HELIOS solution. Axial reflector cross-sections and SPH factors were generated from 1-D homogeneous fuel-heterogeneous reflector HELIOS solution [2].

10. Comments useful for interpreting correctly the results.

[1] Hebert, A., "A Consistent Technique for the Pin-by-pin Homogenization of a Pressurized Water Reactor Assembly", *Nucl. Sci. Eng*., 113, 227 (1993).

[2] Kozlowski, T., C.H. Lee, T.J. Downar, "Application of SPH Factors for VENUS-2 MOX Core Analysis with Pin Homogeneous Cross-sections," accepted for publication, *PHYSOR2002*, Seoul, Korea.

FRAMATOME-ANP GmbH (Germany)

1. **Name of participant(s).**

   W.Timm, S. Misu, D. Porsch

2. **Establishment.**

   FRAMATOME-ANP GmbH (Erlangen, Germany)

3. **Name of code system used**

   CASMO-4 (cell code), MOCA (3-D code)

4. **Bibliographic references for the codes used.**

   CASMO-4, A Fuel Assembly Burn-up Code, Studsvik SOA 2/95 [3]
   MOCA [4]

5. **Origin of cross-section data**

   Studvik's own "L"-library in 70 energy group is used, Most of the data is based on ENDF/B-4. For some isotopes (ex: ^{162}Er or ^{170}Tm) data from JEF-1 and JEF-2.1 are used. The shielded resonance data for Pu- and Gd-isotopes are taken from JEF libraries. Data processing code/method used to obtain the cross-section data use NJOY (different versions).

6. **Spectral calculations and data reduction methods used.**

   The commercially available versions of the code and library of the developer STUDSVIK OF AMERICA INC. have been used. CASMO-4 is a multi-group two-dimensional transport theory code for burn-up calculations on BWR and PWR assemblies. The standard "L-library" contains microscopic cross-sections in 70 energy groups. The CASMO-4 default number of energy groups for MOX fuel was used. Normally, the calculation starts with a simplified geometry and 70 neutron energy groups: 14 fast groups, 13 resonance groups and 43 thermal (below 4eV). In a 2-D transport calculation for a complete bundle geometry 16 energy groups are used, out of which 13 are below 4 eV.

   The calculation sequence normally starts with a simplified geometry. Energy groups are then collapsed as spatial detail is increased. The flux distributions and the eigenvalue are calculated based upon a method of characteristics. A fundamental buckling mode can be used for modifying the results from the transport calculation to include the effects of leakage.

7. **Number of energy groups used in different phases.**

   CASMO can edit cross-section sets with up to 10 groups. In the present case a five-group condensation scheme has been chosen: the energy boundaries of the cross-sections for the 3-D calculations are as seen in Table 1.

Table 1. Energy group condensation structure

Group upper bounds		Fission spectrum	Two-group scheme in-core design calc.
1	10.00 MeV	0.785	1
2	821.0 keV	0.215	1
3	5.53 keV	0.0	1
4	4.00 eV	0.0	1
5	0.625 eV	0.0	2

The fission spectrum assumed here is somewhat harder than the CASMO fission spectrum, but gives an overall better adaptation to the CASMO k_∞ and the CASMO group fluxes. There are some more approximations:

- only isotropic scattering is assumed (P_0);
- (n,2n) reactions are ignored in the five-group scheme;
- the transport cross-section is assumed to be the inverse diffusion constant divided by 3, the in-group scattering cross-section then being the difference between this transport cross-section and the total removal cross-section;
- up-scattering is only taken into account approximately via a correction term in the down-scattering cross-section to the last group (similar to the standard CASMO procedure for the two-group condensation), up-scattering above 0.625 eV is generally small anyway.

8. Cell calculation.

Generally, cross-sections for infinite pin lattice (homogeneous calculations) have been used. For specific materials heterogeneous cell calculations have been performed:

- For the Pyrex pin cell, a (infinite lattice) 3×3 cell has been assumed with one Pyrex pin in the centre being surrounded by eight 3/0 fuel pins. The cross-sections are then condensed only for the central Pyrex pin.
- For the fuel rods adjacent to the baffle reflector it has been investigated whether this environment has an effect on the condensed cross-sections of the fuel row directly adjacent to the baffle and on the cross-sections of the baffle steel. To this end an 8×8 cell has been calculated with two “rows” of water, three “rows” of baffle steel and three “rows” of each fuel type, all rows having a thickness of 1.26 cm and the 8×8 cell having reflective boundary conditions. It was found that only for the UO_2 fuel there was a noticeable effect (the thermal fission and absorption cross-sections are smaller by a few percent near the baffle), whereas the baffle had only a negligible influence on the MOX cross-sections. The five-group cross-section data of the baffle steel have been found to be almost independent of the adjacent fuel type and are taken as identical for the inner and outer baffle.
- A similar CASMO cell calculation has been performed for the interface between the 3.3 (3/0) and the 4.0 (4/0) UO_2 fuel. Here the interface had the strongest effect on the thermal cross-sections of the 4.0 UO_2 fuel, where an increase of around 2% was seen due to increased moderation. The influence on the 3.3 UO_2 cross-sections at this interface is smaller (around 1% decrease) and can be neglected.

In accordance with these CASMO results, the thermal cross-sections of the UO_2 fuel (both 3/0 and 4/0) adjacent to the baffle steel and those of the 4/0 UO_2 fuel at the interface to the 3/0 fuel have been slightly modified in the thermal range below 0.625 eV. One should keep in mind that the effect of these modifications of the cross-sections in a limited number of pins is negligible regarding the core k-effective. Regarding pin powers the impact is only of the order of a few per cent.

9. Other assumptions and characteristics.

In the 3-D core calculations the uniform grid with a pitch of 1.26 cm in x-y direction has also been preserved in all regions outside the fissile zones, i.e. baffle, water, barrel. Therefore baffle and barrel/neutron pad have only been roughly modelled in this uniform grid, i.e. in such a way that the masses (areas) of these materials are approximately preserved. In the quarter core a size of 55×55 "meshes" has been assumed in the x-y direction.

Axially, only two additional materials have been introduced:

- rods with Plexiglas (surrounded by water) above and below the 3/0 UO_2 zone;
- rods with Plexiglas (surrounded by water) above and below the 4/0 UO_2 zone and the 2/2.7 MOX zone.

All grid plate materials have been neglected. For the upper axial reflector a thickness of 13 cm has been assumed and for the lower a thickness of 30 cm.

10. Comments useful for interpreting correctly the results.

In order to get a sufficiently accurate axial power profile in the specified fuel rods, these were split axially into seven almost equidistant regions (around 7 cm per region) and the axial fission rate distribution was then calculated by a simple spline interpolation preserving the rates of these seven axial zones. Since no statistically significant axial asymmetry has been detected, axial profiles have been symmetrised.

All results have been obtained by assuming quarter core symmetry. Comparisons with full core calculations (taking into account the barrel and neutron pad only in one quarter of the core) gave a k-effective which seemed to be around 20 to 30 pcm lower than the symmetrical core (high statistical uncertainty here), so the presence of the barrel seems to slightly increase the k-effective. However the pin power distribution was not affected with full core geometry (no statistically significant effects have been detected).

FRAMATOME-ANP GmbH did not participate in the 2-D benchmark [1]. However, as a test, 2-D calculations with a uniform buckling of 2.4E-3 cm^{-2} have also been performed. Here the k-effective was around 400 pcm lower than in the 3-D calculations. Differences of the 2-D/3-D results regarding pin power distributions appear to be small.

Main results and comments

Cell calculations

Table 2 shows the CASMO-4 k_∞ values of the individual fuel zones and the corresponding values of condensed homogeneous cross-sections.

Table 2. k_∞ values of cell calculations

	CASMO-4 k_∞	CASMO-4 k_∞ 5 group
Oxide 3.3 (3/0)	1.40394	1.40201
Oxide 4.0 (4/0)	1.33469	1.33367
Mox 2.0/2.7	1.25550	1.25472

The CASMO-4 k_∞ values have been calculated with the "L-lib", based on ENDF/B data in 70 energy groups.

Table 2.1. Absorption and fission rates of the heavy metal isotopes in the 2/2.7 MOX zone

Isotope	Absorption	Fission
^{234}U	0.0018014	0.0000499
^{235}U	0.3754927	0.2973021
^{236}U	0.0007096	0.0000270
^{238}U	0.5278478	0.0711410
^{239}Pu	0.9165389	0.6017451
^{240}Pu	0.1896134	0.0019020
^{241}Pu	0.0370322	0.0277846
^{242}Pu	0.0022003	0.0000362
^{241}Am	0.0008104	0.0000119

Table 2.2. Absorption and fission rates of the heavy metal isotopes in the 3/0 UO_2 zone

Isotope	Absorption	Fission
^{235}U	1.1454711	0.9470444
^{238}U	0.4822063	0.0528931

Table 2.3. Absorption and fission rates of the heavy metal isotopes in the 4/0 UO_2 zone

Isotope	Absorption	Fission
^{235}U	1.1496290	0.9372020
^{238}U	0.5166942	0.0627062

In Table 2.3, only the total absorption and fission rates are given. The isotopic rates for specified energy regions cannot be edited directly in CASMO-4, so the results for the three energy regions are missing.

Core calculations

The 3-D core calculations have been performed with the broad energy group Monte Carlo transport code MOCA [4].

The k-effective of the core is:

$$\mathbf{k_{eff} = 1.00110}$$

with an uncertainty of 7 pcm (1 sigma).

The radial fission rate distribution is given in a separate ASCII file (see attachment, which also contains the C/E ratios compared to the measured values). As the measured (and partially interpolated) normalised radial pin power (fission rate) distribution has been published in [1], the MOCA pin power results can be directly compared to the measured values. Table 3 gives an overview of the main results, both for the individual fuel zones and for the total core.

Table 3. Overview of the main results, both for individual fuel zones and the total core

Zone	Power calc.	Power exp.	Power (C/E)	Peaking calc.	Peaking exp.	Peaking (C/E)	1 sigma [%]
UOX 3.3	1.29579	1.33151	0.97317	1.13888	1.14381	0.99568	1.77
UOX 4.0	1.16243	1.16831	0.99497	1.31350	1.33611	0.98308	2.04
MOX 2/2.7	0.62559	0.59258	1.05571	1.75606	1.79722	0.97710	2.58
Total	1.00525	1.00595	0.99930	1.52686	1.56100	0.97813	4.61

Here the "power" is defined as the average of all power factors of the individual fuel zones or of all 325 power factors in the core (as 10 out of the 325 rods are on a diagonal symmetry line in the inner zone, the "mean total power" is not exactly one according to this definition). Generally, a similar behaviour as in many solutions of the 2-D benchmark [1] is seen, i.e. the calculated radial power distribution is flatter than the measured one. Typically, the outer MOX rod powers are overestimated and the rod powers of the inner 3/0 UO_2 zone are underestimated.

The local peaking factors (maximum power factor divided by the "mean power") of the individual zones are also given in the table above. Generally the calculated peaking factors are slightly smaller than the experimental ones which is in accordance with the flatter calculated power distribution. Additionally, the mean deviation of the calculated power distribution of the individual zones is given in the table. These deviations are normally of the same order of magnitude as the average values of the solutions in [1]. Only the deviation for the total core is higher which is due to the fact that the calculated power factors near the periphery are overestimated by almost 10%. This seems to be typical for all solutions in [1] using pin cell homogenised cross-sections.

The calculated normalised axial power profiles are almost identical for all six specified rods. For the central 40 cm of the core the calculated axial power peaking factor is around 1.19 (measured values are not yet available). The detailed axial fission rate distributions of all six specified rods are given in a separate ASCII file (see attachment).

REFERENCES

[1] *Benchmark of the VENUS-2 MOX Core Measurements*, NEA/NSC/DOC(2000)7.

[2] *Blind Benchmark on the 3-D VENUS-2 MOX Core Measurements: Final Specification*, NEA/SEN/NSC/WPPR(2001)1.

[3] Knott, D., B.H. Forssen, M Edenius, *CASMO-4, A Fuel Assembly Burn-up Program Methodology*, Studsvik/SOA-95/2.

[4] Lieberoth, J., "A Monte Carlo Technique to Solve the Static Eigenvalue Problem of the Boltzman Transport Equation", *Nukleonik*, 11, 213-219 (1968).

JAERI (Japan)

1. Name of participant(s).

Yasunobu Nagaya (E-mail: nagaya@mike.tokai.jaeri.go.jp)
Keisuke Okumura (E-mail: okumura@mike.tokai.jaeri.go.jp)
Takamasa Mori (E-mail: mori@mike.tokai.jaeri.go.jp)

2. Establishment.

Japan Atomic Energy Research Institute (JAERI)

3. Name of code system(s) used.

MVP

4. Bibliographic references for the codes used.

[1] Mori, T., M. Nakagawa, *MVP/GMVP: General Purpose Monte Carlo Codes for Neutron and Photon Transport Calculations based on Continuous Energy and Multi-group Methods*, JAERI-Data/Code 94-007 (1994) [in Japanese].

[2] Nakagawa, M. and T. Mori, "Whole Core Calculation of Power Reactors by Use of Monte Carlo Method", *J. Nucl. Sci. Technol*., Vol. 30, No. 7, p. 692 (1993).

[3] Mori, T., M. Nakagawa, M. Sasaki, "Vectorization of Continuous Energy Monte Carlo Method for Neutron Transport Calculation", *J. Nucl. Sci. Technol*., Vol. 29, No. 4, p. 325 (1992).

5. Origin of cross-section data.

- JENDL-3.2 for all nuclides except for Sn (natural). CENDL-2 for Sn (natural).
- JENDL-3.3[4] for all nuclides except for S (natural), Si (natural), Mo (natural) and Sn (natural). JENDL-3.2 for S (natural), Si (natural), Mo (natural), and CENDL-2 for Sn (natural).

6. Spectral calculations and data reduction methods used.

Continuous-energy Monte Carlo calculation.

a) *Resonance shielding*: Taken explicitly for all nuclides and in any energy region (unresolved resonances are treated by probability tables).

b) *Mutual shielding*: Taken explicitly.

c) *Fission spectra*: Nuclide-wise fission spectrum.

d) *(n,2n) reaction*: Taken explicitly.

e) *Weighting spectrum for scattering matrices*: Not necessary.

7. Number of energy groups used in the different phases.

Continuous energy (from 1.0E-5eV to 20MeV) for all phases.

8. Cell calculation.

a) *Type of calculation*: Heterogeneous.

b) *Theory used*: Transport.

c) *Method used*: Monte Carlo.

d) *Calculation characteristics*: Continuous energy.

e) *Histories for cell calculation*: 49 000 000 = 24 500 cycles × 20 000 neutrons (not including 50 cycles for initial guess).

9. Other assumptions and characteristics.

- The 3-D calculation model (quarter-symmetric core model) is constructed based on the report [5] distributed by NEA/SEN/NSC/WPPR. The model includes lower filling, reactor support, bottom and intermediate and upper grids, top and bottom reflectors, top and bottom stops and upper filling axially. It also includes reactor vessel, jacket, neutron pad, barrel, outer and inner baffles radially.

- The neutron pad was assumed to be a part of a cylindrical tube though the real pad does not have uniform thickness.

- We have also performed the full-core calculation to investigate the asymmetric effect of the barrel and neutron pad on the pin power distribution but no difference is seen between the full core and quarter-symmetric models [6]. Thus we employed the quarter-symmetric model to reduce statistical errors.

- There is inconsistency for the gap between the jacket inner wall and the barrel (t4). According to Figure 2 in the report [5], t4 must be t15+t11+e15 (=12.79) but t4 = 11.80. We assumed as follows:

  Gap between the jacket inner wall and the neutron pad = 0.3 cm
  Thickness of the neutron pad = 6.72 cm
  Gap between the neutron pad and the barrel = 5.8 cm

- No data were available for the top and bottom reflectors and stops for MOX pins. Thus we assume that the data are the same as that for 4/0 UO_2 pins.

- The scattering law $S(\alpha,\beta)$ of polyethylene was used for Plexiglas since no scattering law was available.

- Tally regions for pin power distribution include not only the single unit cells of interest but also symmetric cells though the geometry is not symmetric with regard to the diagonal due to the neutron pad.

- Histories for 3-D core calculation: 199 000 000 = 9 950 cycles × 20 000 neutrons (not including 50 cycles for initial guess).
- The average statistical uncertainty for axially integrated pin powers is about 0.13%.
- The average statistical uncertainty for axial pin powers is about 0.66%.
- Other details are descried in reference [6].

10. Comments useful for interpreting correctly the resutls.

REFERENCES

[4] Shibata, K., *et al*. "Japanese Evaluated Nuclear Data Library Version 3 Revision-3: JENDL-3.3", *J. Nucl. Sci. Technol.*, 39, 1125 (2002).

[5] Na, B-C. and N. Messaoudi, *Blind Benchmark on the 3-D VENUS-2 MOX Core Measurements: Final Specification*, NEA/SEN/NSC/WPPR(2001)1.

[6] Nagaya, Y., K. Okumura and T. Mori, "Analysis of VENUS-2 MOX Core Measurements with a Monte Carlo Code MVP", *Proc. Int. Conf. on the New Frontiers of Nuclear Technology: Reactor Physics, Safety and High-performance Computing (PHYSOR 2002)*, 4A-04 (paper index number in CD), Seoul, Korea, 7-10 October (2002).

SCK•CEN (Belgium)

1. **Name of participant(s).**

   Nadia Messaoudi, Hamid Ait Abderrahim

2. **Establishment.**

   SCK•CEN
   Reactor Physics and Myrrha Project Dept.
   Boeretang 200
   B-2400 Mol, Belgium

3. **Name of code system(s) used.**

   MCNP (version 4Ca)

4. **Bibliographic references for the codes used.**

   MCNP A General Monte Carlo Code N-particle Transport Code, Version 4C, J.F. Briesmeister, ed., Los Alamos National Laboratory report, LA-13709-M (April 2000).

5. **Origin of cross-section data.**

   Calculations are made with both the ENDF/B-VI library from the MCNP4C package and the JEF-2.2 library based on JEF-2.2 evaluation (Harm Wienke, *Production and Resting of Vitamin_B6 Multi-group Coupled Neutron/Photon and MCNP-compatible Continuous-energy Cross-section Libraries, Based upon Various Evaluated Cross-section Data Files*, BLG 889, August 2001) except for S (from ENDF/B-VI) and ^{239}Pu, for which the new and corrected CEA evaluation file was used.

6. **Spectral calculations and data reduction methods used.**

   a) *Resonance shielding*: Self-shielding effects in the unresolved resonance range is taken into account by using a probability-table treatment for some isotopes.

   b) *Fission spectra*: Watt fission spectrum.

   c) *Describe how the (n,2n) reaction was treated*: (n,2n) reaction was treated explicitly.

   d) *Weighting spectrum for scattering matrices*: None.

7. **Number of energy groups used in the different phases.**

   Continuous-energy cross-section library was used (from 1.0E-05 eV to 20 MeV).

8. **Cell calculation**

   a) *Type of calculation*: Heterogeneous.

   b) *Theory used*: Transport theory.

c) *Method used*: Monte Carlo method.

d) *Calculation characteristics*: For core calculations, 500 000 particles per cycle with 700 cycles (80 are inactive) were used, for cell calculations, only 1 000 particles per cycle with 1 100 cycles (100 are inactive) were used.

9. Other assumptions and characteristics.

10. Comments useful for interpreting correctly the results.

KAERI (Korea)+NEA

1. **Name of participant(s).**

*Gyu-Hong Roh (e-mail: ghroh@kaeri.re.kr)
**Byung-Chan Na (e-mail: na@nea.fr)

2. **Establishment.**

*Korea Atomic Energy Research Institute, P.O. Box 105, Yuseong, Daejeon, 305-600, Korea
**OECD/NEA, Le Seine St-Germain, 12 Bd des Iles, 92130 Issy-les-Moulineaux, France

3. **Name of code system(s) used.**

MCNP-4B

4. **Bibliographic references for the codes used.**

MCNP: A General Monte Carlo Code N-particle Transport Code, Version 4B, J.F. Briesmeister, ed., Los Alamos National Laboratory report, LA-12625-M (March 1997).

5. **Origin of cross-section data.**

The MCNP continuous-energy neutron cross-section library is newly generated based on ENDF/B-VI release 5 using the nuclear data processing system NJOY97.114 for all the isotopes except Sn from ENDL92. The thermal S(α,β) library TMCCS was used as the reference library, which was produced by LANL. The fractional tolerance used in the NJOY input parameter was 0.1% and the thinning option of the ACER module was not used to improve the accuracy, even though the file sizes are large.

6. **Spectral calculations and data reduction methods used.**

a) *Resonance shielding*: Infinite diluted cross-section library.

b) *Fission spectra*: Watt fission spectrum.

c) *Describe how the (n,2n) reaction was treated*: (n,2n) reaction was treated explicitly.

d) *Weighting spectrum for scattering matrices*: None.

7. **Number of energy groups used in the different phases.**

Continuous-energy cross-section library was used (from 1.0E-05 eV to 20 MeV).

8. **Cell calculation.**

a) *Type of calculation*: Heterogeneous.

b) *Theory used*: Transport theory.

c) *Method used*: Monte Carlo method.

d) *Calculation characteristics*: One quarter of the full 3-D core was explicitly modelled in three-dimensional geometry. In this study, all fuel rods and Pyrex rods were fully modelled including the fuel pellet, fuel gap (*not present in MOX pin cells*), clad and coolant. The radial core components such as, the reactor vessel, jacket, neutron pad, barrel, reflector, outer baffle, inner baffle and inner hole, etc. were also fully modelled. Vertically, the core was modelled from bottom to top such as, lower filling, reactor support, bottom grid, lower reflector, upper grid, upper filling, etc. In order to get the axial fission rate distributions in the core, the core was divided into 25 axial layers and F4 tally card (track length estimate of cell flux) was used for each cell. The number of histories used was 300×10^6 (100 000 neutrons/cycle and 3 000 cycles after 100 inactive cycles).

9. Other assumptions and characteristics.

10. Comments useful for interpreting correctly the results.

KFKI (Hungary)

1. **Name of participant(s).**

   Gábor Hordósy

2. **Establishment.**

   KFKI Atomic Energy Research Institute, Budapest, Hungary

3. **Name of code system(s) used.**

   MCNP-4C

4. **Bibliographic references for the codes used.**

   MCNP™ – A General Monte Carlo N-particle Transport Code, Version 4C, J.F. Breismeister, ed., LA-13709-M, Los Alamos National Laboratory (2000).

5. **Origin of cross-section data.**

   ENDF/B-VI.2 for most isotopes, except the structural material, for which ENDF/B-V was used.

6. **Spectral calculations and data reduction methods used.**

   Probability table treatment was used for the unresolved resonances, as a standard feature in MCNP-4C.

7. **Number of energy groups used in the different phases.**

   Continuous-energy representation.

8. **Cell calculation**

   a) kcode calculation by MCNP-4C.

   b) Monte Carlo.

   c) Monte Carlo.

   d) Calculation characteristics: 25 000 particle per cycle, 50 passive and 500 active cycles were used.

9. **Other assumptions and characteristics.**

10. **Comments useful for interpreting correctly the results.**

    For the axial power distribution calculations the pins were divided into cells with 2 cm height, and the volume averaged fission rate of these segments were used. In the core calculation 37 000 000 active neutrons were used.

KI (Russia)

1. **Name of participant(s).**

   E. Gomin M. Kalugin

2. **Establishment.**

   RRC "Kurchatov Institute"

3. **Name of code system(s) used.**

   MCU-REA

4. **Bibliographic references for the codes used.**

   Gomin, E.A., L.V. Maiorov, "The MCU Monte Carlo Code for 3-D Depletion Calculation", *Proc. of the Int. Conference on Mathematics and Computation, Reactor Physics and Environmental Analysis in Nuclear Applications*, M&C'99, Madrid, Spain (1999), 16.2-12.

5. **Origin of cross-section data.**

   MCU data libraries is DLC/MCUDAT-2.1 based on:

   - ENDF/B-VI, JENDL-3.2, BROND.

   MCU group own evaluations and compilations:

   - LIPAR – parameters of the fully resolved resonances.
   - BFS – phonon spectra library including the ENDF data.
   - KORT – cross-sections for E=0.0253 eV, resonance integrals, etc.

6. **Spectral calculations and data reduction methods used.**

   Monte Carlo.

7. **Number of energy groups used in the different phases**

   Continuous energies.

8. **Cell calculation**

   a) *Type of calculation*: Heterogeneous.

   b) *Theory used*: Transport.

   c) *Method used*: Monte Carlo.

   d) *Calculation characteristics*: Reflecting surfaces, 1.E+6 histories in cell calculations and 40E+6 histories in core calculations, combined collision/absorption estimator of k_{eff} continuous energies.

9. Other assumptions and characteristics.

The 3-D model is based on the benchmark specification provided in the document entitled *Blind Benchmark on the 3-D VENUS-2 MOX Core Measurements*, NEA/SEN/NSC/WPPR(2001)1 without any approximation except on the neutron pad. Neutron pad outer radius was taken as 65.073 cm instead of that specified. Two calculations were performed for the core. In the first run the tallies were fuel rods from 105 to 155 cm. In the second run the tallies were 23 axial zones in each of six fuel pins where axial fission rate distribution were measured.

10. Comments useful for interpreting correctly the results.

None.

GRS+IKE (Germany)

1. **Name of participant(s).**

Winfried Zwermann[1], Margarete Mattes[2]

2. **Establishment.**

[1] Gesellschaft für Anlagen- und Reaktorsicherheit (GRS) mbH
Forschungsgelände
85748 Garching, Germany
Tel: ++49 89 32004-425
Fax: ++49 89 32004-599
Eml: zww@grs.de

[2] Universität Stuttgart, IKE
Pfaffenwaldring 31
70550 Stuttgart, Germany
Tel: ++49 711 685-2136
Fax: ++49 711 685-2010
Eml: mattes@ike.uni-stuttgart.de

3. **Name of code system(s) used.**

MCNP-4C

4. **Bibliographic references for the codes used.**

MCNP – A General Monte Carlo N-particle Transport Code – Version 4C, J.F. Briesmeister, ed., LA-13709-M, (2000).

5. **Origin of cross-section data.**

Point data generated by IKE Stuttgart from:

- JEF-2.2.
- ENDF/B-VI rel. 5.
- JENDL-3.2.

6. **Spectral calculations and data reduction methods used**

None.

7. **Number of energy groups used in the different phases**

Continuous.

8. Cell calculation.

Square pin cells, Monte Carlo transport, continuous energy, 4 000 000 histories (500 cycles, 8 000 neutrons per cycle).

Core calculation: Monte Carlo transport, continuous energy, 40 000 000 histories (10 000 cycles, 4 000 neutrons per cycle), ¼ core.

9. Other assumptions and characteristics.

No S(α, β) data were available for Plexiglas, therefore polyethylene data were taken.

Although, due to the neutron pad, the arrangement is not truly symmetric with regard to the diagonal, each pin fission rate value was calculated by taking the average of pins (i,j) and (j,i).

10. Comments useful for interpreting correctly the results.

SEA (Spain)

1. **Name of participant(s).**

   David López Maganto (dlmaganto@teleline.es)

2. **Establishment.**

   SEA Shielding Engineering and Analysis S.L.
   Avda. de Atenas, 75
   28230 Las Rozas (Madrid)
   Tel: +34 (1) 91 631 78 07
   Fax: +34 (1) 91 631 82 66

3. **Name of computer code system(s) used.**

   MCNP-4C

4. **Bibliographic references for the codes used.**

   MCNP – A General Monte Carlo N-particle Transport Code, Version 4C, J.F Briesmeister, ed., LA-12625-M, Los Alamos National Laboratory.

5. **Origin of cross-section data.**

   ENDF/B-VI for fuel, moderator and some elements of the steel structures, and ENDF/B-V for the rest of elements.

6. **Spectral calculations and data reduction method used.**

   - No special treatment of unresolved resonances.
   - Watt fission spectrum.
   - (n,2n) reaction treated explicitly.

7. **Number of energy groups used.**

   Continuous-energy cross-section library.

8. **Cell calculations**

   a) Heterogeneous model.

   b) Transport theory.

   c) Monte Carlo method.

   d) $2.5 \cdot 10^6$ neutron histories for k_∞ calculations and $4 \cdot 10^7$ for reaction rates calculations.

   e) Uncertainty for energy integrated reaction rates: 0.1%.

9. Other assumptions and characteristics.

Core calculations: $4 \cdot 10^7$ neutron histories for all the calculations, except for the axial fission rates in the MOX zone: $6 \cdot 10^7$ neutron histories. Uncertainty for radial fission rate distribution: <1.00%, Uncertainty for axial fission rate distribution: 2-5%.

10. Comments useful for interpreting correctly the results.

LIST OF CONTRIBUTORS

Authors
Nadia Messaoudi (SCK•CEN, Belgium) and Byung-Chan Na (OECD/NEA)
Problem specification
Byung-Chan Na (OECD/NEA) and Nadia Messaoudi (SCK•CEN, Belgium)
NSC Reviewers
Tomas Lefvert (RIT, Sweden) Takamasa Mori (JAERI, Japan) Pierre D'hondt (SCK•CEN, Belgium) Kevin Hesketh (BNFL, UK)
Benchmark participants
W. Hofmann (FRAMATOME-ANP, Germany) J. Koban (FRAMATOME-ANP, Germany) W. Timm (FRAMATOME-ANP, Germany) S. Misu (FRAMATOME-ANP, Germany) D. Porsch (FRAMATOME-ANP, Germany) D.H. Kim (KAERI, Korea) J.D. Kim (KAERI, Korea) C.S. Gil (KAERI, Korea) J.H. Chang (KAERI, Korea) B-C. Na (OECD/NEA) G.H. Roh (KAERI, Korea) T. Kozlowski (Purdue University, USA) C.H. Lee (Purdue University, USA) T.J. Downar (Purdue University, USA) Y. Nagaya (JAERI, Japan) K. Okumura (JAERI, Japan) T. Mori (JAERI, Japan) N. Messaoudi (SCK•CEN, Belgium) H. Ait Abderrahim (SCK•CEN, Belgium) G. Hordósy (KFKI, Hungary) E. Gomin (KI, Russia) M. Kalugin (KI, Russia) W. Zwermann (GRS, Germany) M. Mattes (IKE, Germany) D.L. Maganto (SEA, Spain)

OECD PUBLICATIONS, 2 rue André-Pascal, 75775 PARIS CEDEX 16
Printed in France.